# REGGE PHENOMENOLOGY

**A.C. IRVING**

*Department of Applied Mathematics and Theoretical Physics,*
*University of Liverpool, P.O. Box. 147, Liverpool L69 3BX, U.K.*

and

**R.P. WORDEN**

*CERN, Geneva, Switzerland*

NORTH-HOLLAND PUBLISHING COMPANY - AMSTERDAM

PHYSICS REPORTS (Section C of Physics Letters) 34, No. 3 (1977) 117–231. NORTH-HOLLAND PUBLISHING COMPANY

# REGGE PHENOMENOLOGY

A.C. IRVING

*Department of Applied Mathematics and Theoretical Physics, University of Liverpool, P.O. Box. 147, Liverpool L69 3BX, U.K.*

and

R.P. WORDEN*

*CERN, Geneva, Switzerland*

Received 16 March 1977

*Contents:*



*Abstract:*

A review is presented of Regge phenomenology in high energy two-body and quasi-two-body scattering.



* Now at Logica Ltd., Little Portland Street, London W1, U.K.

## 1. Introduction

Most high energy collisions between elementary particles result in a multi-body final state in which a cloud of pions take away half the incident energy. In a small number of cases, the particles pass through unchanged. In an even smaller number of cases, they exchange quantum numbers such as charge or strangeness but otherwise, are more or less unchanged. Data for this last class of collision processes show a striking richness and variety – some reaction cross-sections show dips or breaks at fixed momentum-transfer, others do not; spin polarisation properties vary greatly from one reaction to another; cross-sections change by many orders of magnitude over presently accessible energy ranges. The main aim in Regge phenomenology is to understand this huge wealth of experimental facts and to abstract from it a theoretical framework which can be applied to all aspects of hadron physics. In the following review we hope to show that this aim has, to a large extent, been achieved.

Since its introduction into particle physics some fifteen years ago [4], the Regge pole hypothesis has influenced almost every theory or model of the strong interaction. Its importance in strong interactions is two-fold. Firstly, it is so far the only successful implementation of the quantum exchange idea which was so fruitful in the field-theoretic description of electromagnetic interactions. Secondly, it unifies the two main aspects of hadronic collisions – the scattering and spectroscopic properties of hadrons. By the latter, we mean that the same Regge poles which dominate high energy scattering exchange mechanisms also correlate the observed spectrum of hadronic bound states and resonances.

In addition to providing a coherent account of an otherwise bewildering array of two-body scattering data, the underlying ideas of Regge phenomenology have become part of the everyday language of particle physics. They are used routinely in all areas of the subject. One of the aims, in this review, is to describe this achievement of Regge phenomenology which we believe is often overlooked. The debates over specific models have perhaps dulled our appreciation of the great predictive power of the Regge approach.

However, the main purpose of the review is not to eulogise the successes of the past; more important is to survey the live issues of Regge phenomenology. In so doing, we will try to identify the main questions and discuss to what extent they have been satisfactorily answered. We hope the reader will not only be able to acquire or renew familiarity with the consolidated aspects of the subject, but also to assess the important issues lying behind current controversies.

### *1.1. Historical development*

Throughout the early and mid-sixties many workers demonstrated the usefulness of Regge poles for describing the rapidly accumulating data on both elastic and inelastic two-body collisions [8, 6, 15, 20, 21, 29, 23, 24]. With the application of SU(3) to exchange vertices, a coherent picture of exchange mechanisms began to emerge [21]. Data of improved statistical accuracy showed the need for corrections to the basic Regge pole and, in the late sixties, Arnold [17, 30], Kane, Ross [60, 78] and others developed absorption models for Regge cuts, so generalising the $t$-channel approach.

Following the pioneering work of Dolen, Horn and Schmid [42], the almost contemporary development of duality ideas greatly increased the predictive power of the Regge pole model. Being a (complementary) $s$-channel approach, duality provided much-needed constraints on the pole residue functions, and explicit dual model amplitudes were proposed [49]. With the increasing availability of polarisation data, the underlying amplitude structure of the various models incorporating Regge cuts and duality was stringently tested and, as a result, certain systematic features of the amplitudes began

to emerge [60, 50]. At around this time (early seventies), the prospect of a complete understanding of two-body exchange amplitudes in terms of Regge poles and cuts seemed bright [100]. Using double polarization data for $\pi$N scattering, Halzen and Michael [93] demonstrated the value of direct knowledge of amplitude structure. There followed further attempts to unravel the scattering amplitudes from data using a variety of techniques loosely termed "amplitude analysis".

Along with the results of amplitude analyses came a growing realisation that no one absorption model accounted for all the data. The emphasis shifted from model building towards an attempt to find systematic features in amplitude structure [87, 176, 208].

In discussions of Regge phenomenology and its future, one can discern two distinct attitudes (which we shall call "systematic" and "pragmatic"). The systematic, rather optimistic, approach needs little explanation. It is that by further study of experimental data – in particular, data on amplitudes – and with some theoretical prompting, we shall arrive first at some useful empirical rules about the behaviour of Regge cut amplitudes, and then at a calculable theory of Regge cuts. The pragmatic, and in some respects pessimistic, attitude is that there is little progress to be made by current methods of two-body phenomenology, that perhaps Regge cuts are intrinsically complicated objects although the laws governing them may be simple. It is like trying to formulate quantum mechanics from data on the energy levels of mercury – where is the hydrogen atom of Regge phenomenology? According to this view, the basic hypothesis of Regge pole dominance has been established in two-body phenomenology, and its relevance to other hadronic processes recognised. Understanding the subtler features of two-body amplitude structure (and the rules governing Regge cuts) may eventually come from other areas within particle physics. Perhaps, with hindsight, we shall see that we were asking the wrong questions in the first place.

In the concluding section, we shall comment further on the status of the two approaches. The studies of amplitude systematics presented in section 3 and in many of the mini-reviews (section 4) represent the systematic approach to Regge phenomenology. The summary of Regge pole successes (section 2) and the Reggeised Born term model (appendix A) are offered in the spirit of the pragmatic approach.

The success of two-body Regge phenomenology has affected other areas of particle physics in at least three ways.

Firstly, various aspects of Regge behaviour (energy dependence, linear trajectories, etc.) have become desiderata for explicit models and theories. As examples of these, one may mention dual schemes [230, 240] and theories of coloured quarks and gluons (quantum chromodynamics) [155]. Secondly, Regge phenomenology has been an important tool in several diverse areas of study. An obvious example is its use, along with the Mueller generalised optical theorem [77], in analysing inclusive processes. Another, less obvious, example is the role played by Regge concepts in large angle and large transverse momentum scattering [330]. Diffractive scattering is also an area of strong interaction research when Regge ideas and results are in everyday use [291].

Phenomenological success has provided impetus for the development of Regge theory itself. For example, considerable progress in multiparticle Regge theory has resulted [199]. The Gribov Reggeon calculus [57, 296] and its developments have also involved a great deal of interplay with Regge phenomenology, particularly concerning the nature of $j$-plane cuts. (This will be discussed in a later section.)

### 1.2. Plan of the review

The review is arranged into specialist and non-specialist units. We recommend the non-specialist to concentrate on sections 2 (simple features of Regge poles), 3 (absorptive corrections) and 5 (conclusions). Section 4 is more specialised and contains several self-contained mini-reviews of currently interesting topics. We have made little attempt to be complete. However, we hope that personal bias has been sufficiently overcome that our choice of topics, if not our treatment of them, fairly represents recent activity in the field. A particularly noticeable omission is that of diffractive scattering. There are many aspects of the latter which are highly relevant to Regge pole phenomenology but, for reasons of space, we are forced to neglect this rather large subject.

Particular effort has been made to re-emphasise the many simple, yet non-trivial, successes of the Regge pole approach which have become increasingly obscured by technical side-issues. We dwell little on the mathematical derivation of Regge pole formulae and, instead, refer the interested reader to the extensive literature on the subject [41, 75, 305]. Other treatments of the topics presented here may be found in earlier review articles such as those by Jackson [71], Chiu [116], Fox and Quigg [154] and Davier [208].

## 2. Foundations of Regge pole phenomenology

In this section we introduce the basic Regge pole formula as the foundation on which Regge phenomenology is built. We shall argue that this pole formula is highly constrained, highly predictive and successful.

### 2.1. The Regge pole formula

In the late 1960s Regge theory was a subject of enormous technical complexity [see for instance 31] where one had to battle with ghost-killing mechanisms, kinematic constraints, daughters and the like before establishing contact with experimental data. Fortunately the results of all these complexities turn out to be exceedingly simple when expressed in terms of $s$-channel helicity amplitudes [40]. They can be summarised in one formulae (eq. (2.1)) which is adequate for 90% of all phenomenological applications, and which we shall adopt as our starting point. The technicalities which arise on the way have been extensively reviewed [31, 41, 75, 84, 305].

The contribution of a single $t$-channel meson Regge pole at $\alpha(t)$, to an $s$-channel helicity amplitude for the process $12 \to 34$, is given by

$$T_{\lambda_3\lambda_4\lambda_1\lambda_2}(\nu, t) = \frac{1 + \tau \exp\{-i\pi\alpha(t)\}}{\sin \pi\alpha(t)} \cdot g_{\lambda_3\lambda_1}(t) g_{\lambda_4\lambda_2}(t) \cdot (\nu/\nu_0)^{\alpha(t)}. \tag{2.1}$$

$\nu$ is the crossing symmetric energy variable $\frac{1}{2}(s-u)$, where $s = (p_1 + p_2)^2$ and $u = (p_2 - p_3)^2$; $t = (p_3 - p_1)^2$ is the momentum transfer; the signature of the pole is $\tau$ $(= \pm 1)$ and $\nu_0$ is a constant scale factor.

Equation (2.1) is valid in the limit ($\nu \to \infty$, $t$ fixed) to leading order in $1/\nu$. Its most essential properties are

(1) *The energy dependence* comes purely from the factor $(\nu/\nu_0)^{\alpha(t)}$.

(2) *Phase and crossing symmetry.* Since $T(\nu, t)$ is a hermitian analytic function of $\nu$ [even (odd) if $\tau = +1$ $(-1)$] and has a power law behaviour $\nu^{\alpha}$, its phase is uniquely determined. Thus the residue

$g_{\lambda_3\lambda_1}g_{\lambda_4\lambda_2}$ is real and the phase arises solely from the signature factor ($\sim\exp\{-i\pi\alpha/2\}$ if $\tau=+1$ and $i\exp\{-i\pi\alpha/2\}$ if $\tau=-1$). The symmetry under the (crossing) transformation $\nu\to-\nu$ is physically important for relating amplitudes for the $s$-channel process ($12\to34$, $s>0$) to those for the $u$-channel process ($\bar{3}2\to1\bar{4}$, $u>0$). Thus, under crossing, odd signature poles ($\tau=-1$) change sign while even signature ones do not.

(3) *Factorisation.* The Regge pole residue factorises into two vertex functions $g_{\lambda_3\lambda_1}(t)$ and $g_{\lambda_4\lambda_2}(t)$.

(4) *Parity conservation.* The vertex functions obey the parity relations†

$$g_{\lambda_3\lambda_1}=(\tau P)\eta_3\eta_1(-)^{J_3-J_1}(-)^{\lambda_3-\lambda_1}g_{-\lambda_3-\lambda_1}$$
$$g_{\lambda_4\lambda_2}=(\tau P)\eta_4\eta_2(-)^{J_4-J_2}(-)^{\lambda_2-\lambda_4}g_{-\lambda_4-\lambda_2} \tag{2.2}$$

where $J_i$ and $\eta_i$ are the spin and parity of the external particles. $\tau P$ (signature × parity) is known as the naturality of the Regge pole. Equation (2.2) ensures that the parity reflection property of the full amplitude is trivially obeyed:

$$T_{\lambda_3\lambda_4\lambda_1\lambda_2}=\eta_1\eta_2\eta_3\eta_4(-)^{J_3+J_4-J_1-J_2}(-)^{\lambda_3-\lambda_4-\lambda_1+\lambda_2}T_{-\lambda_3-\lambda_4-\lambda_1-\lambda_2}. \tag{2.3}$$

(5) *Kinematic singularities.* In the high energy limit, $s$-channel helicity amplitudes have no kinematic singularities except that those with net helicity flip $n=|\lambda_3-\lambda_1-\lambda_4+\lambda_2|$ vanish in the forward direction as $(-t)^{n/2}$, through angular momentum conservation. Therefore the vertex functions $g(t)$ must behave as

$$g_{\lambda_3\lambda_1}(t)\sim(-t)^{|\lambda_3-\lambda_1|/2} \tag{2.4}$$

near $t=0$. In this way the full amplitude corresponding to single Regge pole exchange behaves as

$$T_{\lambda_3\lambda_4\lambda_1\lambda_2}\sim(-t)^{(n+x)/2} \tag{2.5}$$

where $n+x=|\lambda_3-\lambda_1|+|\lambda_4-\lambda_2|$. Thus it can happen (if $x\neq0$) that a Regge pole amplitude vanishes at $t=0$ more rapidly than angular momentum requires ($\sim(-t)^{n/2}$). For example, an amplitude with $\lambda_3-\lambda_1=1$ and $\lambda_4-\lambda_2=1$ has $n=0$ but $n+x=2$. This solution to the angular momentum constraints, in which each Regge pole individually satisfies them, is called evasion. Another possibility where several poles conspire to satisfy angular momentum and parity constraints has been extensively discussed [e.g. 31] but rejected on phenomenological grounds [84].

We emphasize that eq. (2.1) is an asymptotic formula. In non-leading orders ($\sim\nu^{-1}$ relative to eq. (2.1)) there are several complications. Perhaps the most important is that, for unequal mass kinematics, the physical region boundary is at $t=t_{\min}\neq0$. It is often worthwhile to replace $t$ by $t-t_{\min}$ in kinematic factors such as in eq. (2.1).

### 2.2. Empirical and theoretical constraints

While the properties (1)–(5) listed in §2.1 already make the pole formula usefully predictive, there are further constraints on the allowed trajectories and residue functions which turn it into an indispensable phenomenological weapon of enormous predictive power. The most important of these are

† The relations for particles of "type 1" and "type 2" are superficially different only because of our use of the Jacob and Wick phase factor, $(-)^{J_2-\lambda_2}$, for particle 2 helicity states.

(1) The leading few trajectories dominate above quite moderate energies (in the region of $P_{LAB} \sim 4\,GeV/c$).
(2) Trajectories are linear in $t$.
(3) Residues are fairly structureless functions of $t$ and may be related to the appropriate coupling constants.
(4) Residues have SU(3) symmetry.
(5) Trajectories and residues obey rough exchange degeneracy relations.
(6) Residues obey other constraints such as higher symmetries, vector dominance and factorisation consistency conditions.

Some of these constraints ((2), (5) and (6)) may be regarded as purely theoretical; for example (2) is a feature of dual or quark models. Others rely more heavily on empirical observation and, since it can often be hard to isolate Regge poles from other (Regge cut) contributions to data, are difficult to verify precisely. Nevertheless we have several good reasons to believe them.

(1) *Dominance of leading trajectories*

The leading meson trajectories ($\rho$, $A_2$, $\pi$ and B nonets) are well studied. Much less is known of other possible lower-lying poles. However above some a priori unknown energy, the latter will become negligible because of the factor $\nu^\alpha$ in eq. (2.1). In practice it seems that the leading poles already dominate by $P_{LAB} \sim 4\,GeV/c$, as testified by several approximate (but general) features of the data. Most cross-sections appear to have reached their asymptotic $P_{LAB}^{-n}$ energy dependence ($P_{LAB} \sim \nu/2M$) by $4\,GeV/c$. In addition, the characteristic $t$-dependent features of differential cross-sections and polarisations in general do not change drastically above 4 GeV/$c$. Further evidence that strong low-lying poles are not required comes from the successes of duality where one extrapolates the leading poles to even lower energy, to the resonance region. For baryon exchange processes (section 4I) the situation is less clear-cut.

(2) *Linear trajectories*

The leading Regge trajectories are approximately linear ($\alpha = \alpha(0) + \alpha' t$) with a universal slope $\alpha' = 0.9\,GeV^{-2}$. In spite of its familiarity, this remains one of the most remarkable, and probably most fundamental, facts of hadron physics and is rather ill-understood. Because of its importance for Regge phenomenology we show once again the evidence for linear trajectories in figs. 2.1, 2.2. These show direct evidence (three baryons of the same parity, with spins separated by 2 on a linear trajectory), indirect evidence using exchange degeneracy (four or more particles with spins separated by 1, lying on two exchange degenerate trajectories) and evidence from the high energy scattering region ($\alpha_{eff}$ from $\pi^- p \to \pi^0 n$ data [298] and $\alpha_{eff}$ from $\pi^- p \to \eta n$ data [306] compared to the $\rho$ and $A_2$ trajectories respectively).

(3) *Residue smoothness*

Historically, Regge residues were assumed to be smooth functions of $t$ simply for economy of parameterisation. There is however some evidence to back this assumption of minimal structure compatible with other constraints due to kinematics,† factorisation, etc.

a) There is no evidence from data that the underlying Regge poles have rapidly varying or pathological residue functions for $t < 0$.

† i.e. apart from $(-t)^{|\lambda_3 - \lambda_1|/2}$ angular momentum factors, $s$-channel vertex functions are smooth functions of $t$ e.g. $e^{bt}$. Smoothness is not a precise concept and we do not claim it to be a special property of $s$-channel amplitudes rather than, say, invariant amplitudes.

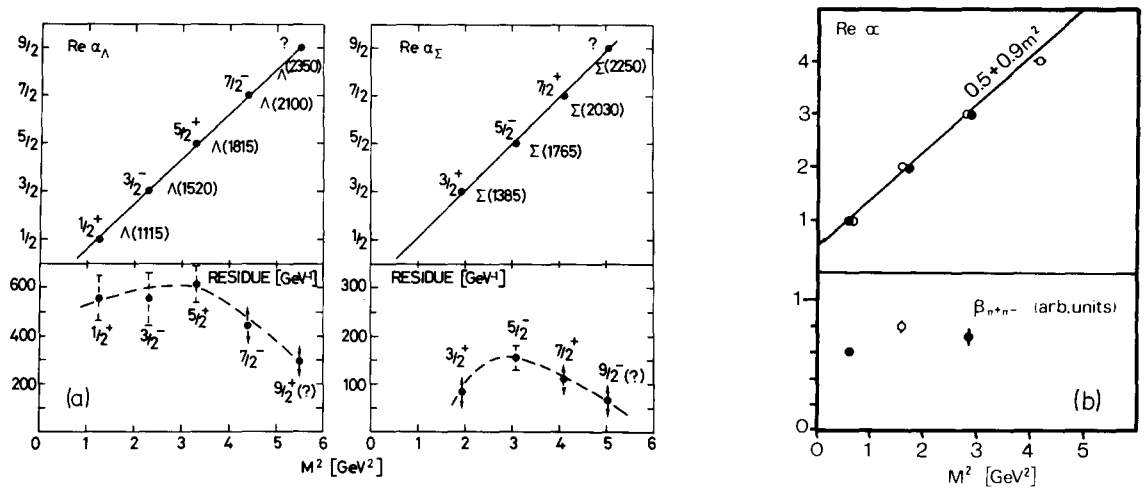


Fig. 2.1. Trajectory and residue functions plotted versus $m^2 \equiv t(>0)$. (a) for $Y^*_{0,1}$ resonances in $\bar{K}N$ (taken from [63]), (b) for mesons decaying into $2\pi$ and $3\pi$ (open and solid points are $I = 0, 1$ respectively).

b) For $t > 0$, residues are often directly measurable from resonance decay widths and coupling constants. Using exchange degeneracy (to relate Regge poles of opposite signature) one may evaluate the same residue at up to four different values of $t$ (as was done for trajectories). Examples are shown in fig. 2.1, which show no evidence for strong fluctuations in residues over a wide $t$ or $u$ range.

c) Residues interpolate smoothly between negative and positive $t$.† One can compare Regge residues in the scattering region (from model fits to data) with residues measured at the particle poles. Such extrapolations can be done, for example, for $\rho$ exchange in $\pi\pi$ scattering (using $\pi\pi$ FESR's to calculate the high energy $\rho$ exchange amplitude); $\rho$ and $\omega$ in $\pi$N, KN scattering and in $\pi$ photoproduction, and for $\pi$ exchange (not a stringent test because of the short extrapolation). Agreement is usually good for individual couplings as well as for flip/non-flip ratios, $F/D$ ratios, etc., even though the residues in the scattering region must be extracted in a model dependent way [76, 322; see also appendix A].

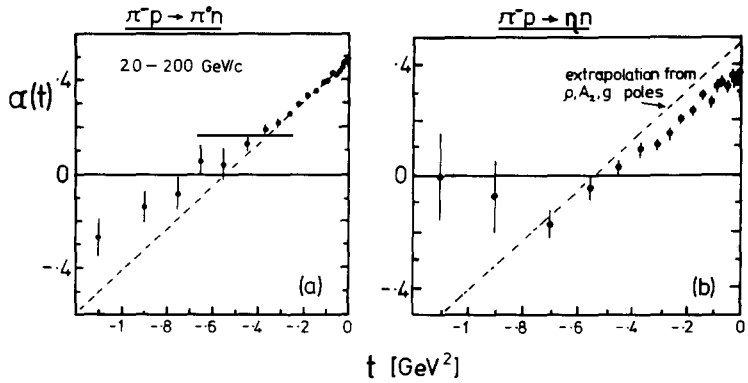


Fig. 2.2. Effective trajectories for (a) $\pi^-p \to \pi^0 n$, (b) $\pi^-p \to \eta n$ in the range 20–200 GeV/$c$ [298, 306].

† Only in the case of the $\Delta$ trajectory (section 4I) does a complicated extrapolation seem necessary.

We have stressed this mundane point of smoothness since it is an important contributor to the economy of the Regge pole formula – one of its greatest attractions.

(4) *Residues have* SU(3) *symmetry*

The phenomenological evidence will be reviewed in section 4C. Here we simply state that there are no known cases of SU(3) violation at the level of residues.

(5) *Exchange degeneracy* is the most controversial adjunct to the Regge pole formula to be introduced in this section. Its phenomenological status is far from clear and will be discussed in sections 4A and B. Here we shall merely describe the residue constraints which would hold in an ideal (?) exchange degenerate world.

These constraints derive from consideration of exotic direct channels such as $K^+p$ or $\pi^+\pi^+$, where resonances are forbidden by the quark model (and are experimentally absent). If the high energy amplitudes are to be dual (i.e. have imaginary parts which are equal in some average sense) to the real low energy amplitudes, then pairs of opposite signature Regge poles must have equal and opposite imaginary parts. This cancellation can only occur exactly if the poles have equal trajectories $\alpha(t)$ and equal residues $g_{\lambda_3\lambda_1}(t)\, g_{\lambda_4\lambda_2}(t)$. For example, to obtain a purely real amplitude in $K^+n \to K^0p$ the $\rho$ and $A_2$ poles must have equal trajectories and residues (including equal flip/non-flip coupling ratios). At $\alpha_{A_2}(t) = 0$ the $A_2$ residue must vanish (to avoid a spurious pole in the amplitude from the $(\sin \pi\alpha(t))^{-1}$ factor. An important consequence of exchange degeneracy (EXD) is therefore that the $\rho$ residue is also zero at $\alpha_\rho(t) = \alpha_{A_2}(t) = 0$, so producing a zero in the full $\rho$-exchange amplitude in $K^+n \to K^0p$. Factorisation then implies that the $\rho$ pole contribution to *any* reaction has a zero at this $t$-value.

Combined with SU(3) symmetry these constraints are very powerful and to find an algebraically consistent solution to them proved a highly non-trivial task. For meson–meson and meson–baryon scattering such a scheme exists and is in reasonable agreement with the known particles and their couplings [for reviews see refs. 74, 235].

Its predictions can be concisely stated by means of duality diagrams [59, 62]: if a process has only a non-planar $s$–$t$ duality diagram, then the $t$-channel exchanges are constrained to give a purely real high energy amplitude (just as if the direct channel were exotic). A typical example is $K^-p \to \omega\Lambda$ shown in fig. 2.3. The Regge exchanges ($K^*$, $K^{**}$) and (K, $K_B$) should combine in pairs to produce a real amplitude. Note that the direct channel is *not exotic* but that the resonances ($Y_0^*$'s) must couple so that their imaginary parts cancel on average.

A very simple and convenient way to remember which amplitudes have zeroes, and where, is to use the Veneziano amplitude prescription for EXD residue functions

$$T(s,t) = \beta\Gamma(J - \alpha(t))(1 + \tau \exp\{-i\pi\alpha(t)\})(\alpha' s)^{\alpha(t)} \tag{2.6}$$

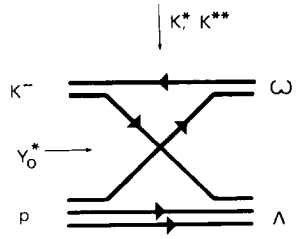


Fig. 2.3. Duality diagram for $K^-p \to \omega\Lambda$. The intermediate states in the $t$ and $s$-channels are respectively $K^*$, $K^{**}$ and $Y^*$ ($I = 0$).

where $J$ is the spin of the lowest particle of the EXD trajectory (1 for $\rho$, $A_2$, 0 for $\pi$, B) and $\beta$ is a real constant. The gamma function contains the pole propagator ($\sim 1/\sin \pi\alpha(t)$) but no zeroes. Amplitude zeroes only occur through the factor $(1+\tau \exp\{-i\pi\alpha(t)\})$. Thus EXD zeroes occur at

$$\begin{aligned} &(\rho, \omega, K^*, B, K_B \ldots) \qquad \alpha(t) = 0, -2, \ldots \\ &(A_2, f, K^{**}, \pi, K \ldots) \qquad \alpha(t) = -1, -3, \ldots \end{aligned} \tag{2.7}$$

We shall discuss, in later sections, the debatable evidence for such zeroes but, for the moment, side with the majority opinion that the zeroes are there.

(6) *Other constraints*

a) *Factorisation consistency.*

The factorised form of the Regge residue, $\beta = g_{\lambda_3\lambda_1} g_{\lambda_4\lambda_2}$ implies obvious numerical relations between pole contributions in different processes. Through analyticity, it also leads to strong consistency conditions on residue zeroes. For example, an EXD zero required in $\pi^+\pi^+ \to \pi^+\pi^+$ (see point (5)) means that the vertex $g(\rho\pi\pi)$ is at least proportional to $\sqrt{\alpha_\rho}$ near $\alpha_\rho = 0$. This implies that any other process, e.g. $\pi N \to \pi N$ has a $\rho$-exchange amplitude at least proportional to $\sqrt{\alpha_\rho}$. To avoid a possible square-root singularity in the full amplitude [27] all other $\rho$ exchange vertices, e.g. $g(\rho NN)$ must also contain such a factor. Thus a zero in $\pi^+\pi^+ \to \pi^+\pi^+$ propagates to all $\rho$-exchange amplitudes. This constraint may be used to deduce the presence of non-factorising (cut) corrections in exchange amplitudes. For example in $pp \to pp$ and $\bar{p}p \to \bar{p}p$ the "$\omega$ exchange" amplitude has a (cross-over) zero at $t = -0.15$. Were this a zero of the $\omega$ Regge pole, it would occur in all $\omega$-exchange processes. Since this is not true experimentally, we conclude that there exist other non-factorising contributions in some or all of these processes.

(b) *Higher symmetries.*

The relations between vertices which follow from $SU(6)_w$, broken through the Melosh transformation or $\ell$-breaking schemes [235] seem to work well for Regge residues. Successful examples include the relation between $\rho$ and $\pi$ pole residues in $\pi$ photoproduction [139] and in vector meson production, the $F/D$ ratios for pseudoscalar and vector couplings to nucleons, the Stodolsky Sakurai $\rho N\Delta$ coupling structure and the $g(\omega B\pi)$ helicity coupling structure in B production [see appendix A]. As in SU(3), these rough agreements could be thought of as resulting from the symmetry working at the pole together with some residue smoothness.

(c) *Vector meson dominance (VMD) and universality.*

VMD gives successful relations between Reggeon–photon and Reggeon–vector meson couplings. The strong qualitative similarities between corresponding photoproduction and vector meson production data are evidence of this [see for example section 4D]. VMD also relates the $\gamma N\bar{N}$ couplings to $\rho N\bar{N}$ and $\omega N\bar{N}$ coupling constants which in turn are related to the $\rho$ and $\omega$ Regge residues. This double extrapolation (photon → vector-meson → Reggeon) is reasonably successful (see e.g. appendix A, table 3). For instance, it relates the smallness of the nucleon isoscalar anomalous magnetic moment to the smallness of the $\omega N\bar{N}$ flip/non-flip ratio [76]. Since the photon couples universally to charges it also predicts equality of $\omega K\bar{K}$ and $\omega N\bar{N}$ residues (universality).

This completes our description of the basic Regge pole formula. To emphasize the predictive power of the approach we present in appendix A a Regge pole model applicable to most processes involving scattering of $0^-, 1^-, 1^+, \frac{1}{2}^+$ or $\frac{3}{2}^+$ particles. The model embodies all the constraints (1) to (5) and is expressed in terms of only 12 phenomenological couplings *all of which* may be theoretically estimated in advance (for

example as in paragraph (6) b,c). The success with which this crude model predicts (typically within a factor two) the cross-sections for arbitrary two-body processes is, we claim, ample proof of the usefulness of the Regge pole model as a powerfully predictive tool.

Before proceeding to more detailed aspects of the scattering data, often beyond the scope of the simple ideas so far discussed, we shall present some of the empirical evidence that the most basic Regge ideas embodied in eq. (2.1) are valid. We argue that this evidence is very strong, so strong that eq. (2.1) is essentially the only possible starting point for analysing high energy two-body quantum number exchange processes.

### 2.3. Simple Regge features of scattering data

(1) *Total cross-section data* give the most direct probe of amplitude energy dependence via the optical theorem,

$$\sigma_T(12) = \frac{1}{(2J_1+1)(2J_2+1)2p_{\mathrm{LAB}}m_2} \sum_{\lambda_1\lambda_2} \mathrm{Im}\, T_{\lambda_1\lambda_2\lambda_1\lambda_2}(\nu, 0). \tag{2.8}$$

Re $T_{\lambda_1\lambda_2\lambda_1\lambda_2}$ $(\nu, 0)$ can also be measured through Coulomb interference, thus giving a unique opportunity to test the phase and energy dependence predictions of the Regge pole model. We write the Regge pole contributions to various elastic processes symbolically

$$\begin{aligned} T(\mathrm{K}^+\mathrm{p}) &= \mathbb{P} + \mathrm{f} + \omega + \mathrm{A}_2 + \rho \\ T(\mathrm{K}^-\mathrm{p}) &= \mathbb{P} + \mathrm{f} - \omega + \mathrm{A}_2 - \rho \\ T(\mathrm{K}^0\mathrm{p}) = T(\mathrm{K}^+\mathrm{n}) &= \mathbb{P} + \mathrm{f} + \omega - \mathrm{A}_2 - \rho \\ T(\bar{\mathrm{K}}^0\mathrm{p}) = T(\mathrm{K}^-\mathrm{n}) &= \mathbb{P} + \mathrm{f} - \omega - \mathrm{A}_2 + \rho \end{aligned} \tag{2.9}$$

$$\begin{aligned} T(\pi^+\mathrm{p}) &= (x)\mathbb{P} + (2)\mathrm{f} + (2)\rho \\ T(\pi^-\mathrm{p}) &= (x)\mathbb{P} + (2)\mathrm{f} - (2)\rho \end{aligned} \tag{2.10}$$

$$\begin{aligned} T(\gamma\mathrm{p}) &= \hat{\mathbb{P}} + (2)\hat{\mathrm{f}} + \hat{\mathrm{A}}_2 \\ T(\gamma\mathrm{n}) &= \hat{\mathbb{P}} + (2)\hat{\mathrm{f}} - \hat{\mathrm{A}}_2. \end{aligned} \tag{2.11}$$

The relative minus signs arise from crossing odd signature poles and from isospin ($\mathrm{p} \to \mathrm{n}$). The factors (2) and $(x)$ are SU(3) clebsches – $x = 1$ if the Pomeron is an SU(3) singlet.

In the range 10–300 GeV total cross-sections (fig. 2.4) have a complicated energy dependence [202] which results from a rising Pomeron component added to the falling Regge pole contributions. If we isolate the odd-signature exchanges $\omega$ and $\rho$ by taking cross-section differences (e.g. $\Delta\sigma(\mathrm{KN}) = \sigma(\bar{\mathrm{K}}\mathrm{N}) - \sigma(\mathrm{KN})$) the picture is much simpler (fig. 2.5). The differences for $\pi$N, KN and NN all fit a power law energy dependence $p_{\mathrm{LAB}}^{-n}$ over the entire range.† The exponents $n$ in fig. 2.5 agree well with the energy dependence $p_{\mathrm{LAB}}^{\alpha(0)-1}$ expected from $\rho$ and $\omega$ trajectories $\alpha(t) = 0.5 + 0.9t$ passing through the particle poles. This represents a test of the most fundamental prediction of Regge poles – their energy dependence over a wide range.

Further differences isolate individual poles so allowing a test of some of the residue systematics which were outlined in §2.2. Such tests have recently been reviewed by Giacomelli [314]. In particular one may investigate the amplitude phases at $t = 0$ for each exchange. Although analyticity also demands a strict relation (see section 2.1) between energy dependence and phase [160, 198], that this be

† $\nu(t=0) = s - m_1^2 - m_2^2 = 2m_2\,(p_{\mathrm{LAB}}^2 + m_1^2)^{1/2} \approx 2m_2\,p_{\mathrm{LAB}}$.

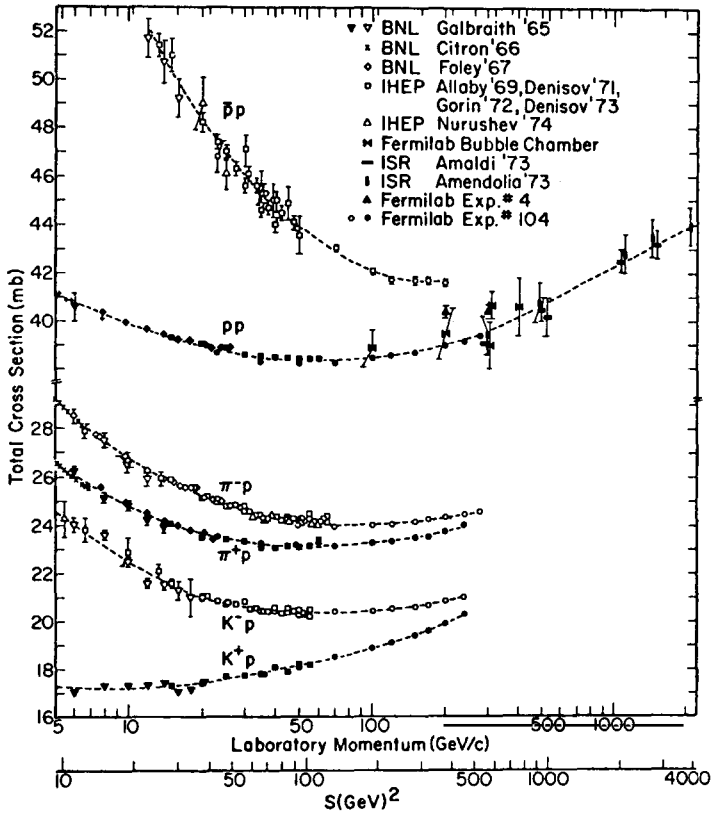


Fig. 2.4. Total cross-sections for $\pi^{\pm}$p, $K^{\pm}$p and $p^{\pm}$p scattering (taken from [314]).

satisfied already at relatively low energies may be regarded as a success of the Regge hypothesis. Figure 2.6 shows the phase in $K^0$-regeneration as a function of energy compared to the Regge prediction, using $\alpha(0) = \frac{1}{2}$.

(2) *Energy dependence of differential cross-sections*

The alpha-effective, $\alpha_{\text{eff}}(t)$, defined by*

$$d\sigma/dt \approx f(t)s^{2\alpha_{\text{eff}}(t)-2} \tag{2.12}$$

summarises the fixed $t$ energy dependence of a cross-section. As extracted from data, the $\alpha_{\text{eff}}$ can be used to make detailed tests of Regge pole (or cut) energy dependence since it should lie close to the trajectory of the dominant exchanged singularity, as a function of $t$. Some sample effective trajectories are shown in fig. 2.7.

For present purposes a somewhat cruder measure of energy dependence suffices. We parametrise the *integrated* cross-section for the process $12 \to 34$ by

$$\sigma(12 \to 34) \sim s^{2\bar{\alpha}-2}. \tag{2.13}$$

Since most reactions have a strong peripheral peak we expect the average trajectory $\bar{\alpha}$ to lie

* As is common practice, we shall use the approximation $s \approx \nu$ for applications of eq. (2.1) at high energies.

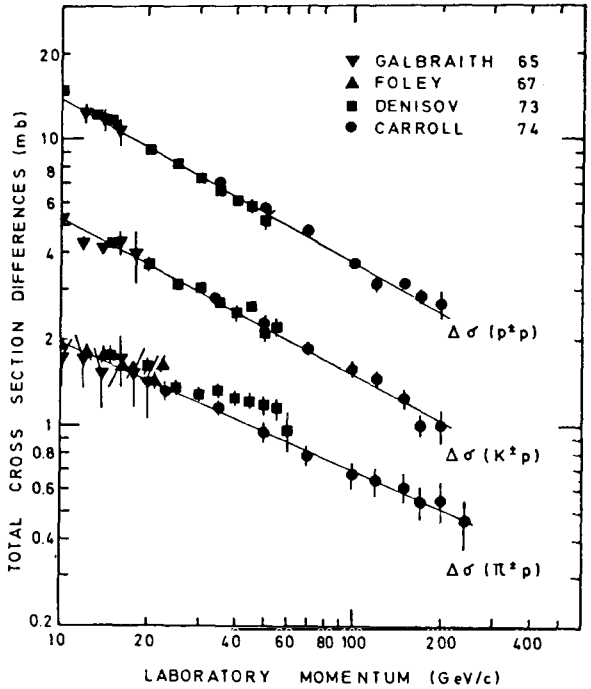


Fig. 2.5. Total cross-section differences corresponding to fig. 2.4 (taken from [314]).

somewhere between $\alpha(0)$ and $\alpha(-0.5)$ (where $\alpha(t)$ is the leading allowed $t$-channel trajectory) – probably nearer $\alpha(0)$. Figure 2.8 contains a few examples of $\sigma$ plotted against $p_{\mathrm{LAB}}$ and the corresponding values of $\bar{\alpha}$. We show a vacuum quantum number exchange process (governed by the Pomeron trajectory, $\alpha(0) \approx 1$), a charge exchange process (governed by the $\rho$ and $A_2$ trajectories, $\alpha(0) \approx \frac{1}{2}$), a hyperchange exchange process (governed by K* and K** trajectories, $\alpha(0) \approx 0.3$), a pion exchange dominated process ($\alpha(0) \approx 0$), a baryon exchange process (governed by the $N_\alpha$ trajectory, $\alpha(0) \approx -\frac{1}{2}$) and finally an exotic exchange process where no single Regge exchange is possible. In this last case the energy dependence is very steep up to around $p_{\mathrm{LAB}} \approx 5$ GeV/$c$ where a somewhat shallower fall-off sets in, perhaps caused by double Regge exchange (exotic Regge cuts).

In all cases the experimental values of $\bar{\alpha}$ correlate well with the theoretical expectations from linear

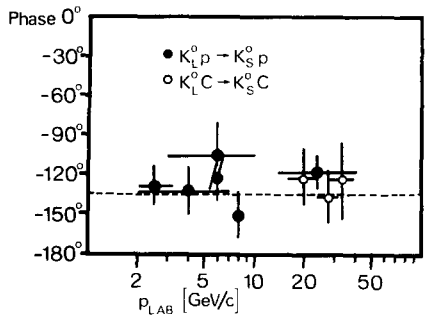


Fig. 2.6. The forward scattering amplitude phase measured in the process $K_L^0 A \to K_S^0 A$ as compared to the Regge pole prediction ($\omega, \rho$ exchange, $\alpha(0) = \frac{1}{2}$). The solid points are for A ≡ hydrogen [110] and the open ones for A ≡ carbon [244]. A trajectory intercept of $\alpha(0) \sim 0.4$ gives best overall agreement with these points ($\sim -126°$).

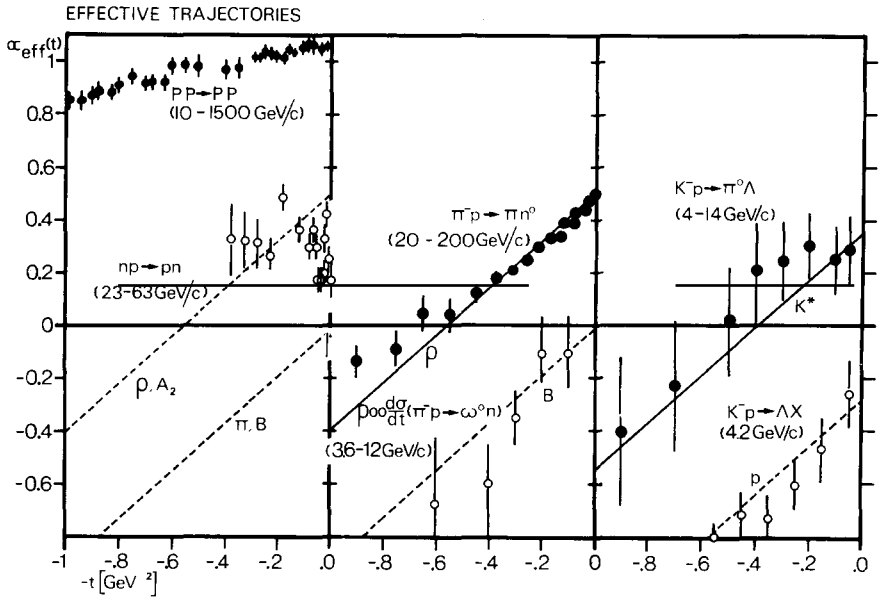


Fig. 2.7. Effective trajectories calculated from the energy dependence of various reactions. The values are from [206, 295, 298, 307, 165, 250]. The trajectory for $K^-p \to \Lambda x$ is calculated from the $m_X^2$ distribution, as described in section 4F. The straight lines are the simplest contributing trajectories (appendix A).

Regge trajectories. Note that the examples chosen all derive from only two initial ($s$-channel) states $K^{\pm}N$, so demonstrating that it is the *t-channel*, not the $s$-channel, which determines the high energy behaviour. The two processes $K^-p \to \pi^-\Sigma^+$ and $K^-p \to \pi^+\Sigma^-$ (fig. 2.8) provide the most convincing evidence of this. In the direct channel they have similar quantum numbers and in fact share the same resonances at low energy. Their $t$-channels however represent respectively, hypercharge exchange and double charge exchange. The data (fig. 2.8) confirm that they have the very different high energy behaviour predicted by the $t$-channel approach.

We stress the universality of this simple and basic Regge pole prediction; with no exceptions, the high energy behaviour of a two-body reaction is governed by the leading Regge poles as prescribed by eq. (2.13). This does not mean that they dominate the amplitudes – there could be other large contributions, whose energy dependence is somehow governed by that of the poles. We shall see that this is indeed the case, and that these extra contributions have important effects on the $t$-dependence of amplitudes. In eq. (2.13) and fig. 2.8 these effects have been hidden by integrating over $t$. Nonetheless, fig. 2.8 gives powerful evidence that Regge poles do control the behaviour of high energy amplitudes.

(3) *Systematics of dominant amplitudes*

For each leading Regge pole it is possible to estimate theoretically, by one means or another, the helicity structure of any vertex i.e. whether it is dominantly helicity-flip ($|\lambda_3 - \lambda_1| = 1$ or $|\lambda_4 - \lambda_2| = 1$) or nonflip ($|\lambda_3 - \lambda_1| = 0$ or $|\lambda_4 - \lambda_2| = 0$). Examples of such estimates for $\pi$, $\rho$ and $A_1$ exchange are summarised in table 3 of appendix A. These together with SU(3) and exchange degeneracy arguments (see also appendix A) suggest the following systematics whose validity has been attested by many varied phenomenological studies [322]. For instance

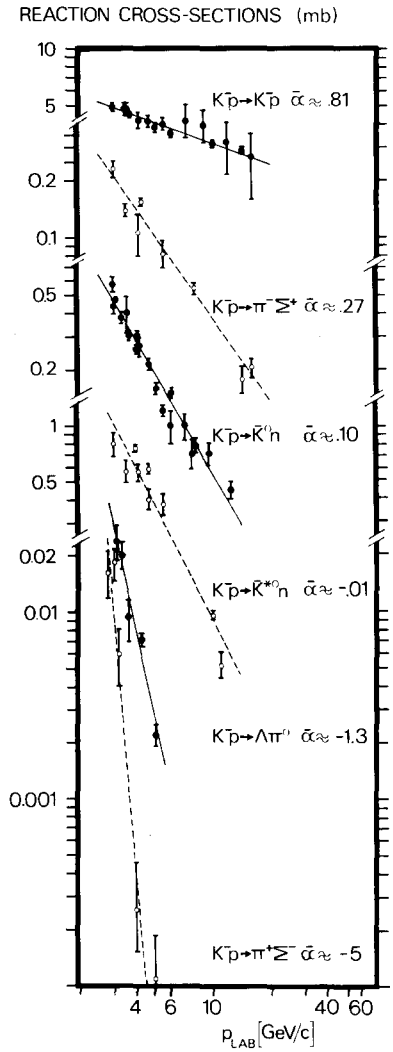


Fig. 2.8. A comparison of the momentum dependences of the reaction cross-sections for $K^-p \to cd$. In each case, an "eye-ball" fit to $p_{LAB}^{2\bar{\alpha}-2}$ is shown (together with the resulting values of $\bar{\alpha}$). The data are from [113, 188, 321, 173, 170, 212, 313, 81, 106, 320, 187]. The cross-sections for $K^-p \to \pi^+\Sigma^-$ have been crudely estimated from $d\sigma/dt$ ($t \simeq 0$) assuming an exponential distribution of slope 1 $GeV^{-2}$.

a) the couplings of $\omega$ and f trajectories to nucleons are mainly helicity-nonflip while $\rho$ and $A_2$ are mainly helicity-flip;
b) K*NΛ, K*NΣ, and the corresponding K** vertices have strong non-flip couplings;
c) the couplings of $\pi$ and B trajectories to nucleons are purely helicity-flip;
d) $\frac{1}{2}^+ \to \frac{3}{2}^+$ transitions (e.g. $p \to \Delta^{++}$) are mainly helicity-flip if mediated by vector or tensor exchange and mainly nonflip if mediated by pseudoscalar exchange;
e) the transition $0^- \to 1^-$ must be pure helicity-flip when mediated by vector or tensor exchange (because of parity, eq. (2.2)) and is mainly non-flip if due to $\pi$-exchange. $0^- \to 0^-$ transitions are trivially nonflip.

From these we can predict, for any given reaction, the net helicity-flip $n = |\lambda_3 - \lambda_1 - \lambda_4 + \lambda_2|$ of the

Table 2.1
The dominant helicity amplitude structure of various processes.

| Processes | Exchanges | Dom. exchange | Dom. amp. | | $n$ | Turnover in data |
|---|---|---|---|---|---|---|
| | | | $n_{top}$ | $n_{bottom}$ | | |
| $\pi^-p\to\pi^0n$ | $\rho$ | $\rho$ | 0 | 1 | 1 | Yes |
| $\pi^-p\to\eta n$ | $A_2$ | $A_2$ | 0 | 1 | 1 | Yes |
| $\pi^-p\to\omega^0n$ | $\rho$, B, Z | $\rho$ | 1 | 1 | 0, 2 | Yes |
| $\pi^-p\to\rho^0n$ | $\pi$, $A_2$, $A_1$ | $\pi$ | 0 | 1 | 1 | Yes |
| $\pi^-p\to\rho^0\Delta^{++}$ | $\pi$, $A_2$ | $\pi$ | 0 | 0 | 0 | No |
| $\pi^+p\to K^+\Sigma^+$ | K*, K** | K*, K** | 0 | 0 | 0 | No |
| $\gamma p\to\pi^0p$ | $\omega$, $\rho$ | $\omega$ | 1 | 0 | 1 | Yes |
| $\gamma p\to\pi^+n$ | $\pi$, $A_2$, B, $\rho$ | $\pi$ (cut) | 1 | 1 | 0, 2 | No |
| $K^+p\to K^+p$ | P, f, $\omega$, $\rho$, $A_2$ | P | 0 | 0 | 0 | No |

dominant amplitudes. An amplitude with $n\neq 0$ is forced by angular momentum conservation to vanish in the forward direction as $(-t)^{n/2}$ so that its contribution to $d\sigma/dt$ vanishes as $(-t)^n$. In any process dominated by helicity flip amplitudes, the cross-section will therefore turn over near $t=0$. Nonflip dominated processes will have no such turnover. The Regge pole predictions for dominant amplitudes can be tested by looking at shapes of $d\sigma/dt$ near $t=0$.

Table 2.1 shows some examples of this test for meson baryon forward scattering. In each case we give the dominant Regge pole, the helicity flip at each vertex $n_1$, $n_2$ and the resulting net helicity flip $n=|n_1\pm n_2|$. In all cases where the dominant net flip $n$ is unique (i.e. $x=0$, $n+x=|n_1|+|n_2|$) the measured differential cross-section confirms the pole prediction. Only in the non-unique cases (e.g. $\pi^-p\to\omega^0n$, or $\gamma p\to\pi^+n$ where $n=0, 2$ for the dominant $\pi$ exchange) can we not successfully predict forward turnovers. Pure pole exchange actually predicts forward turnovers for these processes – in disagreement with data. The resolution of this difficulty, where the turnover results from the pure pole nature of the exchange rather than straightforward angular momentum, will be discussed in section 3.

## 2.4. Summary

In this section we have tried to convey the following ideas:

a) The Regge pole formula is as simple as it could be. In spite of the technicalities of its derivation, eq. (2.1) is the simplest possible, fully general, embodiment of Regge energy dependence, $t$-channel particle poles and basic principles such as $s$–$u$ crossing and angular momentum conservation.

b) The unknowns of the formula (trajectories and residue functions) are strongly constrained, more so than is generally realised. They are limited by SU(3), empirical residue smoothness, factorisation, vector dominance, higher symmetries and exchange degeneracy.

c) Regge pole amplitudes for most conceivable two-body exchange processes can be simply calculated using a complete prescription given in appendix A. These amplitudes are not guaranteed to any specific level of accuracy but may be confidently used to predict the rough features of any process: the differential cross-section magnitude typically to within a factor of 2, its energy dependence in the range $4\to 400\,\mathrm{GeV}/c$, the helicity structure and rough $t$-dependence. For such a range of processes this is no mean achievement.

These ideas constitute the firm foundation on which modern Regge phenomenology is built, and the reason why the data present us with interesting puzzles, as opposed to impenetrable mysteries.

However the Regge pole formula does not unfailingly describe the detailed $t$-dependence of all amplitudes. To understand the dips and breaks in many cross-sections and the behaviour of polarisations we shall need additional ideas. These are the subject of the following section.

## 3. Absorption corrections

In this section we discuss the extra corrections to the Regge pole formulae needed to describe the intricacies of two-body scattering data. There is both theoretical and experimental evidence that Regge poles are often not the only relevant singularities in the $t$-channel $j$-plane. Unitarity in the $t$-channel can, for example, give rise to two-Reggeon cuts. Likewise, $s$-channel unitarity suggests that there will, in general, be corrections to the basic (Born term) Regge pole exchange. The experimental evidence for these additional exchange contributions is well-known. Some simple examples which reflect a failure of the pure Regge pole dominance hypothesis (and are independent of the further trajectory and residue constraints discussed in section 2) are:

1) If a single Regge pole ($\rho$) exchange were to dominate both helicity amplitudes, the polarisation $P$ in $\pi^-p \to \pi^0 n$ would be identically zero. Experimentally it is not [25]. Although $|P|$ is, in fact, not very large, this result was of considerable historical importance in the development of Regge cut models.

2) $P(d\sigma/dt)$ would be equal and opposite for $\pi^-p \to K^0\Lambda$ and $K^-n \to \pi^-\Lambda$ if K* and K** Regge poles alone contributed. This is because $P(d\sigma/dt)$ $(K^0\Lambda) + P(d\sigma/dt)$ $(\pi^-\Lambda)$ involves the phase difference between vector exchange helicity amplitudes, and between tensor exchange ones (no vector/tensor interferences), and should therefore be zero as in (1). This is not true experimentally [80, 55].

3) $d\sigma/dt$ for np CEX should vanish like $t$ (or faster) at $t = 0$ if only Regge poles contribute (see e.g. eq. (2.5): $(n + x)/2 \geq \frac{1}{2}$ for all amplitudes). The data show a forward spike (see §3.1, point (3)).

4) The presence or absence of dips in differential cross-sections which are dominated by the same Regge pole exchange should be correlated. This is experimentally untrue for $\pi^-p \to \pi^0 n$ and $\pi^-p \to \omega^0 n$ – the former has a dip near $t = -0.5$ but the latter has none [329].

5) As in example (4), similar dip structure is expected in the $\omega$-exchange dominated processes $K^0_L p \to K^0_S p$ and $\pi^0 p \to \rho^0 p$. In fact, the data show a dip in the latter at $t = -0.5$ but none in the former [197].

### 3.1. Systematics of corrections to Regge poles

Several areas of study have provided useful pointers to the form of the non-pole-like corrections.

(1) *Cross-over phenomena*: Im $N^{(-)}$

Imaginary parts of odd signature non-flip amplitudes (denoted by $\mathrm{Im}N^{(-)}$) in $\pi p$, Kp and pp elastic scattering may be crudely extracted from the data using the methods outlined in appendix B. $\mathrm{Im}N^{(-)}$ is essentially given by particle/anti-particle cross-section differences. Typical cross-section differences, taken from Ambats et al. [188] are plotted versus $t$ in fig. 3.1. All show a zero, corresponding to the cross-over of elastic cross-sections, at $t \approx -0.15$ in the $\pi p$ case and nearer $t = -0.2$ for Kp and pp. Data in the 6–14 GeV/$c$ range [253] and up to 150 GeV [265] show these "cross-over" zeroes to be roughly independent of energy. In Kp and pp, $\mathrm{Im}N^{(-)}$ has predominantly $\omega$-exchange quantum numbers. Factorisation would suggest that $(d\sigma/dt)(\pi^0 p \to \rho^0 p)$ should also have a dip at $t = -0.2$. In fact (see fig. 3.2) it has a maximum at $t = -0.2$ and, instead, a pronounced dip near $t = -0.5$. Thus,

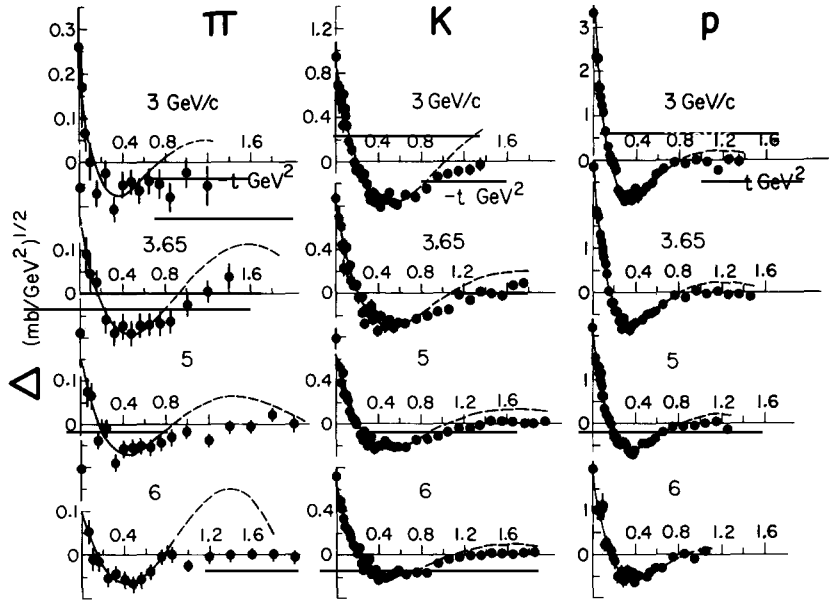


Fig. 3.1. Antiparticle-particle differential cross-section differences $\{\Delta \equiv (\sigma^- - \sigma^+)/(8(\sigma^- + \sigma^+))^{1/2}\}$ for $\pi$p, Kp and pp scattering at 6 GeV/$c$ (taken from [188]). The curves are parametric fits using a form $Ae^{Bt}J_0(b\sqrt{-t})$ suggested by the dual absorptive model [85].

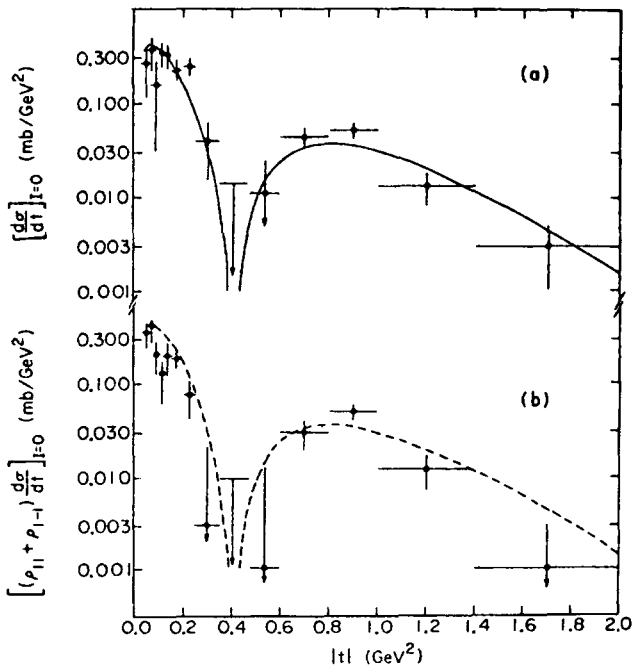


Fig. 3.2. The differential cross-section for $\pi^0 p \to \rho^0 p$ at 6 GeV/$c$. Also shown is the natural parity exchange component $(\rho_{11} + \rho_{1-1})\,d\sigma/dt$ (taken from [157]). The curves are fits based on the dual absorptive model behaviour $J_1(b\sqrt{-t})$.

$\omega$-exchange in Kp and/or in $\pi^0 p \to \rho^0 p$ has non-Regge pole contributions. Since a dip at $t = -0.5$ is what is expected for vector exchanges the most economical conclusion, made on the basis of these data alone, is that it is $\mathrm{Im}N^{(-)}$ in $\pi p$, Kp, and pp which has a non-Regge pole zero structure. This conclusion is reinforced by a comparison of $\mathrm{Re}N^{(-)}$ and $\mathrm{Im}N^{(-)}$ in $\pi N$ which we now discuss.

(2) $\pi N$ *amplitude analysis*: $\mathrm{Re}N^{(-)}$, $\mathrm{Im}F^{(-)}$, $\mathrm{Re}F^{(-)}$

The amplitude analysis which followed the work of Halzen et al. [93] gave evidence that the zero structure of the real parts of non-flip, $\mathrm{Re}N^{(-)}$, and flip, $\mathrm{Re}F^{(-)}$, as well as the imaginary part of the flip were, unlike $\mathrm{Im}N^{(-)}$, consistent with $\rho$ Regge pole behaviour (i.e. $\mathrm{Re} \sim 1 - \cos \pi\alpha(t)$, $\mathrm{Im} \sim \sin \pi\alpha(t)$ near $\alpha(t) = 0$). A summary of the components of $N^{(-)}$ and $F^{(-)}$ as deduced in various analyses may be found in fig. 12 of ref. [154]. The systematics of the corresponding tensor exchange amplitudes, $N^{(+)}$ and $F^{(+)}$, are less well known (see section 4B).

(3) $\pi$-*exchange*

In $\pi$-exchange processes such as $np \to pn$, $\gamma p \to \pi^+ n$ and $\pi^- p \to \rho^0 n$ ($\rho_{11}\, d\sigma/dt$) the $\pi$ pole flips the helicity at both vertices and therefore gives rise to two amplitudes: one with $n = 0$, $x = 2$ (see eq. (2.5)) and the other with $n = 2$, $x = 0$. Thus both vanish as $(-t)^{(n+x)/2} = -t$, although only for the double-flip ($n = 2$) is this a requirement of overall angular momentum conservation. If the $\pi$ pole† dominated, therefore, the cross-sections would vanish as $t^2/(t - \mu^2)^2$ at $t = 0$. Exactly the opposite is true experimentally. For example $d\sigma/dt$ ($np \to pn$) (shown in fig. 3.3) has a large spike [$\sim 1/(t - \mu^2)^2$] which can only be due to the $n = 0$ amplitude having a non-$\pi$ pole contribution. The nature of this contribution is best seen in $\pi^- p \to \rho^0 n$ where the individual amplitudes are well-studied phenomenologically. This is more fully discussed in section 4D. Here, we quote the result that the $n = 0$ amplitude has a slowly varying correction term of order 1 relative to the $\pi$ pole contribution $-t/(t - \mu^2)$. Furthermore, it is to a very good approximation ($\pm 10°$), 180° out of phase with the $\pi$ pole for $|t| < 0.3$.

From studies such as those outlined above one may deduce two approximate, but general, features of the non-pole corrections observed in the data.

(a) They interfere destructively with the Regge pole.

(b) They have a flatter $t$-dependence than the pole.

The result of these corrections is, in general, to sharpen the forward peak in $d\sigma/dt$. In the sense that the width of this peak reflects the range of interaction, the extra contributions are said to make the exchange amplitudes more "peripheral". The concept of peripherality has in fact played a leading role in the discussion of exchange mechanisms and we now review its important features.

### 3.2. Peripherality in impact parameter space

If high energy amplitudes are treated as functions of the final state transverse momentum $\boldsymbol{k}$ ($\boldsymbol{k}^2 = -t$), then by a two-dimensional Fourier transform they may be expressed, equivalently, as functions of a transverse displacement $\boldsymbol{b}$. Since the amplitudes have an azimuthal symmetry (the only azimuthal dependence of $T_n(s, t)$ is $e^{in\phi}$, $n$ = net helicity flip) the transform reduces to

$$T_n(s, b) = \frac{1}{8\pi \bar{q} \sqrt{s}} \int_0^\infty \sqrt{-t}\, d\sqrt{-t} J_n(b\sqrt{t}) T_n(s, t). \tag{3.1}$$

† These arguments apply equally to elementary or Regge pole $\pi$-exchange.

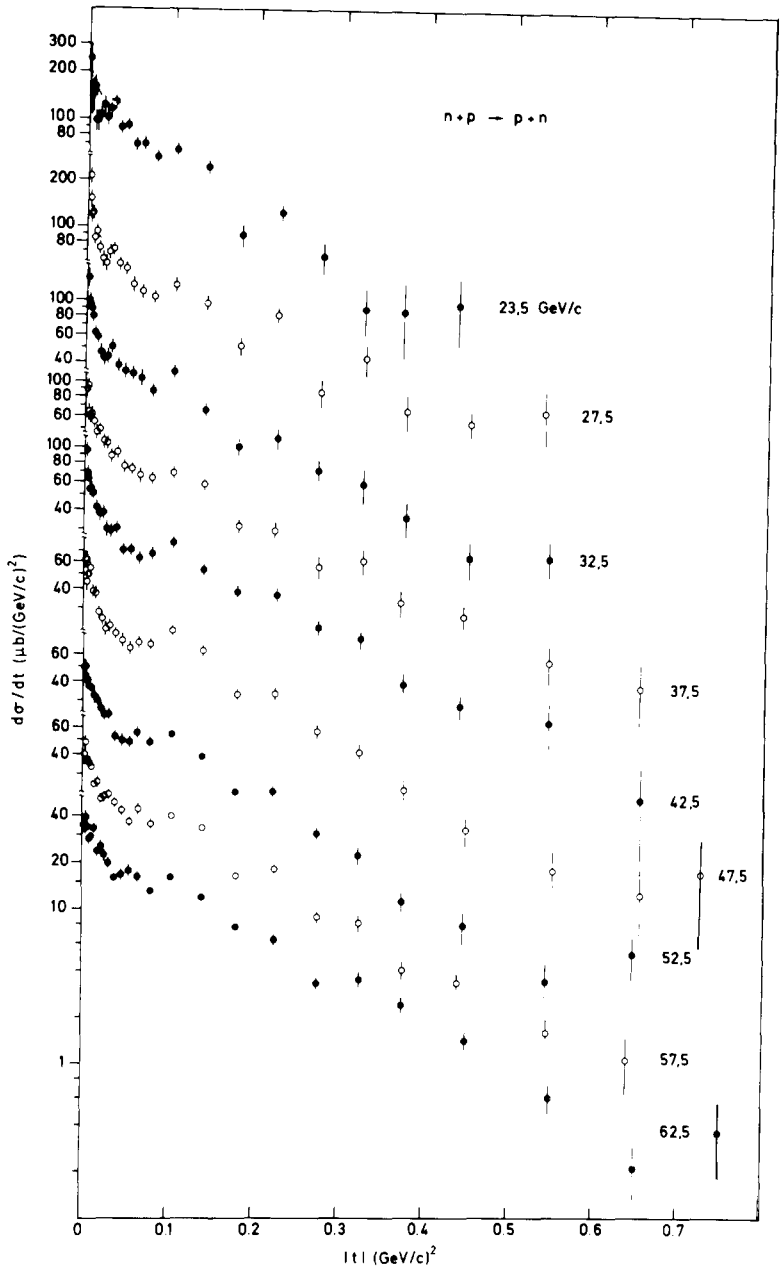


Fig. 3.3. The differential cross-section for np charge-exchange at momenta above 20 GeV/$c$ (taken from [295]).

This defines the impact parameter amplitude, which as $s \to \infty$ is equal to the corresponding partial wave amplitude:

$$T_n(s, b) \approx T_n^J(s), \qquad b \approx Jq. \tag{3.2}$$

(1) *Regge poles in impact parameter space*

For a typical Regge pole amplitude with $n = 0$, the dominant $t$ dependence is roughly exponential

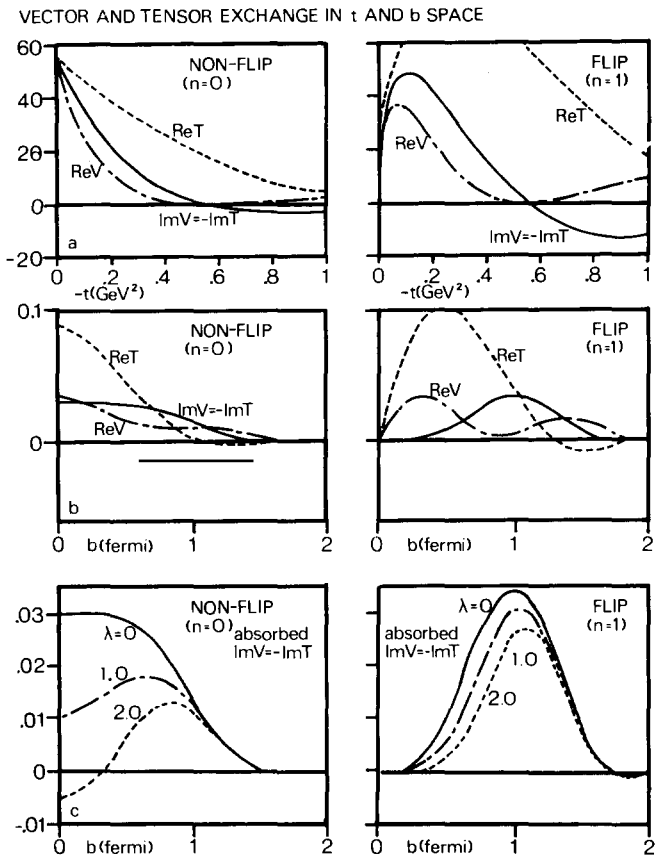


Fig. 3.4. Vector ($\rho$) and tensor ($A_2$) Regge pole exchange amplitudes for $0^-\frac{1}{2}^+$ scattering at 6 GeV/$c$: (a) the model amplitudes of appendix A plotted as a function of $t$, (b) the same amplitudes projected in $b$-space (eq. (3.1)), (c) the result of absorbing the imaginary parts (eqs. (3.4) and (3.6)) with strength $\lambda$ ($\lambda = 1$ corresponds to eq. (3.6) unenhanced). The normalisation is such that $-V = T(\pi^-p \to \pi^0 n)$ as given in appendix A.

(from $\beta(t)$ and $s^{\alpha(t)}$) i.e. $e^{At}$ so that the transform is approximately Gaussian, $\exp(-b^2/4A)$. Amplitudes with $n \neq 0$ will have $T_n(s, b) \sim b^n \exp(-b^2/4A')$.

Experimentally, it seems that non-flip amplitudes are often far from the rather structureless Gaussian form typical of a Regge pole. For example, if we transform the $\mathrm{Im}N^{(-)}$ components described in §3.1 we obtain [85, 108] amplitudes which peak at around $b = 1$ fermi ($\approx 5\ \mathrm{GeV}^{-1}$) and are zero or negative at $b = 0$. A typical result is illustrated in fig. 3.4. This property, concentration of $T_n(s, b)$ within a restricted range of $b$ (near 1 fermi), we shall refer to as "peripherality". The properties of the non flip $\pi$-exchange correction discussed in §3.1 are similar: the $\pi$ Regge pole is large at $b = 0$ while the measured amplitude is considerably depleted in this region (see e.g. fig. 8 of [271]).

For helicity-flip vector and tensor exchange amplitudes the Regge pole zero structure (§3.1) already implies a peripheral form. This is not so surprising, since the typical hadronic scale is around 1 fermi anyway and $T_1(s, b) \approx b$ at $b = 0$.

(2) *Leading resonance peripherality*

The dominant resonances found in $\pi$N phase-shift analyses appear to lie in a "peripheral" band of

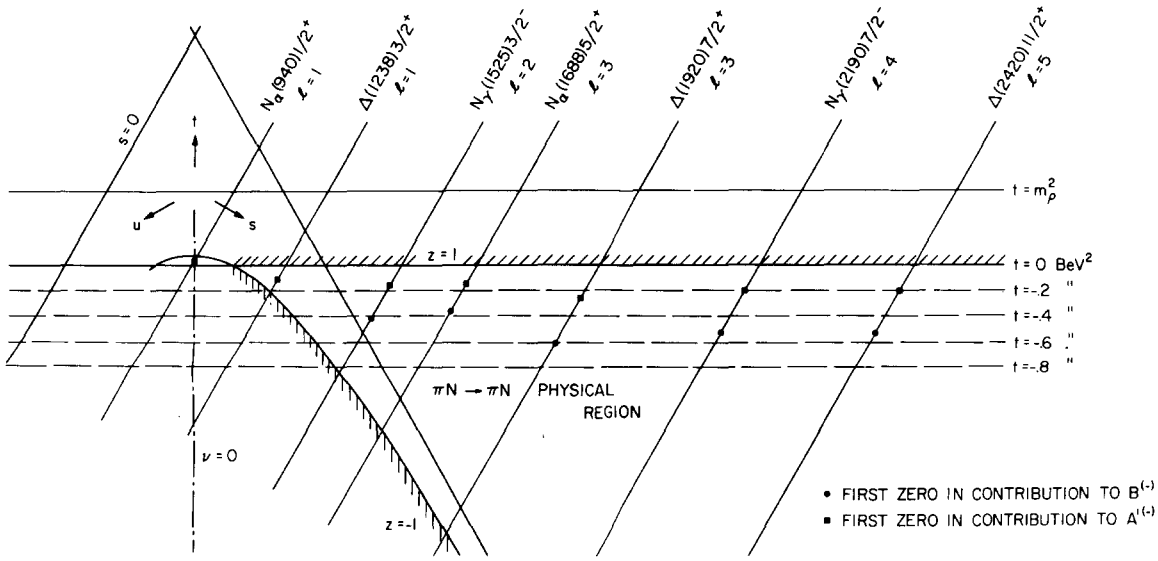


Fig. 3.5. The zeroes of the leading resonance contributions to $A'$ (asymptotically $t$-channel helicity non-flip) and $B$ (asymptotically helicity flip) $\pi$N amplitudes, in the Mandelstam plot. The zeroes all occur near $t \simeq -0.2$ and $t \simeq -0.5$ respectively (figure from [42]).

angular momenta, $J \sim qb_0$ where $b_0 \sim 1$ fermi [42, 95]. It follows that their Legendre zeroes (those of $d^J_{\lambda\mu}(\theta_s)$ in the partial wave sum) tend to lie along lines of fixed $t$, for a given helicity amplitude (fig. 3.5). This is most readily appreciated by considering eq. (3.2) and using the small angle approximation

$$d^J_{\lambda\mu}(\theta_s) \sim J_n(b\sqrt{-t}). \tag{3.3}$$

Zeroes of $d^J_{\lambda\mu}(\theta_s)$ occur at fixed $b\sqrt{-t}$ which for peripheral resonances ($b \approx b_0$) means fixed $t$.

If, by duality, these resonances build up the imaginary parts of high energy amplitudes then the latter will have a peripheral peak in impact parameter and therefore a peripheral zero structure, i.e. zeroes† at $t = -0.2$ in non-flip and $t = -0.6$ in flip amplitudes. The peripherality of dominant resonances seems to be only approximately true in KN scattering, however. The combination dual to $\omega$-exchange is peripheral, but those dual to $A_2$ exchange are apparently not (see section 4B). This last remark is also consistent with the fact that in $\pi N \to \eta N$ there are many non-peripheral (relatively low spin) resonances which couple strongly. Were peripherality a general feature of resonances, this approach to high energy phenomenology [95] would be a powerful one.

A complementary discussion of duality and its applications is contained in section 4H.

### 3.3. *The absorption model*

Amplitude peripherality can be understood in terms of absorption [7, 11]. The most attractive feature of the absorption model is that it relates a phenomenological fact (the peripherality of some exchange amplitudes) to a theoretical fact – the necessity of $j$-plane cuts [9] in a clear and intuitive way.

There are several heuristic derivations of the absorption model [for instance 71] which bring out its physical basis but which, as we shall see, are not adequate for calculating detailed effects. They are

† $J_0(x)$ and $J_1(x)$ have their first zeroes at $x \approx 2.4$ and 3.8 respectively. For $b_0 = 1$ fermi this corresponds to $t = -0.2$ and $-0.6$.

based on the fact that the particles taking part in, say, a charge-exchange reaction, being hadrons, may undergo some strong interaction before or after the basic charge-exchange process. At high energies the most probable initial or final-state interaction is elastic or diffractive scattering (Pomeron exchange), while the basic charge-exchange process is taken to be single Regge pole exchange. Thus the full charge-exchange is the sum of the diagrams shown in fig. 3.6. This picture may be related to the distorted-wave Born approximation of nuclear physics [e.g. 19] where initial and final state wave functions are distorted by the strong interactions. Alternatively it can be derived in an eikonal formalism [30] where the eikonal $\chi$ is a sum of single Reggeon or Pomeron exchange amplitudes. The expansion of the full amplitude $S = e^{i\chi} = 1 + i\chi - \frac{1}{2}\chi^2 \ldots$ produces the multiple scattering diagrams of fig. 3.7. This derivation indicates that the absorptive corrections have something to do with $s$-channel unitarity [71] although the resulting amplitude cannot be said to incorporate full multiparticle unitarity in a realistic way.

In essence, therefore, Regge pole exchange is identified as a single scattering process, and absorption effects represent the multiple scattering corrections. However, problems arise in the practical calculation of these diagrams, the most important of which concerns the intermediate states to be included. In diagrams such as in fig. 3.6 it is obviously wrong to include only elastic intermediate states ($a' = a$, $b' = b$); $a'$ and $b'$ could be any states produced diffractively from the initial state ab. How should one sum over the diffractive states? Does the sum converge at high masses? Should it be truncated at fixed $m_a$ and $m_b$? The "intuitive" derivations of absorption effects are not able to answer these questions. There is another derivation, through the $j$-plane unitarity equations and the Reggeon calculus, which is, in a sense, more rigorous and, at least in principle, allows one to treat the (divergent) sum over diffractive states. Even in this approach there are great practical problems (e.g. what is the helicity and $t$-dependent structure of diffractive amplitudes?) which have so far prevented realistic calculations. We shall discuss the Reggeon calculus in section 4G but for the moment we adopt a more historical approach; first calculating the elastic rescattering diagrams, showing how they give rise to peripherality and then discussing some more or less phenomenologically motivated improvements.

The elastic rescattering corrections in $\pi^- p \to \pi^0 n$ are given by the 4 second order diagrams in fig. 3.6 (the last two must be included to retain $s$–$u$ crossing symmetry). The full amplitude $T_{\text{full}}$ is calculated as the partial wave Regge pole amplitude $T_{\text{pole}}$ multiplied by the partial wave $S$-matrix $S_{\text{el}}$ for elastic scattering (assumed to be identical for $\pi^- p$, $\pi^0 p$, $\pi^+ n$ and $\pi^0 n$ at high energies). We approximate partial-wave amplitudes by impact parameter amplitudes and obtain

$$\begin{aligned} T_{\text{full}} &= T_{\text{pole}}(s, b) S_{\text{el}}(s, b) \\ &= T_{\text{pole}}(s, b) + i T_{\text{pole}}(s, b) T_{\text{el}}(s, b) \end{aligned} \tag{3.4}$$

which is the original Regge pole amplitude plus an absorptive correction $T_{\text{abs}}(s, b) = i\, T_{\text{pole}}(s, b) \cdot T_{\text{el}}(s, b)$. A matrix multiplication over helicities is implied, but we shall assume that the elastic amplitude conserves helicity [70] so that $T_{\text{el}}(s, b)$ is diagonal in helicity. This means absorptive corrections in one helicity amplitude do not depend on pole contributions from another.

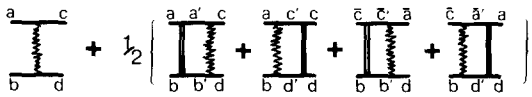


Fig. 3.6. Single and double exchange diagrams which occur in the simplest absorption models. The wavy and double lines represent Reggeon and Pomeron respectively.

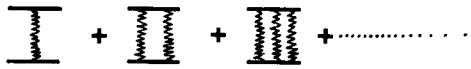

Fig. 3.7. Multiple Regge exchange diagrams which occur in eikonal models.

The simplest first approximation for $T_{el}(s,t)$ which reproduces a constant total cross-section $\sigma_T$ and exponential forward peak ($d\sigma/dt \sim e^{At}$) is,

$$T_{el}(s,t) = 2iq\sqrt{s}\sigma_T e^{At/2} \tag{3.5}$$

giving

$$T_{el}(s,b) = \frac{i\sigma_T}{4\pi A} e^{-b^2/2A} \tag{3.6}$$

where, for $\pi$N elastic scattering, $A \approx 8\,\text{GeV}^{-2}$, $\sigma \approx 23\,\text{mb} \approx 59\,\text{GeV}^{-2}$. Thus the absorption factor in eq. (3.4) is

$$S_{el}(s,b) \approx [1 - 0.6\, e^{-(b/4)^2}] \tag{3.7}$$

so that the central partial waves of the pole amplitude (near $b \approx 0$) are attenuated by a factor 0.4, but in the peripheral waves ($b \approx 1\,\text{fm} \approx 5\,\text{GeV}^{-2}$) the attenuation is negligible (by $\sim 0.9$). This is the origin of peripherality: the rescattering corrections have little effect on peripheral partial waves but are strongly destructive (absorptive) at small impact parameters.

As an example of the amplitude structure in $s$ and $t$, consider approximating a Regge pole amplitude as e.g.

$$T_{pole}(s,t) = \tfrac{1}{2}\beta\, e^{\lambda t}\, i e^{-i\pi\alpha(t)/2}(s/s_0)^{\alpha(t)} \equiv \gamma\, e^{Bt/2} \tag{3.8}$$

where

$$\gamma = \tfrac{1}{2}\beta\, i(e^{-i\pi/2}s/s_0)^{\alpha(0)}, \qquad B = 2\{\lambda + \alpha'(\log(s/s_0) - i\pi/2)\}$$

so that

$$T_{pole}(s,b) = \frac{\gamma/B}{8\pi q\sqrt{s}} e^{-b^2/2B} \tag{3.9}$$

i.e. a Gaussian distribution in $b$-space. From eqs. (3.4), (3.8) and (3.9) and the inverse transform of eq. (3.1):

$$T_n(s,t) = 8\pi q\sqrt{s}\int_0^\infty b\, db J_n(b\sqrt{-t}) T_n(s,b), \tag{3.10}$$

we find

$$T(s,t) = T_{pole}(s,t) + T_{abs}(s,t) = \gamma\, e^{Bt/2} - \gamma\, e^{Bt/2}\left\{\frac{\sigma_T}{4\pi(A+B)} \exp\left(-\frac{B^2 t}{2(A+B)}\right)\right\}. \tag{3.11}$$

It is clear that $T_{abs}(s,t)$ has the rough phenomenological features described in §3.1, i.e. it destructively interferes with $T_{pole}(s,t)$ near $t = 0$ ($T_{abs}/T_{pole} \approx -30\%$) and has a flatter slope in $t$ (half the harmonic mean of the elastic and Regge exchange slopes).

Now consider the $j$-plane structure of $T_{abs}(s,t)$. If $T_{el}(s,t)$ is approximated, more generally, by a Pomeron pole of trajectory slope $\alpha'_P$, $T_{abs}(s,t)$ is given by eq. (3.11) with the replacement $A \to a + 2\alpha'_P \cdot (\log(s/s_0) - i\pi/2)$ where $\alpha_P(t) = 1 + \alpha'_P t$. We see from eq. (3.11) that $T_{abs}(s,t)$ has non-pole-like shrinkage (due to the log $s$ factors in $A$ and $B$). Its $j$-plane structure is most easily seen when expressed as a two-dimensional convolution over transverse momenta

$$T_{abs}(s,\boldsymbol{k}) = \frac{i}{16\pi^2 q\sqrt{s}} \int d^2\boldsymbol{k}_1 T_{pole}(s,\boldsymbol{k}_1) T_{el}(s,\boldsymbol{k}-\boldsymbol{k}_1). \tag{3.12}$$

It is easy to show that this expression is entirely equivalent to the prescription implied by eqs. (3.4), (3.10) and (3.1) which arose more naturally from the point of view of absorption. Thus, the integral over $b$ of the product of two integrals over $\sqrt{-t}$ (each expressible as a Fourier transform with respect to $\boldsymbol{k}$, taking due account of azimuthal dependences) can be written in the form of eq. (3.12) using the Fourier transform convolution theorem.

Since $T_{pole}$ and $T_{el}$ have the behaviour $s^{\alpha(t)}$ and $s^{\alpha_P(t)}$ respectively, the contribution to a particular $\boldsymbol{k}_1$ has $s$ dependence $s^\gamma = s^{\alpha(-\boldsymbol{k}_1^2)+\alpha_P(-(\boldsymbol{k}-\boldsymbol{k}_1)^2)-1}$. Integrating over $\boldsymbol{k}_1$ gives a continuous range of powers $\gamma$ i.e. the form of the contribution of a $j$-plane cut. At fixed $t$ $(= -\boldsymbol{k}^2)$, the branch point is found by maximising $\gamma(\boldsymbol{k}_1^2, t)$. At large $s$, $\gamma_{max}(t)$ coincides with

$$\alpha_c(t) = \alpha(0) + \alpha_P(0) - 1 + \frac{\alpha'\alpha'_P}{\alpha' + \alpha'_P} t \tag{3.13}$$

as deduced from the limit of eq. (3.11)

$$T_{abs}(s,t) \sim (s/s_0)^{\alpha_c(t)} [\log(s/s_0)]^{-1}. \tag{3.14}$$

In particular, if $\alpha'_P = 0$, as was used in eq. (3.5), then $T_{abs}$ behaves like a fixed cut since $\gamma(t) = \alpha_c(t) = \alpha(0)$.

It is important to note that this type of absorptive correction does not spoil the "global" successes of the Regge pole scheme outlined in section 2. The reader may easily satisfy himself that the gross energy dependence of amplitudes, the systematics of dominant helicity amplitudes and SU(3)/EXD predictions for total cross-sections are largely unaffected by absorbing Regge poles.

### 3.4. *Specific absorption models*

Equations (3.4) and (3.5) give rise to an impact parameter profile which, for example, for $\mathrm{Im}N^{(-)}(s,b)$ is not as peripheral as observed (§3.1). The strength of absorption at $b = 0$ is determined by $(T_{pole} - T)/T_{pole}$. This ratio is around 1.2 for the data (e.g. [108]) but only 0.6 in the present over-simplified treatment. Before choosing a method for resolving this difficulty we should note that, if as we have tacitly assumed vector Regge poles do have NWSZ, then the impact parameter distribution is not exactly Gaussian (as in eq. (3.9)) but a little broader. One is therefore nearer to a peripheral bump at $b = 1$ fermi when the input pole has a zero (the precise degree of absorption at $b = 0$ is not too important†). Thus, the actual amount of absorption required to explain the data depends on whether the basic Regge pole amplitudes have NWSZ or not. The historical nomenclature "weak" and "strong" absorption model for these two approaches is readily understood.

† This is because the contribution from $b = 0$ to the integral for $T_{abs}(s,t)$ is small.

(1) *Strong absorption models*

Henyey et al. [46] proposed a single economical solution to the twin problems of (a) insufficient absorption strength (a phenomenological problem) and (b) how to account for inelastic diffractive intermediate states (a theoretical one). They postulated that these intermediate states give approximately the same effect as the elastic ones and so serve only to reinforce the elastic contribution. The absorptive amplitude $T_{\text{abs}}(s, t)$ (eq. (3.11)) was therefore multiplied by a phenomenological factor $\lambda$ (a real constant) which could be different for different amplitudes but was typically of order 2.0.

The effects of this paper were far-reaching. First, the importance of $s$-channel helicity was strongly emphasized by demonstrating how the various helicity amplitudes behaved in different yet characteristic ways when absorbed. A systematic study of $s$-channel helicity amplitude structure resulted. Previously most phenomenology used $t$-channel helicity or invariant amplitudes which have good analytic properties but can be horrendously complicated to use. Second, the introduction of "$\lambda$ factors" focussed attention on the central question – what is the origin of absorption and what determines its strength in various situations? Subsequently, there has been much work on absorption strength systematics [see for instance sections 4A,F,G]. Third, they questioned the existence of NWSZ in pole amplitudes (zeroes in the full amplitude could result from pole/cut interference) and stirred up a lively, but unresolved controversy [97, 98, 100].

Many of the successes of the Strong-Cut Reggeised Absorption Model (SCRAM) have been summarised by Ross et al. [78]. In particular SCRAM can accommodate the strong absorptive effects in $\pi$-exchange processes such as $\gamma p \to \pi^+ n$ and $np \to pn$. There is a useful mnemonic for the amplitudes of SCRAM [78], which are peripheral in $b$-space. One can think of the $b$-space maximum at $b_0 \approx 1$ fermi as a smeared delta-function $\delta(b - b_0)$. This gives a $t$-dependence $J_n(b_0\sqrt{-t})$ for an amplitude of net helicity flip $n$. In particular, non-flip and single flip helicity amplitudes have zeroes at $-t \approx 0.2$ and 0.6 respectively.

(2) *Weak absorption models*

Cohen-Tannoudji et al. [33] and Arnold et al. [37] assumed the existence of NWSZ (from EXD constraints on the basic Regge poles) and used the absorption strength dictated by the elastic $S$-matrix only. The phenomenological success of such models was in part due to their highly constrained and, therefore, predictive nature [144].

The limitations of these "first-generation" strong and weak absorption models soon became apparent and prompted detailed studies of amplitude structure systematics [100] some of which have been summarised in §3.1. A major defect of the SCRAM type models in (1) is that the predominantly imaginary $T_{\text{el}}(s, t)$ (eq. (3.5)) means that $\text{Re}\,T_{\text{pole}}(s, t)$ gets absorbed as strongly as does $\text{Im}\,T_{\text{pole}}(s, t)$ so implying, for example, that $\text{Re}N^{(-)}$ is also peripheral. Experimentally it is not (§3.1). The greatest problems for weak absorption models were that they could not account for the very strong absorptive effects in $\pi$-exchange (§3.1) processes (independent of NWSZ arguments) and that the absorption in, for example, $\text{Im}N^{(-)}$ was not strong enough while that in $\text{Re}N^{(-)}$ was a shade too strong. A second generation of absorption models was developed to cope with these and other difficulties.

(3) *Fancy Pomeron strong absorption models*

Kane and others [158, 319] have shown how one can alter eq. (3.5) so that it represents a Pomeron exchange amplitude which has a sizeable real part at $t \neq 0$, yet which is phenomenologically not too unreasonable (cf. high energy diffractive scattering data). In this way one can arrange to absorb

$\mathrm{Im}N^{(-)}$ much more strongly than $\mathrm{Re}N^{(-)}$, have non-peripheral tensor exchange amplitudes and still retain most of the desirable features of SCRAM.

(4) *Phase-modified weak absorption models*

Ringland et al. [134] and Sadoulet [177] have given ad hoc prescriptions for modifying the absorption phase for vector and tensor exchange to give phenomenologically valid results. Girardi et al. [125] gave a theoretical prescription (based on the dual model) for including secondary cuts (Reggeon–Pomeron–Reggeon) which gave the desired vector and tensor exchange systematics. As at the first generation level ((1) and (2)), the weak absorption approach is considerably more predictive but still cannot account for the very strong ($\lambda_{\mathrm{scram}} = 2.5$ or 3) absorption necessary for $\pi$ exchange.

In fig. 3.8 we compare the description of the $\rho$ and $A_2$ exchange amplitudes of KN CEX scattering afforded by two representative models of types (3) and (4). Fig. 3.4 gives the prediction of the naive Regge model of appendix A. The absorption model components are rather similar (at least for $\rho$-exchange) but this is hardly surprising since both models were constructed with the known amplitude systematics in mind.

### 3.5. Phenomenological status of absorptive models

After a decade's experience with Reggeised absorption models, none of which has proved overwhelmingly superior, several features have been established.

There is evidence of absorption in many two-body amplitudes. It is apparently greatest for zero net helicity flip and in the imaginary parts of vector exchange amplitudes – one can modify the absorbing amplitude "$T_{\mathrm{el}}(s, t)$" in a non-unique way to accommodate this within an absorption model framework. Apart from the case of peripheral scattering, the systematics of absorption strength as a

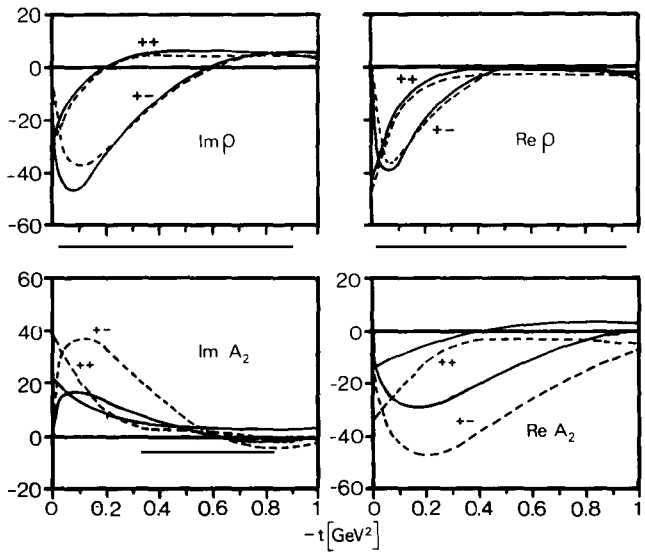


Fig. 3.8. Model amplitudes for $\rho$ and $A_2$ exchange in KN CEX scattering at 6 GeV/$c$. The $s$-channel helicity amplitudes $T_{\frac{1}{2}\frac{1}{2}}$ and $T_{\frac{1}{2}-\frac{1}{2}}$ are labelled "+ +" and "+ −" respectively. The full and dashed curves correspond to the strong and weak absorption models of refs. [319] and [214] respectively. The normalisation is such that $\rho + A_2 = T(K^+n \to K^0p)$ and $d\sigma/dt$ is given by eq. (AA.1) (the amplitudes of fig. 3.4 differ by the factor $-\sqrt{2}$).

function of helicity are not clearly established or understood. Peripherality itself seems to be a fairly general, but not completely universal, aspect of two-body scattering. The energy dependence properties of absorptive corrections seem to vary from process to process. There is a considerable amount of evidence [102, 184, 176] for absorption corrections which have shrinkage more characteristic of Regge poles than of the usual absorption models, (1)–(4). This and other related theoretical points are discussed in section 4G.

We have dwelt little on specific absorption model fits to data. Instead we have taken the view that Regge cut phenomenology has been something of a storm in a tea-cup – from the multitude of analyses performed only a few, albeit important, features have survived (see the previous paragraph and §3.1). Only in a few situations where the amplitudes are well-studied, have the various specific models been stringently tested. In fact, most current models have been specifically modified to pass these tests and one should not therefore be surprised if at a future date the models are found to give incorrect predictions. The main lessons to be learnt come not from the models themselves but from the systematic study of exchange amplitudes to which they have focussed our attention. It is the basic ideas on absorption, gained in this way, which are of most value to the phenomenologist.

### 4A. Are helicity-flip amplitudes Regge pole-dominated?

It has often been suggested [72, 100, 96] that absorption (or other) corrections to helicity flip Regge pole amplitudes are small and may usually be neglected.† Were this true in general, it would constitute a great simplification in the phenomenology of most processes – for instance, by facilitating amplitude analyses and by determining overall phases. We now examine the evidence for and against this hypothesis. Most of the evidence in favour comes from the eight helicity-flip dominated CEX processes $\pi N \to \pi(N, \Delta)$, $\pi N \to \eta(N, \Delta)$, $KN \to K(N, \Delta)$, $\bar{K}N \to \bar{K}(N, \Delta)$.

*4A.1. Evidence for* (we highlight the specific Regge property being tested, in brackets)

F1. *Shrinkage of* $d\sigma/dt$ (energy dependence)

The differential cross-sections of all eight CEX processes shrink with an $\alpha_{\text{eff}}$ (section 2) which is roughly consistent with linear $\rho$ or $A_2$ Regge pole trajectories. In the case of $\pi^- p \to \pi^0 n$ and of $\pi^- p \to \eta n$, in the range $5 < P_{LAB} < 200\,\text{GeV}/c$, this is particularly dramatic (fig. 2.2) although the $A_2$ trajectory slope is a little flat. In strong absorption models [158, 319] $\alpha_{\text{eff}}(t)$ for $\pi^- p \to \pi^0 n$ is expected to have structure at $-t \sim 0.55$ reflecting a move of the dip position with energy (at large $t$, the cut has a slower energy dependence than the pole). Since the data do not show this feature, the simpler explanation in terms of a pure Regge pole (with NWSZ) is hard to resist. (See also the discussion of energy dependence in section 4H.) Nonetheless, one should remember that there are also non-flip dominated processes (e.g. $\pi^+ p \to K^+ \Sigma^+$ and $K_L^0 p \to K_S^0 p$) which are definitely not pure pole dominated but which show strong shrinkage.

F2. $\pi N$ *amplitude analysis (phase)*

The (model independent) amplitude analyses of $\pi N$ scattering [93, 128] show the phase of the helicity flip $I = 1$ amplitude to be in good agreement with that of a $\rho$ Regge pole exchange

† In the absorption model, helicity flip cuts are naturally suppressed, since the absorption correction occurs mainly at small $b$ where the pole amplitude is already small (vanishes at $b = 0$, kinematically). Here we are discussing a further suppression beyond this kinematic one.

$(\sim i \exp\{-i\pi\alpha(t)/2\})$ for $-t \lesssim 0.6$. In addition, both real and imaginary parts have zeros at $t \simeq -0.5$ – the possibility of a *double* zero in the real part is not resolved (insufficient data beyond $t = -0.6$).

F3. *Elastic polarisations (NWSZ)*

If we assume that elastic non-flip amplitudes are to a good approximation pure imaginary (Pomeron dominated) then elastic polarisations measure the real parts of helicity flip amplitudes (see appendix B). For Kp and $\pi$p scattering these agree remarkably well with Regge pole expectations [100]. For pp, $\bar{p}$p and np, similar agreement can only be achieved if a helicity-flip Pomeron is allowed for [273]. The $\pi^+$p and $\pi^-$p polarisation are mirror-symmetric (fig. 4A.1) showing the dominance of $\rho$ exchange over f exchange in the helicity-flip amplitude, and have a double zero at $t = -0.5$, as expected from a $\rho$ pole amplitude (with NWSZ). In interpreting such evidence, one should bear in mind that a pure imaginary non-flip amplitude has been assumed. However, for $\pi$N, amplitude analyses and FESR phase determination indicate that this is a reasonable approximation.

F4. *Dips in* $d\sigma/dt$ *(NWSZ)*

The dips in $\pi^-p \to \pi^0 n$ [22] and $\pi^+p \to \pi^0\Delta^{++}$ [195] at $t \simeq -0.5$ ($\alpha_\rho = 0$) and in $\pi^-p \to \eta n$ [92, 328] and $\pi^+p \to \eta\Delta^{++}$ [195] at $t \simeq -1.4$ ($\alpha_{A_2} = -1$?) are shown in fig. 4A.2. While dips at $t = -0.6$ also emerge naturally from pole/cut interference in strong absorption models, the structure of the $\eta$ production cross-section has so far defied a similar explanation [319]. Two caveats are in order. Since these are *dips* rather than zeroes (there are non-flip amplitudes also contributing), these cross-section data do not provide a strong upper bound on the correction terms present. In addition, it seems that $\alpha_{\text{eff}}^{A_2}$ (fig. 2.2) will not in fact pass through $-1$ at $t \simeq -1.4$, as required by the Regge interpretation.

F5. *$\rho$-exchange FESR (NWSZ and phase)*

All FESR for helicity-flip $\rho$ exchange amplitudes (in $\pi^-p \to \pi^0 n$ [42], $\pi^+p \to \pi^0\Delta^{++}$ [312], KN CEX [217], and $\gamma N \to \pi N$ [139]), show a zero at $-t = 0.5$. The FESR results for other odd-signature helicity flip amplitudes show that the imaginary parts of K* exchange in $\pi N \to K\Lambda$ [211, 289] and of $\omega$ exchange in $\gamma p \to \pi^0 p$ ($E_\gamma > 3$ GeV) [194] also have zeroes near $t = -0.5$ but that the real part of $\omega$ exchange does not have the expected double zero (see remark A1 below).

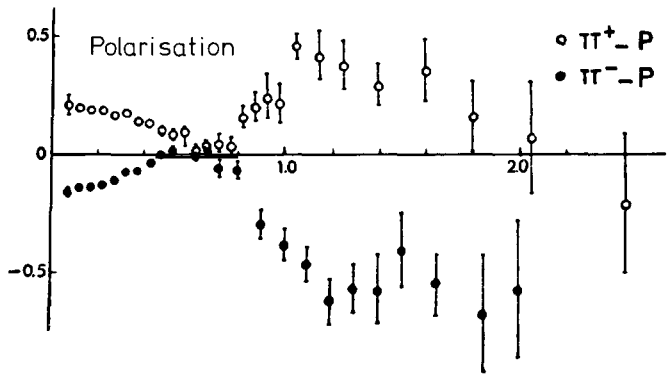


Fig. 4A.1. The polarisation in $\pi^\pm$p elastic scattering at 6 GeV/$c$ (from [68]).

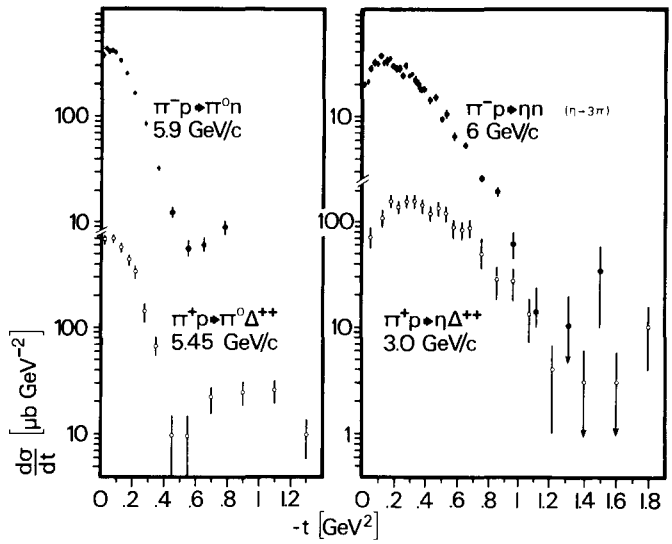


Fig. 4A.2. The differential cross-sections for $\pi^-p \to \pi^0 n$ [22], $\pi^+p \to \pi^0\Delta^{++}$ [195], $\pi^-p \to \eta n$ [328] and $\pi^+p \to \eta\Delta^{++}$ [92], showing a dip at $t = -0.55$ for $\rho$ exchange and a possible dip at $t \simeq -1.2$ for $A_2$ exchange.

F6. *$\pi$-exchange in $\pi^-p \to \rho^0 n$* (energy dependence and phase)

The quantity $\rho_{00}\, d\sigma/dt$ for $\pi^-p \to \rho^0 n$ is dominated by the helicity flip amplitude $P^0_{+-}$ (section 4D) and evidence that it shrinks like a normal Regge pole has been presented [119]. More crucially, in analogy with the polarisation in $\pi^-p \to \pi^0 n$, one can experimentally measure the phase difference between the flip and non-flip amplitudes $P^0_{+-}$ and $P^-_{+-}$ [see appendix B]. They are found to be almost exactly in phase for $0.1 \leqslant -t \leqslant 0.3$ (§4D.1). This lends a measure of support to the assertion that $P^0_{+-}$ is dominated by a $\pi$ Regge pole. However, as discussed in §4D.1, the interpretation of this amplitude is not completely straightforward.

### *4A.2. Evidence against*

A1. *$\pi^0$ photoproduction shrinkage* (energy dependence)

The $\alpha_{\text{eff}}$ for $d\sigma/dt$ ($\gamma p \to \pi^0 p$) [297] is plotted in fig. 4A.3. Also shown is the trajectory of the $\omega$ Regge pole which is expected to dominate this process (in a helicity-flip amplitude). The $\alpha_{\text{eff}}(t)$ is much more reminiscent of a pole + strong cut $\alpha_{\text{eff}}$ (see point F1, above) than of a simple Regge pole. The feature, $\alpha_{\text{eff}}(t) \simeq 0$ for $|t| \geqslant 0.6$, is common to most photoproduction cross-sections.

A2. *$\pi^0$ photoproduction FESR* (phase, NWSZ)

The cross-section for $\gamma p \to \pi^0 p$ looks very similar to that for $\pi^-p \to \pi^0 n$ – forward turnover, dip at $t = -0.5$ and dominated by an odd-signature, helicity flip natural parity exchange. This analogy extends to the imaginary parts of the dominant amplitude (point F5). For the real parts it breaks down, since FESR and fixed-$t$ dispersion relations (FTDR) [194] show that $\gamma p \to \pi^0 p$ has a single zero at $t = -0.2$ rather than a double one at $t = -0.5$. The lack of a full *amplitude* zero at $t = -0.5$ can be most directly seen in the polarised target asymmetry which is linearly proportional to the single flip $\omega$ exchange amplitude yet has a *maximum* at $t = -0.5$ (fig. 4A.4).

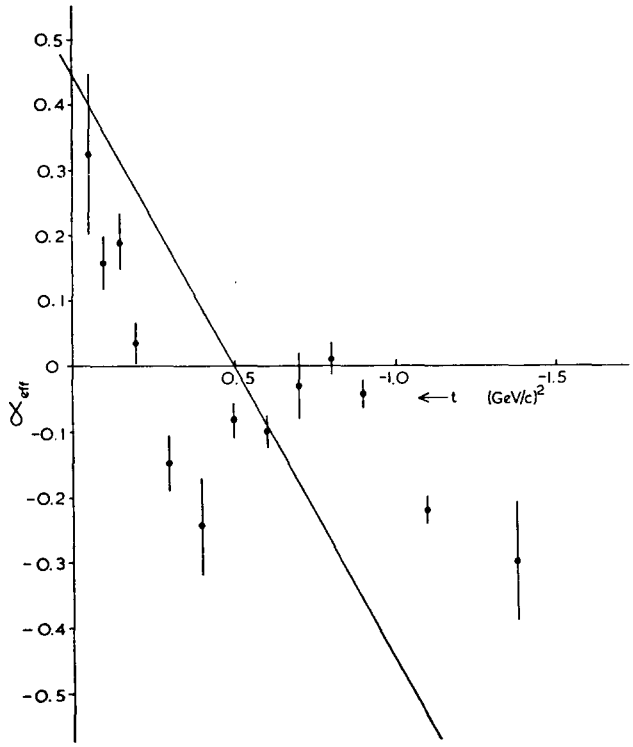


Fig. 4A.3. The effective trajectory for $d\sigma/dt$ ($\gamma p \to \pi^0 p$) is compared with a linear $\omega$ Regge pole trajectory (taken from [297]).

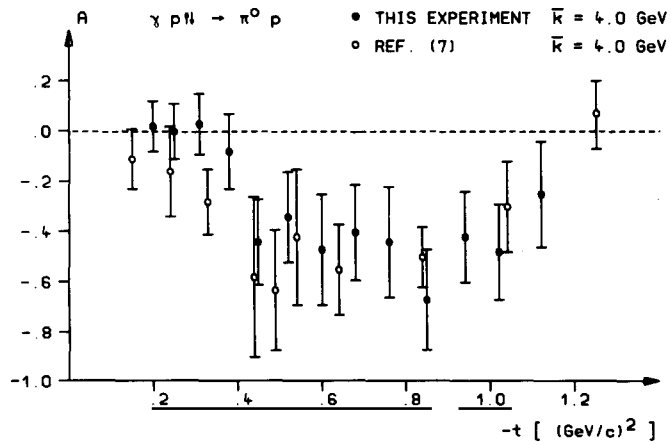


Fig. 4A.4. The polarised target asymmetry $A$ for $\gamma p \to \pi^0 p$ at 4 GeV/$c$ (taken from [146]).

A3. *t-dependence of line-reversal symmetry violation* (NWSZ)

The three pairs of helicity-flip dominated, processes $K^+p \to K^0n/K^-p \to \bar{K}^0n$, $K^+p \to K^0\Delta^{++}/K^-n \to \bar{K}^0\Delta^-$ and $K^-p \to \pi^+\Sigma^-(1358)/\pi^+p \to K^+\Sigma^+(1358)$ are known to violate the line-reversal symmetry expected for EXD Regge poles (see section 4B), the first ("real") cross-section being larger than the second ("rotating"). The cross-section *difference* for a given pair must be largely due to the flip amplitudes. If the latter are Regge pole dominated, this difference, being linear in the vector exchange, is expected to vanish at $\alpha_v(t) = 0$. For $KN \to KN$ and $KN \to K\Delta$ in the 4 to 6 GeV/$c$ region the difference is small near $t = -0.5$ [212, 326] but is not actually zero for KN [216]. For $\Sigma^+(1385)$ production at 10 GeV/$c$ the normalised difference $(\sigma_1 - \sigma_2)/(\sigma_1 + \sigma_2) \simeq (33 \pm 11)\%$ almost independent of $-t(\leq 0.3)$ [249]. It shows no sign of vanishing at $\alpha_{K^*}(t) = 0$, i.e. $t \simeq -0.4$, contrary to our Regge pole hypothesis.

A4. *$\pi$ exchange in $\pi^-p \to f^0n$* (factorisation)

In $\pi^-p \to f^0n$, one of the amplitudes has double helicity flip at the meson vertex, and single flip at the nucleon vertex giving a net single helicity flip. The $\pi$ pole contribution must therefore vanish as $(-t)^{3/2}$ although angular momentum conservation only requires $(-t)^{1/2}$. This amplitude may be extracted from data using rather weak assumptions [278] and has a behaviour compatible with $(-t)^{1/2}$ but not with $(-t)^{3/2}$. It is, in fact, consistent with the Williams absorption prescription (appendix A) which absorbs the extra evasive factor of the pole exchange ($\sim -t$), but leaves the helicity flip piece ($\sqrt{-t}$) unaffected. Here, then, is an example of a helicity-flip amplitude which can be shown to be absorbed. However, it is an amplitude which is rather different (evasive) from the ones to which the present systematics are usually applied (c.f. F1–F6, A1–A3).

Surveying the evidence for pole-dominated helicity-flip amplitudes, we see that little of it is unambiguous. In particular, tests of phases and zeroes at fixed $s$ are only compelling on aesthetic grounds, since recent absorption models have been constructed to *look like* Regge poles in those amplitudes listed in F2–F5. Energy dependence is the only truly unambiguous test of a Regge pole, and here the evidence is against absorption in $\pi^-p \to \pi^0n$. It seems churlish to describe this helicity-flip amplitude, which has the phase, zero structure, factorisation and shrinkage properties of a Regge pole, as being anything other than Regge pole dominated.

On the other hand, the evidence against pole domination in $\gamma p \to \pi^0 p$ is clear cut. The only remark which could be made in defence of pole dominance is that perhaps photoproduction processes are different (cf. $\alpha_{\text{eff}} \simeq 0$ for $-t \geq 0.6$ in all pseudoscalar photoproduction) [260]. In fact, it has recently been claimed [294] that the measured phase difference between $\gamma p \to \pi^0 p$ and its analogous hadronic process $\rho^0 p \to \pi^0 p$ is such that the latter is consistent with ($\omega$) Regge pole behaviour when compared with estimates of the phase in the photoproduction processes (A2).

The only safe conclusion is that many helicity-flip amplitudes appear to be Regge pole dominated although there is definite evidence that some are not.

## 4B. Line-reversal symmetry in charge and hypercharge exchange reactions

The simple $0^{-\frac{1}{2}^+}$ charge and hypercharge exchange (CEX, HYCEX) processes have always occupied a central position in Regge phenomenology, particularly as a testing ground for exchange degeneracy (EXD) and SU(3) symmetry. Table 4B.1 gives the SU(3) relations among them. If the $\rho$

Table 4B.1
SU(3) relations between various CEX and HYCEX processes of the form $0^{-\frac{1}{2}^+} \to 0^{-\frac{1}{2}^+}$.

| Process | SU(3) exchanges | Remarks, and further SU(3) relations |
|---|---|---|
| $\pi^-p \to \pi^0 n$ | $\sqrt{2}\rho$ | $x \equiv \cos\theta - s_T \sin\theta = 1.18$[a] |
| $\pi^-p \to \eta n$ | $x\sqrt{2/3}\,A_2$ | $x' \equiv \sin\theta + s_T \cos\theta = 0.90$ |
| $\pi^-p \to \eta' n$ | $x'\sqrt{2/3}\,A_2$ | |
| $K^+p \to K^0p$ | $\rho + A_2$ | |
| $K^-p \to \bar{K}^0 n$ | $\rho + A_2$ | |
| $K^-p \to \pi^0\Lambda$ | $\frac{1}{\sqrt{2}}(K_\Lambda^* + K_\Lambda^{**})$ | $K_\Lambda^*/\rho = \frac{\lambda}{\sqrt{6}} \frac{3(F/D)+1}{(F/D)+1}$[b] |
| $\pi^-p \to K^0\Lambda$ | $K_\Lambda^* - K_\Lambda^{**}$ | |
| $K^-p \to \pi^-\Sigma^+$ | $K_\Sigma^* + K_\Sigma^{**}$ | $K_\Sigma^*/K_\Lambda^* = \sqrt{6} \frac{(F/D)-1}{3(F/D)+1}$[b] |
| $\pi^+p \to K^+\Sigma^+$ | $-K_\Sigma^* + K_\Sigma^{**}$ | |
| $K^-p \to \eta\Lambda$ | $\frac{3\cos\theta}{\sqrt{6}}(K_\Lambda^* + yK_\Lambda^{**})$ | $y \equiv -\frac{1}{3}(1 + 2s_T \tan\theta) = -0.20$[a] |
| $K^-p \to \eta'\Lambda$ | $\frac{3\sin\theta}{\sqrt{6}}(K_\Lambda^* + y'K_\Lambda^{**})$ | $y' \equiv -\frac{1}{3}(1 - 2s_T \cot\theta) = -4.33$ |

[a] Mixing parameters as discussed in §4C.2.
[b] $\lambda$ is any SU(3) mass-breaking parameter. One choice is [131] $\lambda^{-1} = \{-i\alpha' s\}^{\Delta\alpha}$, $\Delta\alpha \simeq 0.2$.

and $A_2$ Regge pole are parametrised as

$$\rho = \beta_\rho(1 - e^{-i\pi\alpha_\rho})(s/s_0)^{\alpha_\rho} \tag{4B.1}$$

$$A_2 = \beta_{A_2}(1 + e^{-i\pi\alpha_{A_2}})(s/s_0)^{\alpha_A}, \tag{4B.2}$$

then the EXD prediction, $(\alpha_\rho, \beta_\rho) = (\alpha_{A_2}, \beta_{A_2})$, for the KN CEX processes $K^+n \to K^0p$ and $K^-p \to \bar{K}^0n$ gives

$$T(K^0p) = 2\beta(s/s_0)^\alpha \tag{4B.3}$$

$$T(\bar{K}^0n) = -2\beta(s/s_0)^\alpha \cdot e^{-i\pi\alpha}. \tag{4B.4}$$

For obvious reasons, eqs. (4B.3) and (4B.4) are often referred to as "real" and "rotating" (phase) processes. The EXD amplitude structure of the HYCEX line-reversal-related processes (table 4B.1) would be similar.

If eqs. (4B.3,4) are valid for helicity-flip and non-flip amplitudes, then there should be zero polarisation in KN CEX and in the four analogous HYCEX processes. This is certainly not the case in $K^-p \to \bar{K}^0n$ [145] or in the HYCEX reactions, so that at least one amplitude (flip or non-flip) violates EXD. A further consequence of eqs. (4B.3,4) is that cross-sections of pairs of line-reversal related processes should be equal. Historically, this proved difficult to test, because of experimental normalisation uncertainties, but at one stage [73, 69] it seemed that KN CEX was line-reversal symmetric (EXD $\rho$ and $A_2$) while HYCEX was not. Because the former are dominated by helicity flip amplitudes and the latter by non-flip amplitudes, this gave rise to the suggestion [72, 96] that helicity

flip amplitudes are dominated by EXD Regge poles (see also section 4A), while non-flip amplitudes have significant absorptive corrections and hence show EXD violation. Since then, a considerable amount of accurate data on these and related processes has clarified the issue. Bearing in mind the possibility that helicity-flip amplitudes are pole-dominated (section 4A), it is convenient to discuss separately the EXD systematics for helicity flip and non-flip amplitudes.

### *4B.1. Helicity structure of CEX and HYCEX amplitudes*

We define the helicity flip/non-flip amplitude ratio as

$$R = \frac{2m_N}{\sqrt{-t}} \cdot \left. \frac{T_{1/2-1/2}}{T_{N21/2}} \right|_{t=0} . \tag{4B.5}$$

For $\rho$ and $\omega$ couplings to nucleons, this may be estimated from vector meson dominance of nucleon form-factors and gives $R_N^\rho \simeq G_M^V/G_E^V \simeq 4.7$ and $R_N^\omega \simeq G_M^S/G_E^S \simeq 0.9$ [76], i.e. $\rho$ exchange processes are expected to be dominantly helicity-flip. Phenomenologically, $R_N^\rho \simeq 8$ (appendix A). From table 4B.1, using $F/D = -3$ and 0.4 for non-flip and flip respectively (appendix A)†, it follows that $R_\Lambda^{K^*} \sim 3.1$ and $R_\Sigma^{K^*} \sim -1.7$. Furthermore, EXD implies that $R^{\text{tensor}} = R^{\text{vector}}$ ($F/D^{\text{vector}} = F/D^{\text{tensor}}$) so that, while all $0^{-}\frac{1}{2}^{+}$ CEX reactions are expected to be helicity-flip dominated, the $0^{-}\frac{1}{2}^{+}$ HYCEX ones (table 4B.1) should have important non-flip components. Experimentally, the forward dips and forward peaks in the respective processes confirm this.

In $0^{-}\frac{3}{2}^{+}$ CEX and HYCEX production (table 4B.2), the quark model [section 4C] predicts the dominance of the helicity flip amplitudes $H_{3/2\,1/2}$ and $H_{1/2-1/2}$. This is well borne out experimentally ($R_\Delta^\rho \geq 15$).*

Because of the above spin systematics, it is clear that information on helicity-flip amplitudes is best drawn from $0^{-}\frac{1}{2}^{+}$ CEX and $0^{-}\frac{3}{2}^{+}$ HYCEX, while non-flip amplitudes are best studied in $0^{-}\frac{1}{2}^{+}$ HYCEX.

### *4B.2. EXD in helicity-flip amplitudes*

Violations of line-reversal symmetry may be conveniently characterised by the quantity

$$\widetilde{\cos}\,\phi_{VT} \equiv \frac{d\sigma/dt(\text{real}) - d\sigma/dt(\text{rot.})}{d\sigma/dt(\text{real}) + d\sigma/dt(\text{rot.})} = \frac{2|V/T|\cos\phi_{VT}}{1+|V/T|^2} \approx \cos\phi_{VT} \tag{4B.6}$$

if one amplitude is dominant. The latter approximation is useful for $|t| \leq 0.2$ where $|V/T|$ is of order unity. In this $t$ region, the average values of $\cos\phi_{VT}$ are as given in table 4B.3. It is immediately apparent that the common assumption, that flip amplitudes are EXD, is violated in KN and K$\Delta$ CEX and also in $\Sigma(1385)$ production. Particularly noteworthy is that the violation ("real" > "rotating") is *greater* in K$\Delta$ than in KN, although the former is the more dominated by helicity-flip amplitudes. The differential cross-sections for KN and K$\Delta$ CEX at 4 and 6 GeV/$c$ are shown in fig. 4B.1.

FESR studies indicate that the $\rho$ exchange amplitudes in KN scattering are the same as those in $\pi$N scattering (up to a real, $t$-independent, SU(3) Clebsch–Gordon coefficient) [215]. Using the $\rho$-exchange amplitude of Barger and Phillips [52], which is known to reproduce $\pi$N amplitude analyses [93] Elvekjaer and Johnson [215] have decomposed the KN and $\eta$N cross-section and polarisation data to yield the $A_2$ exchange components. The amplitudes at 4 GeV/$c$ are shown in fig. 4B.2. A comparison

† SU(6) predicts $-\infty$ and 1/3 respectively.

* $R_\Delta$ ($=\{R_{1/2-1/2}^2 + R_{3/2\,1/2}^2\}^{1/2}$) may be deduced from the $\Delta$ density matrix elements, in particular $\rho_{33}$ [164].

Table 4B.2
SU(3) relations between various CEX and HYCEX processes of the form $0^{-}\frac{1}{2}^{+} \to 0^{-}\frac{3}{2}^{+}$.

| Process | SU(3) exchanges | Remarks and further SU(3) relations |
|---|---|---|
| $\pi^+p \to \pi^0\Delta^{++}$ | $\sqrt{2}\,\hat{\rho}$ | |
| $\pi^+p \to \eta\Delta^{++}$ | $x\sqrt{2/3}\,\hat{A}_2$[a] | |
| $K^+p \to K^0\Delta^{++}$ | $\hat{\rho} + \hat{A}_2$ | |
| $K^-n \to \bar{K}^0\Delta^-$ | $-\hat{\rho} + \hat{A}_2$ | |
| $K^-p \to \pi^-\Sigma^+(1385)$ | $\hat{K}^* + \hat{K}^{**}$ | $\hat{K}^*/\hat{\rho} = -\lambda/\sqrt{3}$[b] |
| $\pi^+p \to K^+\Sigma^+(1385)$ | $-\hat{K}^* + \hat{K}^{**}$ | |

[a,b] See footnote to table 4B.1.

of the $\alpha_{\text{eff}}$ for $A_2$ exchange in $\pi^-p \to \eta n$ [§4A.1] with that deduced from the phase of the helicity-flip amplitude in fig. 4B.2 ($\sim\exp\{-i\pi\alpha_{\text{eff}}(t)/2\}$) reveals a remarkable similarity. This, together with the observation that $\alpha_\rho(0) - \alpha_{A_2}(0) \sim 0.1$, leads one to consider non-degenerate Regge pole trajectories as a mechanism for the EXD violation in KN CEX [215]. One would expect this mechanism to be even more directly applicable to KΔ CEX with its high proportion of flip amplitudes. The large value of $\widetilde{\cos}\,\phi_{VT}$ in KΔ (0.29 near $t = 0$) would, however, require a much larger trajectory splitting. This simple and attractive mechanism is therefore untenable.

Further evidence on helicity-flip vector/tensor exchange has come from FESR analyses which show that, at least in the region not too far above the cut-off ($p_{\text{LAB}} \sim 1.5\,\text{GeV}/c$), the $\rho$, $A_2$ [217] and $K^*$, $K^{**}$ [211, 289] amplitudes are more than 90° out of phase with the EXD prediction. However, a subsequent analysis of KN scattering by Groom and Martin [267] using the same FESR together with fixed-$t$ dispersion relations (FTDR) to incorporate high energy experimental information, does show the expected EXD sign between $\rho$ and $A_2$ flip amplitudes in the 4–6 GeV/$c$ range. This analysis of $\rho$ and $A_2$ exchange amplitudes in KN provides an independent cross-check of the assumption of

Table 4B.3
$\widetilde{\cos}\,\phi_{VT}$ (eq. (4B.6)), a measure of line-reversal symmetry violation, for various CEX and HYCEX processes. Data are taken from [212, 326, 248, 249, 165].

| Dominant amplitude | Process | $\widetilde{\cos}\,\phi_{VT}\vert_{t=0}$ | $\langle\widetilde{\cos}\,\Phi_{VT}\rangle_{\vert t\vert<0.2}$ | $p_{\text{LAB}}$ GeV/$c$ |
|---|---|---|---|---|
| helicity flip | KN CEX | — | $0.15 \pm 0.05$ | 4 |
| | | | $0.14 \pm 0.08$ | 6 |
| | KΔ CEX | — | $0.29 \pm 0.06$ | 4 |
| | | | $0.27 \pm 0.06$ | 6 |
| | $\bar{K}N \to \pi\Sigma^*$, $\pi N \to K\Sigma^*$ | — | $0.32 \pm 0.07$ | 10.1 |
| helicity non-flip | $\bar{K}N \to \pi\Lambda$, $\pi N \to K\Lambda$ | $0.10 \pm 0.02$ | $0.25 \pm 0.03$ | 4 |
| | $\bar{K}N \to \pi\Sigma$ | $0.06 \pm 0.03$ | $0.16 \pm 0.02$ | 4 |
| | $\pi N \to K\Sigma$ | $0.024 \pm 0.023$ | $0.14 \pm 0.02$ | 10.1 |

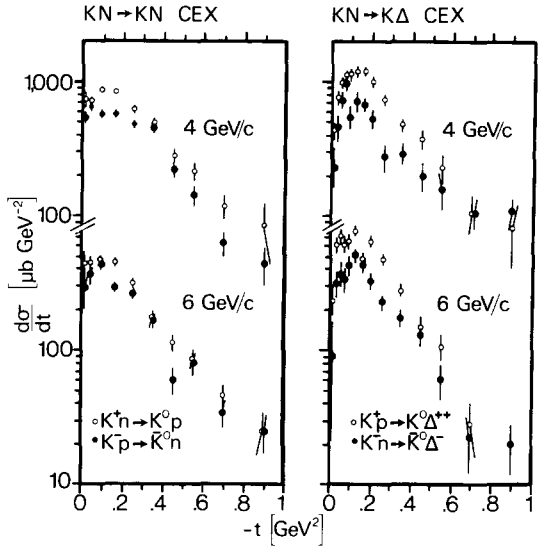


Fig. 4B.1. The differential cross-sections for KN→KN CEX [212] and KN→KΔ CEX [326] at 4 and 6 GeV/$c$.

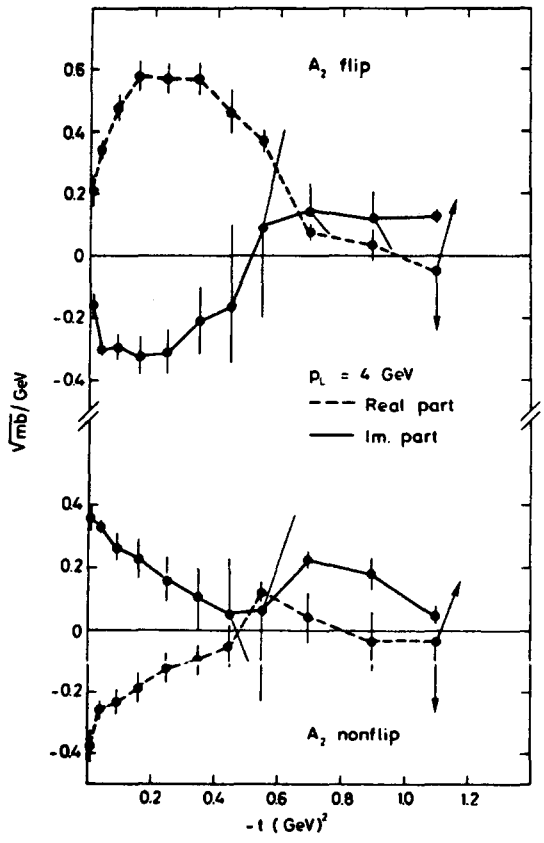


Fig. 4B.2. Helicity flip and non-flip $A_2$ exchange amplitudes from a model-dependence analysis of KN scattering at 4 GeV/$c$ [215]. The line segments joining the points are merely to guide the eye.

Elvekjaer et al. [215] that the $\rho$ amplitudes in $\pi$N and KN satisfy SU(3), and yields $A_2$ exchange amplitudes roughly consistent with theirs. It also underlines the care with which one must interpret high energy predictions obtained from FESR. This point is discussed further in section 4H.

We conclude this section by noting the currently established features of helicity flip amplitudes near 5 GeV/$c$.

(1) The real and imaginary parts of $\rho$ exchange are consistent with the Regge pole behaviour $1-\exp\{-i\pi\alpha_\rho(t)\}$ where $\alpha_\rho(t) \sim 0.5 + 0.9t$ [section 4A].

(2) The phase of $A_2$ exchange in KN CEX is roughly consistent with the Regge phase $\exp\{-i\pi\alpha_{A_2}(t)/2\}$ where $\alpha_{A_2}(t)$ is the observed $\alpha_{\text{eff}}$ of $\pi^- p \to \eta n$.

(3) The EXD prediction $\text{Im}A_2 = -\text{Im}\rho$ is satisfied within errors; there is, however, some EXD violation in the real parts [216].

(4) The EXD violation is typically 15% in the KN CEX cross-section (table 4B.3) but much larger (30%) in the flip dominated $0^-\frac{3}{2}^+$ processes proving that the violation mechanism does not factorise. In particular, it cannot be simply ascribed to $\alpha_\rho(t) - \alpha_{A_2}(t) \neq 0$.

### *4B.3. EXD for non-flip amplitudes*

The evidence against EXD in non-flip amplitudes has always been strong [e.g. 73]. However, the common assumption that line-reversal symmetry is much more seriously violated in HYCEX than in CEX due to the stronger non-flip amplitudes in the former, has been called into question by the recent 10.1 GeV/$c$ data of Berglund et al. [248, 249]. Particular care has been taken to obtain accurate relative normalisation of the differential cross-sections (shown in fig. 4B.3). Averaged for $|t| < 0.2$, $\widetilde{\cos}\,\phi_{VT}$ is only $0.14 \pm 0.02$ for the non-flip dominated $0^-\frac{1}{2}^+$ HYCEX processes, but $0.32 \pm 0.07$ for the analogous flip dominated $0^-\frac{3}{2}^+$ processes. In fact, in the $0^-\frac{1}{2}^+$ case, $\widetilde{\cos}\,\phi_{VT}$ decreases strongly with decreasing $|t|$ ($0.024 \pm 0.023$ at $t = 0$) suggesting that the helicity-flip amplitude could be largely responsible for EXD violation in the $0^-\frac{1}{2}^+$ HYCEX cross sections for $t < 0.2$. Detailed amplitude analysis (§4B.4) is necessary to investigate further this possibility. The $0^-\frac{1}{2}^+$ HYCEX data in the $4 \to 6$ GeV/$c$ range is bedevilled by normalisation uncertainties, but data interpolations [165] show the same $t$-dependence of $\widetilde{\cos}\,\phi_{VT}$ with a mean value ($|t| < 0.2$) not significantly different from KN CEX (table 4B.3). For

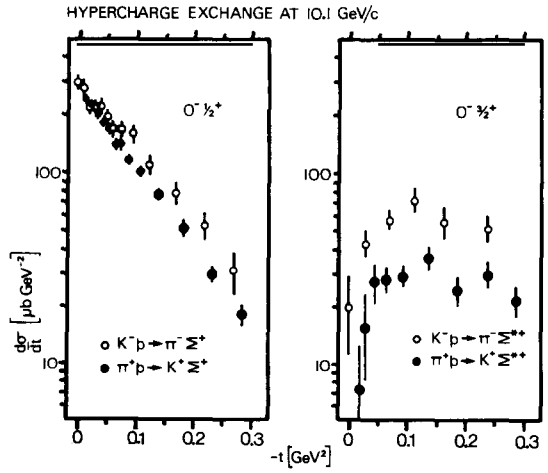


Fig. 4B.3. The differential cross-sections for $0^-\frac{1}{2}^+$ and $0^-\frac{3}{2}^+$ HYCEX at 10.1 GeV/$c$ [248, 249].

$|t| \geq 0.43$ line-reversal symmetry is more seriously violated, particularly for Λ production (see fig. 4B.4). In this region, both flip and non-flip amplitudes are important and detailed amplitude analysis becomes an important tool.

### *4B.4. Amplitude analysis in $0^{-}\frac{1}{2}^{+}$ scattering*

The $\rho$ exchange amplitudes in $0^{-}\frac{1}{2}^{+}$ scattering are now known (~ Regge pole except that Im$\rho$ (non-flip) is peripheral [section 3]). Since most analyses agree on the $A_2$ helicity-flip amplitude (§4B.2 and section 4A) the major remaining uncertainty in CEX scattering concerns the form of the $A_2$ non-flip amplitude. According to the dual absorption [95] and dual peripheral [179] models, $\mathrm{Im}A_2 \simeq -\mathrm{Im}\rho$ and is therefore also peripheral (zero at $t = -0.2$). The least model dependent analyses of KN scattering, to data, are arguably those of Groom et al. [267] and Elvekjaer et al. [215]. Their results (e.g. fig. 4B.2) show that:

Im$A_2$ (non-flip) is not peripheral – it has a single zero at $-t \geq 0.5$.
Re$A_2$ (non-flip) is small (perhaps a double zero) near $\alpha = 0$ in contrast to the $1 + \cos \pi\alpha$ behaviour expected of a Regge pole.

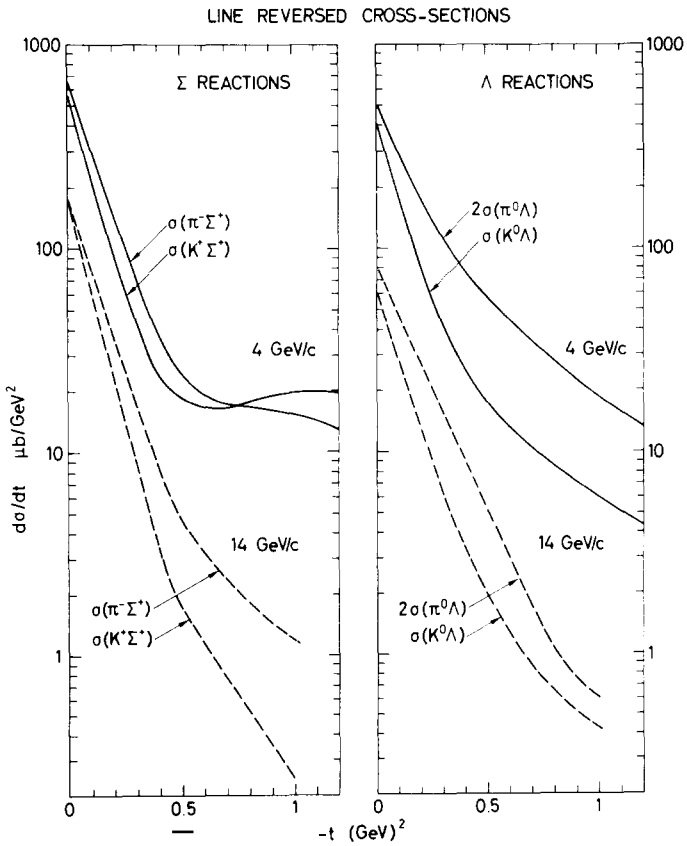


Fig. 4B.4. Hand-drawn interpolations of the available hypercharge exchange cross-sections in the neighbourhood of 4 and 14 GeV/$c$ [165]. The reactions represented are $K^-p \to \pi^-\Sigma^+$, $\pi^+p \to K^+\Sigma^+$, $K^-p \to \pi^0\Lambda$ and $\pi^-p \to K^0\Lambda$.

The EXD violation is proportionally larger in the non-flip cross-section than the flip cross-section for $|t| > 0.2$.

For $|t| < 0.2$, the line-reversal violation in the non-flip cross-section is very small. This last result is consistent with the behaviour of $\widetilde{\cos}\,\phi_{VT}$ in $0^{-\frac{1}{2}+}$ HYCEX.

Measurement of the polarisation in $\pi^- p \to \eta n$ or in $K^+ n \to K^0 p$ near 6 GeV/$c$ would help confirm this picture of $A_2$ exchange.

Amplitude analysis of $K\Delta$ CEX amplitudes requires strong assumptions e.g. on the factorisation of these amplitudes and those in KN [224] or on the helicity structure of the $\rho N\Delta$ and $A_2 N\Delta$ vertices [164, 209]. No generally agreed picture of the origin of the obvious EXD violation has yet emerged. For $\pi N \to K\Sigma^*$ and $KN \to \pi\Sigma^*$, the cascade decay $\Sigma^* \to \Lambda\pi$, $\Lambda \to p\pi$ weakly allows an analysis of transversity amplitudes (up to two undetermined phases) [107] but this sheds little light on EXD breaking. One still has no means of relating the amplitude phases in the separate processes.

The level of understanding in $0^{-\frac{1}{2}+}$ HYCEX is much poorer than in KN CEX despite the relative wealth of experimental facts (including polarisation data). This is because neither K* nor K** can be isolated in a single process as can the $\rho$ in $\pi$N scattering. Three kinds of model dependent amplitude analyses have been performed.

(a) *EXD flip amplitude*

Analyses [109, 165, 148] which use this assumption in order to extract the non-flip vector and tensor amplitudes from $d\sigma/dt$ and polarisation data are unlikely to be fully correct in view of the 15% EXD violation in KN CEX (§4B.2). Since the flip amplitudes are much less important here, a comparable EXD violation should have less effect on the results. Figure 4B.5 shows the original non-flip amplitudes of ref. [165] for $\pi N \to K\Sigma$ at 4 GeV/$c$ and the result of a re-analysis using, as input, a broken EXD flip amplitude with $\alpha_{K^*} - \alpha_{K^{**}} = 0.10$ (cf. §4B.2). The major features are unchanged:

Im$K^*$ is probably peripheral.
Re$K^*$ is roughly consistent with a Regge pole $(1 - \cos \pi\alpha)$ near $\alpha = 0$.
Im$K^{**}$ is not peripheral.

One result which does seem to be sensitive to EXD breaking in the input flip amplitude is the relative magnitudes of $K^*$ and $K^{**}$. The original analysis showed $-\mathrm{Im}K^{**} \gg \mathrm{Im}K^*$ near $t = 0$ contrary to the KN CEX result [154] whereas the reanalysis shows a much smaller effect.

(b) *FESRs and FTDRs*

Argyres et al. [143] have taken a set of imaginary parts for flip and non-flip amplitudes which are consistent with FESR and the analyses described in (a). FTDR are then used to calculate real parts, thus enabling a consistency check of the earlier analyses and, in particular, a check of EXD. They find a small violation of EXD in the real part of the flip amplitudes and non-flip real parts as in (a). An undesirable feature of this analysis is its reliance on a sensitive feature ($-\mathrm{Im}K^{**} \gg \mathrm{Im}K^*$) of the earlier analysis.

(c) *Pole plus effective-cut parametrisation*

Navelet and Stevens [323] have attempted to fit all available $0^{-\frac{1}{2}+}$ HYCEX data (unfortunately omitting the accurate data shown in fig. 4B.3) using loosely parametrised Regge poles for flip amplitudes (to agree with KN CEX) and pole plus effective cuts for non-flip amplitudes. The resulting

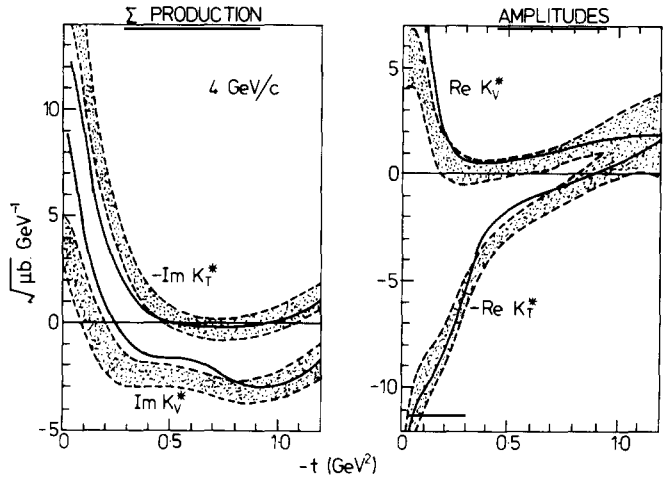


Fig. 4B.5. Odd ($K_{\text{odd}}^*$) and even ($K_{\text{even}}^*$) signature helicity non-flip amplitudes from an analysis of $\bar{K}N \to \pi\Sigma$ and $\pi N \to K\Sigma$ at 4 GeV/$c$ [165] (shaded bands). The full curves, superimposed, are the results of a re-analysis assuming $\alpha_{K^*}(t) - \alpha_{K^{**}}(t) = 0.1$ in the helicity-flip amplitudes (see text).

amplitudes are shown in fig. 4B.6, and are qualitatively similar to those discussed in (a) except that there is slight EXD violation in the flip amplitudes ($\alpha_{K^*} - \alpha_{K^{**}} = 0.05$ and $\beta_{K^{**}} - \beta_{K^*} \sim 15\%$) and that there is smaller EXD violation in the non-flip amplitudes near $t = 0$. (Im$K^{**}$ and Im$K^*$ are more nearly equal.)

In summary, the following features of $0^{-}\frac{1}{2}^{+}$ CEX and HYCEX amplitudes have been established,

(1) Helicity flip amplitudes are roughly consistent with Regge pole behaviour. EXD is only approximately true ($\sim 15\%$) and the violation is in the direction implied by $\alpha_V(t) > \alpha_T(t)$.

(2) The imaginary parts of vector non-flip amplitudes are peripheral, and tensor ones are not (having a zero at about $t = -0.5$). Near $t = 0$, $\mathrm{Im}T \simeq -\mathrm{Im}V$ (as predicted by EXD) for $\rho$ and $A_2$ exchange. This may also be true of HYCEX.

(3) Re$V$ (non-flip) is consistent with Regge behaviour ($\sim 1 - \cos \pi\alpha$).

(4) Re$A_2$ (non-flip) is small near $\alpha = 0$ (unlike Regge). The behaviour of Re$K^{**}$ (non-flip) is unclear but it seems to have a zero between $t = -0.4$ and $t = -0.8$ (Regge $\sim 1 + \cos \pi\alpha$).

### *4B.5. Absorptive models*

Recent comprehensive fits to $0^{-}\frac{1}{2}^{+}$ CEX and HYCEX data have been made using modified absorptive models.

(a) EXD poles + phase-modified weak cuts [134]

Egli et al. [214] have demonstrated that such a highly constrained model (section 3) approximately describes the data. Short-comings, however, include a rather small violation of EXD in KN CEX (no cuts in helicity flip amplitudes, even more crucial in KΔ CEX) yet far too much violation in HYCEX at $t = 0$ ($\widetilde{\cos}\,\phi_{VT} \sim 0.3$ at 10 GeV/$c$ compared to $0.024 \pm 0.023$ in the data). The latter is an inevitable failure of models constructed to only mildly absorb real parts while heavily absorbing imaginary parts.

(b) Modified strong absorption models [158, 319]

These models (section 3) also incorrectly predict $\pi N \to K\Sigma$ and $KN \to \pi\Sigma$ at 10 GeV/$c$ ($\cos \phi_{VT} \sim$

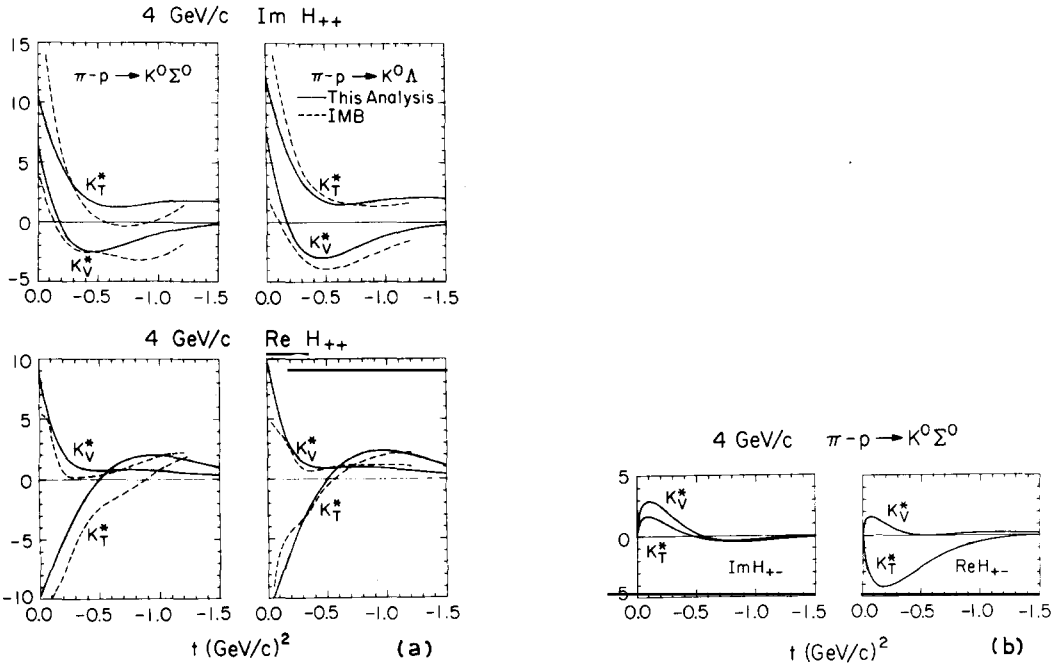


Fig. 4B.6. The amplitudes obtained in model-dependent analyses of hypercharge exchange data at 4 GeV/$c$. (a) The odd ($K_V^*$) and even ($K_T^*$) signature contributions to the helicity non-flip amplitudes ($H_{++}$) in $\pi^-p \to K^0\Lambda$ and in $\pi^-p \to K^0\Sigma^0$. The full and dashed curves correspond to the analyses of refs. [323] and [165] (see text). (b) The helicity-flip amplitude ($H_{+-}$) contributions for $\pi^-p \to K^0\Sigma^0$ [323]. $H_{+-}$ is assumed to be due to EXD Regge poles in the analysis of ref. [165]. Figure taken from [323].

0.3). The small line reversal violation in KN CEX arises from a strong violation of EXD at the pole level ($\alpha_V > \alpha_T$) being redressed by the stronger absorption in the predominating real process. The amplitude systematics are less clear since the final EXD and Regge pole zero structure in $-t$ arises as an "accident" and varies according to the exact version of the model.

Our knowledge of ($\rho$, K*) and ($A_2$, K**) exchange amplitudes has improved significantly over the last few years. Modified absorption models have difficulty in describing their features. In particular it is hard to simultaneously understand why EXD violation in non-flip amplitudes is small at $t = 0$ yet so large near $t = -0.2$ (Im$V$ is peripheral but Im$T$ is not). Another problem for models is the large EXD violation now confirmed in KΔ CEX and Σ* production, in contrast to small violation in KN CEX.

Further insight into the $0^{-\frac{1}{2}^+}$ amplitudes should follow from some experimental results which are expected soon:

$d\sigma/dt$ ($\pi^+p \to K^+\Sigma^+$) at Fermilab energies – one would expect strong absorptive cuts in the helicity non-flip amplitude to be important at large $t$ and to show considerably less shrinkage than K* and K** Regge poles.

Polarisation in $K^+n \to K^0p$ – this will improve the determination of the $A_2$ exchange amplitudes in KN scattering.

Spin-rotation parameters ($R$ and $A$) for $\pi^-p \to K^0\Lambda$ – the quantities $d\sigma/dt$, $P$ and $R$ ($P^2 + R^2 + A^2 = 1$) form a complete set of measurements enabling an amplitude analysis of the combination K*–K** (table 4B.1).

A careful measurement of line-reversal symmetry breaking in $\pi N \to K\Lambda$, $\bar{K}N \to \pi\Lambda$, together with $R$

and $A$ in the latter, would assist a separate determination of $K^*$ and $K^{**}$ amplitudes. Note that since two distinct reactions are involved, this amplitude analysis (unlike $\pi$N) requires additional knowledge of *two* overall phases in order to compare with Regge theory.

## 4C. SU(3) and quark model constraints

Constraints which follow from the quark model and from SU(3) symmetry have proved just as useful in understanding high energy scattering as they have in understanding the hadron mass spectrum and decay rates. In this section, we discuss some tests of these two schemes using high energy data.

### *4C.1. Application of* SU(3) *symmetry to Regge poles*

Tests of SU(3) for decay rates and SU(3) mass-formulae have recently been reviewed by Samois et al. [236] who concluded that, where testable, SU(3) is a good symmetry. At present there is no need to invoke symmetry breaking effects other than the kinematic ones due to mass breaking.

Mass-formulae are rather trivially related to trajectory intercept constraints for Regge poles since

$$\alpha_i(0) = J - \alpha' m_i^2 \tag{4C.1}$$

for each member $i$ of an SU(3) multiplet (spin $J$). Coupling constant constraints are related to Regge residue constraints

$$T_i(s,t) = \beta_i(t) \underbrace{\frac{1 \pm \exp\{-i\pi\alpha_i(t)\}}{\sin \pi\alpha_i(t)} (\alpha' s)^{\alpha_i(t)}}. \tag{4C.2}$$

Note that because high energy scattering is involved, the masses of the four external particles are irrelevant at small $-t$ (cf. ambiguities in the kinematic factors of decay rate formulae). The dependence on the mass of the exchange particle (Reggeon trajectory) is usually confined to the bracketed expression in eq. (4C.2) and provides a natural prescription for unambiguously testing SU(3) i.e. using $\beta(t)$ so defined. In the specific example of resonance production by $\pi$ exchange, one may easily relate $\beta(t)$ to the resonance width $\Gamma$. This gives a specific prescription for testing SU(3) for decay widths which is in better agreement for vector meson decay [171] than the usual naive phase-space prescription [236].

If two Reggeons have similar trajectories (e.g. $\rho$ and $\omega$), then the complete amplitude (eq. (4C.2)) may be used directly for SU(3) comparisons. To the same extent, one may apply SU(3) to absorbed Regge pole amplitudes, provided the absorbing function (e.g. Pomeron) is taken to be an SU(3) singlet. We now give simple examples which highlight the importance of Regge poles in testing SU(3) for amplitudes. Note that one should distinguish between applications using SU(3) alone and those which, in addition, assume absence of exotics. For example, SU(3) alone allows one to write

$$A(K^- p \to \pi^- \Sigma^+) = A(K^- p \to \pi^+ \Sigma^-) \tag{4C.3}$$

$$A(K^- p \to \pi^- \Sigma^+) = A(K^- p \to K^- p) - A(\pi^- p \to \pi^- p). \tag{4C.4}$$

The latter gives rise to a cross-section bound which is amenable to experimental test at high energies [16]

$$\left[\frac{d\sigma}{dt}\left(\pi^-\Sigma^+\right)\right]^{1/2} \geq \left|\left[\frac{d\sigma}{dt}(\pi^- p)\right]^{1/2} - \left[\frac{d\sigma}{dt}(K^- p)\right]^{1/2}\right|. \tag{4C.5}$$

It is obviously violated since, experimentally, the right side tends to a constant in $s$ (at fixed $t$) while the left side drops as $s^{-n}(n>0)$. This is easily understood from a Regge exchange point of view. The right side is due primarily to Pomeron exchange (not pure SU(3) singlet) while the left side is due to K* exchange and these have different energy dependences. Even in the limit of an SU(3) singlet Pomeron, one would not expect eq. (4C.5) to be valid since the K* has a lower intercept than the Pomeron–Reggeon interference term which would then dominate the right side.

If in addition, one assumes absence of (quark model) exotics, stricter relations are obtained. For example (table 4B.2)

$$A\left(K^- p \to \pi^- \Sigma^+(1385)\right) = -\frac{1}{\sqrt{3}} A(K^+ p \to K^0 \Delta^{++}) \tag{4C.6}$$

is an easily testable relation. Again, this is experimentally invalid, as one might have expected since $\alpha_{K^*}(0) < \alpha_\rho(0)$ due to mass breaking (eq. (4C.1)). See §4C.4, however.

### *4C.2. Additional constraints from the quark model*

In fig. 4C.1 is depicted the quark model description of meson–baryon and baryon–baryon scattering processes. Each scattering amplitude is assumed to be made up of the sum of all possible quark–quark sub-amplitudes (quark additivity). The horizontal lines represent spectator quarks which do not affect the scattering amplitude, except in so far as they must couple to the interacting quarks so as to form external hadrons with correct quantum numbers. There are several important consequences of the model:

(a) In the $t$-channel, the exchanged quantum numbers are those of $q_1\bar{q}_3 \to \bar{q}_2 q_4$ (see fig. 4C.1). The amplitude therefore has, from an exchange viewpoint, SU(3) symmetry and absence of exotics.

(b) Furthermore, it has the larger group symmetry, $SU(6)_w$, built in.

(c) If figs. 4C.1(a) and (b) are taken literally, the model may be used to relate meson–baryon and baryon–baryon processes (the same quark sub-amplitude is common to both).

(d) Since the spectator quarks do not interact, spin-flip contributions to the overall amplitude come only from the rather simple sub-process. In terms of transversity (production normal) quantisation,

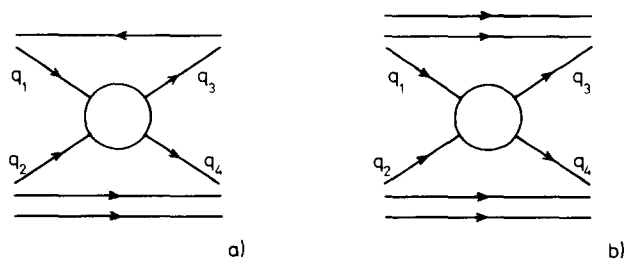


Fig. 4C.1. Meson–baryon and baryon–baryon scattering in the quark model. The horizontal lines represent non-interacting quarks.

only changes of $\Delta m = 0, 2$ are allowed ($\Delta m = 1$ quark amplitudes are zero by parity). This gives rise to restrictions on the allowed overall transversity (or helicity) amplitudes.

Because of (a), many of the simplest quark model results are already realised in any exchange model which has SU(3) symmetry and is restricted to singlet and octet exchange. In fact, some of the best-known and most successful quark model predictions fall into this category and we shall discuss them, below, as SU(3) results. Of course, (b), (c) and (d) give rise to extra constraints and, in particular, (c) and (d) are unique to the quark model. The quark additivity assumption (fig. 4C.1) does not encompass baryon exchange processes. Here, we shall only discuss small-angle scattering and refer to section 4I for a discussion of the SU(3) properties of backward scattering.

When applying SU(3), account must be taken of mixing between isoscalar singlet and octet mesons ($M_1$ and $M_8$). For example for $J^P = 0^-, 1^-$ and $2^+$ the physical particles M($\eta$, $\phi$ or f') and M'($\eta'$, $\omega$ or f) are given by

$$M = -M_1 \sin\theta + M_8 \cos\theta, \qquad M' = M_1 \cos\theta + M_8 \sin\theta. \tag{4C.7}$$

In the quark model,

$$M_1 = \frac{1}{\sqrt{3}}(p\bar{p} + n\bar{n} + \lambda\bar{\lambda}), \qquad M_8 = \frac{1}{\sqrt{6}}(p\bar{p} + n\bar{n} - 2\lambda\bar{\lambda}) \tag{4C.8}$$

(in the usual notation). The additional assumption that $\phi$ (or f') is "magically mixed", i.e. has $\lambda\bar{\lambda}$ as its wave function, implies $\tan\theta = 1/\sqrt{2}$ ($\theta \simeq 35^0$) and that $\phi \not\to \rho\pi$. Thus both $\theta$ and the singlet/octet coupling ratio can be fixed. The quark model shorn of the "magic mixing" assumption fixes the singlet/octet coupling ratio (e.g. $g_{\eta_1\pi A_2}/g_{\eta_8\pi A_2} = g_{\omega_1\pi\rho}/g_{\omega_8\pi\rho} = \sqrt{2}$) but leaves $\theta$ undetermined.

For the $\eta$ and $\eta'$, the quark model prediction $S_T(\equiv g_{\eta_1\pi A_2}/g_{\eta_8\pi A_2}) = \sqrt{2}$ gives rise to a sum rule between hypercharge exchange $\pi^0$, $K^0$, $\eta$ and $\eta'$ production cross-sections which is violated by the data [320]. Mass-mixing formulae suggest $\theta_P = -10.4^0$ (quadratic) or $\theta_P = -23^0$ (linear). The quadratic value of $\theta_P$ (favoured in analyses of meson radiative decays [196]) and the small $t$ hypercharge exchange data suggest a value of $S_T \simeq 1.1$ [320]; see also §4C.3 below.

For the vector and tensor mesons, the quark model predictions are apparently much better. The mass formulae give $\theta_V \simeq 40^0$ and $\theta_T \simeq 31^0$. In fact, the small decay rate of $\phi \to 3\pi$ compared to $\omega \to 3\pi$ may be shown to be compatible with this slight deviation from ideal mixing ($\theta_V \simeq 40^0$ rather than $35^0$) if one uses the quark model wave functions (eq. (4C.8)) and the mixing formulae (e.g. (4C.7)). Recent results on f' production in $\pi N \to K\bar{K}N$ [325] suggest $\theta_T \lesssim 35^0$. For most purposes (e.g. §§4C.3,5) we shall assume magic mixing, $\phi \not\to \rho\pi$, f' $\not\to \pi\pi$, etc.

### *4C.3.* SU(3) *sum rules*

Here we discuss sum rules which are derived by applying SU(3), for a *fixed* (Reggeised) octet exchange, to the complete amplitude. They may therefore be written for any measurable bilinear quantity $\tau$ ($\equiv\sigma$, $d\sigma/dt$, $P(d\sigma/dt)$, or $\rho_{mm'}$ $d\sigma/dt$, etc.). Using tables 4B.1 and 4B.2 we can write

$$\frac{1}{x^2}\tau(\pi^- p \to \eta n) = \tfrac{1}{3}[\tau(K^+ n \to K^0 p) + \tau(K^- p \to \bar{K}^0 n) - \tau(\pi^- p \to \pi^0 n)] \tag{4C.9}$$

$$\frac{1}{x^2}\tau(\pi^+ p \to \eta \Delta^{++}) = \tfrac{1}{3}[\tau(K^+ p \to K^0 \Delta^{++}) + \tau(K^- p \to \bar{K}^0 \Delta) - \tau(\pi^+ p \to \pi^0 \Delta^{++})]. \tag{4C.10}$$

In fig. 4C.2, we present evaluations of these using the most recent data at 6 GeV/$c$. They are fairly well satisfied (at least in shape), suggesting that both the Regge poles themselves, and any corrections to them, are SU(3) symmetric. The discrepancy in magnitude could be resolved by using mixing parameter values corresponding to $x^2$ near one ($S_T < 1$). The most sensitive measure of the mixing parameters will come from high statistics measurements of the ratio $d\sigma/dt\ (\pi^- p \to \eta' n)/d\sigma/dt\ (\pi^- p \to \eta n)$.† Existing data on the $\gamma\gamma$ decay modes of $\eta$ and $\eta'$ give $0.52 \pm 0.15$ for this ratio [317] corresponding to $S_T = 1.04 \pm 0.14$, ($\theta_P = -10.4^0$). If $S_T \geqslant 1$ and $\theta_P \simeq -10^0$ are confirmed, then the discrepancy in the SU(3) sum rule (eq. (4C.9)) must be taken as significant.

Similar sum rules exist for vector-meson production

$$\tau(\pi^- p \to \rho^0 n) + \tau(\pi^- p \to \omega n) = \tau(K^+ n \to K^{*0} p) + \tau(K^- p \to \bar{K}^{*0} n) \tag{4C.11}$$

$$\tau(\pi^+ p \to \rho^0 \Delta^{++}) + \tau(\pi^+ p \to \omega \Delta^{++}) = \tau(K^+ p \to K^{*0} \Delta^{++}) + \tau(K^- n \to \bar{K}^{*0} \Delta^-), \tag{4C.12}$$

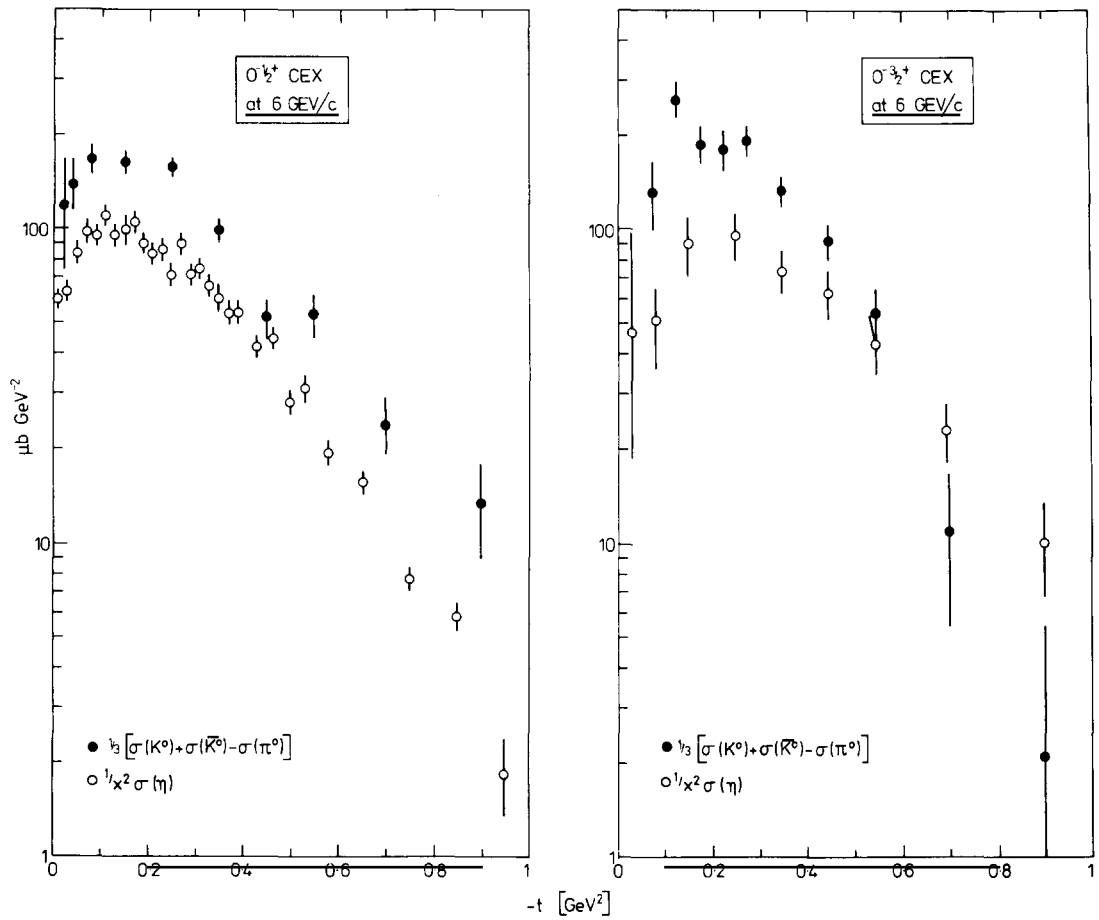


Fig. 4C.2. SU(3) sum rules for $0^-\frac{1}{2}^+$ and $0^-\frac{3}{2}^+$ charge-exchange scattering at 6 GeV/$c$. The mixing parameter $x$ is defined in table 4B.1. The data are from refs. [317, 328, 195, 326]. The symbol $\sigma(\bar{K}^0 n)$ refers to $d\sigma/dt\ (K^- p \to \bar{K}^0 n)$ etc.

† Preliminary data at 8.4 GeV/$c$ [309] show a puzzling difference in the shape of $\eta$ and $\eta'$ $t$-distributions. Integrated over $|t'| < 0.2$, the ratio of cross-section is $0.58 \pm 0.05$.

These have been compared (for $\tau = \rho_{mm'}$ $d\sigma/dt$) with relatively low statistics bubble chamber data in the 4 to 6 GeV/$c$ range and, apart from normalisation inconsistencies, seem to be valid [150, 264]. A complete set of high statistics measurements of each term in eq. (4C.11) has now been made and results are expected shortly [331].

### *4C.4. Mass-broken* SU(3) *relations*

One might hope to, at least partially, allow for SU(3) mass-breaking by noting that the dominant dependence on $\alpha(t)$ of eq. (4C.2) is $\sim(-i\alpha' s)^{\alpha(t)}$. In this way, Martin et al. [131] have used a symmetry-breaking factor

$$\lambda^{-1} = (-i\alpha' s)^{\Delta\alpha}, \tag{4C.13}$$

where $\Delta\alpha = \alpha'(m_{K^*}^2 - m_\rho^2) \simeq 0.2$, to make SU(3) comparisons between $0^{-\frac{1}{2}+}$ charge and hypercharge exchange reactions. In applying SU(3) to different octet exchanges, one must specify the $F/D$ mixing parameter for the octet couplings to baryon vertices, e.g. the $F/D$ for vector and for tensor exchanges, for each helicity coupling. We shall assume (section 4B) that exchanges related by EXD have common $F/D$ ratios. With this assumption, the ratio of $\Lambda$ to $\Sigma$ at $t = 0$ may be used to estimate $(F/D)_{++}$ (helicity non-flip), and the $\Lambda/\Sigma$ ratio for $P$ $d\sigma/dt$ then gives $(F/D)_{+-}$. Broadly, the results are compatible with the global values $(F/D)_{++} = -3$ and $(F/D)_{+-} = 0.4$ quoted in appendix A. Using these parameters and the mass-breaking formula (eq. (4C.13)) one can predict $P$ $d\sigma/dt$ (and hence $P$) in KN charge-exchange in terms of the measured hypercharge exchange polarisation [131]. The results are in tolerable agreement with the data.

The least model-dependent tests of SU(3) between CEX and HYCEX are obtained by eliminating the $F/D$ ratios as, for example, in the relation

$$2\lambda A(K^- p \to \bar{K}^0 n) = \sqrt{6} A(\pi^- p \to K^0 \Lambda) - A(\pi^+ p \to K^+ \Sigma^+). \tag{4C.14}$$

Using this, the cross-section data and polarisation data determine bounds on $|\lambda|^2$. These suggest a value of $|\lambda|^2$ consistent with the dual model expectation (eq. (4C.13)) and, in so doing, provide confidence in this method of applying mass-broken SU(3) symmetry to exchange processes [131].

The complication of $F/D$ values is also avoided in applying SU(3) to $0^{-\frac{1}{2}+} \to 0^{-\frac{3}{2}+}$ or $1^{-\frac{3}{2}+}$ processes. For example, using table 4B.2

$$\tau(K^- p \to \pi^- \Sigma(1385)^+) = \tfrac{1}{3}|\lambda|^2 \tau(K^+ p \to K^0 \Delta^{++}). \tag{4C.15}$$

In fig. 4C.3 we test eq. (4C.15) using $d\sigma/dt$ data at 4 GeV/$c$. Also shown is the analogous "rotating phase" comparison and a plot, versus $p_{LAB}$, using $\tau = \sigma_{\text{integrated}}$. Satisfactory agreement is found.

### *4C.5.* SU(3) *relations between individual amplitudes*

Such tests are only possible where the relevant amplitude analyses are available. In the case of $\rho^0$ and K* production by $\pi$ exchange this is possible and good agreement is found [310, 280, 281] but, as discussed earlier, this could be regarded as a test of SU(3) for decay rates.

Another example, where the exchange amplitudes are reasonably well known, is $\mathrm{Im}N^{(-)}$ (as defined in section 3) which is responsible for cross-over zeroes and is definitely not due to a single Regge pole.

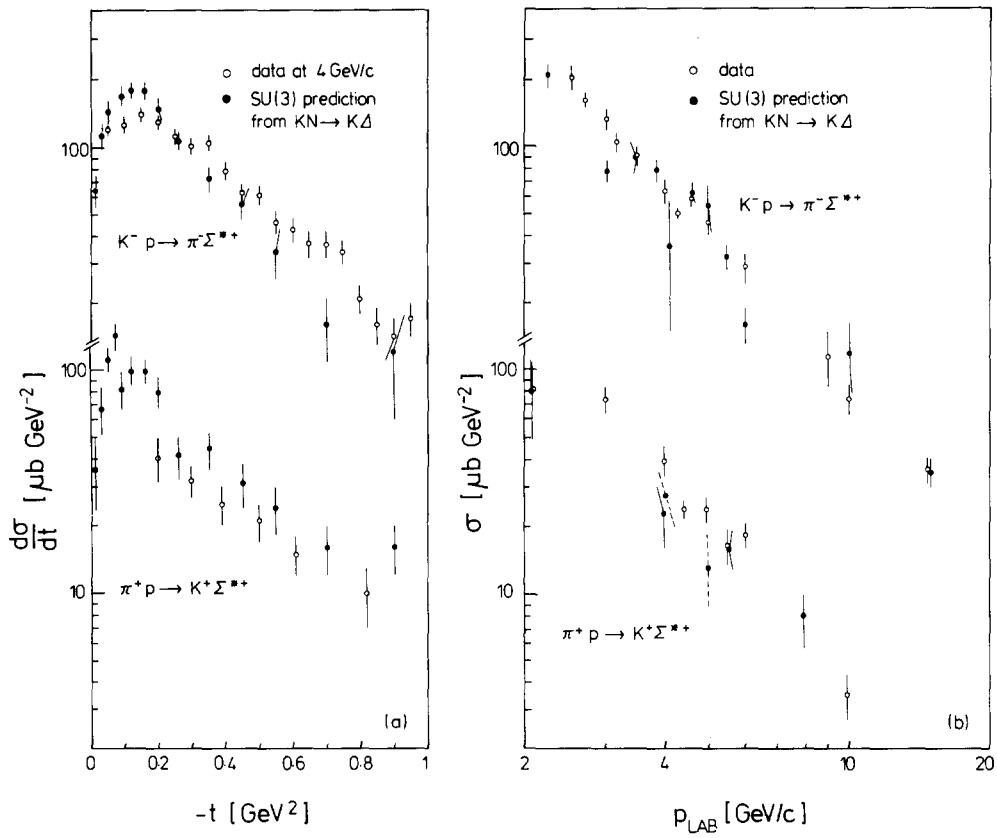


Fig. 4C.3. Differential cross-sections (a) and integrated cross-sections for $K^-p \to \pi^-\Sigma^{*+}$ and $\pi^+p \to K^+\Sigma^{*+}$ (open points) together with predictions from $KN \to K\Delta$ CEX assuming broken SU(3) (eq. (4C.15)) (solid points). The data are from [106, 316, 66, 112] ($\Sigma^{*+}$) and from [326, 223] ($K\Delta$).

In fig. 4C.4 we show a comparison, adapted from ref. [108], of $\mathrm{Im}\omega$ and $\frac{5}{2}\,\mathrm{Im}\rho$ which would be expected to be equal in the SU(3) limit, where the constant, $\frac{5}{2}$, comes from assuming $F/D = -3$. Also shown is $|\lambda|^{-1}\frac{5}{8}\sqrt{3}\,\mathrm{Im}K^*$ from an analysis of $\pi^-p \to K^0\Lambda$ [165]. Apart from the very forward direction, there is a remarkable uniformity in the amplitude magnitude and zero structure.

One may also use total-cross section data to test SU(3) for $\mathrm{Im}N^{(-)}$ ($t = 0$), as a function of energy, SU(3) for $\rho$ exchange in KN and $\pi$N scattering seems to be approximately satisfied† e.g. [193]:

$$\frac{\Delta\sigma_T(K^{\mp}p) - \Delta\sigma_T(K^{\mp}n)}{\Delta\sigma_T(\pi^{\mp}p)} \approx 1.15 \qquad \text{(expect 1)}. \tag{4C.16}$$

It has also been tested at the amplitude level using FESR: Elvekjaer and Johnson [215] have compared FESR for $\rho$ exchange in $\pi$N and KN scattering ($N^{(-)}$ and $F^{(-)}$) and found them to satisfy SU(3).

The advent of high energy hyperon beams will give access to further direct tests. Quigg and Rosner [327] have recently reviewed some interesting possibilities, including various total cross-section differences which will allow tests of SU(3) at baryon vertices independently.

† Hendrick et al. [269] have investigated SU(3), quark model and EXD breaking from total cross-section fits and find parametrisation-dependent violations of SU(3), if substantially unequal $\rho$ and $\omega$ trajectories are tolerated.

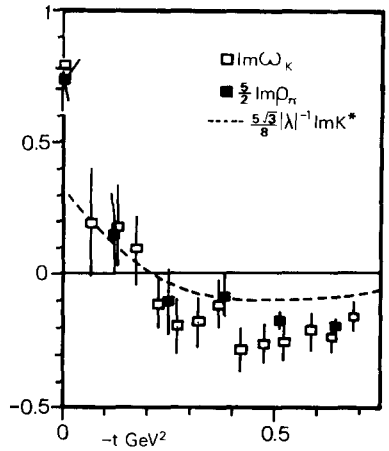


Fig. 4C.4. A test of the universality of vector exchange in $0^{-}\frac{1}{2}^{+}$ scattering, $\mathrm{Im}N^{(-)}$ (see text). The $\rho$ and $\omega$ values are from [108] and the K* curve is from [165].

SU(3) has been strikingly successful in relating amplitudes of more complicated processes. For example, it predicts that, for each spin amplitude (assuming magic mixing)

$$A(\mathrm{K^-p}\to\rho\Lambda)=A(\mathrm{K^-p}\to\omega\Lambda),\qquad A(\pi^-\mathrm{p}\to\mathrm{K^{*0}}\Lambda)=A(\mathrm{K^-p}\to\phi\Lambda). \tag{4C.17}$$

In fig. 4C.5 we show a successful test of the first of these relations using data on the moduli of transversity amplitudes obtained in model-independent amplitude analyses [153]. As is often the case, SU(3) seems to work well even in the presence of strong absorptive corrections and violations of EXD – the EXD Regge poles prediction, $\frac{1}{2}\mathrm{d}\sigma/\mathrm{d}t\ (\phi\Lambda)=\mathrm{d}\sigma/\mathrm{d}t\ (\omega\Lambda)$, is found to be badly violated (see §4D.7).

### *4C.6.* SU(3) *and Regge pole fits*

The success of global Regge pole (and cut) fits to large sets of SU(3) related processes provides some of the most compelling, if not exactly direct or quantifiable, evidence that Regge residues satisfy SU(3) [139, 158, 214, 310, 281]. The qualitative success of the maximum simplicity, EXD, SU(3) Regge pole model of appendix A also speaks loudly for the validity of SU(3).

### *4C.7. Quark model relations between mesons and baryons*

The prediction of relations between meson–baryon and baryon–baryon processes is a non-trivial feature of the quark model. A well-known example of this, which follows directly from the additivity assumption and the equivalence of quarks in mesons and in baryons (see §4C.2), is the prediction [28]

$$\frac{\sigma_T(\bar{\mathrm{p}}\mathrm{p}+\mathrm{pp})}{\sigma_T(\pi^-\mathrm{p}+\pi^+\mathrm{p})}+\frac{1}{2}\frac{\sigma_T(\mathrm{K^+n}+\mathrm{K^-n}-\mathrm{K^-p}-\mathrm{K^+p})}{\sigma_T(\pi^-\mathrm{p}+\pi^+\mathrm{p})}=\frac{3}{2} \tag{4C.18}$$

which basically reflects the relative number of quarks in baryon and meson. At 50 GeV/$c$, the left side of eq. (4C.18) is $(1.73\pm0.02)-(0.01\pm0.005)$, in slight disagreement. A more successful forward scattering relation is that often referred to as "$\omega$ universality" (unlike eq. (4C.18), it involves quantum

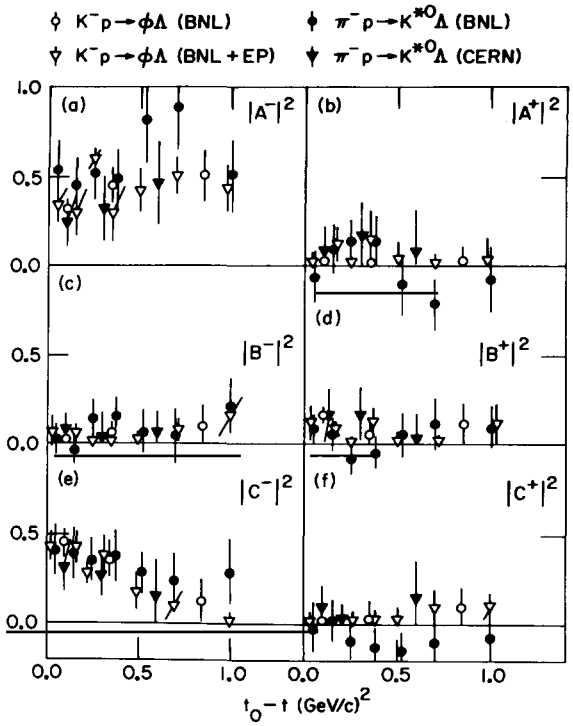


Fig. 4C.5. Transversity amplitude test of the SU(3) relation between $K^-p \to \phi\Lambda$ (open points) and $\pi^-p \to K^{*0}\Lambda$ (solid points) [152]. The quantities $|A_\pm|^2$ etc. are the moduli-squared of particular transversity amplitudes combinations (normalised to one) which are readily obtained from data [152].

number exchange amplitudes),

$$\sigma_T(p^-p - pp) = 3\sigma_T(K^-p - K^+p) - \sigma_T(\pi^-p - \pi^+p). \tag{4C.19}$$

At 50 GeV/$c$ the ratio of left to right sides is $1.14 \pm 0.29$. Lipkin [168] has recently reviewed the status of these and other similar quark model predictions, discussing the assumptions involved and possible reasons for failure.

Bialas and Zalewski [39] have listed many relations between meson and baryon initiated inelastic reactions. Together with $C$-conjugation, such relations give rise to consistency conditions amongst meson–baryon processes which are not always satisfied by the data. For example, the relation

$$\frac{3}{8}\frac{d\sigma}{dt}(\pi^+p \to \eta, \eta'\Delta^{++}) = \frac{d\sigma}{dt}(\pi^-p \to \rho^0 n) - \frac{25}{24}\frac{d\sigma}{dt}(\pi^+p \to \rho^0\Delta^{++}) \tag{4C.20}$$

has little chance of being satisfied because of the different Regge exchanges contributing to both sides ($A_2$ exchange and $\pi + A_2$ exchange). Even when decomposed into natural and unnatural parity exchange components, eq. (4C.20) is not a success. For example, the cancellation on the right-hand side for helicity zero production cannot work because of the very different structure of $\pi$ exchange in each case ($\sim -t$ in $\pi^-p \to \rho^0 n$ but $\sim$ constant in $\pi^+p \to \rho^0\Delta^{++}$).

In studying the relations between the cross-sections† and density matrix elements of meson–baryon

† At finite energies some authors recommend correcting for phase-space effects [e.g. 14]. The procedure for doing this is, however, not unique.

and baryon–baryon processes [39], one also finds that only when the Regge exchange structure is similar, are predictions valid. Thus,

$$\frac{d\sigma}{dt}(pn\to np)=\frac{d\sigma}{dt}(K^+n\to K^0p)+\frac{25}{9}\frac{d\sigma}{dt}(K^+n\to K^{*0}p) \tag{4C.21}$$

is a failure, whereas,

$$\frac{d\sigma}{dt}(pp\to n\Delta^{++})=\frac{8}{3}\frac{d\sigma}{dt}(K^+n\to K^{*0}p) \tag{4C.22}$$

works reasonably well. In fig. 4C.6 various cross-section components are separately shown to satisfy eq. (4C.22) [221]. Not only has the quark model been used here to relate meson and baryon, but also to restrict the number of independent amplitudes in the baryon–baryon process and so obtain a one-to-one correspondence between these and the meson–baryon amplitudes. The constraints imposed on the spin amplitudes are discussed below.

### *4C.8. Constraints on production amplitude spin structure*

Bialas and Zalewski [39] have classified these constraints according to the strength of assumption

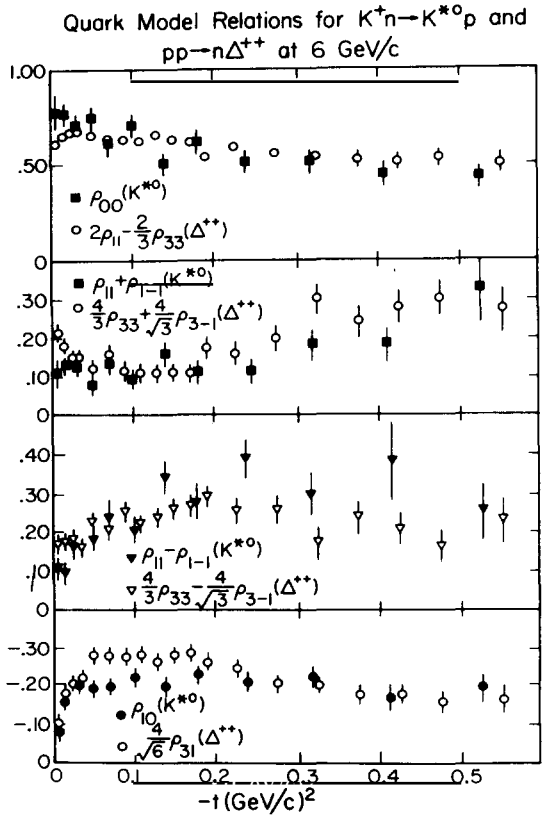


Fig. 4C.6. A test of the quark model relations between the density matrix elements of $pp\to n\Delta^{++}$ (open points) and $K^+n\to K^{*0}p$ (solid points) [221].

used. Class A assumes quark additivity alone. For example, for $\pi N \to \pi\Delta$ one obtains the same $\Delta$ density matrix element predictions as given by the Stodolsky–Sakurai model [10]. In the case of $\pi N \to \rho\Delta$, the $\rho$ and $\Delta$ density matrices are related, e.g.

$$\rho^{11} + \rho^{1-1} = \tfrac{4}{3}(\rho_{3/2\,3/2} + \sqrt{3}\,\mathrm{Re}\,\rho_{3/2-1/2}). \tag{4C.23}$$

These relations are equally valid when formulated for $s$ or $t$-channel helicity quantisation. Class B relations use the additional assumption that two of the eight, otherwise independent, quark–quark

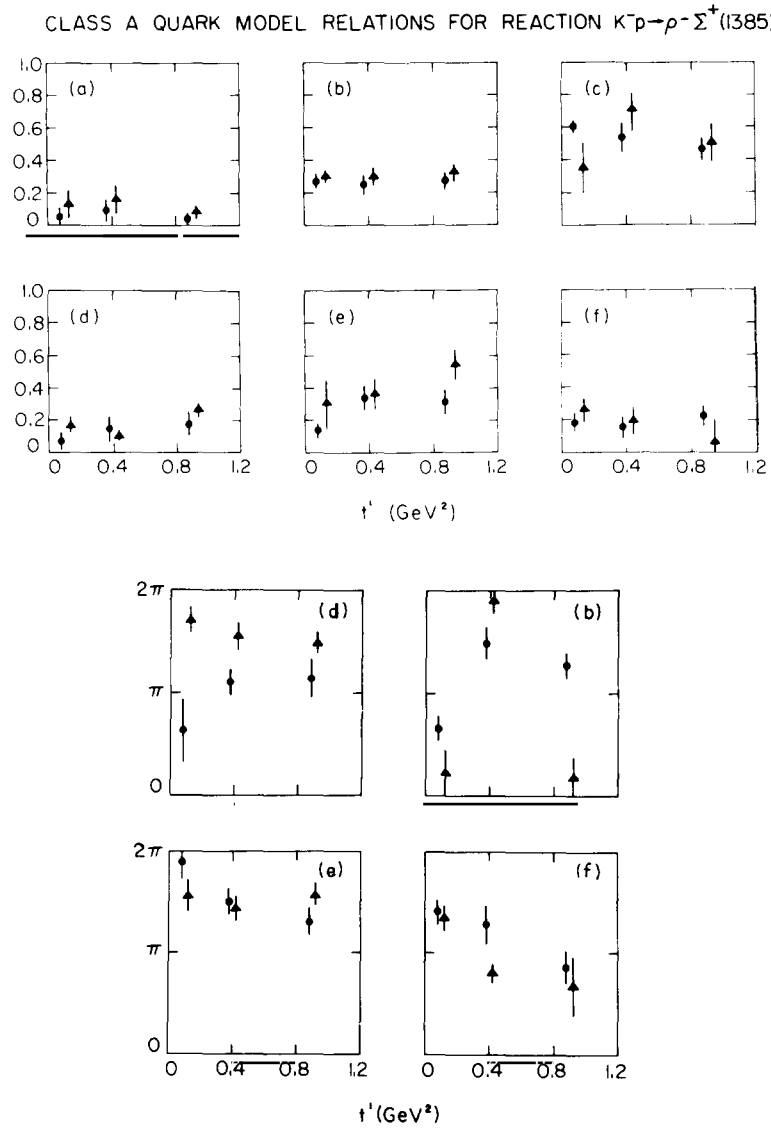


Fig. 4C.7. A test of the quark model class A relations for the 12 transversity amplitude moduli (above) and 8 of the relative phases (below) in $K^-p \to \rho^-\Sigma^{*+}$ [292]. The amplitudes (a)–(f) are shown in pairs (●, ▲) which are expected to be equal in the quark model (see ref. [292] for details). The phases are those relative to the amplitudes in (c) – e.g. (d) is the phase of amplidude (d) relative to (c) etc.

scattering amplitudes are equal. For $\pi N \to \rho\Delta$, for example, relation (4C.23) splits into two stricter ones ($\rho^{11} = \frac{4}{3}\rho_{3/2\,3/2}$, etc.). Class C sets equal a further two quark–quark scattering amplitudes, and relations such as $\mathrm{Re}\,\rho_{10} = 0$ (for $\pi N \to \rho\Delta$) are obtained.

Class B and C results are *not* invariant with respect to rotation between $s$ and $t$-channel quantisation, although those in class B are less dependent on which frame is used than those in C. Many quark model tests have been made using double resonance production data with the conclusion [e.g. 56, 141] that class A and B relations are apparently valid while those of C are significantly violated. Recent high statistics data on the process $K^- p \to \rho^- \Sigma\,(1385)^+$ at 4.2 GeV/$c$ has enabled amplitude analysis to be performed and so allow a direct test of the quark model relations for the transversity amplitudes themselves, including relative phases [292]. Figure 4C.7 shows this test of the class A relations. Apart from one pair of relative phases, the agreement is impressive.

It has been pointed out that many of the successful quark model spin restrictions may also be obtained in Regge models with specific coupling schemes. For example, a "dipole coupling" of Reggeons in $\pi N \to \rho\Delta$ (the N and $\Delta$ coupling dominantly to spin one) can be shown [39, 141] to give rise to class A and B predictions (i.e. those successful experimentally).

The general implications for Regge phenomenology of SU(3) and the quark model can be summarised by these statements:

(a) Where SU(3) does not contradict the common-sense dictated by Regge ideas, it is successful i.e. it is a good symmetry for Regge residues, and also for amplitudes, if one takes account of mass-breaking ($\alpha_{K^*}(t) \neq \alpha_\rho(t)$).

(b) Those quark model results which are also derivable from SU(3) are particularly successful.

(c) Quark model results which relate processes with different Regge exchanges are expected, and found, to be invalid.

(d) Successful quark model relations between spin-amplitudes are usually derivable by other means e.g. Regge models with specific couplings.

(e) In many cases where pure Regge pole dominance and/or exchange-degeneracy are violated, the relations implied by SU(3) and quark additivity are still experimentally valid.

One can therefore contemplate a hierarchy of exchange model constraints, according to decreasing phenomenological precision: (1) SU(3), (2) quark additivity, (3) pure Regge *pole* dominance, (4) exchange degeneracy.

## 4D. Vector meson production and photoproduction

High energy production or scattering of vector particles provides an opportunity to test Regge ideas in a new situation. In particular, new helicity configurations and new exchanges (unnatural parity) are involved. The best measured and understood processes are the set of SU(3) related non-strangeness exchange vector meson production reactions and the single pion photoproduction processes to which they are related by vector meson dominance (VMD). In table 4D.1 we exhibit the exchanged quantum numbers and the SU(3) and VMD relations between the amplitudes. Figure 4D.1 is a pictorial representation of these relationships: there are three basic exchange amplitudes ($I^G = 1^-$, $1^+$ and $0^-$, i.e. those listed in part (a) of the table) the interference terms of which are measurable in the processes listed in parts (b) and (c) of this table. We now discuss the properties of this highly constrained system of amplitudes, using fig. 4D.1 as a guide.

Table 4D.1
The exchange amplitudes in vector meson production and photoproduction. Those in (b) are related to those in (a) by SU(3). Those in (c) are related to (a) and (b) by vector meson dominance and SU(3). Isoscalar unnatural parity exchanges (H, H'?) have been omitted since their SU(3) mixing properties are unknown.

| | Exchange amplitude quantum numbers | |
|---|---|---|
| Process | Natural parity | Unnatural parity |
| $\pi^-p\to\rho^0n$ | $A_2$ | $\pi$ |
| $\pi^-p\to\omega^0n$ | $\rho$ | $B$ |
| $\pi^0p\to\rho^0p$ | $(1/\sqrt{2})\omega$ | - |
| | | a) |
| $\pi^\pm p\to\rho^\pm p$ | $(1/\sqrt{2})(\omega\pm A_2)$ | $\pm(1/\sqrt{2})\pi$ |
| $K^+n\to K^{*0}p$ | $(1/\sqrt{2})(A_2+\rho)$ | $(1/\sqrt{2})(\pi+B)$ |
| $K^-p\to\bar{K}^{*0}n$ | $(1/\sqrt{2})(A_2-\rho)$ | $(1/\sqrt{2})(\pi-B)$ |
| | | b) |
| $\gamma p\to\pi^+n$ | $\nu(A_2-\rho/r)$ | $\nu(\pi-B/r)$ |
| $\gamma n\to\pi^-p$ | $\nu(A_2+\rho/r)$ | $\nu(\pi+B/r)$ |
| $\gamma p\to\pi^0p$ | $(\nu/\sqrt{2})(\omega+\rho/r)$ | $(\nu/r\sqrt{2})B$ |
| $\gamma n\to\pi^0n$ | $(\nu/\sqrt{2})(\omega-\rho/r)$ | $-(\nu/r\sqrt{2})B$ |
| $\gamma p\to\eta p$ | $(x\nu/\sqrt{6})(\rho+\omega/r)$ | $(x\nu/\sqrt{6})B$ |
| $\gamma p\to\eta' p$ | $(x'\nu/\sqrt{6})(\rho+\omega/r)$ | $(x'\nu/\sqrt{6})B$ |
| | | c) |
| $\gamma=\rho+\omega/r$, $r\simeq 2.8$; $\nu^2=\gamma_\rho^2/\pi\alpha\simeq 350$ | | |
| $x=\cos\theta_P-\sqrt{2}\sin\theta_P=1.23$; $x'=-(\sin\theta_P+\sqrt{2}\cos\theta)=-1.22$ | | |

### *4D.1. $I^G=1^-$ exchange in $\pi^-p\to\rho^0n$*

From this process, much has been learned of the properties of $\pi$ exchange and associated cuts (see also sections 4E, F). We briefly recount how Regge exchange information may be inferred from the data. Schlein [35] showed how one may define combinations of helicity amplitudes which are experimentally measurable in $\pi^-p\to\pi^+\pi^-n$: In the $\rho$-region both S and P wave $\pi\pi$ production occurs:

$$\begin{aligned}
&\sigma=|\boldsymbol{P}^0|^2+|\boldsymbol{P}^-|^2+|\boldsymbol{P}^+|^2+|\boldsymbol{S}|^2, \qquad (\rho_{00}-\rho_{11})\sigma=|\boldsymbol{P}^0|^2-\tfrac{1}{2}(|\boldsymbol{P}^+|^2+|\boldsymbol{P}^-|^2),\\
&\rho_{1-1}\sigma=\tfrac{1}{2}(|\boldsymbol{P}^+|^2-|\boldsymbol{P}^-|^2), \qquad \sqrt{2}\,\mathrm{Re}\,\rho_{10}\sigma=\mathrm{Re}(\boldsymbol{P}^0\cdot\boldsymbol{P}^{-*}),\\
&\sqrt{2}\,\mathrm{Re}\,\rho_{0S}\sigma=\mathrm{Re}(\boldsymbol{P}^0\cdot\boldsymbol{S}^*), \qquad \sqrt{2}\,\mathrm{Re}\,\rho_{1S}\sigma=\mathrm{Re}(\boldsymbol{P}^-\cdot\boldsymbol{S}^*),
\end{aligned} \tag{4D.1}$$

where

$$\boldsymbol{P}^{0,-,+}\equiv(P_{++}^{0,-,+},P_{+-}^{0,-,+}), \qquad \boldsymbol{S}\equiv(S_{++},S_{+-}). \tag{4D.2}$$

The P-wave amplitudes $P^\mu_{\lambda'\lambda}$ of definite exchange naturality are defined and discussed in appendix B (§AB.3). The occurrence of scalar products in eq. (4D.1) reflects the fact that no nucleon spin measurements are involved.

To identify individual amplitudes, $L^\mu_{\lambda'\lambda}$, further assumptions are necessary.

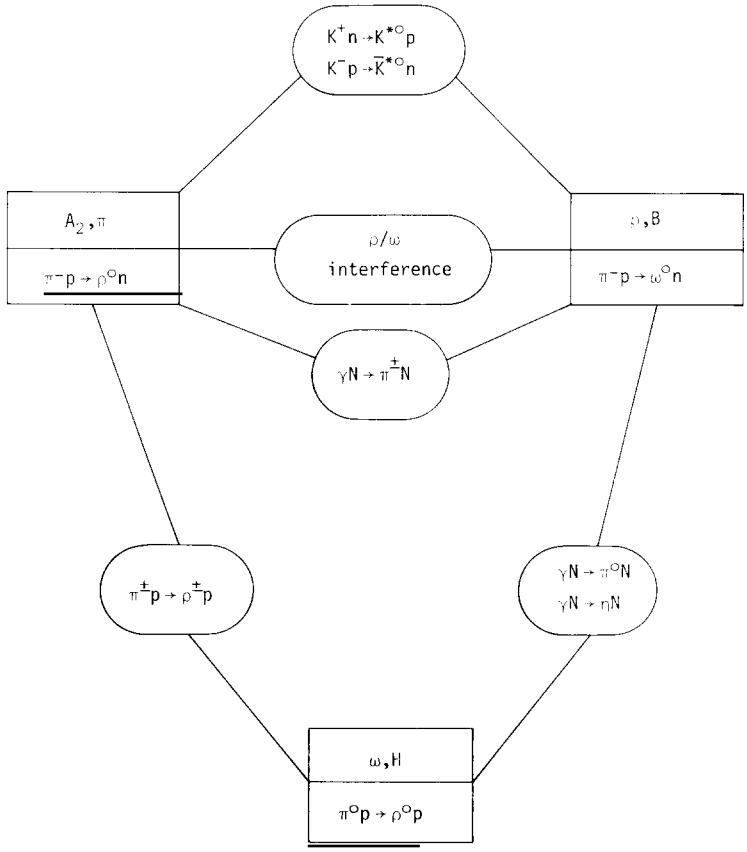


Fig. 4D.1. Relationship between various vector meson production and photoproduction processes. The boxed reactions isolate pure $G$-parity exchanges; the others yield interference information.

(a) Froggatt and Morgan [124] assumed for the unnatural parity combinations $(\boldsymbol{P}^-, \boldsymbol{P}^0, \boldsymbol{S})$
(1) spin coherence: $L^\mu_{+-}/L^\mu_{++}$ is independent of $\mu = 0, -$ and $L = S, P$;
(2) phase coherence: $P^-_{\lambda'\lambda}/P^0_{\lambda'\lambda}$ is real.

These relations would hold for elementary (absorbed) $\pi$ exchange or indeed $\pi$ Regge pole exchange. In fact, they appear to be satisfied by the data to a rather high degree [126].

(b) Estabrooks and Martin [118] have noted that, in the approximation that $A_1$-like $(\lambda' = \lambda)$ exchange may be neglected,† assumption (1) is satisfied and is sufficient, by itself, to enable solution of eqs. (4D.1) since then

$$\boldsymbol{L}^\mu = (0, L^\mu_{+-}); \qquad L = S, P \quad (\mu = 0, -). \tag{4D.3}$$

Figure AA.5 of appendix A shows the moduli $|P^0_{+-}|$, $|P^-_{+-}|$ and $|\boldsymbol{P}^+|$ so deduced from high statistics data at 17.2 GeV/$c$ [225]. Although $|P^0_{+-}|$ has the form expected for $\pi$ exchange $(\sqrt{-t}/(t-\mu^2))$, $|P^-_{+-}|$ shows a forward spike rather than a dip $(-t/(t-\mu^2))$. The latter phenomenon is also well known in the analogous process $\gamma N \to \pi^\pm N$ (see table 4D.1) [26] and has been interpreted in terms of (i) the presence of an opposite parity pole, $\pi_c$ "conspiring" with the $\pi$ [38], (ii) the absorption model ($\pi$ and

† An $A_1$-like exchange ($P^\mu_{++}$, $\mu = 0, -$, s) would enter quadratically in eqs. (4D.1). Recent polarisation measurements (discussed later) suggest $|A_1/\pi|^2 \geq 2$ to 4%. A term of this size does not significantly affect analyses based on eqs. (4D.1).

$A_2$ Regge–Pomeron cuts [60], (iii) the electric Born term model (nucleon $s$ and $u$-channel Born terms) [54] and (iv) the formally similar Williams absorption model [79].

The $\pi$-conspiracy model has been ruled out by factorisation arguments (e.g. [84]) leaving absorption as the favoured interpretation. A stringent test for absorption models of $\pi^-p \to \rho^0 n$ is provided by the data on $\cos\phi_{0-}$ (fig. 4D.2). This measures the phase difference between the $\pi$ exchange amplitudes $P^0_{+-}$ and $P^-_{+-}$ and is defined† in §AB.3 of appendix B. Since $|\cos\phi_{0-}| \simeq 1$, for $|t| \lesssim 0.3$, the $\pi$ pole in $P^0_{+-}$ must be $\sim 180^0$ out of phase with the $\pi$ cut in $P^-_{+-}$. Models based on the Williams prescription have this feature by construction. General absorption models however do not, since the phases of pole and cut tend to be unequal except near $t = 0$. In fig. 4D.2, is shown the prediction of a model proposed by Field and Sidhu [222]. The helicity amplitude predictions of a simplified Regge pole model (using the Williams prescription for $\pi$ absorption) are shown in fig. AA.5 and give a good account of the data ($\xi_{0-}\cos\phi_{0-} = \pm 1$, by construction).

The natural parity component of $\pi^-p \to \rho^0 n$ is thought to be dominated at large $t$ by $A_2$ exchange, and at small $t$ by the same $n = 0$ (cut) correction associated with $\pi$ exchange. Note that $P^{\pm}_{+-}$ are just the sum and difference of the same two ($n = 0$ and $n = 2$) helicity amplitudes ($T_{+1\,1/2-1/2}$). The relative proportions of $A_2$ pole, $\pi$ cut and $A_2$ cut present in $|P^+|$ are illuminated by the latter's energy dependence ($\alpha_{\text{eff}}(t)$). This is shown in fig. 4D.3 for $\pi^-p \to \rho^0 n$ and charged $\pi$ photoproduction: for $|t| \gtrsim 0.3$ it is clear that $A_2$ exchange is important but, near $t = 0$, the energy dependence is more characteristic of $\pi$ exchange. Taken together with the phase-coherence evidence, this suggests that the $A_2$–Pomeron cut in $T^1_{+-}$ is small compared to the $\pi$ cut. The rise of $\alpha_{\text{eff}}(t)$ near $t \simeq 0.2$ must then be interpreted as due to $\pi$ cut and $A_2$ pole interference. This effect is very difficult to reproduce quantitatively in absorption models, since the flat $t$-dependence of the strong $\pi$ cut forces it to dominate the $A_2$ out to $t$ values where $\alpha_{\text{eff}}(A_2)$ is itself near zero [222]. The simple "Regge pole plus Williams" model (appendix A) does, however give a qualitative account of this feature (fig. 4D.3).

Two other aspects of (Reggeised) $\pi$ exchange are highlighted in $|P^0_{+-}|$. Firstly, it has been pointed out that $\alpha_{\text{eff}}(t)$ for this quantity (from 6 to 17 GeV/$c$) shows less shrinkage than expected of a typical Regge pole ($\alpha' \lesssim 0.4$ rather than 0.9), [222]. Secondly, and perhaps not unconnected with the first,

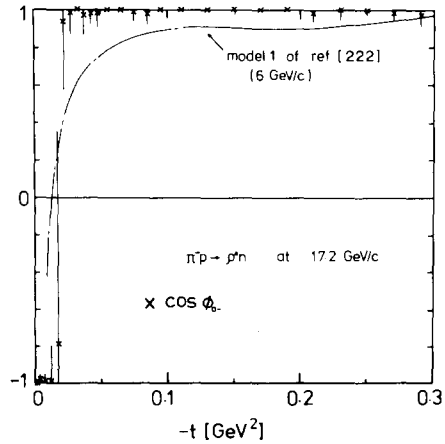


Fig. 4D.2. The phase coherence $\cos\phi_{0-}(\times)$ of the amplitudes $P^0$ and $P^-$ in $\pi^-p \to \rho^0 n$ at 17.2 GeV/$c$ extracted (see §4D.1) assuming spin-coherence [169].

† Spin coherence ($\xi_{0-} = 1$) has been assumed in extracting $\cos\phi_{0-}$.

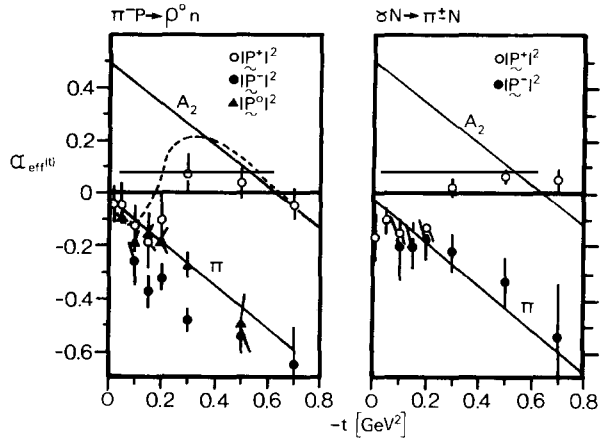


Fig. 4D.3. The $\alpha_{\text{eff}}$ parameter deduced from $\pi^-p \to \rho^0 n$ and $\gamma N \to \pi^\pm N$ data [271] in the range 3 to 17 GeV. The natural and unnatural parity exchange components are treated separately. The full lines represent $\pi$ and $A_2$ Regge trajectories and the dashed curve is the prediction of the simple model given in appendix A.

there is little sign of a zero or dip at $-t \sim 0.5$ as might be expected of a pure pole – a smooth $t$-dependence in $P^{0t}_{++}$ (in the $t$-channel), the only $\pi$ exchange amplitude, should give rise to a zero at $-t = m_\rho^2 - m_\pi^2$ in $P^0_{+-}$ ($s$-channel) because of a zero in the crossing matrix. In models, the lack of a zero can be accounted for by allowing a $\pi$ coupling to $P^-_{++}$ ($t$-channel) (as in fact required by dual models) [172] or simply by evaluating the crossing matrix at $t = m_\pi^2$ as in the Williams model. Formally, these give the same result. The possibility therefore exists that $P^0_{+-}$ is not such a clear-cut example of pure Regge pole exchange in an $n = 1$ amplitude as is often supposed (see section 4A).

Information on the spin structure at the nucleon vertex of $\pi^-p \to \rho^0 n$ and $\gamma p \to \pi^+ n$ is still fragmentary. However, recent measurements of $\pi^-p \to \pi^+\pi^- n$ on a polarised target have shown a sizeable $A_1$-like exchange – see §4E.4. For the natural parity exchange polarisation component $T_+$ (eq. (AB.15)), the dominant contribution is expected to have the form $\text{Im}[\pi_{\text{cut}} A_2^*]$. In fig. 4E.3, the predicted polarisation [228] is shown to agree well with experiment [299].

In summary, the amplitude structure of $\pi$ and $A_2$ exchange in $\pi^-p \to \rho^0 n$ is reasonably well understood. Figure AA.5 bears witness to this. The most remarkable feature from the point of view of absorption models is the high degree of phase-coherence between the unnatural parity amplitudes. The corresponding quantum number exchange in $\gamma N \to \pi^\pm N$ shows the same qualitative features as $|\boldsymbol{P}^+|$ and $|\boldsymbol{P}^-|$ in $\pi^-p \to \rho^0 n$. Some quantitative (VMD violating) differences are discussed in section 4F.

### *4D.2. $I^G = 1^+$ exchange in $\pi N \to \omega N$*

Figure 4D.4 shows the quantities $|\boldsymbol{P}^0|^2$, $|\boldsymbol{P}^\pm|^2$ and $\xi_{0-} \cos\phi_{0-}$ for $\pi^-p \to \omega^0 n$ as measured at 6 GeV/$c$ [329]. If the unnatural parity exchange is dominated by B Regge pole exchange, then just as for $\pi$ exchange in §4D.1, one expects $|\boldsymbol{P}^0|^2 (= |P^0_{+-}|^2)$ to vanish at $t = 0$ and $\xi_{0-} \cos\phi_{0-} = 1$. The data on the other hand imply the presence of a strong amplitude $P^0_{++}$ (finite at $t = 0$) which has been interpreted as Z exchange, Z ($J^{PC} = 2^{--}$) being the potentially EXD partner of the $A_1$ [228, 318]. Such a component would indeed make $\xi_{0-} \cos\phi_{0-}$ vanish at $t = 0$ as observed in the data. Because of this extra complication, it is not possible to solve for the components $|P^{0\prime}_+|$, $|P^-_{+-}|$ and $\cos\phi_0$ as in $\pi^-p \to \rho^0 n$.

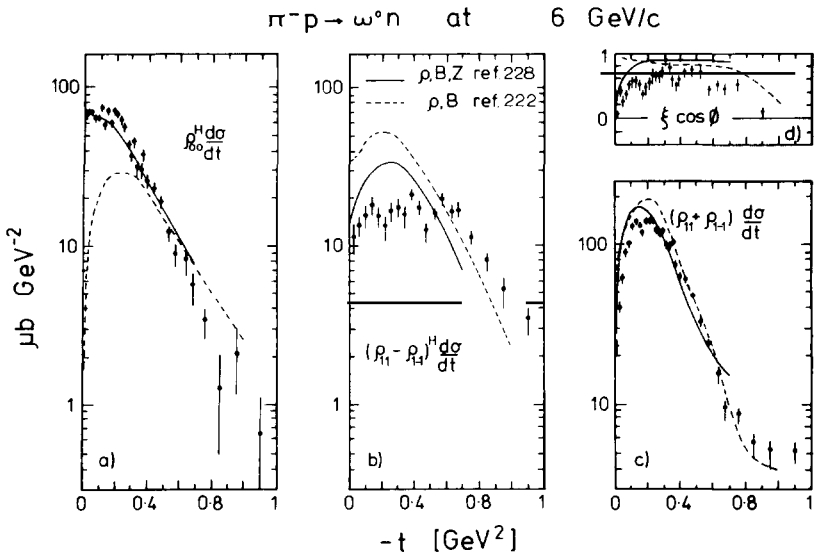


Fig. 4D.4. Data for $\pi^- p \to \omega^0 n$ at 6 GeV/$c$ [329] compared with the model predictions of refs. [228] (full curve) and [222] (dashed curve). $\xi \cos \phi$ is the spin-averaged phase difference defined in eq. (AB.14), (taken from ref. [318]).

The fact that $\rho_{11}\, d\sigma/dt$ is finite at $t = 0$ implies (just as in $\pi^- p \to \rho^0 n$ and $\gamma N \to \pi^\pm N$) that a non-evasive (cut) correction is present. However its nature is rather obscure. The dramatic forward turnover in $|P^+|^2$ which is presumably dominated by the $n = 0$, $x = 2$ $\rho$ exchange amplitude, suggests that this cut is rather small with respect to $\rho$ exchange. (Contrast the factor of 10 drop in cross-section at $t = 0$ with the peak in $\pi^- p \to \rho^0 n$.) However, one is then surprised that the pronounced dip at $-t = 0.6$, characteristic of $\rho$ Regge pole exchange, is not seen. The VMD-related process $\gamma p \to \eta p$ also shows a smooth behaviour of $|P^+|^2$ [301].

In summary, two unnatural parity Regge pole exchanges ($B$, $Z$) are important in $\pi N \to \omega N$ (see also section 4E). The natural parity component seems to be dominated by $\rho$ Regge pole exchange at least for $|t| \lesssim 0.4$. Whether or not cuts are important at larger $t$ is less clear. Models with and without NWSZ have been considered [222, 228] but none gives a very convincing account of all the data. Information on the energy dependence of the various components of $\pi N \to \omega N$ would help disentangle the details of the exchange mechanisms. Some information at 8 and 12 GeV/$c$ [307] is available but is not yet sufficient to show up any anomalies in the $\alpha_{\text{eff}}(t)$ of $|P^+|^2$ near $-t = 0.6$.

### *4D.3. $I^G = 0^-$ exchange in $\pi^0 p \to \rho^0 p$*

Information on $\pi^0 p \to \rho^0 p$ comes from combining data ($d\sigma/dt$ and density matrix elements) for $\pi^\pm p \to \rho^\pm p$ and $\pi^- p \to \rho^0 n$ so as to eliminate $I = 1$ exchange. The cross-section is dominated by the natural parity component $|P^+|^2$, has a turnover in the forward direction and a deep dip near $-t = 0.5$ (fig. 3.2). This is in agreement with the simple Regge expectation of $\omega$ exchange contributing dominantly to $P^+_{++}$ ($n = 1$), (see, for example, [171]). The unnatural parity components, being small, are difficult to isolate. Small but non-zero values of $\rho_{00}$ and $\mathrm{Re}\rho_{10}$ at 2.7 GeV/$c$ have been interpreted as evidence of isoscalar, unnatural parity (H) exchange [132]. Non zero values of $|P^-|^2$ could arise, in absorption models, as a result of absorbing a natural parity pole contribution to $P^+_{+-}$. However $\omega$ couples weakly to such an amplitude.

The energy dependence of $\pi^0 p \to \rho^0 p$ is roughly consistent with $\omega$ exchange [171]. Studies of the VMD related process $\gamma p \to \pi^0 p$ are potentially more useful for elucidating amplitude structure. This is because of the availability of high statistics, high energy data and of FESR information [139, 194, 297]. Table 4D.1 shows that $\gamma p \to \pi^0 p$ actually has small contributions from $I = 1$ exchange ($\rho$, B and Z) – small because of the VMD suppression factor $1/r$ ($\sim \frac{1}{3}$) and because the $\rho$ couples much more weakly ($\times \frac{1}{3}$) to the non-flip nucleon vertex than does the $\omega$. Again, $\gamma p \to \pi^0 p$ is dominated by $|\boldsymbol{P}^+|^2$ which has a turnover at $t \sim 0$ and, at $t = -0.5$, a dip which is somewhat shallower than in $\pi^0 p \to \rho^0 p$. The $I = 0$ component of $\gamma p \to \pi^0 p$ and the cross-section for $\pi^0 p \to \rho^0 p$ approximately satisfy vector meson dominance (a relative factor of $\gamma_\rho^2/\pi\alpha \simeq 350$) [274]. This simple picture is partially destroyed by the $\alpha_{\text{eff}}(t)$ information from $\gamma p \to \pi^0 p$ (shown in fig. 4A.3). The effective trajectory is not linear in $t$ (as expected for an $\omega$ Regge pole) but has a dip-bump structure characteristic of pole/cut interference effects. Indeed strong cut models give a good description of this quantity [139]. In these models, the dip at $-t = 0.5$ is due to pole/cut cancellation in an $n = 1$ amplitude, the pole itself having no NWSZ (see also section 4A). However Barker et al. [194] have used FTDR and FESR to show that $P^+_{++}$ has a phase which is not at all typical of absorption models (old or new) – at 4 GeV the imaginary part has the usual zero near $-t = 0.5$ but the real part is apparently much more strongly absorbed, with a zero at $-t = 0.2$. Further light is shed on the production amplitudes by a measurement of the relative phase between $\rho^0 p \to \pi^0 p$ and $\gamma p \to \pi^0 p$ using nuclear physics techniques applied to $\gamma A \to \pi^0 A$ [294]. A non-zero (i.e. VMD-violating) phase difference is observed which is consistent with that expected (near $t = -0.2$) if $\gamma p \to \pi^0 p$ has the phase deduced by Barker et al. [194] and $\rho^0 p \to \pi^0 p$ is Regge pole dominated. This would be a tempting solution to the paradox of the apparent simplicity of $\pi^0 p \to \rho^0 p$ yet complexity of $\gamma p \to \pi^0 p$. There exists other evidence of the importance, and occasional strange behaviour, of cut effects in photoproduction ([260] and section 4F).

The three basic exchange components discussed in §4D.1–§4D.3 can be made to yield even more information by studies of their mutual interference terms (see fig. 4D.1). We now discuss these using some of the techniques outlined in appendix B.

### *4D.4. $\rho$–$\omega$ interference and related phenomena*

As discussed in appendix B (§AB.5) the interference between the $I^G = 1^+$ and $1^-$ exchanges is measurable in four experimentally independent ways:

(1) Since $\omega$ has a small ($\sim 1\%$) branching ratio into $\pi^+\pi^-$, one can use data on $\pi N \to \pi^+\pi^- N$ to measure the relative phases of the $\rho$ and $\omega$ production amplitudes.

(2) By a similar token, $\rho$ and $\omega$ production amplitudes can be observed to interfere in $\pi N \to \pi^+\pi^-\pi^0 N$. A detailed discussion of these phenomena is contained in [318].

(3) Assuming SU(3) for the vector meson couplings (table 4D.1), the difference between $K^+ n \to K^{*0} p$ and $K^- p \to \bar{K}^{*0} n$ observables is proportional to the same interference.

(4) Assuming VMD, the difference between $\gamma p \to \pi^+ n$ and $\gamma n \to \pi^- p$ yields the same information as (3).

If $A(\rho)$ and $A(\omega)$ represent the $I^G = 1^-$ and $1^+$ exchange amplitudes respectively, then the various methods respectively give access to

(1) $A(\rho)A(\omega)^*$

(2) $\text{Im}[A(\rho)A(\omega)^*]$

(3), (4) $\text{Re}[A(\rho)A(\omega)^*]$,

where a sum over nucleon spins is implicit. Studies of $\rho$–$\omega$ interference effects (method (1)) [220, 229] and K* production (method (3)) [228] show that $\pi$ exchange in $\boldsymbol{P}^0$ interferes only weakly with the

corresponding $G = +$ component (B exchange). Depending on the particular measurement, phase differences $\phi(\rho) - \phi(\omega)$ of from $65^0$ to $100^0$ are observed. For EXD Regge poles, $90^0$ is expected. There are indications from $\rho$–$\omega$ interference in $2\pi$ and in $3\pi$ ((1) and (2)) that the spin coherence in $\boldsymbol{P}^0$ is less than 1.0 (see §AB.5). This and the lack of a turnover in $|\boldsymbol{P}^0|^2$ for $\pi^-p \to \omega^0 n$ provides the strongest evidence of the existence of Z exchange in $P^0_{++}$ [318].

Interference effects in $\boldsymbol{P}^-$ are small and show $\phi(\rho) - \phi(\omega) \geq 90^0$, for $|t| \geq 0.1$, also in rough agreement with $\pi$ and B exchange dominated models.

In §§4D.1 and 4D.2, it was deduced that $\boldsymbol{P}^+$ in $\pi^-p \to \omega^0 n$ was dominated by $\rho$ exchange while its counterpart in $\pi^-p \to \rho^0 n$ was dominated by the $\pi$ cut, for $|t| < 0.1$, and $A_2$ Regge pole for $|t| > 0.2$. The phase difference $\phi(\rho) - \phi(\omega)$ is thus expected to swing rapidly from the second to third quadrants as $|t|$ increases. Results from methods (1), (3) [228] and (4) [139] confirm this simple qualitative picture.

Since the interference term in $\boldsymbol{P}^+$ is linearly proportional to the $\rho$ exchange amplitude, it offers a more sensitive test for the NWSZ than does $|\boldsymbol{P}^+|^2$ [139]. Figure 4D.5 shows that this term, isolated from photoproduction data (4), shows no trace of a zero near $-t = 0.6$. (See also §4D.2.)

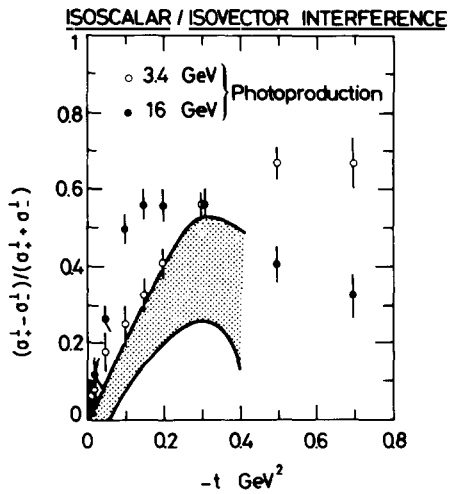


Fig. 4D.5. The normalised difference between $\pi^+$ and $\pi^-$ photoproduction by natural parity exchange (data points). The analogous interference term (between odd and even $G$-parity exchanges) from $KN \to K^*N$ at 4 GeV/$c$ (see §4D.4) is shown by the shaded region [271].

## *4D.5. Interference between $I^G = 0^-$ and $1^-$ exchanges*

Charged $\rho$ production measures interference between $\omega$ and $A_2$-like exchanges. In the case of $\rho$ and $A_2$ exchange, each has similar nucleon helicity structure and the amplitudes therefore have a high degree of spin coherence. However, since $\omega$ is dominantly helicity non-flip and $A_2$ dominantly flip at nucleon vertices, the opposite is true in $\pi^\pm p \to \rho^\pm p$. It is therefore not surprising that the data [157] show little or no interference.

Isolation of an interference term in $|\boldsymbol{P}^0|^2$ would also require very accurate relative normalisation of $\pi^\pm p \to \rho^\pm p$ and $\pi^- p \to \rho^0 n$ since each is dominated by $\pi$ exchange. Such an interference would be sensitive to the presence of H exchange.

### 4D.6. Interference between $I^G = 0^-$ and $1^+$ exchanges

The interference of $\omega$ and $\rho$-like exchanges is measurable in neutral pseudoscalar photoproduction (assuming SU(3), as in table 4D.1). In fact, measurement of $d\sigma/dt$ and $\Sigma$ (the polarised photon asymmetry) for $\gamma p \to \pi^0 p$, $\eta p$ and $\gamma n \to \pi^0 n$ enables one to isolate the $I = 0$ and 1 exchanges, and their interference, in $|\boldsymbol{P}^+|^2$ and $|\boldsymbol{P}^-|^2$ [274]. Although $\Sigma$ for $\gamma n \to \pi^0 n$ is not yet known, there is already sufficient information to allow some discussion of these quantities. The contributions to $|\boldsymbol{P}^+|^2$ from $I = 0$ and 1 are very similar in magnitude (up to the VMD factor of ~350), and in shape, to their hadronic counterparts. For the reasons put forward in §4D.5, these $\omega$ and $\rho$-like amplitudes are expected to have small spin coherence. However, unlike $\omega$ and $A_2$, the $\omega$ and $\rho$ amplitudes are expected to have similar phases (SU(3) symmetry) and so there is more chance of an interference effect. The data do show an interference in $\boldsymbol{P}^+$ (basically a reflection of $d\sigma/dt\ (\gamma p \to \pi^0 p) > d\sigma/dt \cdot (\gamma n \to \pi^0 n)$) which is roughly consistent with SU(3) symmetry assuming $F/D \simeq -3$ (0.4) for nucleon helicity non-flip (flip) [274].

$|\boldsymbol{P}^-|^2$ for $I = 0$ is surprisingly large and is in fact comparable with the $I = 1$ component (normalisation: $\boldsymbol{P}^-(\pi^0 p) = \boldsymbol{P}^-(I = 0) + (1/r)\boldsymbol{P}^-(I = 1)$, see table 4D.1). This result reflects the experimental fact that $\Sigma(\gamma p \to \eta p) > \Sigma(\gamma p \to \pi^0 p)$ [301], a result which few Regge cut models predicted, since they usually generate unnatural parity exchange in $\gamma p \to (\pi^0, \eta)p$ by B exchange and/or absorption of the $\rho$ exchange in $P^-_{+-}$ (both are $I = 1$). Realistic models for neutral photoproduction must therefore contain isoscalar unnatural parity Regge poles e,g, H exchange [139].

### 4D.7. Hypercharge exchange processes

In processes such as $\pi^- p \to K^{*0}\Lambda$ and $K^- p \to \omega\Lambda$ sufficient experimental observables are available (with an unpolarised target, 10 out of the 12 pieces of independent information) to enable meaningful amplitude analyses [105] and to constrain tightly Regge fits [122]. Until recently, limited experimental statistics allowed only qualitative statements about the exchange mechanisms. New high statistics bubble chamber data on $K^- p \to (\rho, \omega, \phi)\Lambda$ [245] will allow more detailed analyses.

Assuming SU(3) and magic mixing of the $\omega$ and $\phi$ (or equivalently, the quark model) one obtains the amplitude relations (section 4C),

$$\boldsymbol{P}^\mu(K^- p \to \rho^0 Y) = \boldsymbol{P}^\mu(K^- p \to \omega Y) \tag{4D.3}$$

$$\boldsymbol{P}^\mu(\pi^- p \to K^{*0} Y) = \boldsymbol{P}^\mu(K^- p \to \phi Y), \tag{4D.4}$$

where $Y = \Lambda^0$, $\Sigma^0$ or $\Sigma(1385)^0$. Where testable, these relations are found to be well satisfied (see section 4C). The further assumption of EXD Regge poles leads to the equivalence of the amplitude moduli in eqs. (4D.3, 4D.4) in close analogy with the line-reversal symmetry relations discussed in section 4B:

$$|\boldsymbol{P}^\mu(K^- p \to \rho^0 Y)|^2 = \tfrac{1}{2}|\boldsymbol{P}^\mu(K^- p \to \phi Y)|^2. \tag{4D.5}$$

High statistics, high energy, data for the sum of the $Y = \Lambda^0$ and $Y = \Sigma^0$ final states is available at 13 GeV/$c$ [302] where it is found that eq. (4D.5) is well-satisfied for $|\boldsymbol{P}^+|^2$ within small errors (fig. 4D.6). At 4.2 GeV/$c$, the "real" process is some two times larger than the "rotating", in keeping with the usual CEX and HYCEX line-reversal violation systematics. It is, however, the opposite effect to the breaking found in the SU(3) analogous processes $K^+ n \to K^{*0} p$ and $K^- p \to \bar{K}^{*0} n$ at 4 to 6 GeV/$c$ where the mechanism is $\pi$-cut/$\rho$ exchange interference (see §4D.4). Since the K and its cuts are relatively

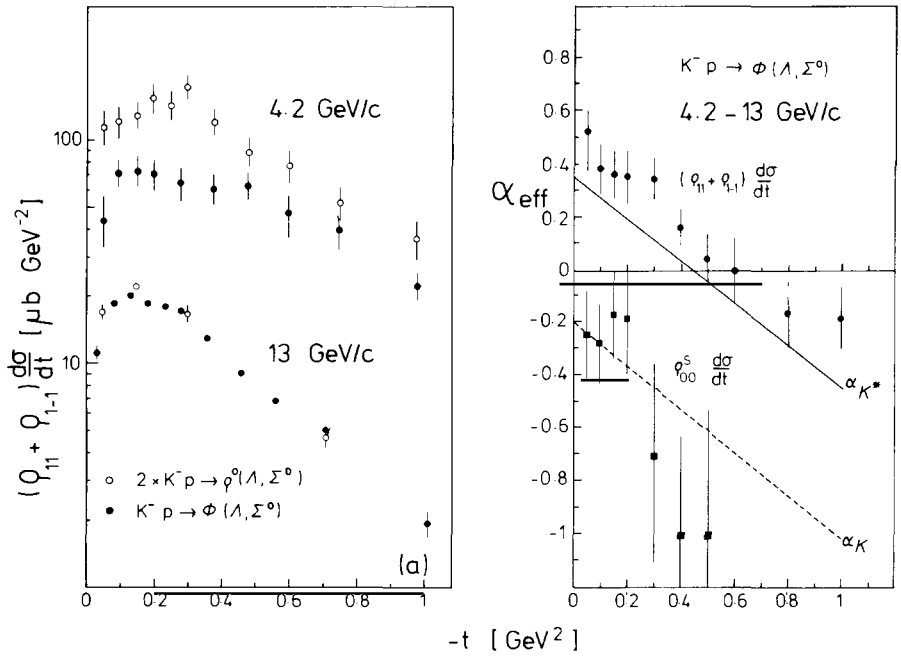


Fig. 4D.6. (a) A test of the EXD and SU(3) predictions for $K^- p \to \rho(\Lambda^0,\Sigma^0)$ and $K^- p \to \phi(\Lambda^0,\Sigma^0)$ by natural parity exchange. (b) Effective trajectories for the natural parity and unnatural parity exchange components of the same data [245, 106, 302]. At 4.2 GeV/$c$, both $\rho(\Lambda,\Sigma)$ and $\omega(\Lambda,\Sigma)$ data (equivalent by SU(3)) have been used.

less important and $\boldsymbol{P}^+$ is dominated by the nucleon non-flip component (K* exchange), this difference is not so surprising. The EXD breaking seems to be in $|\boldsymbol{P}^+_{++}|^2$ itself and decreases rapidly with energy (apparently zero at 13 GeV/$c$).

There is little firm evidence of EXD breaking in $|\boldsymbol{P}^0|^2$ either at 4 or 13 GeV/$c$. However $|\boldsymbol{P}^-|^2$ shows large breaking (a factor of 2 to 7) at 13 GeV/$c$. Since $|\boldsymbol{P}^-|^2$ is expected to be a rather opaque conglomeration of poles and cuts no immediate conclusions follow. In fig. 4D.6, are shown the $\alpha_{\text{eff}}(t)$ values for $|\boldsymbol{P}^+|^2$ and $|\boldsymbol{P}^0|^2$. Both show skrinkage and are respectively similar to K* and K Regge trajectories.

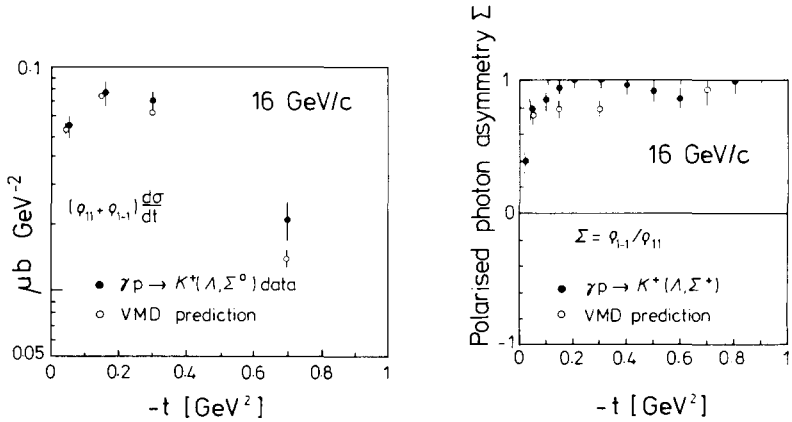


Fig. 4D.7. Comparison of $\gamma p \to K^+(\Lambda,\Sigma^0)$ data [53, 284] with predictions based on vector meson dominance (see §4D.7) and the data of fig. 4D.6.

Cross-section and polarised photon asymmetry data for the VMD related process $\gamma p \to K^+(\Lambda + \Sigma^0)$ are available at 16 GeV/$c$. Since $\gamma \sim \rho + \frac{1}{3}\omega + \sqrt{\frac{2}{3}}\phi$ one can make a VMD comparison using hadronic data for $\rho p \to K^+(\Lambda + \Sigma^0)$ and $\phi p \to K^+(\Lambda + \Sigma^0)$ which are respectively "rotating" and "real" processes. One can make the plausible assumption that these are respectively given by the $K^- p \to \phi(\Lambda + \Sigma)$ and $K^- p \to \rho(\Lambda + \Sigma)$ data and that the necessary, but not crucial, amplitude phase difference is given by the naive EXD argument ($\sim e^{-i\pi\alpha(t)}$). The result of such a VMD comparison, scaled to 16 GeV/$c$, is shown in fig. 4D.7. The agreement is rather close except that (as is often the case, see section 4F) the fraction of natural parity exchange is higher for photoproduction.

### *4D.8. Charge-exchange $\phi$ and $\omega$ production*

Simple Regge exchange ideas predict $\pi N \to \omega N$ and $\pi N \to \phi N$ to have identical production properties up to an overall scale factor, $Z = g^2_{\phi\rho\pi}/g^2_{\omega\rho\pi} \simeq 1/400$ (as estimated from $\Gamma_{\phi\to 3\pi}/\Gamma_{\omega\to 3\pi}$). For the natural parity exchange components $|\boldsymbol{P}^+|^2$, this appears to be true at 6 GeV/$c$, the ratio being $0.0023 \pm 0.0004$ [304]. However, the unnatural parity components $|\boldsymbol{P}^0|^2$ have different behaviours – $\phi N$ has a much flatter $t$-dependence and drops as $s^{-5}$ between 4 and 6 GeV/$c$. This very rapid energy dependence, also seen in $d\sigma/dt$ from just above threshold [192], has been interpreted in terms of double exchange diagrams [300]. However, since the anomalous behaviour appears to be in the overall unnatural parity exchange amplitudes $|\boldsymbol{P}^0|$, this mechanism would require an unnatural $\otimes$ natural parity exchange structure (not the K $\otimes$ K diagram considered). Since the leading single Regge exchanges are so suppressed ($Z \sim 1/400$), it is clear that any exchange model for $\pi N \to \phi N$ will have to contain some sort of higher order diagram (unitarity, Regge–Regge cut, etc.).

### *4D.9. Vector meson and $J^P = \frac{3}{2}^+$ baryon production*

With the obvious exception of $I = 0$ exchange, all the exchange mechanisms and SU(3) relationships discussed in §4D.1 to §4D.8 may also be studied in processes involving the production of a $J^P = \frac{3}{2}^+$ baryon in the final state. In these reactions, the natural parity exchanges are largely confined to helicity flip baryon vertices (see appendix A) while the unnatural parity poles can now contribute to all baryon helicity states but, in contrast to the nucleon case, predominantly to helicity non-flip. The CEX processes such as $\pi^+ p \to \rho^0 \Delta^{++}$ and $K^+ p \to K^{*0} \Delta^{++}$ are well described by the simplest Regge pole with Williams pion absorption model (see, for example fig. AA.4). They provide a useful source of information on non-evasive overall helicity non-flip $\pi$ exchange ($n = 0$, $x = 0$) in contrast to $\pi^- p \to \rho^0 n$, etc., which are dominated by $n = 1$ amplitudes. Because of the large number of helicity states involved, analysis of $\pi^+ p \to \rho^0 \Delta^{++}$ into amplitudes is more complicated than for $\pi^- p \to \rho^0 n$ (§4D.1). With extra model-dependent assumptions (basically the testable quark model baryon coupling scheme) it is possible to obtain the amplitude structure from the decay angular distributions of $\pi N \to \pi\pi\Delta$ (containing all but three of the required pieces of information) [164, 324]. In particular, one may extract the usually unobtainable relative phase between natural and unnatural parity exchange amplitudes – for example, between $P^0_{+-}$ and $P^+_{+-}$ (in a similar notation as for $\pi^- p \to \rho^0 n$). This phase [324] shows precisely the behaviour expected in the simplest $\pi$ cut and $A_2$ exchange models. In §4D.4 this phase behaviour was indirectly inferred from natural–natural interferences.

For the HYCEX reactions such as $K^- p \to \rho\Sigma(1385)$ even more information is available in principle (22 out of 23 independent measurable quantities). At present, lack of statistics prevents detailed conclusions being drawn from such analyses. However many of the constraints implied by duality

(real amplitudes) and the quark model (class A and B relations, see section 4C) are apparently satisfied [292].

In summary, the exchange mechanisms of vector production processes are now understood to roughly the same extent that $0^{-}\frac{1}{2}^{+}$ scattering was understood in the late sixties. The detailed knowledge of amplitude phases from polarisation measurements, etc., is not yet sufficient to enable discussion of peripherality of imaginary parts and other technical issues – compare our present knowledge of $\rho$ exchange in $\pi^- p \to \omega^0 n$ and in $\pi^- p \to \pi^0 n$. Nonetheless, the basic exchanges have been identified and considerable progress in establishing the non-pole-like correction systematics has been made. Forthcoming polarisation studies and high energy, high statistics data are expected to accelerate this progress considerably.

## 4E. Unnatural parity exchanges

Unnatural parity Regge pole exchanges are, in general, less well studied than the dominant natural parity poles ($\rho$, $A_2$, etc). This is both because they are lower lying and because they only occur in processes with rather complicated spin structure e.g. baryon–baryon scattering or vector meson production. According to the $L$-excitation quark model there are four nonets of unnatural parity mesons which should give rise to sizeable exchange contributions. These have $J^{PC} = 0^{-+}$, $1^{+-}$, $1^{++}$ and $2^{--}$, corresponding to $q\bar{q}$ states of $^{2s+1}L_J = {}^1S_0$, ${}^1P_1$, ${}^3P_1$ and ${}^3D_2$ respectively, and are listed in table 4E.1. Some of their expected and observed properties are also summarised in the table.

Table 4E.1

Summary of the expected and observed properties of unnatural parity Regge poles. Masses in brackets are estimated assuming EXD with the corresponding trajectory in the LH part of the table ($\alpha' = 0.82$). The symbols "?" and "??" signify an unclear experimental or theoretical status (the second symbol denotes a greater degree of confusion).

| a) | | $J^{PC} = 0^{-+}$ | | | | | $J^{PC} = 1^{+-}$ | | | | | |
|---|---|---|---|---|---|---|---|---|---|---|---|---|
| Regge pole | $\alpha(0)$ | Production | Exchange | | Shrinkage | Regge pole | Mass [MeV] | Production | Exchange | | Shrinkage |
| | | | Seen | Expected | | | | | Seen | Expected | |
| $\pi$ | −0.02 | yes | yes | yes | yes | B | 1235 | yes | yes | yes | yes |
| $\eta$ | −0.25 | yes | no | no | – | H | (1235) | no | ? | ? | – |
| $\eta'$ | −0.75 | yes | no | no | – | H' | (1460) | no | no | no | – |
| K | −0.20 | yes | yes | yes | yes | $K_B$ | 1300? | ? | ?? | ? | – |

| b) | | $J^{PC} = 1^{++}$ | | | | | $J^{PC} = 2^{--}$ | | | | | |
|---|---|---|---|---|---|---|---|---|---|---|---|---|
| Regge pole | $\alpha(0)$ | Production | Exchange | | Shrinkage | Regge pole | Mass [MeV] | Production | Exchange | | Shrinkage |
| | | | Seen | Expected | | | | | Seen | Expected | |
| $A_1$ | ~0 | no | yes | small | – | Z | (1560) | no | yes | yes | ? |
| D | −0.35 | yes | no | no | – | $Z_0$ | (1690) | no | no | no | – |
| E | −0.64 | yes | no | no | – | $Z_0'$ | (1795) | no | no | no | – |
| $K_A$ | −0.39? | ? | ?? | ? | – | $K_Z$ | (1700) | no | ?? | ? | – |

### *4E.1. Relative importance of unnatural parity exchanges*

We list some of the features which govern the "visibility" in the data of a particular Regge pole. The first 5 points are relevant to both natural and unnatural parity exchange:

(1) The lower the mass for a given spin, the higher lying is the trajectory, and hence the more important the exchange at high energies ($\sim s^{\alpha(t)}$).

(2) If the lowest state on the trajectory has a small mass, then the resulting singularity can have a strong influence on the physical region, e.g. for the pion $1/\sin \pi\alpha(t) \sim 1/(t-\mu^2)$.

(3) Odd signature exchanges ($\sim 1-\exp\{-i\pi\alpha(t)\}$) are suppressed with respect to even ones near $\alpha(t)=0$ (e.g. B/$\pi$ and $A_1$/Z near $t=0$ and $\rho/A_2$ near $-t=0.6$). Even signature exchanges are suppressed near $\alpha(t)=-1$, i.e. usually well away from $t=0$. This assumes a NWSZ structure.

(4) Because target and projectile in general have non-zero isospin, $I=1$ exchange is much more readily isolated than $I=0$ which usually occurs along with $I=1$ and requires non-trivial data analysis (cf. the discussion of $\pi^-p\to\rho^0n$ and $\pi^\pm p\to\rho^\pm p$ in section 4D).

(5) Strange ($I=\frac{1}{2}$) EXD partners are difficult to separate since there are no $G$-parity constraints (e.g. K and $K_B$ always occur together).

Two further considerations are specific to unnatural parity poles.

(6) SU(6) predicts [12] that, for the $1^{++}$ and $0^{-+}$ couplings to octet baryons, the $F/D$ mixing parameters are $\frac{2}{3}$. Couplings analogous to KN$\Sigma$ and $\eta$NN are therefore expected to be small. The $I=0$ exchanges in table 4E.1 have been listed in order of increasing mass ($m_{H'} > m_H$). Apart from $\eta, \eta'$, their mixing properties are not known experimentally. If they are magically mixed, cf. the $\omega$ and $\phi$, then one expects only the $\omega$-like exchange to couple strongly to nucleons.

(7) For $I=0$ or 1 meson exchanges, $C$-parity constrains their couplings to nucleons,

$$g_{\lambda_4\lambda_2}(t) = CP(-)^{\lambda_4-\lambda_2} g_{\lambda_2\lambda_4}(t). \tag{4E.1}$$

($P$, $C$ are the parity and $C$-parity of the exchange.) Together with eq. (2.2) this implies

$$g_{\lambda_4\lambda_2}(t) = C\tau g_{-\lambda_2-\lambda_4}(t), \tag{4E.2}$$

so that the $\pi$ and B nonets ($CP=-1$) couple only to helicity flip while the $A_1$ and Z nonets ($C\tau=-1$) couple only to non-flip. Note that all natural parity exchanges have $CP=C\tau=+$ (as predicted for example by the quark model) so that no helicity coupling constraints exist in that case.

(8) For strange meson couplings to octet baryons, eq. (4E.1) does not apply except in the limit of exact SU(3) (e.g. equal N and $\Sigma$ masses). In principle, therefore, off-diagonal helicity couplings can exist for $(K, K_B)$ and $(K_A, K_Z)$ (see for example [318] and appendix A).

Although one expects all the trajectories in table 4E.1 to contribute to two-body processes, many exchanges will be difficult to observe in practice, because of considerations like the above. For example, the $\eta$ [(4), (6)], $\eta'$ [(1), (4)], $A_1$ [(3)], $K_A$, $K_B$, $K_Z$ [(8)] are not expected to show themselves easily. In the next subsections some of the more likely candidates are discussed.

### *4E.2. $\pi$ and* B *exchange*

The pion satisfies all criteria for a prominent exchange and consequently it has been relatively well studied. Because of the short extrapolation distance to $t=m_\pi^2$, its coupling strength in a given process can be successfully predicted (see, for example, section 4D and appendix A). There are no known exceptions to this.

In evasive amplitudes ($x\neq 0$, eq. (2.5)) some form of absorption is apparently present. The Williams

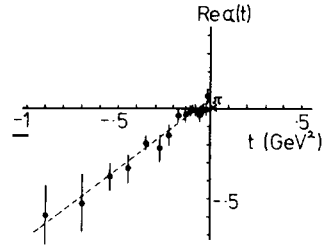


Fig. 4E.1. The effective trajectory deduced from $\pi^- p \to \pi^0 \pi^0 n$ data in the range 2 to 50 GeV/$c$ [252]. The best-fit straight-line $[(0.04 \pm 0.04) + (0.74 \pm 0.14)t]$ passes close to the $\pi$ pole (marked by ×).

model provides a simple and reliable method of describing these effects (see appendix A), except that there appears to be some mass-dependence of the absorption strength (see section 4F). There is firm evidence of some degree of shrinkage in $\pi$ exchange but the precise value of the trajectory slope is not reliably known ($\alpha' \sim 0.2$–$0.8$). Figure 4E.1 shows a recent determination of $\alpha_{\text{eff}}(t)$ from $d\sigma/dt \cdot (\pi^- p \to \pi^0 \pi^0 n)$ which should be dominated by $\pi$ exchange [252]. Although it is consistent with $\alpha' \sim 0.8$, the result beyond $t = -0.2$ depends critically on the use of data at $p_{\text{LAB}} = 2$ GeV/$c$. The same is true of determinations from $\pi^- p \to \rho^0 n$ (§4D.1) where the shrinkage is largely due to a shoulder in the $t$-distributions of the low energy (3 or 4 GeV/$c$) data.

B exchange is expected, and observed in $\pi N \to \omega N$, $\omega\Delta$ (§4D.2). Its phase relative to $\pi$ exchange has been measured in $\rho$–$\omega$ interference experiments (§4D.4) and is roughly as expected of an odd signature Regge pole with a trajectory similar to that of the $\pi$. The $\alpha_{\text{eff}}$ measured in $\pi^+ p \to \omega \Delta^{++}$ from 3 to 16 GeV/$c$ [200] shows a small degree of shrinkage ($\alpha'_{\text{eff}} \approx 0.6 \pm 0.3$ for $\rho_{00}\, d\sigma/dt$ in the $t$-channel).

### *4E.3. Strangeness exchange*

The small mass of the K meson allows it to show up in the same way as the $\pi$, but to a lesser extent. One expects K-exchange in processes such as $K^- p \to \phi\Lambda$ (dominantly $n = 1$, cf. $\pi^- p \to \rho^0 n$) and $K^- p \to \phi\Sigma^*(1385)$ ($n = 0$) and $\bar{p}p \to \bar{\Lambda}\Lambda$ ($n = 0$, $x = 2$, cf. $\bar{p}p \to \bar{n}n$). Figure 4E.2 shows a comparison of $\rho_{00} \cdot d\sigma/dt$ for $K^- p \to \phi\Sigma^*(1385)$ and for $\pi^+ p \to \rho^{*0}\Delta^{++}$ where the latter has been multiplied by the SU(3)

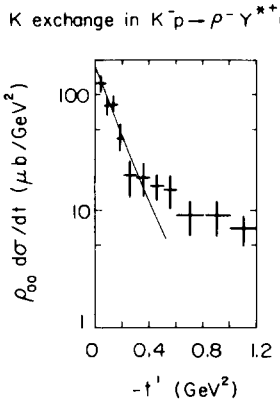


Fig. 4E.2. $\rho_{00}\, d\sigma/dt$ ($K^- p \to \rho^- \Sigma^{*+}$) data [292] compared with the broken SU(3) (§4C.4) K exchange prediction made from $\pi$ exchange in $\rho_{00} \cdot d\sigma/dt$ ($\pi^+ p \to \rho^0 \Delta^{++}$) (solid curve).

factor 6 and a factor $(t - m_\pi^2)^2/(t - m_K^2)^2$ to help take account of SU(3) mass-breaking. The agreement is very satisfactory.

Figure 4D.6 shows evidence for shrinkage of K exchange. It must however be remembered that $|P^0|^2$ (defined in §4D.1) contains contributions from both K and $K_B$ exchange. In fact, one expects an EXD $K_B$ contribution ($\sim 1 - \exp\{-i\pi\alpha(t)\}$) to dominate beyond $-t = 0.2$ or 0.4. The absorptive corrections to K exchange are not well studied and could provide additional insight into the behaviour of $\pi$ exchange itself. For example, the two pairs of line-reversed reactions ($np \to pn$, $\bar{p}p \to \bar{n}n$) and $\Lambda p \to p\Lambda$, $\bar{p}p \to \bar{\Lambda}\Lambda$) should illuminate the comparative properties of $\pi$ and K cuts.

The evidence for $K_A$ and $K_Z$ exchange contributions, which theoretically could be sizeable (see appendix A), is ambiguous because of points (5) and (8) above. Non-zero values of the unnatural parity exchange polarisation $T_0$ (see appendix B) imply the presence of both flip and non-flip nucleon helicities [105, 121] but not necessarily both (K, $K_B$) and ($K_A$, $K_Z$) exchange.

### *4E.4.* $A_1$*-like exchanges*

Because of point (3) above, $A_1$ Regge pole exchange is expected to be small near $t = 0$ if $\alpha_{A_1}(0) \approx 0$. However the unnatural parity exchange polarised target asymmetry for $\pi^- p \to \rho^0 n$ has recently been measured at 17.2 GeV/$c$ [299] and is non-zero (fig. 4E.3). The non-flip amplitude $|P^0_{++}|$, containing the $A_1$-like exchanges, can be estimated from this preliminary data (§AB.4) to be at least 15–20% of the dominant $\pi$-exchange amplitude for $|t| < 0.3$. The origin of this relatively large amplitude is not yet understood.

The EXD partner of the $A_1$, the Z Regge pole, is not suppressed at $\alpha = 0$ and estimates [272] suggest a significant contribution to $\pi N \to \omega N$ in agreement with data for $\rho_{00}\, d\sigma/dt$ [329] and indications from $\rho$–$\omega$ interference effects (§4D.4). Figure 4E.4 shows the expected $\rho_{00}\, d\sigma/dt$ distributions for $\pi^- p \to \omega^0 n$ and $\pi^+ n \to \omega^0 p$ in two models with [228] and without [222] Z exchange. At small $t$ there is small spin coherence in the first model since $\pi N \to \omega N$ is dominated by Z ($P^0_{++}$) and $\pi N \to \rho N$ by $\pi$ exchange ($P^0_{+-}$) so that little difference is expected between the $\pi^+ n$ and $\pi^- p$ reactions. Preliminary data are in agreement with this [329].

Axial exchanges with $\tau C = -1$ thus seem to be significant in resonance production processes. Little is yet known of their Regge properties (phase, shrinkage) nor yet of possible absorption systematics.

To summarise, the quark model predicts a rich spectrum of unnatural parity exchanges each of

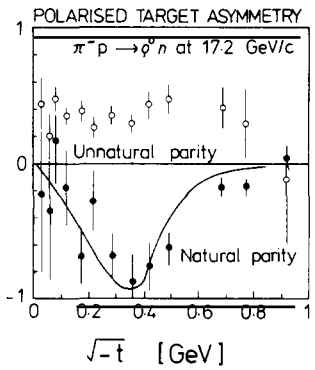


Fig. 4E.3. The polarised target asymmetry associated with (eq. (4B.15)) natural parity exchange (solid points) and unnatural parity exchange (open points) in $\pi^- p \to \rho^0 n$ at 17 GeV/$c$ [299]. The solid curve is a theoretical prediction [228].

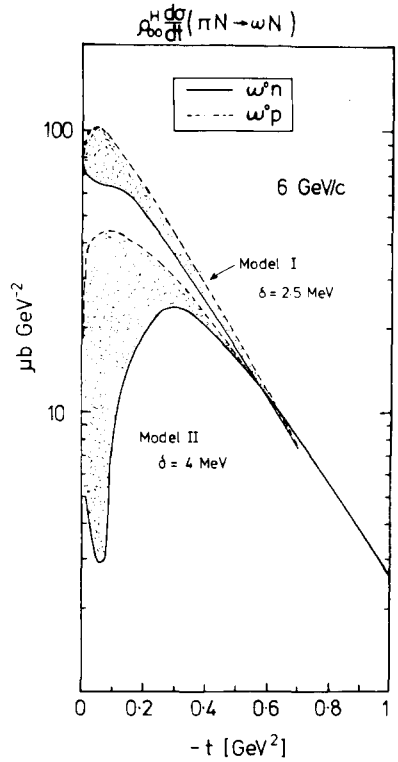


Fig. 4E.4. Theoretical predictions of two models (I [228] and II [222]) for the $\rho$–$\omega$ interference effects expected in $\pi^+ n \to \omega^0 p$ and $\pi^- p \to \omega^0 n$ at 6 GeV/$c$.

which will contribute to some or other reaction. However, for various reasons, only a few of these exchanges are expected to be easily detectable in practice. Exchanges with $\pi$-like quantum numbers ($\tau C = +$) are well-studied – those with $A_1$-like quantum numbers ($\tau C = -$) also play an important role, but are less well understood.

## 4F. External mass dependence of exchange mechanisms

The increasing abundance of resonance production data has shed light on two important questions: what is the relation between produced resonances and how do their production mechanisms depend on their mass and spin? These questions reflect both the spectroscopic and dynamical (or scattering) aspects of hadron physics. For example, a study of $\pi^- p \to \pi^+ \pi^- n$ is expected to yield spectroscopic information ($\pi\pi$ phase shifts and resonance parameters) and, at the same time, illuminate the production systematics of $\pi^- p \to (\rho^0, f, g^0, h \ldots) n$. From one viewpoint, we are looking at the Regge trajectory $\alpha(m^2)$ for $m^2 > 0$. From another viewpoint we are studying Reggeon-particle scattering as a function of $t_{\pi\pi}$ and $m^2$ (see fig. 4F.1a and b). This interplay between produced and exchanged hadronic states is of fundamental interest.

An important feature of most exchange processes is the presence of absorptive corrections, some of whose properties are best understood from direct channel or geometrical arguments (section 3)

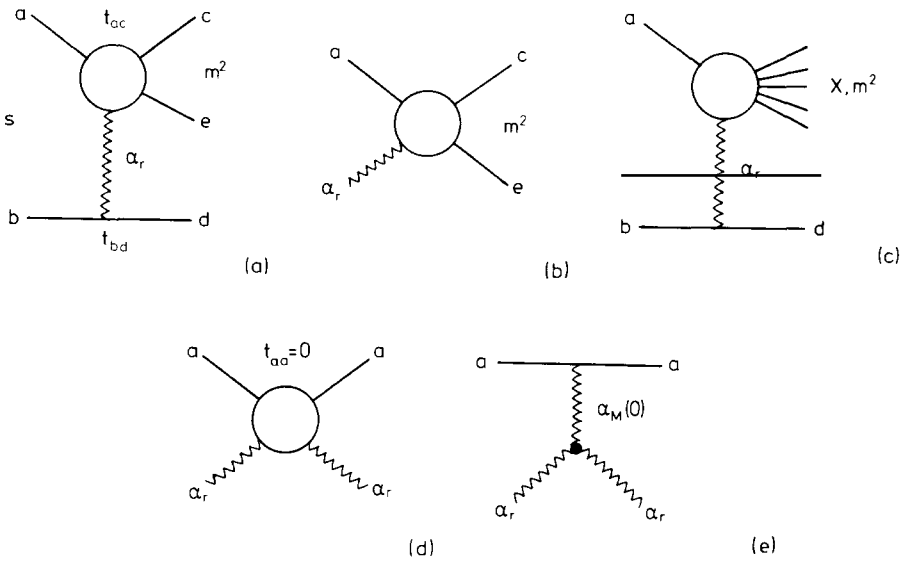


Fig. 4F.1. High energy production amplitudes [(a), (c)] and related Reggeon-particle scattering amplitudes [(b), (d)]. Amplitude (e) is a Regge pole approximation to (d).

while others are more directly related to the $t$-channel (section 4G). In either approach, the variable $m^2$ should provide a useful tool in our efforts to clarify the nature and origin of absorption.

Reggeon-particle scattering can be conveniently studied in two regimes:

(1) Single-particle inclusive processes (fig. 4F.1c) are related via the Muller–Regge approach [77] to a forward elastic Reggeon–particle scattering amplitude (fig. 4F.1d). This relation is the Reggeon–particle scattering analogue of the optical theorem for particle–particle collisions.

(2) From an exclusive two-particle production amplitude (fig. 4F.1a) one can obtain, by factorisation, a Reggeon–particle goes to particle–particle scattering amplitude (fig. 4F.1b). A similar procedure (but assuming elementary $\pi$ exchange) is used in the Chew–Low method of extracting $\pi\pi$ scattering cross-sections [1].

### *4F.1. Reggeon–particle scattering and finite-mass sum rules*

It has been demonstrated [e.g. 117, 129, 135] that so-called finite-mass sum rules (FMSR) may be written for the amplitude of fig. 4F.1d. In analogy with FESR for particle–particle scattering, the constraint imposed by duality can make such sum rules highly predictive, i.e. the known high energy (or mass) Regge behaviour and low energy resonance contributions are strongly correlated. In particular, the FMSR give rise to correlations between the exchanged trajectory and the produced system, through the triple-Regge formula [199] for the high mass behaviour

$$\frac{d^2\sigma}{dt\, dm^2} \sim \frac{1}{s}(m^2)^{\alpha_M(0)}(s/m^2)^{2\alpha_r(t)}. \tag{4F.1}$$

The extra factor $(s/m^2)^{2\alpha_r(t)}$ (byond the obvious $(m^2)^{\alpha_M(0)}$) is difficult to justify, in anything less than a full mathematical derivation. The variable $s/m^2$ can, however, be thought of as the available (sub-) energy in this particular Regge limit.

A rather attractive experimental test of eq. (4F.1) is presented in fig. 4F.2. This shows the value of $\alpha_r(t)$ obtained by fitting eq. (4F.1) to data on the inclusive processes $K^-p \to \Lambda X$ both in the target fragmentation region ($\alpha_r \sim \alpha_{K^*}$) and in the beam fragmentation region ($\alpha_r \sim \alpha_N$). Two, distinct, linear trajectories are obtained [250].

Hoyer, Roberts and Roy [161] have investigated the phenomenology of the FMSR by saturating the low-mass side of the sum rule with resonance production cross-sections (the high mass side has the triple-Regge behaviour, eq. (4F.1)). One obtains an expression of the form

$$\left[\frac{d\sigma^R}{dt}\right]_{\alpha_r} \sim (m^2)^{\alpha_M(0)-2\alpha_r(t)} \tag{4F.2}$$

where $\alpha_M$ is the leading trajectory dual to the resonances (R) which dominate the final state X (see fig. 4F.1e). Equation (4F.2) has three simple and directly testable consequences [161]:

(1) The ratio of exchange contributions due to natural and unnatural parity Regge poles is

$$\mathcal{R}^R(m^2) \equiv \left[\frac{d\sigma^R}{dt}\right]_{\alpha UP} \Big/ \left[\frac{d\sigma^R}{dt}\right]_{\alpha NP} \approx (m^2)^{2(\alpha_{NP}-\alpha_{UP})} \approx m^2 \tag{4F.3}$$

if $\alpha_{UP}(0) \approx 0$ and $\alpha_{NP}(0) \approx 0.5$ i.e. natural parity exchange is relatively less important for higher mass resonances.

(2) $$\left[\frac{d\sigma^{R_2}}{dt}\right]_{\alpha_r} \Big/ \left[\frac{d\sigma^{R_1}}{dt}\right]_{\alpha_r} \approx (m_2^2/m_1^2)^{\alpha_M(0)-2\alpha_r(t)} \tag{4F.4}$$

for production of resonances $R_i$ of mass $m_i$, i.e. the relative abundance of two resonances in a given channel depends on the exchanged trajectory: higher masses are favoured by lower-lying trajectories.

(3) $$\left[\frac{d\sigma^R}{dt}(t=t_1)\right]_{\alpha_r} \Big/ \left[\frac{d\sigma^R}{dt}(t=t_2)\right]_{\alpha_r} \approx (m^2)^{2\alpha'(t_2-t_1)} \tag{4F.5}$$

i.e. resonance production $t$-distributions flatten (antishrink) with increasing mass.

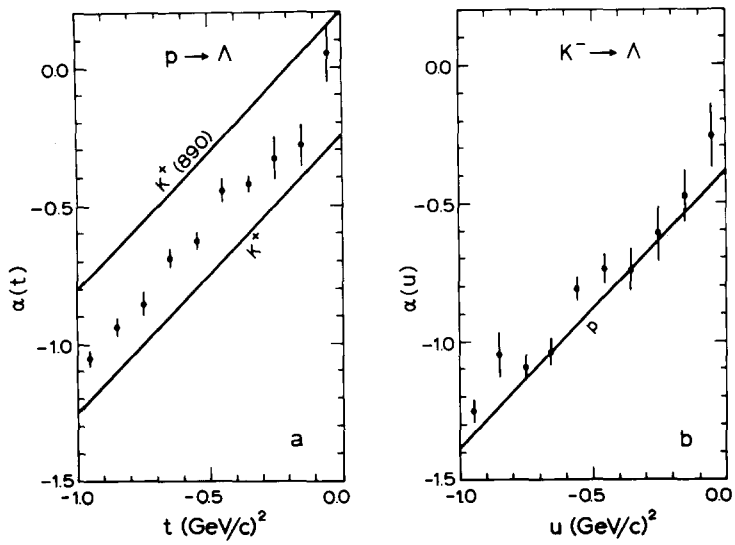


Fig. 4F.2. Effective trajectories deduced [250] from $K^-p \to \Lambda X$ at 4.2 GeV/$c$ using a triple-Regge parametrisation in the target fragmentation region (meson exchange) and in the beam fragmentation region (baryon exchange).

Hoyer et al. [161] found (1)–(3) to be compatible with available data on $\pi N \to XN$ and $KN \to XN$. In fig. 4F.3 the $\pi$ exchange contributions in $\rho$, f and g production are compared with eq. (4F.2). The agreement, here, is not surprising since the $\pi$ exchange sum rule (using data at small $t_{NN}$) is very close to an FESR for on-shell $\pi\pi$ scattering. Also shown is a comparison of eq. (4F.3) with data on $KN \to KX$ ($\omega + f$ and $\pi$ exchange). Recent data on $\pi^- p \to \pi^+ \pi^- n$ has allowed a more precise study of the ratio $\mathcal{R} \equiv UP/NP$ ($\sim \pi/A_2$) as a function of mass. It is found to be compatible with eq. (4F.3) [169, 227, 278]. An analogous study of the ratio of $B/\rho$ exchange in $\pi N \to \omega N$ and $\pi N \to A_2 N$ at 4 GeV/$c$ [263] again shows rough consistency with eq. (4F.3).

In these applications, the mass-dependence studied was that of a meson resonance system (which was itself used to isolate the natural and unnatural parity exchange components of interest). One may also study the mass-dependence of the baryon system recoiling against a given vector meson. For example Paler et al. [282] have measured the K* density matrix elements in the inclusive processes $K^- p \to K^{*-} X^+$ and $K^{*0} X^0$ at 14.3 GeV/$c$. Figure 4F.4 shows the quantity $\mathcal{R}(=UP/NP) = (\rho_{00} + \rho_{11} - \rho_{1-1})/(\rho_{11} + \rho_{1-1})$ as a function of $m_X^2$. The expected increase of the unnatural parity fraction is clearly observed. Chung et al. [259] have compared $\mathcal{R}(m^2)$ for production of the $\Delta(1236)$ and of its

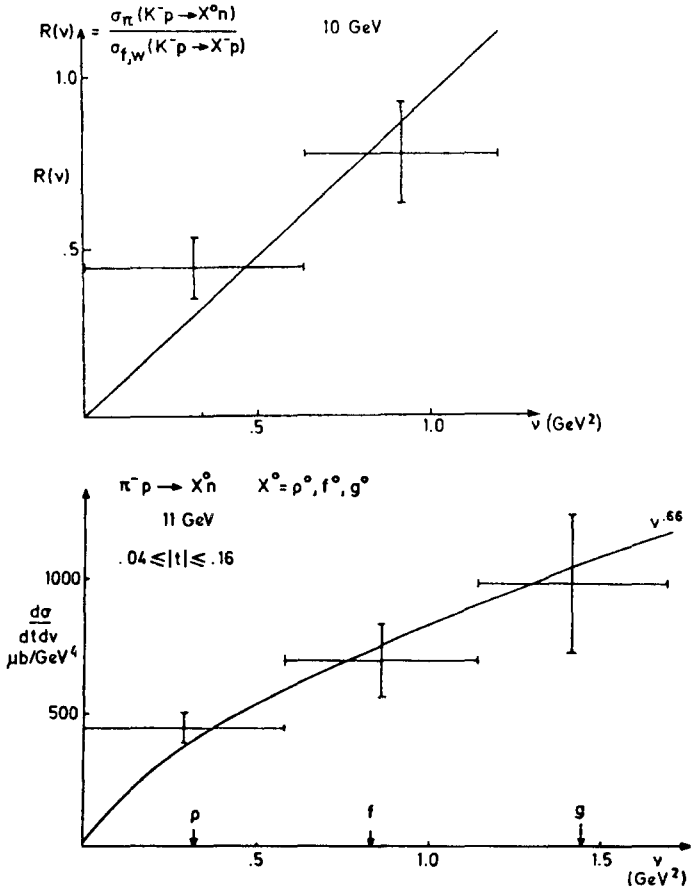


Fig. 4F.3. Below: finite mass sum rule for $\pi^- p \to Xn$ at 11 GeV ($\nu \sim m^2$). Above: the finite mass sum rule prediction for the ratio of unnatural to natural parity exchange compared to data for $K^- p \to XN$ [161].

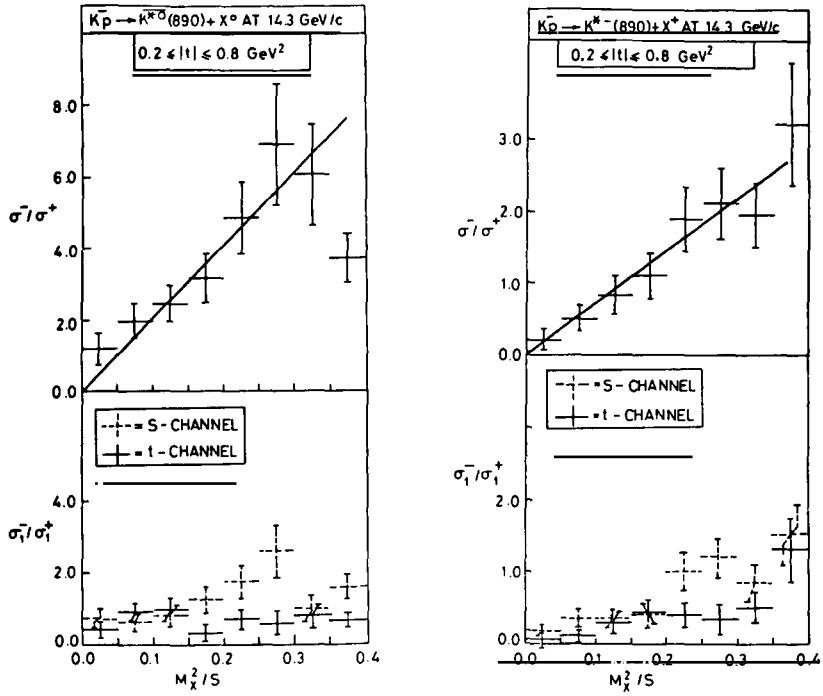


Fig. 4F.4. The ratio of unnatural to natural parity exchange as a function of $m^2/s$ in $K^-p \to K^{*0}X$ and $K^-p \to K^{*-}X$ at 14.3 GeV/$c$ [282]. $\sigma_-$ and $\sigma_+$ are the unnatural and natural parity exchange components projected from the cross-section by the vector-meson density matrix combinations $(\rho_{00} + \rho_{11} - \rho_{1-1})$ and $(\rho_{11} + \rho_{1-1})$ respectively. $\sigma_{1\pm}$ refer to the $s$ or $t$-channel helicity one projections only $(\sigma_{1+} \equiv \sigma_+)$.

$J^P = 7/2^+$ recurrence ($\Delta(1880)$) in association with the $\rho$ and $\omega$. Again, the data show an increase, consistent with $\mathcal{R}\alpha m^2$.

Equation (4F.4) may be used to predict one resonance production cross-section from another. For example Sorensen [238] has successfully predicted $\pi N \to BN$ from a knowledge of $\pi N \to \eta N$ ($A_2$ exchange).

### *4F.2. Exclusive two particle production processes*

Hoyer and Kwiecinski [162] have established FESR for Reggeon–particle goes to particle–particle scattering amplitudes (figs. 4F.1a and b). Together with semi-local duality, these give, e.g. for $ab \to ced$, relations between the resonance production amplitudes of the form

$$\langle \mathrm{Im}\, T_r^R \rangle \sim (m^2)^{\alpha_M(t_{ac}) - \alpha_r(t_{bd})}, \tag{4F.6}$$

where $T_r^R$ is the amplitude for production of resonance $R$ by exchange of Reggeon $\alpha_r$, in the limit $s \gg m^2$. Strictly speaking, these sum-rules are only derivable in the further limit $s_{ed}/s = 0$ (see fig. 4F.1a). Otherwise, the Reggeon particle amplitude has additional (uncalculable) singularities which contribute to the FESR contour integral. This analytic structure has been demonstrated in dual resonance and field theory models [162].

By comparison with FMSR (eq. (4F.2)) the FESR derivation is more complicated and model-dependent. However, the fact that the FESR apply, in the first instance, to individual (helicity) amplitudes rather than cross-sections can make them a more powerful and specialised tool in the

analysis of resonance production data. Also, the dependence on $t_{ac}$ (eq. (4F.6)) gives them additional phenomenological power. Another even more specific approach is the factorised $B_5$ dual model amplitude advocated by Michael [172] as a means of obtaining a four-point amplitude with one particle off-shell (Reggeised). As the Veneziano model is an explicit solution of conventional FESR, so these "dual vertices" are, in a sense, specific solutions of the above off-shell FESR [in particular they give the same predictions for $\mathcal{R}(m^2)$ (eq. (4F.3)) as do eqs. (4F.2) and (4F.6)]. Their very specific character allows the calculation of one resonance production amplitude, $T_r^{R_2}(s,t,m^2)$, from another, $T_r^{R_1}(s,t,m^2)$, where $R_1$ and $R_2$ lie on the same EXD trajectory.

Hoyer et al. [226] have tested the off-shell FESR (eq. (4F.6)) using high statistics data for $\pi^-p\to\pi^+\pi^-n$ at 17.2 GeV/$c$. They conclude that, overall, the sum-rules connecting $\rho$ and f production are well-satisfied. In particular, the $A_2\pi\to\pi\pi$ off-shell FESR works well for $|t_{pn}|\geq 0.3$, suggesting that natural parity $\rho$ and f production are indeed dominated by $A_2$ exchange in this $t$-region, and that non-evasive (cut) corrections are unimportant here. This is in contrast to conventional absorption models (section 3) which generate increasingly large corrections at large $t$. It is also found that the $\pi$-exchange sum-rules require the presence of a $t$-channel helicity one Reggeised $\pi$ coupling consistent in magnitude with that predicted by the $B_5$ approach [172, 228] (see also §4D.1).

### *4F.3. Absorption strength as a function of mass*

The non-evasive cut correction associated with helicity non-flip $\pi$ exchange is one of the most cleanly identifiable absorptive effects. In appendix B (§AB.6) it is shown how the relative cut strength ($C/\pi(m^2)$) in various processes may be determined from the data. Ochs and Wagner [174] have used a generalised Williams model (i.e. with variable cut strength) to describe $\pi^-p\to\pi^+\pi^-n$ (summing over all $\pi\pi$ partial waves) and found a smooth decrease in absorption strength such that $C((1.8\,\text{GeV})^2)/C(m_\rho^2)\approx 0.35$. They also noted a comparable decrease with $m^2$ in $KN\to K\pi N$ data. Martin [169] has examined the ratio $C/\pi(m^2)$ for P, D and F wave $\pi\pi$ production separately and shown it to be a strong function of mass, but not of $\pi\pi$ spin. The combined (P, D, F wave) mass dependence of $C$ [169] is shown in fig. 4F.5.

Comparison of $\pi^-p\to\rho^0n$ ($m^2=m_\rho^2$) with charged-pion photoproduction ($m^2=0$) and electroproduction ($m^2\equiv q^2<0$) might also be expected to reveal mass-dependent effects. It has been shown [271] that the well-known violations of the naive vector meson dominance relation between $\rho$ production and $\pi$ photoproduction can be most simply accounted for by postulating a mass-

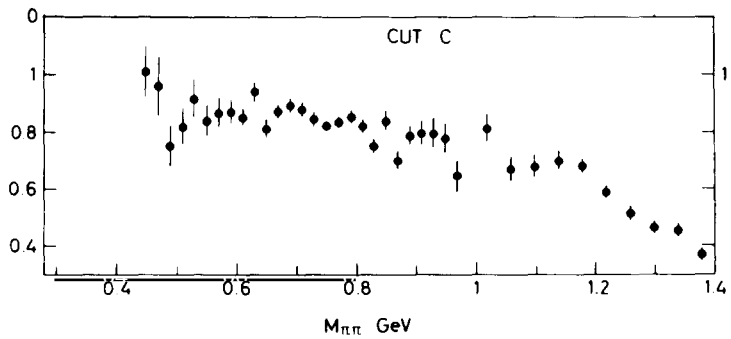


Fig. 4F.5. The mass-dependence of the effective absorption strength $C$ (measured relative to the dominant $\pi$ exchange amplitude) as deduced from data on $\pi^-p\to\pi^+\pi^-n$ at 17.2 GeV/$c$ [169].

dependence of the $\pi$ cut such that $C(m^2=0)/C(m^2=m_\rho^2)\approx 1.4$. As explained in §AB.6, this is readily deduced from the polarised photon asymmetry data ($\Sigma$) and its $\rho$ production analogue (see fig. 4F.6). A continuing increase in $C(m^2)$ as $m^2$ becomes negative can also economically account for some VMD violations in the electroproduction data [271, 239].

So little is known about cuts in other (non-$\pi$ exchange) resonance production processes, that studies of absorption mass-dependence must be considered to be in their infancy. A particularly interesting system is $\pi^0 p\to\rho^0 p$, $\gamma p\to\pi^0 p$ and $\pi^0$ electroproduction, all supposedly dominated by $\omega$ exchange (§4D.3). The dip at $t\approx -0.5$ in the first two may plausibly be the NWSZ of the $\omega$ Regge pole or a pole-cut interference effect. A mass-dependence in the absorption strength could distinguish between these particular possibilities by giving rise to a shift in the dip position observed in $\pi^0$ electroproduction [94]. A recent measurement of the latter process [254] at $\sqrt{s}=2.55$ GeV shows a dramatic $q^2$-dependence relative to $q^2=0$ (the dip disappears) but, unfortunately, is not easily interpretable in terms of either a Regge pole or any known absorption model. Conclusive evidence for a decrease of absorption strength with increasing mass of the produced object is so far confined, therefore, to $\pi$-exchange processes. Whether or not $\pi$-exchange is special in this respect remains to be seen.

Explanations of the decrease can be described as, qualitative incomplete or highly speculative. In the best documented case of $\pi^- p\to\pi^+\pi^- n$, it has been suggested [183] that the cut has contributions from both $\pi$ and $A_2$ absorption. Since the ratio $A_2/\pi$ is known to decrease with $m^2$ (eq. (4F.3)) the $A_2$ cut and hence, to some extent, the total cut should decrease with $m^2$. Quantitatively, however, this effect is much smaller than that observed. It has also been suggested [169] that there may be a connection between the small absorption found in higher mass resonance production and the anomalously low nuclear absorption of multi-pion states as observed in coherent $3\pi$ and $5\pi$ production from nuclei. There have also been various speculations concerning the $q^2$ dependence of the geometrical and absorptive properties of the photon. In view of the very different interaction characteristics of the electromagnetic current near $q^2=m_\rho^2$ (hadronic) and in the deep inelastic region, in practice $q^2\lesssim -1$ (point-like), it is not surprising if its absorptive properties are a strong function of $q^2$.

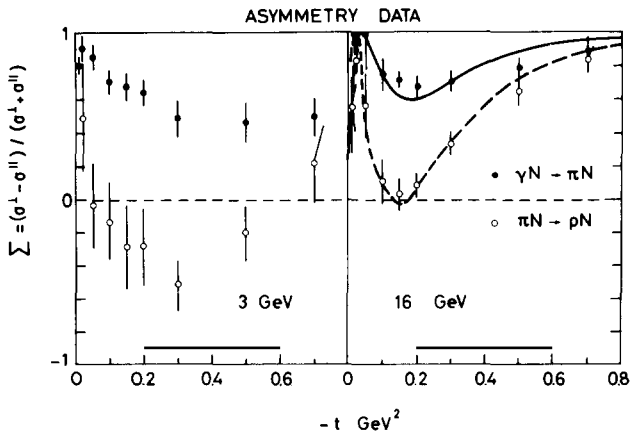


Fig. 4F.6. The polarised photon asymmetry in $\gamma p\to\pi^+ N$ (solid points) compared with the analogous quantity in $\pi^- p\to\rho^0 n$ ($\rho_{1-1}/\rho_{11}$) [271]. Strict vector dominance predicts these to be equal. The curves are the fit obtained in a model which takes account of mass-dependent effects [271].

## 4G. Theoretical aspects of Regge cuts

A major aim of Regge phenomenology has been to deduce, from the data, as much as possible about $j$-plane singularities and to find empirical regularities on which a theory of high energy scattering might be based. It is complemented by a theoretical approach in which one tries to calculate high energy amplitudes from first principles. This has mainly been done through Gribov's Reggeon calculus and the closely related $j$-plane unitarity equations. Although most of the interest has centred around elastic scattering and the nature of the Pomeron, the results are equally applicable to quantum-number exchange processes, in particular to the Reggeon–Pomeron cuts (absorptive corrections) whose importance we have already recognised.

In this section we review the practical constraints on Regge cut structure which emerge from the Reggeon calculus and related considerations. It turns out that although the calculus offers, in principle, a complete scheme for calculating cuts, in practice many unknowns remain and the major results are more in the nature of boundary conditions on the cuts (e.g. particular properties of the branch points) than solutions. Nevertheless, these boundary conditions will become increasingly important as energies rise.

### *4G.1. Reggeon unitarity equations and the Reggeon calculus*

By considering 4-particle unitarity in the $t$-channel, and picking out Regge poles in the 2-particle subchannels one can derive a set of Reggeon unitarity equations [18, 138]

$$\mathrm{disc}_j a(j,t) = \int \mathrm{d}^2\boldsymbol{k}_1\,\mathrm{d}^2\boldsymbol{k}_2 \Delta(t,t_1,t_2)\delta(\alpha_1(t_1)+\alpha_2(t_2)-j-1) N_{\alpha_1\alpha_2}(\boldsymbol{k}_1,\boldsymbol{k}_2) N_{\alpha_1\alpha_2}(\boldsymbol{k}_1,\boldsymbol{k}_2)^*, \tag{4G.1}$$

$$\begin{aligned}\mathrm{disc}_j N_{\alpha_1\alpha_2}(\boldsymbol{k}_1,\boldsymbol{k}_2) = \int \mathrm{d}^2\boldsymbol{k}_1'\,\mathrm{d}^2\boldsymbol{k}_2' \Delta(t,t_1',t_2')\delta(\alpha_1'(t_1')+\alpha_2'(t_2')-j-1) \\ \times N_{\alpha_1'\alpha_2'}(\boldsymbol{k}_1',\boldsymbol{k}_2') B_{\alpha_1'\alpha_2'\alpha_1\alpha_2}(\boldsymbol{k}_1',\boldsymbol{k}_2',\boldsymbol{k}_1,\boldsymbol{k}_2)^*,\end{aligned} \tag{4G.2}$$

$$\begin{aligned}\mathrm{disc}_j B_{\alpha_1'\alpha_2'\alpha_1\alpha_2}(\boldsymbol{k}_1',\boldsymbol{k}_2',\boldsymbol{k}_1,\boldsymbol{k}_2) = \int \mathrm{d}^2\boldsymbol{k}_1''\,\mathrm{d}^2\boldsymbol{k}_2'' \Delta(t,t_1'',t_2'')\delta(\alpha_1''(t_1'')+\alpha_2''(t_2'')-j-1) \\ \times B_{\alpha_1'\alpha_2'\alpha_1''\alpha_2''}(\boldsymbol{k}_1',\boldsymbol{k}_2',\boldsymbol{k}_1'',\boldsymbol{k}_2'') B_{\alpha_1''\alpha_2''\alpha_1\alpha_2}(\boldsymbol{k}_1'',\boldsymbol{k}_2'',\boldsymbol{k}_1,\boldsymbol{k}_2)^*.\end{aligned} \tag{4G.3}$$

These equations are shown diagrammatically in fig. 4G.1. $a(j,t)$ is a $t$-channel partial-wave amplitude for a particle–particle scattering process, continued to complex $j$ and evaluated at $t=-\boldsymbol{k}^2$. Viewed from the $t$-channel, $\alpha_1$ and $\alpha_2$ are two intermediate state Regge poles with $s$-channel transverse momenta $\boldsymbol{k}_1$ and $\boldsymbol{k}_2$ ($t_i=-\boldsymbol{k}_i^2$ and $\boldsymbol{k}=\boldsymbol{k}_1+\boldsymbol{k}_2$). The $N_{\alpha_1\alpha_2}$ are Reggeon–particle scattering amplitudes evaluated at $j=\alpha_1+\alpha_2-1$ ("Gribov vertices"). Likewise, the $B_{\alpha_1'\alpha_2'\alpha_1\alpha_2}$ are Reggeon–Reggeon scattering amplitudes evaluated at $j=\alpha_1+\alpha_2-1=\alpha_1'+\alpha_2'-1$.

Despite their technically complicated derivation, the physical importance of these equations is very clear. disc $a(j,t)$ is the discontinuity, across the 2-Reggeon cut, of the $t$-channel partial-wave amplitude – precisely the discontinuity which controls the high energy ($s$) behaviour of the cut contributions, via the Mellin transform:

$$T(s,t) = \int_{\alpha_c}^{-\infty} \mathrm{d}j\,\mathrm{disc}_j a(j,t)\,\mathrm{e}^{-\mathrm{i}\pi j/2} s^j. \tag{4G.4}$$

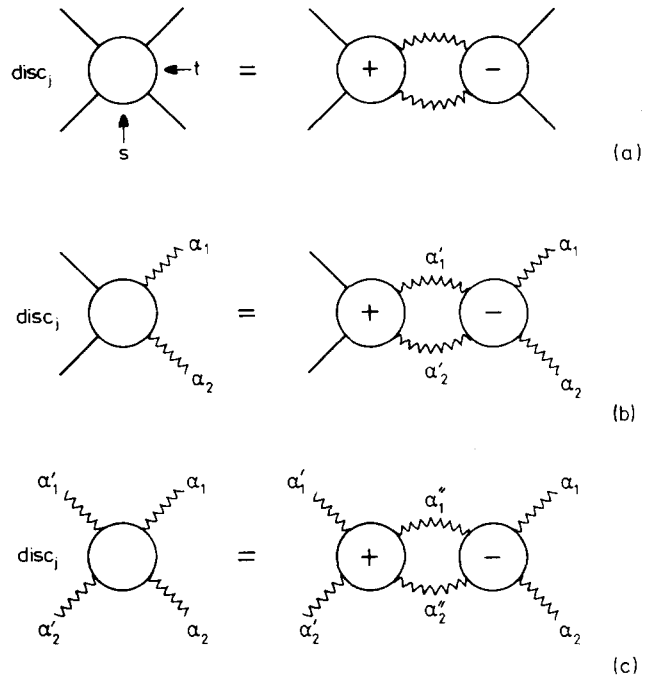


Fig. 4G.1. Reggeon unitarity equations in the $t$-channel $j$-plane.

Given a reliable model for the vertices $N_{\alpha_1\alpha_2}$, one can therefore calculate, for instance, a Reggeon–Pomeron cut amplitude. Similar equations can be written for $n$-Reggeon ($n \geq 3$) intermediate states in the $t$-channel, giving the contribution of an $n$-Reggeon cut to high energy amplitudes.

The Reggeon calculus, first derived by Gribov [44] from high energy limits of Feynman diagrams, may be viewed as a formal field-theory solution to the unitarity equations [243]. With it one can, in principle, calculate quite complicated effects, such as interactions between Reggeons, and $t$-channel iterations (see fig. 4G.2). However, there is no reason to believe that the vertices of the theory (including couplings to external particles) are particularly simple so that practical calculations are not yet possible.

The basic entities of the Reggeon calculus are factorising Regge poles. The observed Pomeron, for instance, may be thought of as built up from an underlying "bare" Pomeron pole via higher order diagrams of the calculus. This gives rise to anomalous powers of $\log s$ in the total cross-section at asymptotic energies [233, 185]. When calculating Regge–Pomeron cuts it is usual to regard the Pomeron as a factorising pole and ignore the multi-Pomeron diagrams at present (sub-ISR) energies.† This is because, in this regime, the "rising" component of the total cross-section is not large, and tests of

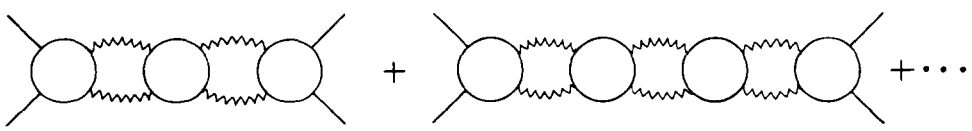


Fig. 4G.2. $t$-channel iterations.

† There is nonetheless, a possibility that the "full" self-consistent Pomeron pole (satisfying the $t$-channel unitarity equations) may also factorise.

Pomeron factorisation in diffractive and inclusive processes are all successful [276]. Even with the approximation of only one Reggeon and one Pomeron $t$-channel intermediate states, we do not have a complete calculational scheme for Regge–Pomeron cuts, but as we shall see, several useful results can be derived.

### *4G.2. Results for Regge–Pomeron cuts*

We shall divide the $(j, t)$ plane into four regions where different physical effects predominate:

| | | | |
|---|---|---|---|
| A: | intersection of pole and cut | $t \simeq 0$ | $j \simeq \alpha_{\text{pole}}(0)$ |
| B: | tip of the cut | $t \neq 0$ | $j \simeq \alpha_{\text{cut}}(t)$ |
| C: | near the pole | $t \neq 0$ | $j \simeq \alpha_{\text{pole}}(t)$ |
| D: | the rest. | | |

Of course, these regions (indicated in fig. 4G.3) are not well-defined. In fact, one of the main interests in this approach is to ascertain the useful extent of each region and its approximations.

A. *Intersection of pole and cut*

This is the infrared region of the Reggeon field theory (all momenta $\boldsymbol{k}$ and "energies" $(j - \alpha_{\text{pole}}(0))$ are small) where it can be solved, without neglecting multi-Pomeron diagrams, in a number of ways, notably by use of the renormalisation group equations [233, 185]. Using the latter, rather general method, it can be shown that results in this region are rather insensitive to the details of the input Reggeon field theory [255]. The case of meson Regge trajectories has been treated by Abarbanel and Sugar [186] who find solutions in which the Regge pole behaviour at $t = 0$ is modified by an "anomalous dimension" power of log $s$:

$$T(s, 0) \sim s^{\alpha(0)} (\log s)^{-\gamma} \tag{4G.5}$$

where $-\gamma = 1/12$ to first order in the $\epsilon$-expansion. They also find that the perturbation of the trajectory from its input linear form, caused by interaction with the cuts, is fairly weak near $t = 0$.

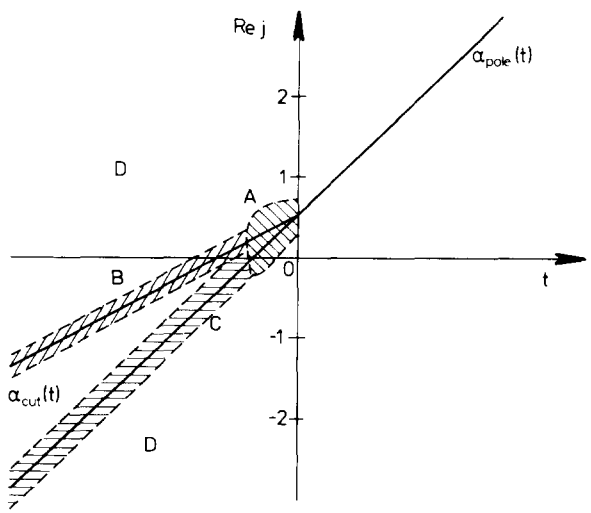


Fig. 4G.3. Regions of the $j$-plane useful in the discussion of Reggeon–Pomeron cut properties. The regions A, B, C and D are defined in the text.

B. *Tip of the cut*

Bronzan and Jones [32] have given an argument that the cut discontinuity cannot be finite at the branch point, but must be "softened" to be consistent with $t$-channel unitarity. Some rather artificial-looking counter-examples to this have been given [151, 147] but in the Reggeon calculus this softening of the discontinuity does occur. The cause of it can be seen in eq. (4G.3). Suppose disc $B_{\alpha_1\alpha_2;\alpha_1\alpha_2}$ is constant near the branch point, then the branch point singularity must be logarithmic. This implies that the integral on the RHS has a $\log^2(j-\alpha_c)$ behaviour. Thus disc $B \sim \log^2(j-\alpha_c)$, which contradicts the original assumption. The only simple solution is of the form [18, 201]

$$B \sim [A(j,t) + \log(j-\alpha_c)]^{-1} \tag{4G.6}$$

near the branch point. This $1/\log(j-\alpha_c)$ singularity of $B$ propagates through the other unitarity eqs. (4G.2,3) and appears in $a(j,t)$. Therefore disc $a(j,t)$ has the softened $1/\log^2(j-\alpha_c)$ behaviour.

The softening will only be visible in that $j$-plane region where $\log(j-\alpha_c)$ is much larger than the unknown function $A(j,t)$. In the Reggeon calculus the softening is brought about by the $t$-channel iterations diagrams of fig. 4G.2, so that the numerical importance of the softening depends on the size of the four-Reggeon vertices in fig. 4G.1. Collins and Fitton [260] have presented phenomenological evidence that hard cuts are appropriate in photoproduction but that for most hadronic processes $A(j,t)$ must be small, the cuts softened, and the cut discontinuity dominated instead by $j \sim \alpha_{\text{pole}}(t)$ (region C).

We know two other properties of the Regge–Pomeron cut discontinuity near the branch point; the discontinuity has the same parity as the parent Regge pole [275], and it factorises [332]. Contributions with opposite parity, or which do not factorise, are suppressed by a factor $(j-\alpha_c)$ near the branch point (suppressed by $1/\log s$ in $T(s,t)$). To leading order in $\log s$, then, Regge–Pomeron cuts factorise and have the same parity as the Regge pole.†

These rules are fairly academic at sub-30 GeV energies and difficult to test [see for example 287]. One clear-cut case is that of $\pi$ exchange (see section 4D) where the full cut amplitude obviously violates the parity and factorisation rules – showing that the tip of the cut is far from dominating these particular amplitudes. As energies increase, however, the tip of the cut naturally becomes more important, so that rules such as these may be of use at NAL-SPS energies.

C. *The region near the pole*

In this region the pole-cut interaction diagrams (or "enhancement diagrams") [44] of fig. 4G.4 become important. Qualitatively, their effect is to give the pole trajectory $\alpha(t)$ an imaginary part and the cut discontinuity a Breit–Wigner form in the neighbourhood of the pole position. Using the language of the non-relativistic two-dimensional scattering analogy ($\boldsymbol{k}$ is momentum, and $\alpha(0)-j$ energy), the Reggeon is unstable for $t<0$ being able to decay into a Reggeon and Pomeron. It therefore acquires a width, and the two-particle cut (Reggeon–Pomeron) has a Breit–Wigner form. A more formal justification directly in terms of $t$-channel unitarity can be made [104].

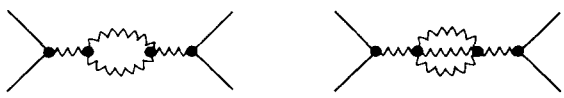

Fig. 4G.4. Pole enhancement diagrams occurring in the Reggeon calculus.

† At finite energies, the absorption model, for example, allows cuts of both parities in evasive amplitudes ($x \neq 0$ in eq. (2.5)).

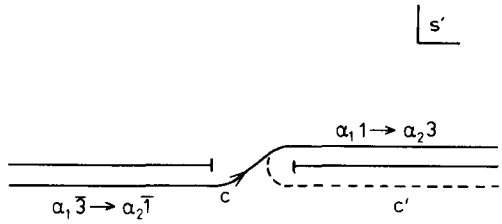


Fig. 4G.5. Integration contour used in the Schwartz sum rule for a Reggeon–particle scattering amplitude.

Beyond these qualitative statements, little is known. The size of $\mathrm{Im}\alpha(t)$ depends on the triple-Regge couplings of fig. 4G.4. These couplings, however, are necessarily nonplanar [44] and therefore not the familiar triple Regge couplings which are phenomenologically accessible in inclusive experiments [111]. A number of Regge analyses using pole-enhanced cuts have been reported [175, 262, 260]. Their attractiveness stems from some evidence that cuts at large $-t$ often seem to share the same shrinkage properties as the basic Regge pole. This evidence, from $\alpha_{\text{eff}}(t)$ studies of differential cross-sections, model dependent amplitude analysis, and FESR analyses (section 4H), has been summarised by Ringland [176] and Schrempp [287].

D. *The rest*

We have separated off the two regions where, for a clear dynamical reason, some higher order diagrams of the Reggeon calculus become important. One could also investigate the possibility that, for the rest of the $(j, t)$ plane, the perturbative expansion of the Reggeon calculus is rapidly convergent so that only the lowest diagram (fig. 4G.1) is important. This diagram involves the couplings $N_{\alpha_1\alpha_2}$ of the Reggeons to the external particles.

The Gribov vertex $N^{13}_{\alpha_1\alpha_2}$ is a partial-wave amplitude for the $t$-channel process $\alpha_1 + \alpha_2 \to \bar{1} + 3$ (Reggeon + Reggeon → particle + particle) evaluated at $j = \alpha_1 + \alpha_2 - 1$. Since the appropriate kinematic-singularity-free (KSF) amplitude has Regge behaviour $\sim s^{j-\alpha_1-\alpha_2}$ (see e.g. eq. (4F.1)) this particular $j$-value corresponds to a "fixed-pole behaviour" $\sim s^{-1}$. In addition, it is at a wrong-signature point so the partial wave amplitude (or "fixed pole residue") can be evaluated by a superconvergence sum rule [36]

$$N^{13}_{\alpha_1\alpha_2}(t) = \int_C A^{13}_{\alpha_1\alpha_2}(s', t)\, \mathrm{d}s' \tag{4G.7}$$

where $A(s', t)$ is the KSF amplitude and $s'$ the energy variable appropriate to $\alpha_1 1 \to \alpha_2 3$. The contour of integration C is shown in fig. 4G.5. Clearly C may be distorted to the contour C', for example, so that only resonances in the direct channel $\alpha_1 1 \to \alpha_2 3$ (but not the u' channel $\alpha_1 \bar{3} \to \alpha_2 \bar{1}$) contribute to the integral. To make practical use of this result, i.e. to sum the resonance contributions in the $s'$ channel, requires further theoretical input as discussed, for example, in the next section.

### *4G.3. Duality constraints on Regge cuts*

Duality techniques, when combined with Reggeon calculus results, can give rise to useful constraints on Reggeon–Pomeron and Reggeon–Reggeon cuts. For example, Finkelstein [86] has pointed out that if either the $s'$ or $u'$ cut in $A^{13}_{\alpha_2\alpha_2}(s', t)$ (see eq. (4G.7) and fig. 4G.5) is absent then the contour C may be closed so that it contains no singularities, and hence $N^{13}_{\alpha_1\alpha_2}$ will vanish. According to duality this

happens if one cannot draw a *planar* ($s'u'$) duality diagram for the process $\alpha_1 1 \to \alpha_2 3$. This selection rule ensures, for instance, that although Reggeon–Reggeon cuts may contribute to the HYCEX processes such as $\bar{K}N \to \pi\Sigma$, they do not occur in the SU(3)-related KN CEX reactions (section 4B). Further, more specific, selection rules for Reggeon–Reggeon cuts have been derived from these arguments using SU(3) and EXD constraints [140, 125]. These lead to a suppression of Regge–Regge cuts in $\pi$N charge-exchange.

Attempts have been made to sum the resonance contributions in eq. (4G.7) using FMSR duality to relate the sum to a triple-Regge vertex [210]. However, as discussed in paragraph C of §4G.2, this coupling is a peculiar non-planar one about which little is known phenomenologically.

Recently, several dual schemes for generating a Reggeon or Pomeron singularity via unitarity have been investigated [163, 182, 258]. In these approaches, the contributions in the unitarity expansions are classified according to their topological properties (e.g. the number of non-planar loops involved). Chew and Rosenzweig [257] have used such techniques to achieve renormalisation corrections to input Regge poles which could account for SU(3) and EXD breaking. This occurs when a higher-order contribution can be dual-transformed to a single Regge exchange contribution with a "renormalisation" loop inserted. In some cases the higher (for example the second) order term, because of the non-planar properties of the graph, does not so transform and represents a genuine Reggeon–Pomeron cut (see also the discussion of the Finkelstein selection rule). Duke [308] has pointed out that, in this way, the topological expansion properties of the Pomeron, in a given channel, determine the nature of the related Reggeon–Pomeron cuts. For example, since the number of twisted loops in expansions of $K^-p$, $\pi^-\Sigma^+$, $\pi^+p$ and $K^+\Sigma^+$ are different, the Reggeon–Pomeron cuts in $K^-p \to \pi^-\Sigma^+$ and $\pi^+p \to K^+\Sigma^+$ should have different strengths (weaker in the former, in agreement with experiment).

### *4G.4. The Reggeon calculus and cut amplitude systematics*

We have seen how the main difficulty with the Reggeon calculus is that, while giving us a framework, it does not suggest many useful approximations for practical calculations. Only in certain special regions, such as the tip of the cut, can testable predictions be made. We therefore suggest that the main use of the Reggeon calculus will instead be as a source of clues on how to look for systematics of cut amplitudes. Two examples will illustrate this point.

The lowest-order cut diagram (fig. 4G.1) gives an amplitude which depends on a product of two factors – the Gribov vertices in the diagram. The spin-dependence of the amplitude is governed by that of the two vertices. However, each Gribov vertex depends only on the spin-state of the two particles coupled to it. In the past, searches for cut strength systematics have concentrated on the net-helicity flip of amplitudes (e.g. section 4A). The Reggeon calculus strongly suggests that, aside from certain obvious kinematic factors, cut strengths will depend not so much on net helicity flip so much as on the helicity flip at each vertex.

A more speculative remark can be made about the Gribov vertices themselves. These are integrals of a Reggeon–particle scattering amplitude over $s'$ at fixed $t$(eq. (4G.7)). $s$-channel helicity amplitudes do not have simple analytic properties in the $s$-plane at fixed $t$, but $t$-channel helicity amplitudes do – they can be regularised to give KSF amplitudes with Regge behaviour $s'^{\alpha - M}$, where $M$ depends on the $t$-channel helicities of the Reggeon *and of the external particles.* This suggests that the systematics of Gribov vertices (and so, of cuts) will depend most simply on $t$-channel helicity, not $s$-channel helicity.

In support of these two remarks, we recall that the clearest examples of strong Regge cuts (section 3) occur in amplitudes where a nucleon→nucleon transition has zero helicity-flip in the $t$-channel. These examples are $\pi$ exchange ($np \to pn$, $\gamma p \to \pi^+ n$ and $\pi^- p \to \pi^+ \pi^- n$), $\rho$ exchange (the non-flip amplitude of $\pi^- p \to \pi^0 n$) and $\omega$ exchange ($Kp \to Kp$ and $\gamma p \to \pi^0 p$). These suggest that $t$-channel non-flip nucleon→nucleon transitions have a particularly strong Gribov vertex. The last example ($\gamma p \to \pi^0 p$) clearly shows the inadequacy of net helicity flip as a basis for systematics; on that basis, $\gamma p \to \pi^0 p$ and $\pi^- p \to \pi^0 n$ should be very similar. In practice (section 4A), one has strong cuts and the other does not. The difference can be attributed to their different spin structure at the nucleon vertex.

One can, of course, cite amplitudes with nucleon $t$-channel helicity non-flip vertices where the presence of strong cuts is by no means established – for example, those which dominate $\rho_{00}\, d\sigma/dt \cdot (\pi^- p \to \rho^0 n)$ (section 4A) and $pp \to n\Delta^{++}$. However, the point being made is that the Reggeon calculus can be an important and positive influence on our approach to the phenomenology of Regge cuts.

## 4H. Duality in two-body scattering

"It vanished quite slowly, beginning with the end of the tail, and ending with the grin, which remained some time after the rest of it had gone."

"Alice in Wonderland", Lewis Carroll.

Duality is one of the most attractive theoretical ideas to have emerged from Regge phenomenology [42]. The idea that direct-channel resonances are somehow equivalent to (dual to) crossed-channel Regge poles has found applications in all areas of hadron physics – in inclusive and multibody reactions, as well as in the two-body processes where it was discovered. The study of dual models has become a theoretical field in its own right, with an elaborate formalism and some startling similarities to gauge field theories.

The reasons for the popularity of duality are not hard to find. Any theory which claims equivalence between A and B, allows one to use A where B is complicated, and vice versa. One can have one's cake and, in a dual sense, eat it. Duality therefore, has enormous potential to unify disparate phenomena. However, it can only give a real simplification if the basic concept can be clearly stated and experimentally tested. It is in two-body physics, where the energy-dependence of individual amplitudes is best studied, that the most stringent tests of duality can be made. We now survey some tests in an attempt to answer the question – "Does duality really work?".

### *4H.1. Defining duality in the presence of Regge cuts*

Statements of duality in two-body scattering are most easily phrased in terms of finite-energy sum rules (FESR) which are identities following strictly from analyticity: if the crossing-odd amplitude $T^{(-)}(\nu, t)$ is integrated round the contour of fig. 4H.1, Cauchy's theorem implies

$$\int_a^b T^{(-)}(\nu, t)\, d\nu = -\int_b^c T^{(-)}(\nu, t)\, d\nu \tag{4H.1}$$

where $|a| = |b| = |c| = \nu_c$, a cut-off energy. The LHS of this sum-rule ($|\nu| < \nu_c$) is calculable from experiment. Provided the exact high energy amplitude (for *all* complex $\nu$: $|\nu| = \nu_c$) is used in the RHS, this equation is only an expression of fixed-t analyticity and not yet one of duality.

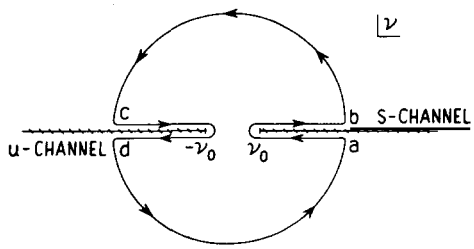


Fig. 4H.1. Contour, in the $\nu$-plane, used in the derivation of an FESR [184].

*Definition:* The hypothesis of duality is, simply, that to evaluate the semi-circular contour (RHS of eq. (4H.1)) one can use a Regge model containing only *leading* (high-lying) $j$-plane singularities (Regge poles, cuts, etc.). We note the following important features of this definition:

(a) It is non-trivial and testable. One uses phase-shift amplitudes to calculate the LHS, and, if a high energy model satisfying the above criteria can be found, the amplitude in question is said to satisfy duality. The concept of "leading singularities" can be made quantitative, e.g. $-\frac{1}{2} \leqslant j \leqslant \frac{1}{2}$.

(b) The original hope of using only Regge *poles* on the RHS (so that Regge poles could be said to be "dual to resonances") cannot be realised – duality without Regge cuts is meaningless. As discussed in section 3, the $\rho$ exchange helicity non-flip amplitude Im $N^{(-)}$ in $\pi^- p \to \pi^0 n$ has a zero at $t = -0.2$. This is not a property of the $\rho$ Regge pole but a pole/cut cancellation effect. Since the low-energy resonances also possess this zero (fig. 3.5), it is only possible to satisfy the sum rule by including both Regge poles *and* cuts. Figure 4H.2 shows a sum-rule for Im$N^{(-)}$, and the (disastrous) effect of neglecting

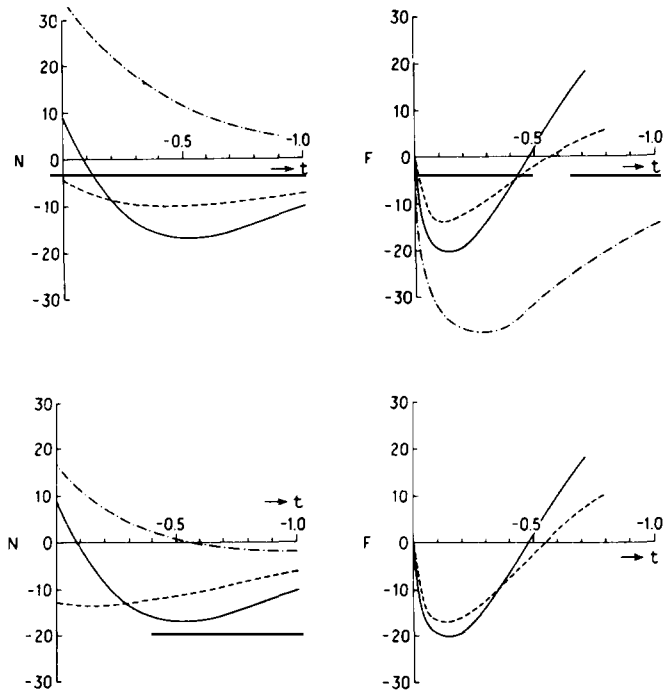


Fig. 4H.2. Comparison of FESR integrals for $\pi$N charge exchange helicity flip and non-flip amplitudes (full curve) with the second generation cut models of Hartley and Kane [158] (above) and Ringland et al. [134] (below). The dotted curves are the Regge pole contributions (taken from [184]).

Regge cuts. Including Regge cuts, however, has an unpleasant side-effect – unlike Regge poles, cut discontinuities are not localised in the $j$-plane and so one must introduce the above arbitrary, but essential, restriction on $j$. If there is no restriction, low-lying singularities which are not constrained at high energy could dominate the sum rule ($|\nu| \lesssim \nu_c$) and rob it of much of its practical content.

(c) Duality, in this FESR sense, can be violated in two ways. Firstly, in a given reaction, there could be *intrinsic* low-lying $j$-plane contributions so that *no* high energy model could be invented so as to satisfy our criteria for phenomenological duality. Secondly, although a given reaction amplitude is dual according to our definition, there is no guarantee that every Regge model for this amplitude, which fits the data adequately at high energies ($p_{\mathrm{LAB}} \gtrsim 4\,\mathrm{GeV}/c$), will itself satisfy duality. We shall try to maintain this distinction in the following survey of duality tests. The first, and most basic type of failure, implies the invalidity of duality as a general property of nature. The second could be used as a criterion for choosing between competing high energy models [184].

### *4H.2. Tests of duality*

(a) $\pi^- p \to \pi^0 n$

Figure 4H.2 shows the FESR for the helicity-flip $\pi N$ charge-exchange amplitude compared with typical high energy models. The good agreement was one of the foundation-stones of duality. Remarkably, all known helicity flip $\rho$ exchange FESR show this good agreement [242], so one may conjecture that duality is at least a property of helicity-flip $\rho$ exchange amplitudes. The ambiguities associated with Regge cuts are not serious here, presumably because the cuts are relatively weak. The non-flip FESR for $\mathrm{Im}N^{(-)}$ (also shown in fig. 4H.2) shows the same cross-over zero as the high energy data. In a general sense (see note (c) above), $\mathrm{Im}N^{(-)}$ is certainly dual. However, the second generation absorption models shown in fig. 4H.2 and discussed in section 3, are not dual. They cannot reproduce the zero structure because of their low-lying $j$-plane singularities [184]. Figure 4H.3 shows a typical cut-discontinuity in the $J$-plane. One concludes that $\pi N$ CEX amplitudes seem to be "dual" but that current models for the non-flip amplitude are not.

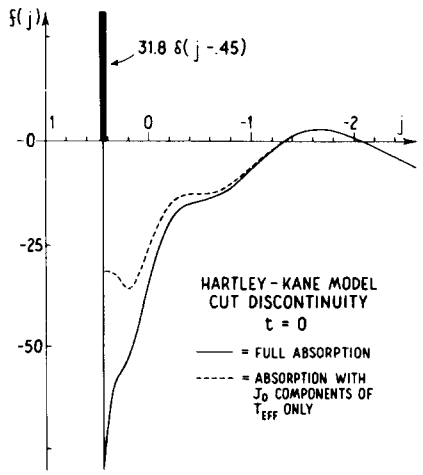


Fig. 4h.3. A typical Regge cut model [158] $j$-plane discontinuity. The $\delta$-function at $j = 0.45$ is the input Regge pole. (Figure taken from [184].)

(b) KN *charge exchange*

Helicity-flip $\rho$ and $A_2$ exchange FESR integrals [217] are shown in fig. 4H.4. Also shown are high energy amplitudes deduced from an analysis of all high energy KN scattering data using fixed-$t$ dispersion relations to help constrain the parameters [267] (see also §4B.2). As discussed above, the $\rho$ exchange FESR and high energy amplitude have the same structure. However, the $A_2$ FESR and high energy amplitude are rather different – of opposite sign, in fact. To the extent that the amplitude analysis results are correct, the $A_2$ exchange amplitude is clearly not dual. Note that the high energy $\rho$ and $A_2$ imaginary parts ($p_{LAB} > 3\,GeV/c$) are roughly exchange degenerate ($\mathrm{Im}A_2 \sim -\mathrm{Im}\rho$). There appear to be low-lying $j$-plane contributions which destroy this relationship in the FESR and, within our definition, violate duality.

(c) $K^-p \to \pi^0\Lambda$

The analogous FESR integrals for helicity-flip K* and K** exchange in $K^-p \to \pi^0\Lambda$ and $\pi^-p \to K^0\Lambda$ also exhibit [211, 289] this "anti-exchange degenerate" sign, while indications from high energy analyses (§4B.4) are that the true high energy amplitudes are likely to be closer to exchange-degenerate. Again, this amounts to a failure of phenomenological duality.

(d) $\gamma p \to \pi^0 p$

A complete analysis of the high energy amplitudes for this process has not yet been possible. However, all model-dependent approaches are in agreement that the well-known cross-section dip at $t = -0.5$ is associated with a zero in the imaginary part of the helicity-flip amplitude†, just as in $\pi^-p \to \pi^0 n$. However, unlike $\pi N$ charge-exchange, the $\pi^0$ photoproduction FESR does not show a zero near $t = -0.5$ [139, 194]. In a qualitative sense, the amplitude does not appear to be dual. This peculiar behaviour of the FESR can, in fact, be fitted by strong cut absorption models [139] and dual absorption models [179]; but in these cases the FESR is satisfied by a complicated mixture of

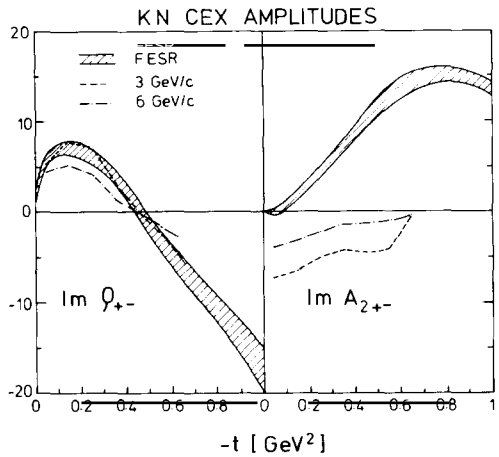


Fig. 4H.4. The helicity-flip KN charge exchange FESR integrals [217] corresponding to $\rho$ and $A_2$ exchange (shaded region). The corresponding high energy amplitudes at 3 and 6 GeV/$c$ [267] are shown by the broken lines. The relative scale between the FESR and high energy amplitudes is arbitrary (chosen so that the $\rho$ exchange results correspond in magnitude).

† This amplitude is dominated by $\omega$ exchange (helicity non-flip at the nucleon vertex).

high-lying and low-lying $j$-plane singularities. This, as we discussed in §4H.1, cannot be taken as positive evidence for duality.

### *4H.3. Duality results in the presence of duality violation*

There are probably some two dozen amplitudes whose high energy behaviour is sufficiently understood, and whose low-energy phase-shifts are well enough known to make meaningful tests of duality using FESR [242]. The half-dozen we have selected (§4H.2) are fairly typical and were chosen because, taken individually, each gives a definite result. The overall picture which emerges is not encouraging: although it appears to work sometimes (e.g. the $\rho$ exchange amplitudes in $\pi$N and KN CEX) it is clearly not a general property of all two-body amplitudes. This conclusion is based on one particular kind of duality test. There are, of course, other tests – in particular of exchange degeneracy (e.g. section 4B) and the many other relations between Regge residues which must hold in schemes which incorporate duality and SU(3) symmetry [74]. However, we believe that the FESR tests are the most important because they are the most direct.

In view of the importance of duality in many areas of particle physics, it is an urgent priority to discover what can be salvaged of its original predictive power.† Perhaps the violations are restricted to a certain class of amplitudes? Since duality was, from the first, a phenomenological rather than theoretical concept, one can expect little theoretical guidance in establishing the origin of duality violation. Below, we discuss briefly some applications of duality which, in the light of these violations, deserve a critical re-examination.

(a) *Two-component duality* [45, 43]

This is the hypothesis that resonances are dual to non-diffractive exchanges while background (non-resonant) is dual to the Pomeron. The validity of this is questionable. For example if $A_2$ exchange in $K^+n \to K^0p$ does not satisfy duality (example (b) in §4H.2), this hypothesis cannot be reliably used to separate f and $A_2$ exchange from Pomeron exchange in $K^{\pm}p$ elastic scattering.

(b) *Exchange degeneracy*

Although the masses of the $(\rho, \omega, K^*)$ and $(A_2, f, K^{**})$ are roughly compatible with exchange degenerate trajectories, the quantitative FESR evidence for exchange degeneracy (EXD) is weak. Again, consider $K^+n \to K^0p$. The naive implication of duality is that, since there are no known resonances in $K^+n$ scattering, the imaginary part of the amplitude should be small and so the high energy imaginary part should be correspondingly small. If taken to be zero, this implies EXD of the $\rho$ and $A_2$ exchange amplitudes. However, we know that the imaginary part of the helicity flip $A_2$ amplitude changes sign between $\nu = \nu_c$ (anti-EXD sign) and higher energies. Thus, the EXD prediction at high energies ($p_{LAB} \gtrsim 4\,\text{GeV}/c$) seems to hold approximately in spite of, rather than because of, the FESR duality arguments.

(c) *The dual absorptive model*

Here the FESR evidence rests largely on $\pi^-p \to \pi^0n$ where, for some reason, the fixed $-t$ zero structure persists even at the level of each resonance. According to this model the imaginary part of the $A_2$ non-flip amplitude in KN CEX should also have a "peripheral" zero at $t = -0.2$. Neither the

† The reader's attention is drawn to the quotation at the head of this section.

FESR nor the high energy amplitude have this zero (§4B.4). The failure of this model seems to be due to the fact that not all strongly coupled resonances are peripheral, rather than a failure of duality. This is clear since, if each resonance contribution did have a zero at $t = -0.2$, then by analyticity so would the high energy amplitude, irrespective of duality.

(d) *Semi-local duality and FMSR*

In $\pi N \to \pi N$ and in $\pi N \to \pi \Delta$ [90, 312] duality is satisfied in an especially simple way with each resonance itself possessing the zero structure (at $t = -0.2, -0.5$) found at high energies. In these, rather unique, cases one can therefore perform an FESR average over a much smaller range of $\sqrt{\nu}$ (e.g. 1 GeV) and still approximate the Regge result. This is known as semi-local duality. In the examples where FESR duality, if satisfied, is satisfied in a complicated way (e.g. $\gamma p \to \pi^0 p$) or not satisfied at all (KN), such a procedure would clearly be incorrect. In view of this, the application of semi-local duality to finite mass sum-rules (FMSR) where it plays an important role (see section 4F), cannot be reasonably expected to meet with more than qualitative success.

(e) *Dual model amplitudes*

The interest in dual amplitudes has long passed from being a strictly phenomenological one to being a theoretical one. The appeal of the Veneziano model which embodies crossing, Regge behaviour, and direct channel (resonance) poles in one simple two-parameter ($\beta, \alpha'$) expression is easy to understand. Its original motivation, as an explicit solution of FESR, is now less compelling. Veneziano amplitudes are an idealised solution to what turns out to be an idealised constraint (duality).

(f) *Quark/duality diagram results*

Such diagrams [59, 62] may be used to summarise EXD results such as discussed in (b) and those obtained from them using SU(3). They may also be used, for example, as a calculus for approximating multi-resonance production by multi-Regge exchange. This is an application of local duality and subject to the caveats discussed in (d) above. They are also used to state results such as the Finkelstein selection rule (section 4G) where the precise reliance placed on the validity of duality is difficult to evaluate.

In summary, it appears that quantitative results depending on FESR duality, in particular semi-local duality, have a very narrow basis of experimental motivation. Nonetheless, those results which depend on the more trivial aspect of duality that a scattering amplitude may be expanded in terms of its singularities (in $s$ or $j$) in *either* direct or crossed channels, are likely to remain. The extent to which a few leading singularities dominate seems to be less than was at first hoped, and to vary from reaction to reaction.

## 4I. Baryon exchange

In this section, we do not attempt a comprehensive survey of baryon exchange, but limit ourselves to a comparison with meson exchange and a review of some recent phenomenological developments. Many aspects of backward scattering have been reviewed by Barger and Cline [50], Berger and Fox [82, 83] and by Storrow and Winbow [181, 288].

### 4I.1. Peculiarities of baryon exchange

Several features complicate the analysis of baryon exchange processes in terms of Regge poles.

(1) McDowell symmetry of meson–baryon amplitudes [3] means that for each $u$-channel exchange of given signature, there must be two trajectories $\alpha^{\pm}(\sqrt{u})$ of opposite parity (parity doublets) which contribute. The trajectories and residues ($\beta^{\pm}(\sqrt{u})$) are analytic functions of $\sqrt{u}$ (as are the amplitudes themselves), and obey

$$\alpha^{+}(\sqrt{u}) = \alpha^{-}(-\sqrt{u}), \qquad \beta^{+}(\sqrt{u}) = -\beta^{-}(-\sqrt{u}). \tag{4I.1}$$

Thus, the nucleon trajectory, $N_\alpha$, must be accompanied by an opposite parity trajectory of partner states obeying eq. (4I.1). If $N_\alpha$ has a linear trajectory then such states will be degenerate in mass, since

$$\alpha^{-}(-\sqrt{u}) = \alpha^{+}(\sqrt{u}) = \alpha_0 + \alpha'(\sqrt{u})^2. \tag{4I.2}$$

Experimentally, such parity doublets seem to be absent [137], so that Regge models must have a mechanism for suppressing the unwanted states in the spectrum. Many other Reggeisation problems are intimately connected with McDowell symmetry.

(2) Because of the existence of two related trajectories, the energy dependence due to a single fermion Regge pole is (cf. eq. (4I.2))

$$\mathrm{d}\sigma/\mathrm{d}u \sim s^{\alpha(\sqrt{u})+\alpha(-\sqrt{u})-2}, \tag{4I.3}$$

so that the shrinkage properties of the data reflect only that part of the trajectory's $u$-dependence which is even in $\sqrt{u}$. In fig. 4I.1 we show two examples (taken from [181]) of $\Delta_\delta$ trajectories which fit the positive $u$ spectrum, one of which is odd in $\sqrt{u}$, therefore has no physical parity doublets, and gives no shrinkage. The other is even in $\sqrt{u}$, has degenerate parity doublets, and has "normal" Regge pole shrinkage. Lack of shrinkage in the data, therefore, does not necessarily imply non-Regge pole behaviour in baryon exchange processes.

(3) In contrast to forward scattering, non-zero polarisation can arise from a single baryon Regge exchange. This is because the parity doublets may have non-degenerate trajectories (i.e. with terms odd in $\sqrt{u}$), and so different Regge phases.

(4) Measurement of the nucleon polarisation $P$ in $aN\uparrow \to Nb$ can be used [142] to separate out the contributions of natural ($M^{+}$) and unnatural ($M^{-}$) $u$-channel parity exchange for $u<0$. For example in $0^{-}\frac{1}{2}^{+}$ scattering,

$$|M^{\pm}|^2 = \frac{1}{2}\frac{\mathrm{d}\sigma}{\mathrm{d}u}(1 \mp P). \tag{4I.4}$$

This information is, however, considerably less useful to the phenomenologist than the analogous decomposition for meson exchanges, since at $u=0$, $|M^{+}| = |M^{-}|$ necessarily. The extrapolation to $u>0$ yields little information about which parity of pole is being exchanged. It is an analogous conspiracy to that which occurs in forward $\gamma p \to \pi^{+} n$, where the spike in $M^{+}$ for $t<0$ is actually a result of $\pi$ pole exchange in $M^{-}$ for $t>0$. In the backward case, this conspiracy occurs in *every* process, and one has no a priori knowledge of the fundamental (parity doubled) pole exchanges. To obtain this, a specific extrapolation model is required.

(5) For forward meson–baryon processes, the $t$-channel quantum numbers isospin, parity and $G$-parity are easily controlled by selecting the final state meson, its charge and its polarisation. For

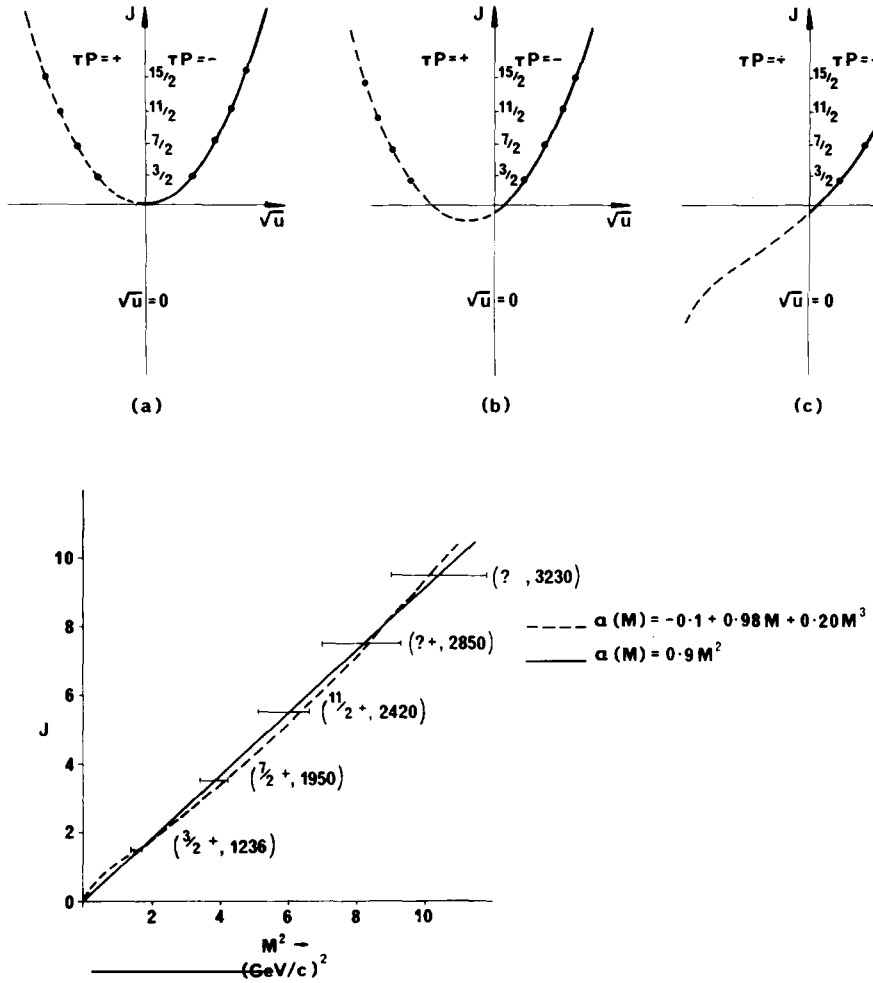


Fig. 4I.1. (a)–(c) Three of the possible baryon trajectory behaviours giving rise to (a) degenerate parity doublets, (b) non-degenerate parity doublets, (c) no physical parity doublets. Below: the Chew–Frautschi plot corresponding to possibilities (a) (full curve) and (c) (dashed). Figure taken from ref. [181].

backward scattering, only the $u$-channel isospin can be easily controlled. Even photon or vector meson polarisation measurements are not particularly useful in sorting out the exchange mechanisms.

(6) In general, backward peaks are much smaller than forward ones. In terms of direct channel partial waves, this results from cancellations between waves. It is therefore not surprising that resonant effects persist to relatively high energies (see fig. 4I.2). The Regge region in backward processes appears not to set in until 6 GeV/$c$ or more.

The above problems are general and common to all Regge models. There are further problems encountered in building specific models.

(7) Unlike forward scattering, FESR are not useful in constructing model amplitudes for MB scattering. These would require information on the $MM \to B\bar{B}$ channel, below the $B\bar{B}$ threshold.

(8) Exchange degeneracy patterns for baryon trajectories are less well-established. The constraints which follow from SU(3) symmetry and absence of exotics in crossed channels can not be exactly

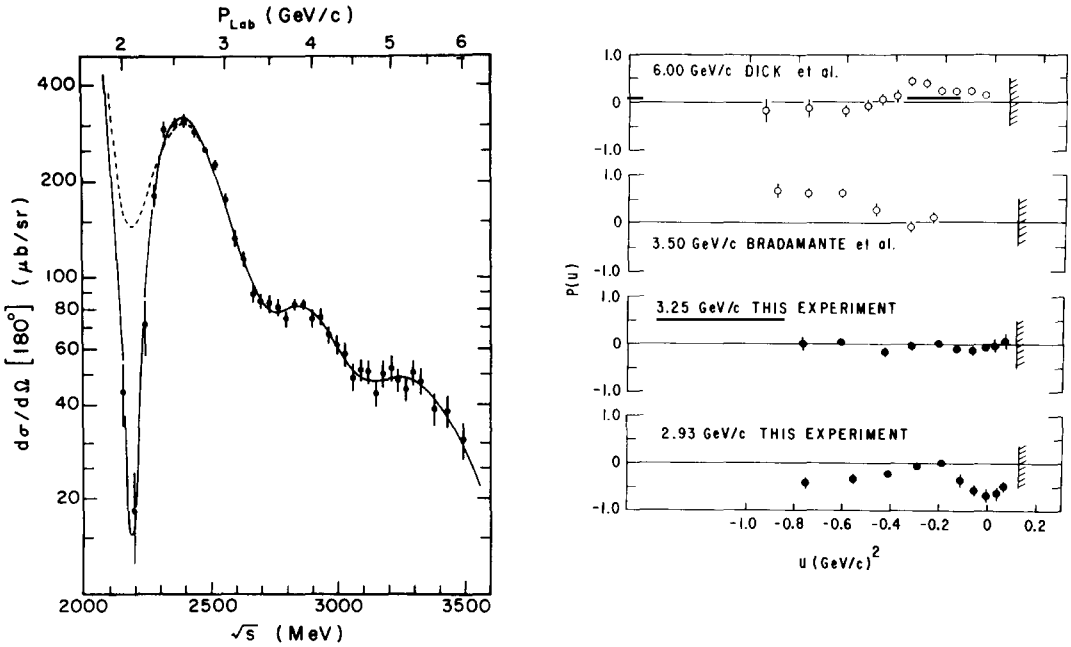


Fig. 4I.2. The backward differential cross-section for $\pi^+p$ elastic scattering as a function of energy [277]. Also shown is the polarisation in $\pi^-p \to \pi^-p$ near the backward direction, at various energies [293].

satisfied by the leading trajectories. One must ignore some of the constraints, introduce extra trajectories or break SU(3) in order to obtain solutions. The major results, EXD between $\alpha$ and $\gamma$ and between $\beta$ and $\delta$ trajectories (e.g. $N_\alpha$, $N_\gamma$ and $N_\beta$, $\Delta_\delta$), are, however, common to all schemes [51, 61, 103].

There is one notable positive element in this comparison with meson exchange:

(9) The baryon resonance spectrum is very well known up to quite high spins (from phase-shift analysis of formation experiments). The residues for $u > 0$ (decay widths) are in general much better known than the meson ones.

It is obvious that the direct tests of Regge pole exchange used in section 2 are almost impossible to apply to baryon exchange. We cannot directly interpret shrinkage properties, the connection between scattering and spectrum or Regge phase relations. The only well-established feature of the data which speaks positively for Regge dominance is the approximate consistency, in all known cases, of $\alpha_{\text{eff}}(u \simeq 0)$ with the Regge expectation (eq. (4I.3)).

### *4I.2. Backward πN scattering*

The more recent progress in understanding backward $\pi$N scattering may be traced in a series of papers by Storrow and Winbow [181, 288]. In addition to the difficulties discussed in §4I.1, there are apparently inconsistencies between experimental data sets e.g. in $d\sigma/du$ $(\pi^+p \to p\pi^+)$ near 6 GeV/$c$ and in $d\sigma/du$ $(\pi^-p \to n\pi^0)$ [261]. These inconsistencies are not only in normalisation but, more seriously, in shape.

The existence of a set of 5 measurements $\sigma(p\pi^+)$, $\sigma(p\pi^-)$, $\sigma(n\pi^0)$, $P(p\pi^+)$, $P(p\pi^-)$ near 6 GeV/$c$ allows incomplete analysis of the amplitude structure to be performed. The three cross-section

measurements ($\sigma \equiv d\sigma/du$) allow a resolution of the isospin triangle:

$$A(p\pi^+) = \tfrac{1}{3}(2A^{1/2} + A^{3/2}), \qquad A(p\pi^-) = A^{3/2}, \qquad A(n\pi^0) = \tfrac{1}{3}\sqrt{2}(A^{1/2} - A^{3/2}), \tag{4I.5}$$

where the $A^I$ are spin-averaged amplitudes of definite $u$-channel isospin. In fig. 4I.3 (taken from ref. [159]) we show $|A^{1/2}|^2$ and the relative phase $\cos\phi_{13}$. $|A^{1/2}|^2$ has an approximate double zero at $u \simeq -0.15$ while $|A^{3/2}|^2$ (the $p\pi^-$ cross-section) has no remarkable structure. The zero in $|A^{1/2}|^2$ is a reflection of the dip structure in $\sigma(p\pi^+)$ and $\sigma(n\pi^+)$ which are traditionally described as due to the NWSZ, at $\alpha(u) = -\frac{1}{2}$, of the $N_\alpha$ Regge trajectory which is taken as linear in $u$. Because of this, and the fact that one can choose residue parametrisations which extrapolate comfortably to the $\pi$NN coupling constant, the $N_\alpha$ contribution to backward $\pi$N is often treated as a simple Regge pole with a linear trajectory (and the parity doublets at $\sqrt{u} = m_N$ etc. suppressed by arranging suitable zeroes in the residue function). Encouragement in this direction is afforded by the shrinkage observed in $\alpha_{\text{eff}}(\pi^+ p \to p\pi^+)$ (fig. 4I.4, see also remark (2) above).

Exchange degeneracy of the $\Delta_\delta$ and $N_\beta$ trajectories, and the absence of an $N_\beta$ state at $J^P = \frac{1}{2}^-$, imply zeroes at $\alpha_\Delta = \frac{1}{2}, -\frac{3}{2}\ldots$ in the residue of the $\Delta_\delta$ Regge pole which should dominate $|A^{3/2}|^2$, [47]. Thus, for linear trajectories, one expects no dips in $|A^{3/2}|^2$ for $|u| \lesssim 1$, and a value of $\cos\phi_{13} = -1/\sqrt{2}$ near $u = 0$. The data (fig. 4I.3), however, show $\cos\phi_{13} = +0.7$ near the value $(1/\sqrt{2})$ expected, if the $\Delta_\delta$ residue does *not* contain the NWSZ [82]. Another strange feature of $\cos\phi_{13}$ is its approximate double zero near $u = -0.15$, rather than a *single* zero reflecting that in $A^{1/2}$ [181]. The lack of shrinkage in $\alpha_{\text{eff}}(\pi^- p \to p\pi^-)$ is a further indication, if one were needed, that $\Delta$ exchange is not simple – it could be

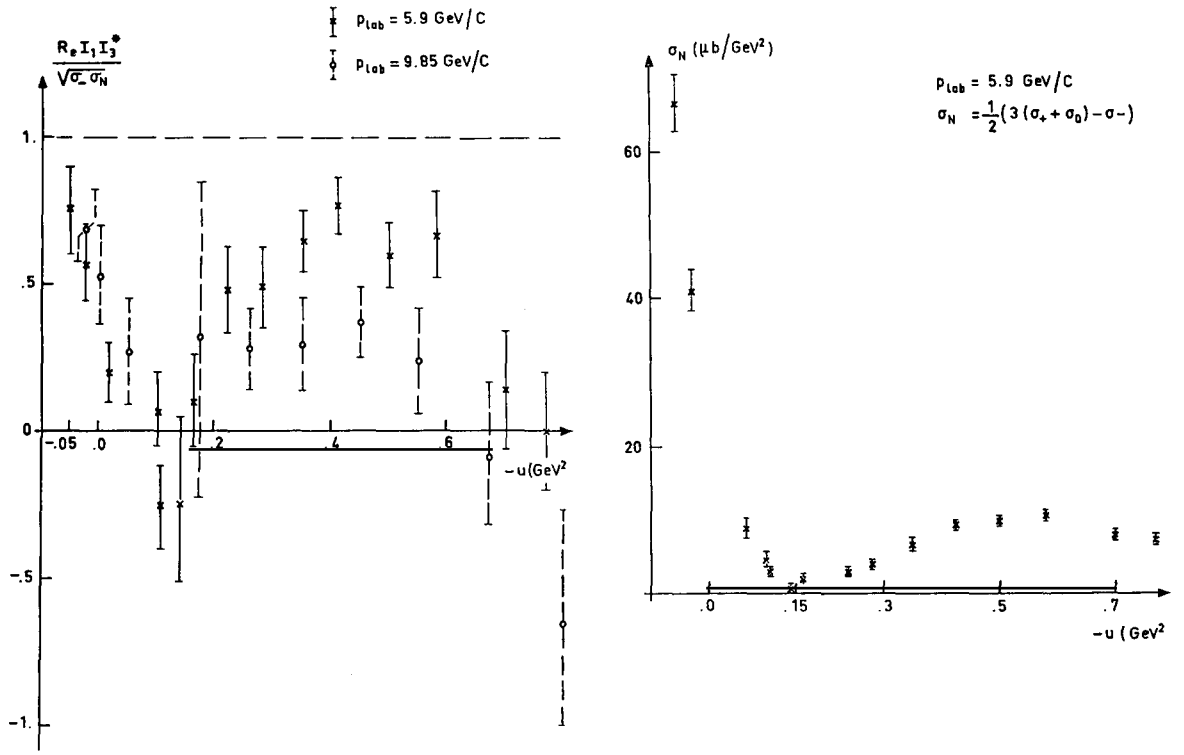


Fig. 4I.3. The $I = \frac{1}{2}$ exchange component $\sigma_N$ in backward $\pi$N scattering at 5.9 GeV/$c$, and the corresponding spin-averaged phase difference $(\text{Re}I_1 I_3^*/\sqrt{\sigma_- \sigma_N} = \xi \cos\phi_{13})$ between $I = \frac{1}{2}$ and $I = \frac{3}{2}$ exchange [159]. The $I = \frac{3}{2}$ intensity, $\sigma_-$ (not shown), is just the backward $\pi^- p$ scattering differential cross-section.

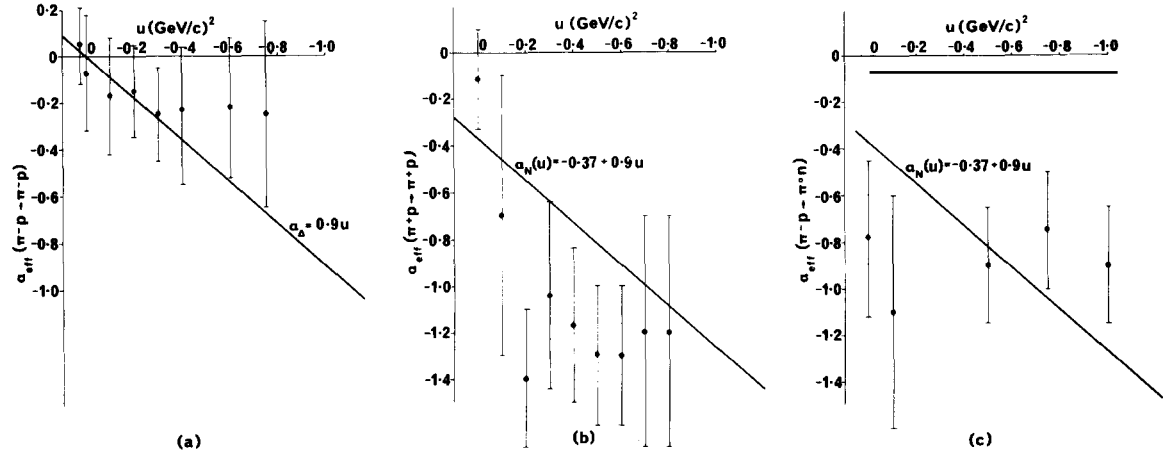


Fig. 4I.4. Effective trajectories for backward $\pi$N scattering, (a) $\pi^-p\to p\pi^-$, (b) $\pi^+p\to p\pi^+$ and (c) $\pi^-p\to n\pi^0$ [181].

because $\alpha_\Delta(\sqrt{u})$ is a dominantly odd function of $\sqrt{u}$ or because strong absorptive corrections are present.

To make a spin decomposition of $A^{1/2}$ and $A^{3/2}$ requires some assumptions to supplement the polarisation information. Several such model-dependent amplitude analyses have been performed [120, 159, 191, 288]. The most natural assumptions are made about the Regge pole nature of the $A^{1/2}$ amplitudes ($N_\alpha$ and possibly $N_\gamma$ exchange) although other choices are arguable. No particularly clear or compelling picture of the $A^{3/2}$ amplitudes emerges. Specific cut models [82] do not give a satisfactory description (particularly of $P(\pi^-p\to p\pi^-)$) but, unlike forward scattering, it is difficult to isolate the systematics of their failure uniquely. Such Regge pole (and cut) models as there are, all agree on one feature: that whereas the $N_\alpha$ (and $N_\gamma$, if included) extrapolate satisfactorily to the pole position, the extrapolated width of the $\Delta(1236)$ is always much too narrow (even when a residue zero at $\alpha = \frac{1}{2}$ is included).

Since the above analyses were performed, new measurements of $d\sigma/du$ ($\pi^-p\to n\pi^0$) from 2.6 to 8 GeV/$c$ have been performed [261]. The "dip" previously thought to be at $u \simeq -0.2$ now appears to be at around $-0.3$ and is very much shallower than previously measured. Over the range 4.3 to 8 GeV/$c$ there is now significant evidence of shrinkage ($\alpha'_{\text{eff}} \simeq 0.6$) whereas previously there was none [fig. 4I.4]. It is claimed that important radiative corrections [237] have, for the first time, been taken into account. Since these corrections are different for different charged particles it seems likely that isospin analyses (discussed above) and SU(3) comparisons (below) may have to be critically re-examined. In this review, we can only take the existing data at face-value.

Tests of line-reversal symmetry between $\bar{p}p\to\pi^+\pi^-$ and $\pi^-p\to p\pi^-$ and between $\bar{p}p\to\pi^-\pi^+$ and $\pi^+p\to p\pi^+$ have been made with 5 GeV/$c$ $\bar{p}p$ data by Chabaud et al. [115]†. The first of these comparisons seems to hold only approximately for $|u| < 1$, and is badly violated at larger $u$ ($\bar{p}p$ is low). The $p\pi^+$ comparison is approximately valid for $|u| \geq 0.4$ but no $\bar{p}p$ data exist in the interesting dip region. That there is better agreement for the mixed isospin channel ($p\pi^+$) than for the pure "$\Delta$ exchange" process, is somewhat surprising. However, one should remember that $\Delta$ exchange does behave less like a simple Regge-pole than $N_\alpha$ (see above). Smaller angle data for $\bar{p}p\to\pi^-\pi^+$ [$t_{\min}$ (5 GeV/$c$) $\simeq -0.08$] is needed to allow a comparison with the dip seen in $\pi^+p\to p\pi^+$ at $u = -0.15$.

† Line-reversal tests are made by comparison of cross-sections at fixed $t$ (or $u$) and fixed $s$. Corrections for the unequal flux-factors ($\bar{p}p$ and $\pi p$ incident) must also be made. This prescription corresponds to equal corrected cross-sections if dominated by a single Regge pole $\sim s^\alpha$ or $\nu^\alpha$.

### *4I.3.* SU(3) *related processes*

The SU(3) relation given by eq. (4C.4) is also valid for backward scattering – it makes no assumptions about the nature of the exchanges. From it, a triangular inequality between $\pi^-p\to p\pi^-$, $K^-p\to\Sigma^+\pi^-$ and $K^-p\to pK^-$ may be deduced

$$\left|\left[\frac{d\sigma}{du}(p\pi^-)\right]^{1/2}-\left[\frac{d\sigma}{du}(\Sigma^+\pi^-)\right]^{1/2}\right|\leq\left[\frac{d\sigma}{du}(pK^-)\right]^{1/2}. \tag{4I.6}$$

In Regge language, the first two processes are due to $\Delta$ exchange (plus possible exotics), while backward $K^-p$ elastic scattering is pure exotic (a $K^{*+}$–nucleon Regge–Regge cut?). It thus forms a simple and interesting system within which to test exchange ideas. At high energies, the RHS should rapidly tend to zero, and the $p\pi^-$ and $\Sigma^+\pi^-$ cross-sections approach equality. Recent measurements of the LHS at 3 and 5.1 GeV/$c$ [270] show that the shapes of the $p\pi^-$ and $\Sigma^+\pi^-$ differential cross-sections are different, but that the inequality (eq. (4I.6)) is still satisfied thanks to the non-zero "forbidden" peak measured in $K^-p\to pK^-$ at around 3 and 5 GeV/$c$ [114]. However, detailed measurements at 4.2 GeV/$c$ [321] show a different picture. At this energy, $d\sigma/du\ (pK^-)|_{u=0}$ has an upper limit of 0.25 $\mu$b GeV$^{-2}$ rather than the large value of ~2.5 $\mu$b GeV$^{-2}$ suggested by interpolation of the 3 and 5 GeV/$c$ data. The bounds on $p\pi^-$ and $\Sigma^+\pi^-$ are therefore much tighter but, miraculously, at this energy the differential cross-sections (and even the polarisations) are equal within errors (fig. 4I.5). We conclude that, although the exotic amplitude has not yet settled down to its asymptotic behaviour, SU(3) seems, nonetheless, to be well satisfied.

The supposed simplicity of $N_\alpha$ exchange makes it an obvious candidate for SU(3) applications. Kayser and Hayot [127] have successfully predicted $d\sigma/du$ $(\pi^+p\to p\pi^+)$ ($N_\alpha$ dominated) from $d\sigma/du$ $(K^+p\to pK^+)$ ($\Lambda_\alpha$ dominated)†. The comparison of normalisation implies $F/D\simeq 0.8$. From an $N_\alpha$, $\Delta_\delta$ pole and weak cut model for $\pi^\pm p$ scattering they have also successfully predicted the differential cross-sections for $K^-n\to\Lambda\pi^-$ and $K^-n\to\Sigma^0\pi^-$ (also $N_\alpha$, $\Delta_\delta$ dominated). Recently Gula et al. [268] have used a highly simplified, duality-motivated, Regge pole amplitude (the baryon exchange equivalent of the model proposed in appendix A) to relate $N_\alpha$ exchange in $\pi^+p\to p\pi^+$ and $K^-p\to\Lambda\pi^0$ ($F/D\simeq 2$). They point out that the constant residue approximation of the Veneziano amplitude, in the high energy limit for $u<0$, can be readily continued to $u>0$ in such a way as to avoid parity doublets.

The process whose amplitude spin structure is best-known is $\pi^-p\to\Lambda K^0$, for which a complete amplitude analysis [measurement of $d\sigma/dt$, $P$ and $R$ (or $A$)] has been performed at 5 GeV/$c$ [247]. The flip/non-flip amplitude ratio is intimately connected to the exchange parity, since [181]

$$\frac{T_{+-}}{T_{++}}\underset{s\to\infty}{\approx}\frac{\tilde{A}}{B\sqrt{u}}=\frac{\hat{F}^+(\sqrt{u})+\hat{F}^+(-\sqrt{u})}{\hat{F}^+(\sqrt{u})-\hat{F}^+(-\sqrt{u})} \tag{4I.7}$$

where $\tilde{A}\equiv A+m_N B$ and $B$ are the usual invariant amplitudes, $T_{\lambda'\lambda}$ the usual $s$-channel helicity amplitudes, and $\hat{F}^\pm(\sqrt{u})$ $(=-\hat{F}^\mp(-\sqrt{u}))$ are the $u$-channel regularised parity-conserving helicity amplitudes. For example, in the absence of physical parity doublets,

$$\tilde{A}/B|_{u=m_R^2}=\tau_R\eta_R m_R \tag{4I.8}$$

for a resonance of mass $m_R$ and naturality $\tau_R\eta_R$. For $\pi^-p\to\Lambda K^0$ in the range $|u|\leq 0.4$, it is found that

† SU(3) comparisons between exchanges with unequal trajectories must use an SU(3) mass-breaking prescription similar to that outlined in section 4C (eq. (4C.13)).

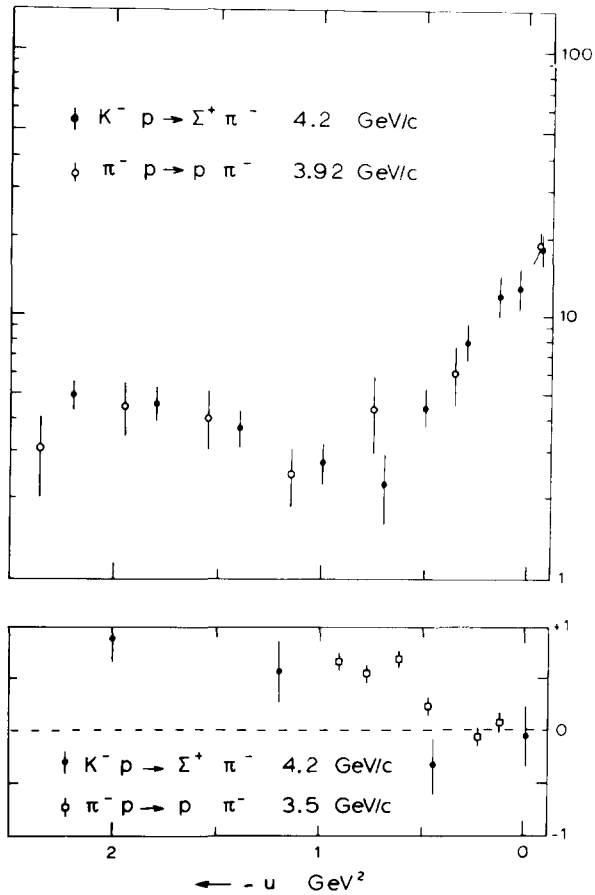


Fig. 4I.5. A test of SU(3) for Δ exchange in $K^-p \to \Sigma^+\pi^-$ and $\pi^-p \to p\pi^-$. Above, are the differential cross-sections ($\mu$b GeV$^{-2}$) and below, the polarisation [321].

$|\tilde{A}/B| \simeq 0.5$ and $\sin\phi_{AB} \simeq -1$ ($\phi_{AB} = \arg(\tilde{A}/B)$). Schmid and Storrow [136] have anticipated such a result, using a knowledge of the resonance coupling signs, in a Regge pole model with EXD $\Sigma_\alpha, \Sigma_\gamma$ and $\Sigma_\beta, \Sigma_\delta$ pairs of trajectories. (In fact, many of the amplitude analysis results [247] can be anticipated from the known Λ polarisation, since, when $P = +1$, $R^2 \simeq A^2 \simeq 0$.) The agreement between the model of ref. [136] and the essential features of the amplitude analysis, shows that it is possible to establish the same consistency between the mass spectrum and the scattering region (using the simplest extrapolation models) as was achieved for meson exchange.

### *4I.4. Photoproduction and vector-meson production*

Forward photoproduction has its unique problematic features (section 4D). In view of the parlous state of backward $0^{-\frac{1}{2}+}$ phenomenology, it therefore comes as no surprise to learn that backward photoproduction has very few transparent, well-tested, or well-understood qualities. Berger and Fox [83] have summarised some experimental systematics of $d\sigma/du$ ($\gamma N \to N\pi$)

(a) no appreciable shrinkage
(b) $s$-dependence $\sim s^{-3}$
(c) $u$-dependence $\sim e^{u}$
(d) no dip structures in $u$.

Regge pole models with exactly linear trajectories (see point (2) of §4I.1) cannot reproduce feature (a). Features (c) and (d) reflect directly on the baryon couplings to $\gamma N$ as compared to $\pi N$. Most models explain the filling in of the $N_\alpha$ dip in $\gamma N \to N\pi$ as due to relatively strong coupling of the $N_\gamma$ and $N_\beta$ trajectories. In addition, one can go some way to reproducing lack of shrinkage by arranging that $I = \frac{1}{2}$ exchange ($\alpha_{N_\alpha}(0) \simeq -\frac{1}{2}$) dominates for small $u$ but $I = \frac{3}{2}$ ($\alpha_\Delta(0) \simeq 0$) dominates for $-u > 0.5$ [67]. This assignment is not seriously contradicted by the ratio $d\sigma/du\ (p\pi^0)/d\sigma/du\ (n\pi^+)$ which is sensitive to the $u$-channel isospin decomposition. One still expects shrinkage at large $|u|$ ($\geqslant 1$) but data are as yet inconclusive. Berger and Fox [83] recommend $\alpha_{\text{eff}}$ studies of $\gamma p \to \Delta^{++}\pi^-$ (pure $I_u = \frac{3}{2}$) and $\gamma d \to pn$ (pure $I_u = \frac{1}{2}$) for more direct tests of shrinkage.

In summary, $\gamma N \to N\pi$ has all the ambiguities and problems of $\pi N \to N\pi$ plus extra ones associated with having 4 complex amplitudes but, as yet, only one measurement ($d\sigma/du$). The lack of precise data over a range of energies also inhibits any really worthwhile tests of exchange models.

Recently, $d\sigma/du$ and $\rho_{mm'}$ data for $\pi^+ n \to p(\rho^0, \omega, f)$ have become available at 4 GeV/$c$ [218] and 6 GeV/$c$ [207]. Vector meson dominance relates an appropriate sum of helicity one $\rho$ and $\omega$ production cross-sections to $d\sigma/du$ ($\gamma p \to n\pi^+$). The incoherent sum of $\rho$ and $\omega$ are even flatter in $u$ than photoproduction although the VMD comparison is valid within the limits of the unknown $\rho$–$\omega$ interference term [204]. There is no evidence of dips at $u = -0.2$ in any of the quantities $\rho_{00}$, $\rho_{11} \pm \rho_{1-1}$ or $d\sigma/du$.

The global features of $\rho$, $\omega$ and f production at backward angles appear similar.

## 5. Conclusions

In the early sections of the review we emphasised the established successes of Regge pole theory and Regge phenomenology. These have led to a situation where one can predict (reliably) the gross energy dependence and amplitude structure of any two-body reaction. In view of the scant information available from other sources on the underlying dynamics of the strong interaction, this is no mean achievement. It was also argued that the corrections to the Regge pole formula (absorption, Regge cuts, etc.) are an intrinsic and significant feature of hadronic amplitudes and deserve careful study in their own right. Before taking stock of the current state and future prospects of Regge phenomenology, we enumerate a few general points which have emerged in our survey.

(1) Above laboratory momenta of 4 GeV/$c$ or so, every measured two-body reaction has a cross-section whose energy dependence is in agreement with that expected in a Regge pole model.

(2) Every Regge pole exchange, which is expected to contribute significantly in scattering processes, can be observed in the data – there are no anomalous "missing" Regge trajectories.

(3) There is firm evidence of absorption or Regge cut corrections in many amplitudes – particularly those helicity amplitudes with no net helicity-flip.

(4) The cruder properties of these corrections ($t$-dependence flatter than the corresponding pole contribution and an approximately destructive relative phase) are understood in terms of the physically intuitive absorption model or Regge–Pomeron cuts. There are many subtler, but nevertheless well-established, features awaiting a proper understanding.

(5) SU(3) and, to a lesser extent, quark model constraints on Regge residues lead to an accurate and economical description of the data. Even in the presence of (absorptive?) corrections, the physical amplitudes appear to satisfy SU(3) symmetry.

(6) Exchange degeneracy provides a rough guide to the relative strength of opposite signature exchanges. However, unlike SU(3), there are many examples where it is seriously violated and in a manner which is ill-understood.

(7) Whereas Regge poles provide a straightforward connection between the meson spectrum ($t > 0$) and forward high-energy scattering ($t < 0$), the analogous connection for baryon exchange processes is complicated and of less immediate phenomenological value.

We now return to the question raised in the introduction – has Regge phenomenology far to go? Are there exciting discoveries still to be made by studying high-energy two-body scattering amplitudes, or would effort be better spent exploring other avenues?

The grounds for pessimism are simply stated: there have been no great breakthroughs in recent years, models have been discredited one by one, the Regge cuts we study are second-order effects and, since coupling constants are large, they will be difficult to calculate in any theory. However, viewed in the context of a larger project (the attempt to understand the strong interactions), Regge phenomenology still seems as likely to open the way to important new discoveries as do other areas of study viz. multiparticle final states, large $p_T$ phenomena, diffractive processes and resonance spectroscopy. The last two, in common with Regge phenomenology, involve simple, well-defined final states allowing measurement of amplitudes rather than cross-sections. Theoretical ideas can therefore be stringently tested. Amongst the best three areas where amplitudes can be measured, two-body Regge phenomenology is distinguished by the richness and variety of its data. Because of this, Regge phenomenology has reached the healthy situation where sufficient experimental systematics have been established that (a) one can rigorously discriminate between current theoretical models and (b) the building materials for new ones are in reasonable supply. (Compare this on the one hand, with atomic physics where the basic theoretical model is far in advance of the experimental applications and, on the other, with large $p_T$ physics where models abound but data, though plentiful, cannot discriminate.)

Theoretical progress, in the near future, is expected to evolve in two main directions. Firstly, within the framework of the Reggeon calculus, one might anticipate progress in understanding the shrinkage and factorisation properties of Regge cuts. This should go hand-in-hand with the measurement of familiar two-body processes at very high energies ($p_{LAB} \geq 100\,\text{GeV}/c$) and large momentum-transfers ($|t| > 1\,\text{GeV}^2$). The second area of theoretical research involves various "dual unitarisation" schemes. Here, the proposal is to classify hadronic amplitudes according to their dual topology, obtain solutions of the unitarity equation for each topology and then calculate the physical amplitude as a perturbation expansion in increasing topological complexity. This may well have practical repercussions for exchange degeneracy violation, exotic exchange and the relation between diffractive and non-diffractive scattering [257].

On the experimental front, much more information is expected to be available on the production of unnatural parity states ($A_1$, H, D, E, etc.), and of high spin resonances ($J \geq 2$). Polarisation measurements of increasing sophistication are being attempted. For example, "complete measurements" of the spin structure of hypercharge exchange reactions and of proton–proton scattering will shortly be available. Understanding the nature of the corrections to Regge poles will require two complementary types of experimental study. Firstly, information on the $t$-dependence and phase of each amplitude can only come from these detailed polarisation studies (which are limited to conventional energies). This reflects on the detailed structure of the associated $j$-plane discontinuity. Secondly, to illuminate

the precise nature of the branch point singularity, one requires additional two-body data at very high energies.

The recent discoveries of new high mass mesons $J/\chi$ [190] and associated charmed mesons [315] have, so far, had little impact on the basic problems of Regge pole dynamics. This is mainly because their small couplings to "conventional" hadrons, and high masses, inhibit participation in the normal hadronic world of large cross-sections and whose dynamics are characterised by masses of 1 GeV or less. Of course, the extra quantum number may give some insight into the nature of SU(3) breaking and related phenomena.

The role of Regge phenomenology is not so much to obtain and test a complete theory of hadronic scattering as to reduce the data to a coherent form suitable for motivating or suggesting such a theory. To this extent, it has served, and should continue to serve, a very useful function.

**Acknowledgements**

We are very grateful to Diane Ho for her efficient and cheerfully-given assistance in the preparation of the manuscript. One of us (ACI) thanks his colleagues at Liverpool for their encouragement and tolerance during the course of this work.

## Appendix A. Reggeised Born term model

In this appendix we present a simple Regge pole model which explicitly satisfies the theoretical and phenomenological constraints discussed in §2.2. Because of these constraints, the relevant Regge residues (coupling constants) can be estimated theoretically, so giving the model considerable predictive power.

### *AA.1. Amplitude structure*

We use the $s$-channel helicity amplitudes of section 2, but rewrite the helicity subscripts in a form suggestive of factorisation. In terms of these, the differential cross-section for $ab \to cd$ is,

$$\frac{d\sigma}{dt} = \frac{389.3}{(2s_a+1)(2s_b+1)64\pi m_b^2 p_L^2} \sum_{\lambda_i} |T^{\lambda_c\lambda_a}_{\lambda_d\lambda_b}(s,t)|^2 \,\mu b\,\mathrm{GeV}^{-2}. \tag{AA.1}$$

If $ab \to cd$ is mediated by the exchange of Reggeon e, the amplitude is factorised (see fig. AA.1) into the form

$$T^{\lambda_c\lambda_a}_{\lambda_d\lambda_b}(s,t) = -V^{\lambda_c\lambda_a}_{e}(ca) \cdot R[s,\alpha_e(t)] \cdot V^{e}_{\lambda_d\lambda_b}(db). \tag{AA.2}$$

Each vertex factor $V$ is written as the product of a helicity coupling $\beta$ and a kinematical "half-angle" factor:

$$V^{\lambda_c\lambda_a}_{e}(ca) = \beta_e^{\lambda_c\lambda_a}(ca) \cdot (-t'/4M^2)^{|\lambda_c-\lambda_a|/2}. \tag{AA.3}$$

Here, $t'$ is $t - t_{\min}$ and $M$, the nucleon mass, is introduced for dimensional reasons. The factorised

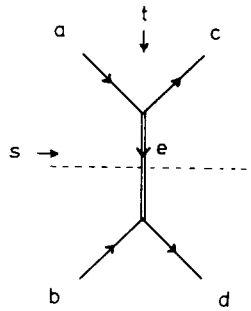


Fig. AA.1. Kinematics and factorisation convention for the Born term model of appendix A.

Regge residue $\beta_e^{\lambda_c\lambda_a}$ (ca) is taken to be a constant and is therefore proportional to the coupling constant $(g^2_{ace}/4\pi)^{1/2}$ which would arise in a one meson exchange Born term calculation [13].

The crucial extrapolation from $t = m_e^2$ to $t < 0$ employs an ansatz suggested by the high energy limit of a Veneziano amplitude. Thus, we write the Reggeised propagator for e as

$$R[s, \alpha_e(t)] = \tfrac{1}{2}[1 + (-)^{s_e}\exp\{-i\pi\alpha_e(t)\}]\Gamma[l_e - \alpha_e(t)](\alpha')^{1-l_e}(\alpha' s)^{\alpha_e(t)} \tag{AA.4}$$

where $l_e$ is the spin of the lowest state occuring on the EXD trajectory and $\alpha' = 0.9\,\mathrm{GeV}^{-2}$. Note that since

$$\alpha_e(t) - s_e = \alpha'(t - m_e^2), \tag{AA.5}$$

$R[s, \alpha_e(t)]$ reduces, in the neighbourhood of $t = m_e^2$, to

$$R[s, \alpha_e \approx s_e] \approx s^{s_e}/(m_e^2 - t), \tag{AA.6}$$

the meson-exchange Born term result. Using eqs. (AA.2), (AA.3) and (AA.6), the identification of the residues ($\beta$) and coupling constants can be made.

Parity conservation at each vertex (eq. (2.2)) implies

$$\begin{aligned} V_e^{\lambda_c\lambda_a}(\mathrm{ca}) &= \tau_e\eta_c\eta_a(-)^{s_c - s_a + \lambda_c - \lambda_a} V_e^{-\lambda_c - \lambda_a}(\mathrm{ca}), \\ V^e_{\lambda_d\lambda_b}(\mathrm{db}) &= \tau_e\eta_d\eta_b(-)^{s_d - s_b - \lambda_d + \lambda_b} V^e_{-\lambda_d - \lambda_b}(\mathrm{db}), \end{aligned} \tag{AA.7}$$

where $\tau_e(=\eta_e(-)^{s_e})$ is the naturality of e, and $\eta_i$ is the intrinsic parity of particle i. "Upper" and "lower" vertices are related by

$$V_e^{\lambda_c\lambda_a}(\mathrm{ca}) = (-)^{s_a - \lambda_a + s_c - \lambda_c} V^e_{\lambda_c\lambda_a}(\mathrm{ca}). \tag{AA.8}$$

### *AA.2. Evaluation of couplings*

Table AA.1 exhibits the types of process which we shall consider. Alongside each type are listed the prototype couplings from which each particular reaction may be calculated. Table AA.2 lists the relevant Regge trajectory parameters. Having identified the prototype couplings from the reaction directory (table AA.1), their numerical values are obtained from table AA.3. Overall "best fit" values of these have been obtained by studying the model's predictions for many well-measured processes. Also listed in table AA.3 are theoretical estimates obtained from resonance decay widths, vector dominance etc. (the precise origin of each is indicated). In most cases, the phenomenological and theoretical values are found to be compatible and the theoretical value is therefore adopted.

We assume (§2.2)

(1) exchange degeneracy of trajectories and couplings,

(2) SU(3) symmetry of couplings,

(3) SU(3) mass breaking is manifested only in the trajectory functions which appear in $R[s, \alpha_e(t)]$ e.g. $\alpha_\pi(t) - \alpha_K(t) \approx 0.2$ (see table AA.2).

With these assumptions, one need consider only $\rho$, $\pi$ and $A_1$ as representative of the leading SU(3) octet exchanges.

To facilitate the evaluation of the specific couplings in each process, we give (in tables AA.4($\rho$), AA.5($\pi$) and AA.6($A_1$)) most of the useful SU(3), SU(2) and EXD-related couplings.

Table AA.1

The processes described by the model are listed together with the prototype couplings required. The latter are chosen to be those most conveniently and reliably estimated theoretically (table AA.3). The specific couplings are then obtained from these using SU(3) symmetry (tables AA.4–6).

| Process ab→cd | Prototype couplings: e(ca) or e(db) | |
|---|---|---|
| | Natural parity | Unnatural parity |
| $0^-0^- \to 0^-0^-$ | $\rho(\pi\pi)$ | – |
| $*\frac{1}{2}^+\frac{1}{2}^+ \to \frac{1}{2}^+\frac{1}{2}^+$ | $\rho$(NN) | $\pi$(NN) |
| $0^-\frac{1}{2}^+ \to 0^-\frac{1}{2}^+$ | $\rho(\pi\pi)$, $\rho$(NN) | – |
| $0^-\frac{1}{2}^+ \to 0^-\frac{3}{2}^+$ | $\rho(\pi\pi)$, $\rho(\Delta N)$ | – |
| $0^-\frac{1}{2}^+ \to 1^-\frac{1}{2}^+$<br>$1^-\frac{1}{2}^+ \to 0^-\frac{1}{2}^+$ | $\rho(\omega\pi)$, $\rho$(NN) | $\pi(\rho\pi)$, $\pi$(NN)<br>$A_1(\rho\pi)$, $A_1$(NN) |
| $0^-\frac{1}{2}^+ \to 1^-\frac{3}{2}^+$<br>$1^-\frac{1}{2}^+ \to 0^-\frac{3}{2}^+$ | $\rho(\omega\pi)$, $\rho(\Delta N)$ | $\pi(\rho\pi)$, $\pi(\Delta N)$ |
| $*\frac{1}{2}^+\frac{1}{2}^+ \to \frac{1}{2}^+\frac{3}{2}^+$ | $\rho$(NN), $\rho(\Delta N)$ | $\pi$(NN), $\pi(\Delta N)$ |
| $*\frac{1}{2}^+\frac{1}{2}^+ \to \frac{3}{2}^+\frac{3}{2}^+$ | $\rho(\Delta N)$ | $\pi(\Delta N)$ |
| $0^-\frac{1}{2}^+ \to 1^+\frac{1}{2}^+$ | $\omega(B\pi)$, $\rho$(NN) | –† |
| $0^-\frac{1}{2}^+ \to 1^+\frac{3}{2}^+$ | $\omega(B\pi)$, $\rho(\Delta N)$ | –† |

* a and c may also be $\frac{1}{2}^+$.

† Coupling possible but neglected.

Table AA.2

The Regge exchanges and trajectory intercepts $\alpha_0$. $s_e$ is the spin of the corresponding meson exchange and $l_e$ the minimum value achieved by $s_e$ on the exchange degenerate trajectory. The trajectory slope is taken as $\alpha' = 0.9$.

| e | $s_e$ | $l_e$ | $\alpha_0$ |
|---|---|---|---|
| $\rho$, $\omega$(K*)<br>$A_2$, f(K**) | 1<br>2 | 1 | 0.5 (0.35) |
| $\pi$(K)<br>B($K_B$) | 0<br>1 | 0 | $-\alpha' m_\pi^2 (-\alpha' m_K^2)$ |
| $A_1(K_A)$<br>$Z(K_Z)$ | 1<br>2 | 1 | 0 (−0.25) |

## *AA.3. Limits of application*

Aside from the case of $\pi$ and related exchanges, we neglect absorptive effects. This is partly because we are primarily interested in a Born term model and partly because there exists no comparably simple (far less reliable) means of calculating absorptive corrections in general (section 3). In the case of $\pi$ exchange these remarks do not apply. Firstly, one cannot reasonably neglect absorption in those $\pi$ exchange amplitudes which vanish at $t = 0$ for a pure pole, but for which data show a forward spike (e.g. $np \to pn$ or $\gamma p \to \pi^+ n$). Secondly, there does exist a parameter-free prescription which describes $\pi$ exchange absorption in a successful, if ill-understood, manner. We implement this prescription, known as the Williams model (see §4D.1) as follows

*Williams model*

Each Regge pole amplitude can be written (see eq. (AA.3)) as

$$T^{\lambda_c\lambda_a}_{\lambda_d\lambda_b} = -(-t'/4M^2)^{(n+x)/2} \cdot \beta_e^{\lambda_c\lambda_a}\beta^e_{\lambda_d\lambda_b} \cdot R[s, \alpha(t)], \tag{AA.9}$$

where $n, x$ are defined in eq. (2.5). In the case of $\pi$ exchange, the Williams prescription [79] is to evaluate the amplitude (apart from the essential angular momentum conservation factor $(-t')^{n/2}$ and the pole propagator) at $t = m_\pi^2$. Thus, the corrected $\pi$ exchange amplitude becomes‡

$$T^{\lambda_c\lambda_a}_{\lambda_d\lambda_b}(\text{abs.}) = -(-t'/4M^2)^{n/2} \cdot (-m_\pi^2/4M^2)^{x/2} \cdot \beta_e^{\lambda_c\lambda_a}\beta^e_{\lambda_d\lambda_b} \cdot R[s, \alpha(t)]. \tag{AA.10}$$

Table AA.3

The basic coupling strengths $\beta$. The "overall best-fit" values and theoretically estimated values are compared. The former were estimated by ensuring that overall helicity-flip dominated processes are well reproduced. In cases where the *ratio* of helicity couplings is not well determined by data, the theoretical value is used. Other couplings are related to those by exact EXD, SU(3) and isospin. The relevant SU(3) tables are catalogued.

| Exchange | Coupling | Phenom. value | Theoretical estimate | Origin of theoretical estimate | SU(3) Table |
|---|---|---|---|---|---|
| | $\beta_\rho(\pi^0\pi^-)$ | 8.0 | 8.3 | $\Gamma_{\rho\to\pi\pi} = 143$ MeV | AA.4a |
| | $\beta_\rho^{\lambda_\omega=1}(\omega\pi^-)$ | 13.0 | 16.6 | Gell-Mann, Sharp, Wagner model for $\Gamma_{\omega\to 3\pi}$ [5] | 4b |
| | $\beta^\rho_{1/2\ 1/2}$(np) | 2.3 | 5.9 | VMD of nucleon form-factors [76] | 4c |
| | $_{1/2-1/2}$ | 18.4 | 27.7 | | |
| $\rho$ | $\beta^\rho_{1/2-1/2}(\Delta^{++}\text{p})$ | 12.5 | 10–13 | VMD of transition form-factor [322] | 4d |
| | $_{3/2\ 1/2}$ | $\sqrt{3}$† | $\sqrt{3}$† | | |
| | $_{1/2\ 1/2}$ | 0 | 0 | Quark model [39] | |
| | $_{3/2-1/2}$ | 0 | 0 | | |
| $(\omega)$ | $\beta_\omega^{\lambda_B=0}(B^+\pi^+)$ | 3.0 | 6.1 | $\Gamma_{B\to\omega\pi} = 135$ MeV, | 4e |
| | $\lambda_B = +1$ | 2.2† | 2.2† | $\lvert F_0\rvert^2 = 0.10$ [203] | |
| | $\beta_\pi^{\lambda_\rho=0}(\rho^0\pi^-)$ | 4.40 | 4.40 | $\Gamma_{\rho\to\pi\pi} = 143$ MeV | 5a |
| | $\lambda_\rho = +1$ | 3.45† | 3.45† | Crossing matrix evaluated at $t = \mu^2$ [79] | |
| | $\beta^\pi_{1/2-1/2}$(np) | 35.7 | 35.7 | $g^2_{\pi NN}/4\pi = 14.4$ | 5b |
| $\pi$ | | 0 | 0 | *CP* invariance | |
| | $\beta^\pi_{1/2\ 1/2}(\Delta^{++}\text{p})$ | −5.3 | −6.46 | $\Gamma_{\Delta\to\pi N} = 115$ MeV | 5c |
| | $_{1/2-1/2}$ | −4.27† | −4.27† | Crossing matrix evaluated at $t = \mu^2$ | |
| | $_{3/2-1/2}$ | −5.91† | −5.91† | | |
| | $_{3/2-1/2}$ | 5.11† | 5.11† | | |
| | $\beta_{A_1}^{\lambda_\rho=0}(\rho^0\pi)$ | 6.76* | 6.76 | $\Gamma_{A_1\to\rho\pi} = 140$ MeV, *l*-broken | 6a |
| | $\lambda = 1$ | 0.74† | 0.74† | $SU(6)_w$ [272] | |
| $A_1$ | $\beta^{A_1}_{1/2\ 1/2}$(np) | 5.0* | 6.2 | Axial VMD of weak form factor [272] | 6b |
| | $_{1/2-1/2}$ | 0 | 0 | *CP* invariance | |

† The *ratio* of this coupling to the first entry is presented.

* Only the product of these couplings is phenomenologically testable.

‡ We neglect $t_{min}$ everywhere except in $(-t')^{n/2}$.

Table AA.4

The SU(3), SU(2) Clebsches for couplings of the vector and tensor exchanges.

| e \ ca | $\pi^-\pi^-$ | $\eta_8\pi^0$ | $K^+K^+$ | $K_SK_L$ | $K^+\pi^+$ | $\pi^-K^-$ | $\eta_8\bar{K}^0$ |
|---|---|---|---|---|---|---|---|
| $\rho^0$ | $-1$ | · | $\frac{1}{2}$ | $-\frac{1}{2}$ | · | · | · |
| $A_2^0$ | · | $\frac{1}{\sqrt{3}}$ | $\frac{1}{2}$ | · | · | · | · |
| $\omega$ | · | · | $\frac{1}{2}$ | $\frac{1}{2}$ | · | · | · |
| $f$ | 1 | · | $\frac{1}{2}$ | · | · | · | · |
| $\overline{K^{*0}}$ | · | · | · | · | $\frac{1}{\sqrt{2}}$ | $-\frac{1}{\sqrt{2}}$ | $\frac{\sqrt{3}}{2}$ |
| $\overline{K^{**0}}$ | · | · | · | · | $-\frac{1}{\sqrt{2}}$ | $-\frac{1}{\sqrt{2}}$ | $-\frac{1}{2\sqrt{3}}$ |
| $\beta_e(ca)/\beta_\rho(\pi^0\pi^-)$ | | | | | | | a) |

| e \ ca | $\rho^-\pi^-$ | $\omega\pi^0$ | $K^{*+}K^+$ | $K^{*-}K^-$ | $\phi\bar{K}^0$ | $K^{*+}\pi^+$ | $\omega\bar{K}^0$ | $\rho^-K^-$ |
|---|---|---|---|---|---|---|---|---|
| $\rho^0$ | · | 1 | $\frac{1}{2}$ | $\frac{1}{2}$ | · | · | · | · |
| $A_2^0$ | $-1$ | · | $\frac{1}{2}$ | $-\frac{1}{2}$ | · | · | · | · |
| $\omega$ | 1 | · | $\frac{1}{2}$ | $\frac{1}{2}$ | · | · | · | · |
| f | · | · | $\frac{1}{2}$ | $-\frac{1}{2}$ | · | · | · | · |
| $\overline{K^{*0}}$ | · | · | · | · | $-\frac{1}{\sqrt{2}}$ | $-\frac{1}{\sqrt{2}}$ | $\frac{1}{2}$ | $-\frac{1}{\sqrt{2}}$ |
| $\overline{K^{**0}}$ | · | · | · | · | $\frac{1}{\sqrt{2}}$ | $\frac{1}{\sqrt{2}}$ | $\frac{1}{2}$ | $-\frac{1}{\sqrt{2}}$ |
| $\beta_e^{\lambda_e=1}(ca)/\beta_\rho^{\lambda_\omega=1}(\omega\pi^-)$ | | | | | | | | b) |

| e \ db | pp | $\Sigma^+p$ | $\Lambda n$ |
|---|---|---|---|
| $\rho^0$ | $\frac{1}{\sqrt{2}}(F/D+1)$ | · | · |
| $A_2^0$ | $\frac{1}{\sqrt{2}}(F/D+1)$ | · | · |
| $\omega$ | $\frac{1}{\sqrt{2}}(3F/D-1)$ | · | · |
| f | $\frac{1}{\sqrt{2}}(3F/D-1)$ | · | · |
| $\overline{K^{*0}}$ | · | $F/D-1$ | $-\frac{1}{\sqrt{6}}(3F/D+1)$ |
| $\overline{K^{**0}}$ | · | $F/D-1$ | $-\frac{1}{\sqrt{6}}(3F/D+1)$ |
| $(1+F/D)\beta^e_{\lambda_d\lambda_b}(db)/\beta^\rho_{\lambda_n\lambda_p}(np)$; $(F/D)_{++}=-3$ $(F/D)_{+-}=0.4$ | | | c) |

Table AA.4 (*Continued*)

| e \ db | $\Delta^+ p$ | $\Sigma^+(1385)p$ |
|---|---|---|
| $\rho^0$ | $\sqrt{\frac{2}{3}}$ | · |
| $A_2^0$ | $\sqrt{\frac{2}{3}}$ | · |
| $\overline{K^{*0}}$ | · | $\frac{1}{\sqrt{3}}$ |
| $\overline{K^{**0}}$ | · | $\frac{1}{\sqrt{3}}$ |
| $\beta^e_{1/2-1/2}(db)/\beta^\rho_{1/2-1/2}(\Delta^{++}p)$ | | d) |

| e \ ca | $B^-\pi^-$ | $H_B\pi^0$ | $K_B^+K^+$ | $K_B^-K^-$ | $K_B^+\pi^+$ | $B^-K^-$ |
|---|---|---|---|---|---|---|
| $\rho^0$ | · | $-\frac{1}{\sqrt{3}}$ | $\frac{1}{2}$ | $\frac{1}{2}$ | · | · |
| $A_2^0$ | $-1$ | · | $\frac{1}{2}$ | $-\frac{1}{2}$ | · | · |
| $\omega$ | 1 | · | $\frac{1}{2}$ | $\frac{1}{2}$ | · | · |
| f | · | · | $\frac{1}{2}$ | $-\frac{1}{2}$ | · | · |
| $\overline{K^{*0}}$ | · | · | · | · | $-\frac{1}{\sqrt{2}}$ | $-\frac{1}{\sqrt{2}}$ |
| $\overline{K^{**0}}$ | · | · | · | · | $\frac{1}{\sqrt{2}}$ | $-\frac{1}{\sqrt{2}}$ |
| $\beta_e^{\lambda_c=0}(ca)/\beta_\omega^{\lambda_B=0}(B^+\pi^+)$ | | | | | | e) |

Table AA.5

SU(3), SU(2) Clebsches for couplings of the pseudoscalar and axial vector ($J^{PC} = 1^{+-}$) exchanges. Isospin zero exchanges have been ignored.

| e \ ca | $\rho^-\pi^-$ | $\omega\pi^0$ | $K^{*+}K^+$ | $K^{*-}K^-$ | $\phi\bar{K}^0$ | $K^{*+}\pi^+$ | $\omega\bar{K}^0$ | $\rho^-K$ |
|---|---|---|---|---|---|---|---|---|
| $\pi^0$ | $-1$ | · | $\frac{1}{2}$ | $-\frac{1}{2}$ | · | · | · | · |
| $B^0$ | · | 1 | $\frac{1}{2}$ | $\frac{1}{2}$ | · | · | · | · |
| $\overline{K^0}$ | · | · | · | · | $\frac{1}{\sqrt{2}}$ | $\frac{1}{\sqrt{2}}$ | $\frac{1}{2}$ | $-\frac{1}{\sqrt{2}}$ |
| $\overline{K_B^0}$ | · | · | · | · | $-\frac{1}{\sqrt{2}}$ | $-\frac{1}{\sqrt{2}}$ | $\frac{1}{2}$ | $-\frac{1}{\sqrt{2}}$ |
| $\beta_e^{\lambda_c=0}(ca)/\beta_\pi^{\lambda_\rho=0}(\rho^0\pi^-)$ | | | | | | | | a) |

Table AA.5 (*Continued*)

| e \ db | pp | $\Sigma^+$p | $\Lambda$n |
|---|---|---|---|
| $\pi^0$ | $\frac{1}{\sqrt{2}}(F/D+1)$ | · | · |
| $B^0$ | $\frac{1}{\sqrt{2}}(F/D+1)$ | · | · |
| †$\overline{K^0}$ | · | $F/D-1$ | $-(3F/D+1)/\sqrt{6}$ |
| †$\overline{K^0_B}$ | · | $F/D-1$ | $-(3F/D+1)/\sqrt{6}$ |
| $(1+F/D)\beta^e_{+-}(db)/\beta^\pi_{+-}(np)$; $F/D=\frac{2}{3}$ | | | b) |

| e \ db | $\Delta^+$p | $\Sigma^*(1385)$p |
|---|---|---|
| $\pi^0$ | $\sqrt{\frac{2}{3}}$ | · |
| $B^0$ | $\sqrt{\frac{2}{3}}$ | · |
| $\overline{K^0}$ | · | $1/\sqrt{3}$ |
| $\overline{K^0_B}$ | · | $1/\sqrt{3}$ |
| $\beta^e_{1/2\,1/2}(db)/\beta^\pi_{1/2\,1/2}(\Delta^{++}p)$ | | c) |

† See note on K exchange in §AA.3.

Table AA.6

SU(3), SU(2) Clebsches for couplings of the axial vector ($J^{PC}=1^{+-}$) and tensor ($2^{--}$) exchanges.

| | |
|---|---|
| $\beta^{A_{e^{-0}}}_{e^{-0}}(ca)/\beta^{A_\rho}_{A_1}{}^{=0}(\rho^0\pi^-) = \beta^{A_{e^{-0}}}_{e^{-0}}(ca)/\beta^{A_\rho}_{\pi}{}^{-0}(\rho^0\pi^-)$ (i.e. use table AA.5a with $\pi\to A_1$, $B\to Z$) | a) |
| $\beta^e_{+-}(db)/\beta^{A_2}_{+-}(np) = \beta^{e'}_{+-}(db)/\beta^\pi_{+-}(np)$ (i.e. use table AA.5b with $\pi\to A_1$, $B\to Z$) $F/D=\frac{2}{3}$ | b) |

For $\pi+B$ (or simply B) exchange we also use eq. (AA.10) where $R$ is, of course, the correctly signatured propagator. Note that in this model the energy dependence of pole and cut is the same.

SU(3) *mass breaking*

Since SU(3) is not a good symmetry for masses we must have a separate prescription for K exchange absorption. The replacement

$$(-t)^{x/2}\to(-\tfrac{1}{2}m_K^2)^{x/2} \tag{AA.11}$$

(rather than $(-m_K^2)^{x/2}$) turns out to be phenomenologically reasonable.

The only other situation where mass-breaking is explicitly taken into account, is in relating the K(NY) (Y = $\Lambda$ or $\Sigma$) and $\pi$(NN) couplings. Although the flip couplings may be related by unbroken SU(3) (see table AA.5), an $s$-channel non-flip KNY coupling arises through mass-breaking in the $s$–$t$ crossing matrix. Thus

$$\frac{\beta^K_{++}(YN)}{\beta^K_{+-}(YN)}=\frac{m_Y-m_N}{2m_N}. \tag{AA.12}$$

*Line-reversal symmetry breaking*

Since vector and tensor exchanges are taken to be EXD, the model cannot attempt to describe the line-reversal inequalities as observed, for example, in $\pi N \to KY/\bar{K}N \to \pi Y$ and in KN CEX. It does, however, give a reasonable account of that observed in np and $\bar{p}p$ CEX by virtue of the $\pi$ cut interfering with $\rho$ Regge pole exchange.

*Polarisation observables*

It is obvious that polarisation observables which are sensitive to the imaginary parts of density matrix elements are, in general, incorrectly given by the model which predicts equal phases for helicity amplitudes when a single (or a single EXD pair of) Regge poles is exchanged. For example, $P(\pi^- p \to \pi^0 n)$ is identically zero. In cases where there is more than one Regge contribution, polarisation can occur in the first order estimate. For example, in $\pi^- p \to \rho^0 n$, the model predicts non-zero polarisation in both natural and unnatural parity exchange components. Suitable formulae for calculating such polarisation contributions can be found in §AB.4.

## *AA.4. Some examples*

We give some examples of varying complexity, both to illustrate the calculational procedure and to demonstrate the typical accuracy to be expected of the model. Two of the examples are described in detail.

A. $\pi^- p \to \pi^0 n$

1) From table AA.1, the prototype couplings are $\rho(\pi\pi)$ and $\rho(NN)$.

2) From table AA.4a, $\rho$ exchange is the only $I = 1$ exchange allowed. The trajectory parameters are listed in table AA.2. Eq. (AA.4) then gives the required propagator $R$.

3) The meson vertex is given by table AA.3 directly, $V_\rho(\pi^0\pi^-) = \beta_\rho(\pi^0\pi^-) = 8.0$.

4) The two baryon couplings are also found in table AA.3,

$$V^\rho_{++}(np) = 2.3, \qquad V^\rho_{+-}(np) = 18.4\sqrt{-t}/2M.$$

5) The helicity amplitudes are therefore $T_{+\pm} = V_\rho R V^\rho_{+\pm}$.

6) Equation (AA.1) now gives the differential cross section. Note that parity implies $|T_{-\mp}| = |T_{+\pm}|$. The resulting cross-section is compared to data in fig. AA.2. Figure AA.3 contains an analogous comparison for the SU(3)-related processes $K^- p \to (\eta, \eta')\Lambda$ (section 4B).

B. $K^+ p \to K^{*0}\Delta^{++}$

1) The prototype couplings required (see table AA.1) are $\rho(\omega\pi)$, $\rho(\Delta N)$ (natural parity exchange) and $\pi(\rho\pi)$, $\pi(\Delta N)$ (unnatural).

2) The exchanges occur in EXD pairs (see tables AA.4b, 5a) so that one can form $R(\pi + B)$ and $R(\rho + A_2)$ at once.

3) $V^{\lambda=0,1}_{\pi+B}(K^{*+}K^+)$ and $V^{\lambda=1}_{\rho+A_2}(K^{*+}K^+)$ are calculated from table AA.3 using tables AA.5a and 4b respectively. Isospin then gives the vertices $V(K^{*0}K^+)$.

4) The baryon couplings are derived from tables AA.3, 5c and 4d.

5) In calculating $T^{\lambda_{K^{*0}}}_{\lambda_\Delta \lambda_N}$ as the sum over exchange contributions ($\pi + B$ and $\rho + A_2$), one uses the vertex parity relations of eq. (AA.7). For the $\pi + B$ amplitudes the absorption prescription of eq. (AA.10) is now applied.

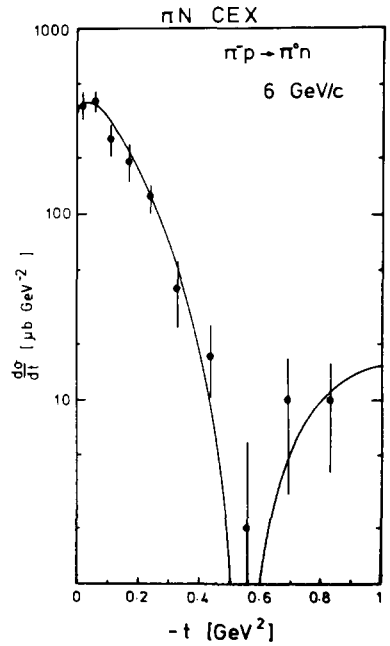


Fig. AA.2. Comparison of model and data [48] for $\pi^- p \to \pi^0 n$ at 6 GeV/$c$.

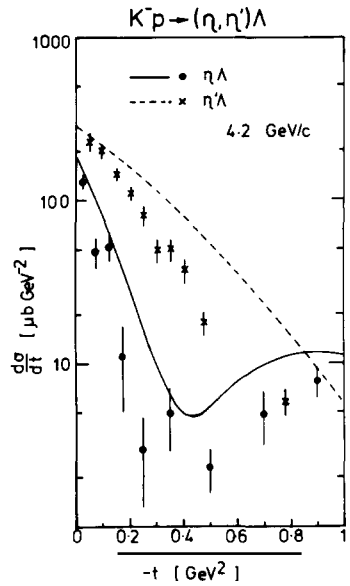


Fig. AA.3. Comparison of model and data [246] for $K^- p \to \eta\Lambda$ and $K^- p \to \eta'\Lambda$ at 4.2 GeV/$c$.

6) The cross-section and $s$-channel density matrix elements may be calculated using

$$\rho^{mm'}_{nn'} \frac{d\sigma}{dt} = \sum_{\lambda_a \lambda_b} T^{m\lambda_a}_{n\lambda_b} T^{m'\lambda_a *}_{n'\lambda_b}. \tag{AA.13}$$

Figure AA.4 contains a comparison of data and predictions for the quantities $\rho_{00}\, d\sigma/dt$, $(\rho_{11} \pm \rho_{1-1}) \cdot d\sigma/dt$. The analogous quantities for $\pi^- p \to \rho^0 n$ at 17.2 GeV/$c$ (an absolute prediction) are shown in fig. AA.5.

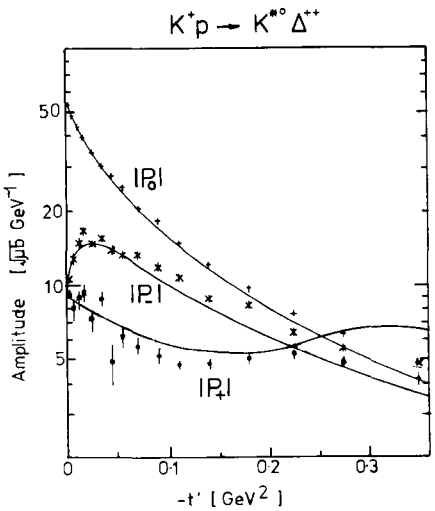


Fig. AA.4. Model predictions for $|P_0| = [\rho_{00}\, d\sigma/dt]^{1/2}$, $|P_\pm| = [(\rho_{11} \pm \rho_{1-1})\, d\sigma/dt]^{1/2}$ in $K^+ p \to K^{*0}\Delta$ compared with data at 13 GeV/$c$ [311].

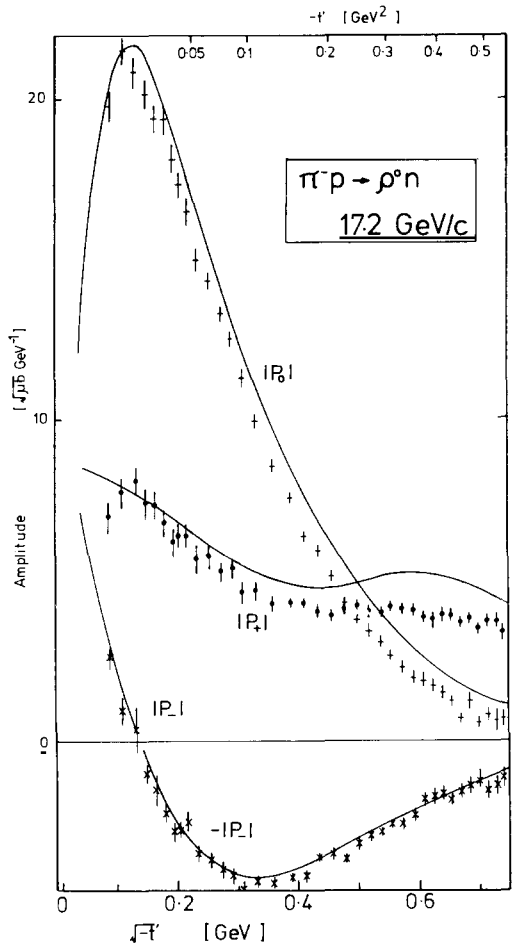


Fig. AA.5. Model predictions for $|P_0|$, $|P_\pm|$ (see caption to fig. AA.4) in $\pi^-p \to \rho^0 n$ compared to data at 17.2 GeV/$c$ [225, 169].

In arriving at the best overall coupling values listed in table AA.3, most reliance has been placed in describing well-measured processes and, in particular, those amplitudes thought to be least affected by absorption. Thus, it is often the case that the model overestimates processes dominated by net helicity flip zero e.g. $\pi^+p \to K^+\Sigma^+$. When necessary, the *average* of line-reversal related processes has been used to help establish coupling strengths (e.g. $K^+p \to K^0\Delta^{++}$ and $K^-n \to \bar{K}^0\Delta^-$).

Differential cross-sections are accurate, typically, to within a factor of two. Considering the lack of parameters, simplicity of calculation, large range of processes and large kinematic region ($P_{LAB} > 4$ GeV/$c$, $|t| < 1$ GeV$^2$) involved, it represents an astonishingly good summary of the high energy data. It is intended that these, simply calculated, model amplitudes provide a useful standard with which to compare data and facilitate discussions of features such as EXD or SU(3) breaking and absorptive corrections.

## Appendix B. Interference techniques for amplitude extraction

In this appendix we give some examples of relatively direct methods for obtaining amplitude information from experimental observables. Each application, the results of which are discussed in

the text, is intended to single out a specific feature of the exchange mechanism. This is achieved using relationships of the general form,

$$\text{Observable} = \left.\begin{matrix}\text{Re}\\ \text{or}\\ \text{Im}\end{matrix}\right\} [(\text{known amplitude}) \cdot (\text{interesting amplitude})^*]. \tag{AB.1}$$

Of course, the usefulness of the resulting information depends (1) on how well known is the "known amplitude" and (2) on the validity of neglecting further amplitudes (where this is necessary).

### *AB.1. Elastic cross-overs and* $\mathrm{Im}N^{(-)}$

In the notation of section 3, the crossing odd (even) helicity flip and non-flip amplitudes for elastic scattering Xp and $\bar{\mathrm{X}}$p are $F^{(-)}$ ($F^{(+)}$) and $N^{(-)}$ ($N^{(+)}$) respectively, where

$$\begin{aligned}\frac{\mathrm{d}\sigma}{\mathrm{d}t}(\bar{\mathrm{X}}\mathrm{p}) &= |F^{(+)} + F^{(-)}|^2 + |N^{(+)} + N^{(-)}|^2\\ \frac{\mathrm{d}\sigma}{\mathrm{d}t}(\mathrm{Xp}) &= |F^{(+)} - F^{(-)}|^2 + |N^{(+)} - N^{(-)}|^2.\end{aligned} \tag{AB.2}$$

Useful combinations of these are

$$\begin{aligned}\Sigma &\equiv \frac{1}{2}\left[\frac{\mathrm{d}\sigma}{\mathrm{d}t}(\bar{\mathrm{X}}\mathrm{p}) + \frac{\mathrm{d}\sigma}{\mathrm{d}t}(\mathrm{Xp})\right] = |F^{(+)}|^2 + |F^{(-)}|^2 + |N^{(+)}|^2 + |N^{(-)}|^2\\ \Delta &\equiv \frac{1}{2}\left[\frac{\mathrm{d}\sigma}{\mathrm{d}t}(\bar{\mathrm{X}}\mathrm{p}) - \frac{\mathrm{d}\sigma}{\mathrm{d}t}(\mathrm{Xp})\right] = 2\,\mathrm{Re}[F^{(+)}F^{(-)*} + N^{(+)}N^{(-)*}].\end{aligned} \tag{AB.3}$$

Davier and Harari [85] demonstrated that if (1) $N^{(+)}$ is dominated by a pure imaginary Pomeron ($N^{(+)} = \mathrm{i}|\mathbb{P}|$), (2) $|N^{(+)}|^2$ dominates $\Sigma$, and (3) $|N^{(+)}| \gg |F^{(+)}||F^{(-)}/N^{(-)}|$ then

$$\Sigma \approx |N^{(+)}|^2 \approx |\mathbb{P}|^2, \qquad \Delta \approx 2|\mathbb{P}|\,\mathrm{Im}N^{(-)}, \tag{AB.4}$$

i.e.

$$\mathrm{Im}N^{(-)} \approx \Delta/(2\Sigma^{1/2}). \tag{AB.5}$$

Typical results are shown in fig. 3.1. Carnegie et al. [256] have shown how one may improve on these approximations given a rough knowledge of some of the smaller amplitudes. In any case, the results are in broad agreement with those obtained by model-independent amplitude analysis [93, 128].

### *AB.2. Elastic polarisation and* $\mathrm{Re}F^{(\pm)}$

The elastic polarisation can be written, in the notation of §AB.1,

$$\begin{aligned}P\frac{\mathrm{d}\sigma}{\mathrm{d}t}(\bar{\mathrm{X}}\mathrm{p}) &= -2\,\mathrm{Im}[(N^{(+)} + N^{(-)})(F^{(+)} + F^{(-)})^*]\\ P\frac{\mathrm{d}\sigma}{\mathrm{d}t}(\mathrm{Xp}) &= -2\,\mathrm{Im}[(N^{(+)} - N^{(-)})(F^{(+)} - F^{(-)})^*].\end{aligned} \tag{AB.6}$$

Just as in §AB.1, we form the combinations

$$\Sigma_P \equiv -2\,\mathrm{Im}[N^{(+)}F^{(+)*} + N^{(-)}F^{(-)*}]$$
$$\Delta_P \equiv -2\,\mathrm{Im}[N^{(+)}F^{(-)*} + N^{(-)}F^{(+)*}], \tag{AB.7}$$

and make the same approximations ((1)–(3)). Then

$$\Sigma_P \approx -2|\mathbb{P}|\,\mathrm{Re}\,F^{(+)} - 2\,\mathrm{Im}[N^{(-)}F^{(-)*}],$$
$$\Delta_P \approx -2|\mathbb{P}|\,\mathrm{Re}\,F^{(-)}. \tag{AB.9}$$

Thus,

$$\mathrm{Re}\,F^{(-)} \approx -\Delta_P/(2\Sigma^{1/2}). \tag{AB.10}$$

In the case of $\pi^{\pm}$p scattering, one can, in addition, calculate Re $F^{(+)}$ (from eq. (AB.8)) using the measured value of $P(\mathrm{d}\sigma/\mathrm{d}t)$ $(\pi\mathrm{p}\to\pi^0\mathrm{n})$ $(\equiv -4\,\mathrm{Im}N^{(-)}F^{(-)*})$. The use of such techniques has been discussed by Phillips [100] and examples are given in section 4A. The interesting structure in the real parts occurs near $-t = 0.5$ other than $-t = 0.2$ as in §AB.1. In the larger $t$-range the assumptions (1) to (3) are more questionable.

### *AB.3. Spin and phase coherence in vector meson production*

It is convenient to define naturality-conserving helicity amplitudes $P^{\mu}_{\lambda'\lambda}$ for the process $0^{-\frac{1}{2}+}\to 1^{-\frac{1}{2}+}$ in terms of the helicity amplitudes $T_{\mu\lambda'\lambda}$ of section 1, by

$$P^0_{\lambda'\lambda} \equiv T_{0\lambda'\lambda}, \qquad P^{\pm}_{\lambda'\lambda} \equiv \frac{1}{\sqrt{2}}(T_{1\lambda'\lambda} \pm T_{-1\lambda'\lambda}). \tag{AB.11}$$

In terms of these, the differential cross-section and measurable vector meson density matrix elements are given by

$$\begin{aligned}
\sigma &\equiv \mathrm{d}\sigma/\mathrm{d}t = \sigma_0 + \sigma_- + \sigma_+ \\
\sigma_0 &\equiv \rho_{00}\sigma = |P^0_{++}|^2 + |P^0_{+-}|^2 \\
\sigma_{\pm} &\equiv (\rho_{11} \pm \rho_{1-1})\sigma = |P^{\pm}_{++}|^2 + |P^{\pm}_{+-}|^2 \\
\sqrt{2}\,\mathrm{Re}\,\rho_{10}\sigma &= \mathrm{Re}[P^0_{++}P^{-*}_{++} + P^0_{+-}P^{-*}_{+-}].
\end{aligned} \tag{AB.12}$$

(Only 3 of the 4 quantities $\sigma$, $\sigma_0$, $\sigma_{\pm}$ are independent.) Note that the natural ($P^+$) and unnatural ($P^0, P^-$) parity amplitudes add incoherently, and that the only measurable interference term is

$$P^0_{++}P^{-*}_{++} + P^0_{+-}P^{-*}_{+-} = \xi_{0-}\sqrt{\sigma_0\sigma_-}\,e^{i\phi_{0-}}. \tag{AB.13}$$

The product

$$\xi_{0-}\cos\phi_{0-} = \sqrt{2}\,\mathrm{Re}(\rho_{10}\sigma)/[\sigma_0\sigma_-]^{1/2} \tag{AB.14}$$

is measurable in unpolarised (nucleon) experiments and has some useful properties ($0 \leqslant \xi_{0-} \leqslant 1$, $-1 \leqslant \cos\phi_{0-} \leqslant 1$):

(1) $\xi_{0-} = 1$ (i.e. $P^0$ and $P^-$ are "spin-coherent") if and only if $P^0_{\lambda'\lambda}/P^-_{\lambda'\lambda}$ is independent of $\lambda'$, $\lambda$. A trivial way of satisfying this is if only one nucleon helicity configuration (+ + or + −) is involved. Such a situation would hold in $\pi^-\mathrm{p}\to\rho^0\mathrm{n}$ if $\pi$ exchange (which couples only to + −) dominated $P^0$ and $P^-$ (see section 4D).

(2) $\xi_{0-}|\cos\phi| = 1$ (i.e. $P^0$ and $P^-$ are spin *and* phase coherent) if and only if the ratio $P^0_{\lambda'\lambda}/P^-_{\lambda'\lambda}$ is *real* and independent of $\lambda'$, $\lambda$. As discussed in section 4D, $\pi$ exchange and its associated cuts in $\pi^-p\to\rho^0n$ appears to satisfy this. In general, when one nucleon helicity vertex dominates (++ or +−), $\xi_{0-}\cos\phi_{0-}$ measures directly the relative phase between $P^0$ and $P^-$. To be sure that one helicity dominates, nucleon polarisation studies (§AB.4) are necessary.

### *AB.4. Polarisation in vector meson production*

In terms of the amplitudes for $0^{-\frac{1}{2}+}\to 1^{-\frac{1}{2}+}$ defined in §AB.3, the transversely polarised target asymmetry $T$ and transverse recoil polarisation $P$ are given by

$$\begin{aligned} T_\sigma &= T_0\sigma_0 + T_-\sigma_- + T_+\sigma_+ \\ T_0\sigma_0 &= -2\,\mathrm{Im}[P^0_{++}P^{0*}_{+-}] \\ T_\pm\sigma_\pm &= -2\,\mathrm{Im}[P^\pm_{++}P^{\pm *}_{+-}] \end{aligned} \tag{AB.15}$$

and

$$\begin{aligned} P\sigma &= P_0\sigma_0 + P_-\sigma_- + P_+\sigma_+ \\ P_0 &= -T_0, \qquad P_\pm = \pm T_\pm. \end{aligned} \tag{AB.16}$$

$T_0$ and $T_\pm$ are all separately measurable, either in a transversely polarised target experiment (e.g. as in $\pi^-p\to\rho^0n$ [166, 299]) or in an unpolarised experiment like $K^-p\to\rho\Lambda$ where the $\Lambda$ and $\rho$ decay correlations give polarisation information [105, 121].

If the target is longitudinally polarised then one may also measure

$$\begin{aligned} I_{+0}\sigma &\equiv 2\,\mathrm{Im}[P^+_{++}P^{0*}_{++} + P^+_{+-}P^{0*}_{+-}] \\ I_{+-}\sigma &\equiv 2\,\mathrm{Im}[P^+_{++}P^{-*}_{++} + P^+_{+-}P^{-*}_{+-}], \end{aligned} \tag{AB.17}$$

i.e. the phase between natural (+) and unnatural (o, −) parity exchange becomes measurable.

In the case of $\pi^-p\to\rho^0n$ (§4D.1) $T_0$ measures the interference between $A_1$-like exchanges in $P^0_{++}$ and the well-established $\pi$-exchange amplitude $P^0_{+-}$. Assuming $|P^0_{+-}|^2 \gg |P^0_{++}|^2$ (for $t\neq 0$), one can estimate

$$|A_1/\pi| = |P^0_{++}/P^0_{+-}| \geqslant \tfrac{1}{2}|T_0|. \tag{AB.18}$$

Other examples are discussed in sections 4D,E.

### *AB.5. ρ-ω interference and related phenomena*

Measurements of the reaction pairs ($K^+n\to K^{*0}p$, $K^-p\to\bar{K}^{*0}n$), ($\gamma p\to\pi^+n$, $\gamma n\to\pi^0p$), ($\pi^+n\to\pi^+\pi^-p$, $\pi^-p\to\pi^+\pi^-n$) and ($\pi^+n\to\pi^+\pi^-\pi^0p$, $\pi^-p\to\pi^+\pi^-\pi^0n$) yield information on the relative phase of the $\rho$ and $\omega$ CEX production amplitudes $A(\rho)$ and $A(\omega)$ (see section 4D). The amplitude relations are

$$\begin{aligned} K^+n\to K^{*0}p \quad &\propto \quad A(\rho)+A(\omega) \\ K^-p\to\bar{K}^{*0}n \quad &\propto \quad A(\rho)-A(\omega), \end{aligned} \tag{AB.19}$$

$$\begin{aligned} \gamma p\to\pi^+n \quad &\propto \quad A(\rho)-A(\omega)/r \\ \gamma n\to\pi^-p \quad &\propto \quad A(\rho)+A(\omega)/r, \end{aligned} \tag{AB.20}$$

$$\begin{aligned} \pi^+ n \to \pi^+\pi^- p \quad &\propto \quad A(\rho) - \epsilon B(m_{2\pi}^2) A(\omega) \\ \pi^- p \to \pi^+\pi^- n \quad &\propto \quad A(\rho) + \epsilon B(m_{2\pi}^2) A(\omega), (m_{2\pi} \sim m_\rho \pm \Gamma_\rho) \end{aligned} \tag{AB.21}$$

$$\begin{aligned} \pi^+ n \to \pi^+\pi^-\pi^0 p \quad &\propto \quad i\epsilon A(\rho) - A(\omega) \\ \pi^- p \to \pi^+\pi^-\pi^0 n \quad &\propto \quad i\epsilon A(\rho) + A(\omega), (m_{3\pi} \sim m_\omega) \end{aligned} \tag{AB.22}$$

where $r \approx 3$ (quark model), $B(m_{2\pi}^2)$ is proportional to the $\rho$ decay Breit–Wigner amplitude, and $\epsilon$ ($\approx 0.035$) is a small $\rho$–$\omega$ mixing parameter related to the $\omega \to 2\pi$ branching ratio [222, 318]. The production phase information is contained in the interference terms

$$\begin{aligned} I^\mu &\equiv P^\mu_{++}(\rho) P^\mu_{++}(\omega)^* + P^\mu_{+-}(\rho) P^\mu_{+-}(\omega)^* \\ &\equiv \xi^\mu_{\rho\omega} \exp(i\phi^\mu_{\rho\omega}) [\sigma_\mu(\rho)\sigma_\mu(\omega)]^{1/2}, \end{aligned} \tag{AB.23}$$

where $\xi^\mu_{\rho\omega}$, so defined, is the spin-coherence between $\rho$ and $\omega$ production in meson helicity state $\mu$, and $\phi^\mu_{\rho\omega}$ is the spin-averaged relative production phase [cf. eq. (AB.13)]. For example, measurement of $\sigma_\mu(K^{*0}p) - \sigma_\mu(\bar{K}^{*0}n)$ [see eq. (AB.19)] yields Re $I^\mu$ (assuming SU(3) symmetry at the meson vertex), and hence $\xi^\mu_{\rho\omega} \cos\phi^\mu_{\rho\omega}$. $\sigma_\mu(\pi^+ n) - \sigma_\mu(\pi^- p)$ [see eq. (AB.20)] also measures $\xi^\mu_{\rho\omega} \cos\phi^\mu_{\rho\omega}$ (assuming VMD). $\sigma_\mu(\pi^+\pi^- p) - \sigma_\mu(\pi^+\pi^- n)$ measures Re $[B(m^2) I^\mu]$ and so, in principle, by varying $m^2$, yields $\xi^\mu_{\rho\omega}$ and $\phi^\mu_{\rho\omega}$ separately. In practice, $\xi^\mu_{\rho\omega}$ is not well constrained [229]. Since $\epsilon \sim$ real, $\sigma(\pi^+\pi^-\pi^0 p) - \sigma(\pi^+\pi^-\pi^0 n)$ (see eq. (AB.22)) yields $\xi^\mu_{\rho\omega} \sin\phi^\mu_{\rho\omega}$. All four types of measurement yield information on the same pairs of production amplitudes, and all have proved invaluable in constraining vector production models. In particular, the first convincing evidence for B exchange came from measurements of $\phi^0_{\rho\omega}$ in $\pi^+\pi^-$ production, i.e. in its interference with the relatively well-understood $\pi$-exchange. Sections 4D and 4E contain many examples.

### *AB.6. Absorption strength as a function of mass*

The existence of (absorptive) cuts in non-flip evasive ($n = 0$, $x \neq 0$) $\pi$ exchange amplitudes is well-known [sections 3, 4D]. Since there is little evidence of cuts in $n = 1$, $x = 0$ $\pi$ exchange amplitudes, at small $-t$, one might hope to learn about the cuts by interfering these $n = 0$ and 1 amplitudes. In §AB.3 it is shown how $\xi_{0-} \cos\phi_{0-}$ ($\alpha$ Re $\rho_{10}$) in $\pi^- p \to \rho^0 n$ measures the relative pole/cut phase. In terms of the Williams model one expects near $t = 0$ (section 4D)

$$\begin{aligned} P^0_{+-} \quad &\propto \quad \sqrt{-t}/(t - \mu^2) \\ P^-_{+-} \quad &\propto \quad [-2t/(t-\mu^2) + C(m^2)]/m \\ P^+_{+-} \quad &\propto \quad [C(m^2)]/m \end{aligned} \tag{AB.24}$$

where $C(m^2) \approx 1$ for $m = m_\rho$.
Thus

$$\text{Re}\,\rho_{10}\, d\sigma/dt \sim -\sqrt{-t}[\mu^2 + t + (C-1)(\mu^2 - t)] \tag{AB.25}$$

so that the value of $C(m^2)$, the effective cut, may be phenomenologically evaluated from the position in $-t$ at which the data for Re $\rho_{10}$ (or $\cos\phi_{0-}$) has a single zero. This technique may also be used in $\pi^+$ electroproduction where measurement of Re $\rho_{10}\, d\sigma/dt$, as a function of $q^2$, allows an estimate of $C(q^2)$ [section 4F].

Near $t = 0$, one may also use the approximation

$$\Sigma \equiv \frac{\sigma_+ - \sigma_-}{\sigma_+ + \sigma_-} \underset{t\to 0}{\approx} \frac{-2t}{C(m^2)(\mu^2 - t) + 2t} \tag{AB.26}$$

to calculate $C(m^2)$ from the small $t$ data. This is particularly useful in comparisons of photoproduction and vector-meson production [section 4F].

One may also test the Williams model prediction (or indeed that of any simple absorption model), that $C = 1$ is independent of spin as well as mass (e.g. for $\pi^- p \to f^0 n$ as well as $\pi^- p \to \rho^0 n$). In this case, where the $\pi$ exchange couples to different spins, it is convenient to use $t$-channel quantisation for the meson helicity. In the case of general spin $L(P \to L)$, and approximating the crossing-matrix for $t \approx 0$, eqs. (AB.24) become

$$\begin{aligned} L_{+-}^{0(t)} &\propto \sqrt{-t}/(t - \mu^2) \\ L_{+-}^{1-(t)} &\propto C(L, m^2)\sqrt{\tfrac{1}{2}L(L+1)}/m. \end{aligned} \tag{AB.27}$$

(Note that the $\pi$ pole does not couple to the $t$-channel unnatural parity helicity 1 amplitude.) If the $L_{+-}^{\mu(t)}$ can be isolated (section 4F), the $L$ and $m^2$ dependence of $C(L, m^2)$, so defined, can be studied [169]. If, on the other hand, $C$ is *assumed* to be independent of $L$, it can be more directly obtained from the ratio $\langle Y_1^J \rangle / \langle Y_0^J \rangle$ of the $t$-channel $\pi\pi$ angular distribution moments using eqs. (AB.27) [174].

## References


[1] G.F. Chew and F.E. Low, Phys. Rev. 113 (1959) 1640.
[2] M. Jacob and G.C. Wick, Ann. Phys. 7 (1959) 404.
[3] S.W. MacDowell, Phys. Rev. 116 (1959) 774.
[4] G.F. Chew and S.C. Frautschi, Phys. Rev. Letters 7 (1961) 394.
[5] M. Gell-Mann, D. Sharp and W.G. Wagner, Phys. Rev. Letters 8 (1962) 261.
[6] R.J.N. Phillips, Phys. Letters 3 (1962) 21.
[7] N.J. Sopkovitch, Nuovo Cimento 26 (1962) 186.
[8] B.R. Desai, Phys. Rev. Letters 11 (1963) 59.
[9] S. Mandelstam, Nuovo Cimento 26 (1963) 1113, 1127, 1148.
[10] L. Stodolski and J.J. Sakurai, Phys. Rev. Letters 11 (1963) 90.
[11] K. Gottfried and J.D. Jackson, Nuovo Cimento 34 (1964) 735.
[12] F. Gursey and L.A. Radicati, Phys. Rev. Letters 13 (1964) 299.
[13] J.D. Jackson and H. Pilkuhn, Nuovo Cimento 33 (1964) 906.
[14] S. Meshkov, G.A. Snow and G.B. Yodh, Phys. Rev. Letters 12 (1964) 87.
[15] R.J.N. Phillips, Phys. Letters 10 (1964) 344.
[16] H.D.I. Abarbanel and C. Callan, Phys. Letters 16 (1965) 191.
[17] R.C. Arnold, Phys. Rev. Letters 14 (1965) 657.
[18] V.M. Gribov, I.Y. Pomeranchuk and K.A. Ter-Martirosyan, Phys. Rev. 139B (1965) 184.
[19] J.D. Jackson, High Energy Physics, eds. C. de Witt and M. Jacob (Gordon and Breach, New York, 1965).
[20] R.J.N. Phillips and W. Rarita, Phys. Rev. Letters 14 (1965) 502.
[21] R.J.N. Phillips and W. Rarita, Phys. Rev. 139B (1965) 1336.
[22] A.V. Stirling et al., Phys. Rev. Letters 14 (1965) 763.
[23] A. Ahmadzadeh and C.H. Chan, Phys. Letters 22 (1966) 692.
[24] J. Arbab and C.B. Chui, Phys. Rev. 147 (1966) 1045.
[25] P. Bonamy et al., Phys. Letters 20 (1966) 75.
[26] G. Buschorn et al., Phys. Rev. Letters 17 (1966) 1027; 18 (1967) 571.
[27] R.J. Eden, P.V. Landshoff, D.I. Olive and J.C. Polkinghorne, The analytic $S$-matrix (Cambridge University Press, 1966).
[28] H.J. Lipkin and F. Scheck, Phys. Rev. Letters 16 (1966) 71.
[29] D.R.O. Morrison, Phys. Letters 22 (1966) 528.
[30] R.C. Arnold, Phys. Rev. 153 (1967) 1523.
[31] L. Bertocchi, Proc. Heidelberg Conf. on Elementary Particles, 1967, ed. H. Filthuth (North-Holland Publ. Co., Amsterdam, 1968).
[32] J.B. Bronzan and C.E. Jones, Phys. Rev. 160 (1967) 1494.

[33] G. Cohen-Tannoudji, A. Morel and H. Navelet, Nuovo Cimento 48A (1967) 1075.
[34] M. Le Bellac, Phys. Letters 25B (1967) 524.
[35] P.E. Schlein, Phys. Rev. Letters 19 (1967) 1052.
[36] J. Schwarz, Phys. Rev. 159 (1967) 1269.
[37] R.C. Arnold and M.L. Blackmon, Phys. Rev. 176 (1968) 2087.
[38] J.S. Ball, W.R. Frazer and M. Jacob, Phys. Rev. Letters 20 (1968) 518.
[39] A. Białas and K. Zalewski, Nucl. Phys. B6 (1968) 448, 465, 478, 483.
[40] G. Cohen-Tannoudji, A. Morel and Ph. Salin, Nuovo Cimento 55A (1968) 412.
[41] P.D.B. Collins and E.J. Squires, Regge poles in particle physics (Springer, Berlin, 1968).
[42] R. Dolen, D. Horn and C. Schmid, Phys. Rev. 166 (1968) 1768.
[43] P.G.O. Freund, Phys. Rev. Letters 20 (1968) 1235.
[44] V.N. Gribov, Soviet Phys. JETP 26 (1968) 414.
[45] H. Harari, Phys. Rev. Letters 20 (1968) 1395.
[46] F. Henyey, G.L. Kane, J. Pumplin and M. Ross, Phys. Rev. Letters 21 (1968) 946.
[47] K. Igi, S. Matsuda and Y. Oyanagi, Phys. Rev. Letters 21 (1968) 580.
[48] I. Manelli et al., Phys. Rev. 168 (1968) 1515.
[49] G. Veneziano, Nuovo Cimento 57A (1968) 190.
[50] V.D. Barger and D.B. Cline, Phenomenological theories of high energy scattering (Benjamin, New York, 1969).
[51] V. Barger and C. Michael, Phys. Rev. 186 (1969) 1592.
[52] V. Barger and R.J.N. Phillips, Phys. Rev. 187 (1969) 2210.
[53] A.M. Boyarski et al., Phys. Rev. Letters 22 (1969) 1131.
[54] C.F. Cho and J.J. Sakurai, Phys. Letters 30B (1969) 119.
[55] D.J. Crennel et al., Phys. Rev. Letters 23 (1969) 1347.
[56] W. De Baere et al., Nuovo Cimento 61A (1969) 397.
[57] V.N. Gribov, Sov. J. Nucl. Phys. 9 (1969) 369.
[58] A.S. Goldhaber, G.C. Fox and C. Quigg, Phys. Letters 30B (1969) 249.
[59] H. Harari, Phys. Rev. Letters 22 (1969) 562.
[60] F.S. Henyey, G.L. Kane, J. Pumplin and M. Ross, Phys. Rev. 182 (1969) 1579.
[61] J. Mandula, J. Weyers and G. Zweig, Phys. Rev. Letters 23 (1969) 266.
[62] J.L. Rosner, Phys. Rev. Letters 22 (1969) 689.
[63] C. Schmid, Nuovo Cimento Letters 1 (1969) 165.
[64] P. Sonderegger and P. Bonamy, contr. to Lund Conf. (1969);
P. Sonderegger, High Energy Collisions, 3rd Int. Conf. on high energy physics (Stony Brook, 1969).
[65] M.A. Virasoro, Phys. Rev. Letters 22 (1969) 37.
[66] S.P. Ying et al., Phys. Letters 30B (1969) 289.
[67] V. Barger and P. Weiler, Nucl. Phys. B20 (1970) 615.
[68] M. Borghini et al., Phys. Letters 31B (1970) 405.
[69] A. Firestone et al., Phys. Rev. Letters 25 (1970) 958.
[70] F. Gilman, J. Pumplin, A. Schwimmer and L. Stodolsky, Phys. Letters 31B (1970) 387.
[71] J.D. Jackson, Rev. Mod. Phys. 42 (1970) 12.
[72] M. Jacob, Proc. Brandeis summer school (MIT press, 1970) Vol. 2.
[73] K.-W. Lai and J. Louie, Nucl. Phys. B19 (1970) 205.
[74] J. Mandula, J. Weyers and G. Zweig, Ann. Rev. Nucl. Sci. 20 (1970) 289.
[75] A.D. Martin and T.D. Spearman, Elementary particle theory (North-Holland, Amsterdam, 1970).
[76] C. Michael, Springer Tracts in Modern Physics, Vol. 55 (Springer-Verlag, Berlin, 1970) p. 174.
[77] A. Mueller, Phys. D2 (1970) 2963.
[78] M. Ross, F.S. Henyey and G.L. Kane, Nucl. Phys. B23 (1970) 269.
[79] P.K. Williams, Phys. Rev. D1 (1970) 1312.
[80] M. Abramovich et al., Nucl. Phys. B27 (1971) 477.
[81] M. Aguilar-Benitez et al., Phys. Rev. D4 (1971) 2853.
[82] E.L. Berger and G.C. Fox, Nucl. Phys. B26 (1971) 1.
[83] E.L. Berger and G.C. Fox, Nucl. Phys. B30 (1971) 1.
[84] P.D.B. Collins, Phys. Reports 1C (1971) 103.
[85] M. Davier and H. Harari, Phys. Letters 35B (1971) 239.
[86] J. Finkelstein, Nuovo Cimento 5A (1971) 413.
[87] G.C. Fox, Phenomenology in particle physics 1971, eds. C.B. Chiu et al. (Caltech, Pasadena, 1971).
[88] F.D. Gault and H.F. Jones, Nucl. Phys. B30 (1971) 68.
[89] F.D. Gault, A.D. Martin and G.L. Kane, Nucl. Phys. B32 (1971) 429.

[90] Y. Gell et al., Nucl. Phys. B33 (1971) 379.
[91] F.J. Gilman, J. Pumplin, A. Schwimmer and L. Stodolsky, Phys. Letters 31B (1970) 387.
[92] D.F. Grether et al., Phys. Rev. Letters 26 (1971) 792.
[93] F. Halzen and C. Michael, Phys. Letters 36B (1971) 367.
[94] H. Harari, Proc. 1971 Int. Symp. on electron and photon interactions at high energies (Cornell, 1971) p. 299.
[95] H. Harari, Ann. of Phys. 63 (1971) 432.
[96] A.C. Irving, A.D. Martin and C. Michael, Nucl. Phys. B32 (1971) 32.
[97] C. Lovelace, Phenomenology in Particle Physics, eds. C. Chiu et al. (Caltech, 1971).
[98] C. Lovelace, Proc. Amsterdam Conf. on Elementary Particles (1971).
[99] A.D. Martin and C. Michael, Phys. Letters 37B (1971) 513.
[100] R.J.N. Phillips, Proc. Amsterdam Int. Conf. on Elementary Particles (1971).
[101] G. Plaut, Nucl. Phys. B35 (1971) 221.
[102] C. Schmid, Phenomenology in Particle Physics, eds. C. Chiu et al. (Caltech, 1971).
[103] C. Schmid and J.K. Storrow, Nucl. Phys. B29 (1971) 219.
[104] F. Zachariasen, CERN preprint TH1290; Proc. 10th Internationale Universitätswochen Kernphysik, Schladming, 1971.
[105] M. Abramovich, A.C. Irving, A.D. Martin and C. Michael, Phys. Letters 39B (1972) 353.
[106] M. Aguilar-Benitez et al., Phys. Rev. D6 (1972) 29.
[107] M. Aguilar-Benitez, S.U. Chung, R.L. Eisner and R.D. Field, Phys. Rev. Letters 29 (1972) 749.
[108] V. Barger, K. Geer and F. Halzen, Nucl. Phys. B44 (1972) 475.
[109] V. Barger and A.D. Martin, Phys. Letters 39B (1972) 379.
[110] V.K. Birulev et al., Phys. Letters 38B (1972) 452.
[111] J.B. Bronzan, Phys. Rev. D6 (1972) 1130.
[112] CERN-HERA data compilation, CERN/HERA 72-1.
[113] CERN-HERA data compilation, CERN/HERA 72-2.
[114] V. Chabaud et al., Phys. Letters 38B (1972) 446.
[115] V. Chabaud et al., Phys. Letters 41B (1972) 209.
[116] C.B. Chiu, Ann. Rev. Nucl. Sci. 22 (1972) 255.
[117] M.B. Einhorn, J. Ellis and J. Finkelstein, Phys. Rev. D5 (1972) 2063.
[118] P. Estabrooks and A.D. Martin, Phys. Letters 41B (1972) 350.
[119] P. Estabrooks and A.D. Martin, Phys. Letters 42B (1972) 229.
[120] C. Ferro-Fontan, CERN preprint TH1490 (1972).
[121] R.D. Field, Phys. Letters 39B (1972) 389.
[122] R.D. Field, R.L. Eisner and M. Aguilar-Benitez, Phys. Rev. D6 (1972) 1863.
[123] A. Firestone and E. Colton, Caltech preprint CALT-68-353 (1972).
[124] C.D. Froggatt and D. Morgan, Phys. Letters 40B (1972) 655.
[125] G. Girardi et al., Nucl. Phys. B47 (1972) 445.
[126] G. Grayer et al., Nucl. Phys. B50 (1972) 29.
[127] B. Kayser and F. Hayot, Phys. Rev. D6 (1972) 2423.
[128] R.L. Kelly, Phys. Letters 39B (1972) 635.
[129] J. Kwiecinski, Nuovo Cimento Letters 3 (1972) 619.
[130] J.S. Loos and J.A.J. Mathews, Phys. Rev. D6 (1972) 2436.
[131] A.D. Martin, C. Michael and R.J.N. Phillips, Nucl. Phys. 43B (1972) 13.
[132] W. Michael and G. Gidal, Phys. Rev. Letters 28 (1972) 1475.
[133] L. Moscoso et al., Phys. Letters 40B (1972) 285.
[134] G. Ringland et al., Nucl. Phys. B44 (1972) 395.
[135] A.I. Sanda, Phys. Rev. D6 (1972) 280.
[136] C. Schmid and J.K. Storrow, Nucl. Phys. B44 (1972) 269.
[137] J.K. Storrow, Nucl. Phys. B47 (1972) 174.
[138] A.R. White, Nucl. Phys. B50 (1972) 93, 130.
[139] R.P. Worden, Nucl. Phys. B37 (1972) 253.
[140] R.P. Worden, Phys. Letters 40B (1972) 260.
[141] G.S. Abrams and K.W.J. Barnham, Phys. Rev. D7 (1973) 1395.
[142] J.P. Ader, C. Meyers and Ph. Salin, Nucl. Phys. B58 (1973) 621.
[143] E.N. Argyres, A.P. Contogouris, J.J. Holden and M. Svec, Phys. Rev. D8 (1973) 2068.
[144] S.A. Adjei et al., Ann. Phys. 75 (1973) 405.
[145] W. Beusch et al., Phys. Letters 46B (1973) 477.
[146] W. Bienlein et al., Phys. Letters 46B (1973) 131.
[147] D. Branson, Nuovo Cimento 15A (1973) 217.

[148] C.B. Chiu and E. Ugaz, Phys. Letters 43B (1973) 327.
[149] G. Ciapetti et al., Nucl. Phys. B64 (1973) 58.
[150] G. Ciapetti et al., Nucl. Phys. B66 (1973) 350.
[151] M. Creutz, F.E. Paige and L.L. Wang, Phys. Rev. Letters 30 (1973) 343.
[152] R.D. Field, Proc. Tallahassee $\pi\pi$ Conference, Florida State Univ., 1973.
[153] R.D. Field, R.L. Eisner, S.U. Chung and M. Aguilar-Benitez, Phys. Rev. D7 (1973) 2036.
[154] G.C. Fox and C. Quigg, Ann. Rev. Nucl. Sci. 23 (1973) 219.
[155] H. Fritzsch, M. Gell-Mann and H. Leutwyler, Phys. Letters 47B (1973) 365.
[156] G.R. Goldstein, J.F. Owens and J. Rutherford, Nucl. Phys. B53 (1973) 197.
[157] H.A. Gordon, K.-W. Lai and J.M. Scar, Phys. Rev. D8 (1973) 779.
[158] B.J. Hartley and G.L. Kane, Nucl. Phys. B57 (1973) 157.
[159] F. Hayot and A. Morel, Phys. Rev. D8 (1973) 223.
[160] G. Höhler, Lectures at the Tehran Summer School and at the Triangle Seminar on Low Energy Hadron Interactions, Smolenice, 1973.
[161] P. Hoyer, R.G. Roberts and D.P. Roy, Nucl. Phys. B56 (1973) 173.
[162] P. Hoyer and J. Kwiecinski, Nucl. Phys. B60 (1973) 26.
[163] Huan Lee, Phys. Rev. Letters 30 (1973) 719.
[164] A.C. Irving, Nucl. Phys. B63 (1973) 499.
[165] A.C. Irving, A.D. Martin and V. Barger, Nuovo Cimento 16A (1973) 573.
[166] J.D. Kimel and E. Reya, Nucl. Phys. B58 (1973) 513.
[167] N. Levy, W. Majerotto and B.J. Read, Nucl. Phys. B55 (1973) 493.
[168] H. Lipkin, Phys. Reports 8C (1973) 173.
[169] A.D. Martin, Proc. 4th Int. Symp. on multiparticle hadrodynamics, Pavia, 1973; CERN report TH 1741.
[170] G.C. Mason and C.G. Wohl, Nucl. Phys. B58 (1973) 1.
[171] C. Michael, Nucl. Phys. B57 (1973) 292.
[172] C. Michael, Nucl. Phys. B63 (1973) 431.
[173] R.J. Miller et al., Nuovo Cimento Letters 6 (1973) 491.
[174] W. Ochs and F. Wagner, Phys. Letters 44B (1973) 271.
[175] C. Pajares and D. Shiff, Nuovo Cimento Letters 8 (1973) 237.
[176] G.A. Ringland, Proc. Int. Conf. on elementary particles, Aix-en-Provence, 1973, Suppl. of Journal de Physique, Tome 34, Fasc. 11-12 C1-1973.
[177] B. Sadoulet, Nucl. Phys. B53 (1973) 135.
[178] P. Salin, Proc. Int. Symp. on Electron and Photon Interactions at High Energies, Bonn, 1973.
[179] B. Schrempp and F. Schrempp, Nucl. Phys. B54 (1973) 525.
[180] D.J. Sherden et al., Phys. Rev. Letters 30 (1973) 1230.
[181] J.K. Storrow and G. Winbow, Nucl. Phys. B53 (1973) 62; B54 (1973) 560.
[182] G. Veneziano, Phys. Letters 43B (1973) 413.
[183] R.P. Worden, Proc. Daresbury Study Weekend on $\pi$ exchange (1973).
[184] R.P. Worden, Nucl. Phys. B58 (1973) 205.
[185] H.D.I. Abarbanel and J.B. Bronzan, Phys. Letters 48B (1974) 345; Phys. Rev. D9 (1974) 2397.
[186] H.D.I. Abarbanel and R.L. Sugar, Phys. Rev. D10 (1974) 721.
[187] C.W. Akerlof et al., Phys. Rev. Letters 33 (1974) 119.
[188] I. Ambats et al., Phys. Rev. D9 (1974) 1179.
[189] E.N. Argyres, A.P. Contogouris and J.P. Holden, Phys. Rev. D9 (1974) 1340.
[190] J.J. Aubert et al., Phys. Rev. Letters 33 (1974) 1404;
J.-E. Augustin et al., Phys. Rev. Letters 33 (1974) 1406.
[191] T.M. Aye and A.K.M.A. Islam, J. Phys. A: Math. Nucl. Gen. 7 (1974) 1141.
[192] D.S. Ayres et al., Phys. Rev. Letters 32 (1974) 1463.
[193] V. Barger, Proc. 17th Int. Conf. on High Energy Physics, London, 1974, p. I-193.
[194] I.S. Barker, A. Donnachie and J.K. Storrow, Nucl. Phys. B79 (1974) 431.
[195] I.J. Bloodworth et al., Nucl. Phys. B81 (1974) 231.
[196] A. Bramon and M. Greco. Phys. Letters 48B (1974) 137.
[197] G. Brandenberg et al., Phys. Rev. D9 (1974) 1939.
[198] J.B. Bronzan, G.L. Kane and U. Sukhatme, Phys. Letters 49B (1974) 272.
[199] R.C. Brower, C.E. De Tar and J.H. Weis, Phys. Reports 14C (1974) 257.
[200] W.F. Buhl et al., Phys. Letters 48B (1974) 388.
[201] J.L. Cardy and A.R. White, Nucl. Phys. B80 (1974) 12.
[202] A.S. Carroll et al., Phys. Rev. Letters 33 (1974) 928, 932.
[203] V. Chaloupka et al., Phys. Letters 51B (1974) 407.

[204] J.A. Charlesworth et al., Nucl. Phys. B79 (1974) 375.
[205] P.D.B. Collins and A. Fitton, Nucl. Phys. B68 (1974) 125.
[206] P.D.B. Collins, F.D. Gault and A. Martin, Nucl. Phys. B83 (1974) 241.
[207] S. Dado et al., Phys. Letters 50B (1974) 275.
[208] M. Davier, Proc. Summer Inst. on particle physics, SLAC, 1974, Vol. 1.
[209] J.P. De Brion and R. Peschanski, Nucl. Phys. B81 (1974) 484.
[210] B.R. Desai, Phys. Letters 50B (1974) 494.
[211] R.C.E. Devenish, C.D. Froggatt and B.R. Martin, Nucl. Phys. B81 (1974) 330.
[212] R. Diebold et al., Phys. Rev. Letters 32 (1974) 904.
[213] J. Dronkers and P. Kroll, Nucl. Phys. B82 (1974) 130.
[214] E. Egli, D.W. Duke and N.W. Dean, Phys. Rev. D9 (1974) 1365.
[215] F. Elvekjaer and R.C. Johnson, Nucl. Phys. B83 (1974) 142.
[216] F. Elvekjaer and R.C. Johnson, Nuovo Cimento Letters 11 (1974) 561.
[217] F. Elvekjaer and B.R. Martin, Nucl. Phys. B75 (1974) 388.
[218] M.J. Emms et al., Phys. Letters 51B (1974) 195.
[219] P. Estabrooks, A.D. Martin and C. Michael, Nucl. Phys. B72 (1974) 454.
[220] P. Estabrooks et al., Nucl. Phys. B81 (1974) 70.
[221] R.D. Field, Proc. 17th Int. Conf. on High Energy Physics, London, 1974.
[222] R.D. Field and D.P. Sidhu, Phys. Rev. D10 (1974) 89.
[223] K.J. Foley et al., Phys. Rev. D9 (1974) 42.
[224] G. Girardi and H. Navelet, Nucl. Phys. B83 (1974) 377.
[225] G. Grayer et al., Nucl. Phys. B75 (1974) 189.
[226] P. Hoyer, P. Estabrooks and A.D. Martin, Phys. Rev. D10 (1974) 80.
[227] B. Hyams et al., Phys. Letters 51B (1974) 272.
[228] A.C. Irving and C. Michael, Nucl. Phys. B82 (1974) 282.
[229] S.L. Kramer et al., Phys. Rev. Letters 33 (1974) 505.
[230] S. Mandelstam, Phys. Reports 13C (1974) 259.
[231] W. Männer, Proc. IVth Int. Conf. on experimental meson spectroscopy, Boston, 1974.
[232] B.R. Martin and F. Elvekjaer, Nucl. Phys. B75 (1974) 388.
[233] A.A. Migdal, A.M. Polyakov and K.A. Ter-Martirosyan, Phys. Letters 48B (1974) 239; Zh. Eksp. Teor. Fiz. 67 (1974) 84.
[234] M.L. Perl, High energy hadron physics (John Wiley and Sons, New York, 1974).
[235] J.L. Rosner, Phys. Reports 11C (1974) 189.
[236] N.P. Samios, M. Goldberg and B.T. Meadows, Rev. Mod. Phys. 46 (1974) 49.
[237] M.R. Sogard, Phys. Rev. D9 (1974) 1486.
[238] C. Sorensen, Phys. Letters 49B (1974) 86.
[239] L.G.F. Vanryckeghem, Phys. Letters 53B (1974) 272.
[240] G. Veneziano, Phys. Reports 9C (1974) 199.
[241] A.B. Wicklund et al., contrib. paper, London Conf., 1974.
[242] R.P. Worden, Proc. London Conf., 1974.
[243] H.D.I. Abarbanel et al., Phys. Reports 21C (1975) 119.
[244] K.-F. Albrecht et al., Nucl. Phys. B93 (1975) 237.
[245] Amsterdam-CERN-Nijmegen-Oxford collaboration CERN/D.Ph.II/Phys. 75-17.
[246] Amsterdam-CERN-Nijmegen-Oxford collaboration CERN/D.Ph.II/Phys. 75-20.
[247] P. Astbury et al., Nucl. Phys. B99 (1975) 30.
[248] A. Berglund et al., Phys. Letters 57B (1975) 100.
[249] A. Berglund et al., Phys. Letters 60B (1975) 117.
[250] R. Blokzijl et al., Nucl. Phys. B98 (1975) 401.
[251] V.N. Bolotov et al., contrib. paper, Palermo Conf., 1975.
[252] V.N. Bolotov et al., Serpukhov preprint IHEP 75-148 (1975).
[253] G. Brandenburg et al., Phys. Letters 58B (1975) 367.
[254] F.W. Brasse et al., Phys. Letters 58B (1975) 464.
[255] G. Calucci and R. Jengo, Nucl. Phys. B84 (1975) 413.
[256] R.K. Carnegie et al., Phys. Letters 58B (1975) 371.
[257] G.F. Chew and C. Rosenzweig, Phys. Letters 58B (1975) 93.
[258] Chan Hong-Mo, J.E. Paton and Tsou Sheung Tsun, Nucl. Phys. B86 (1975) 479; B92 (1975) 13.
[259] S.U. Chung et al., Phys. Letters 57B (1975) 384.
[260] P.D.B. Collins and A. Fitton, Nucl. Phys. B91 (1975) 332.
[261] G. De Marzo et al., Phys. Letters 56B (1975) 487.

[262] B.R. Desai and P.R. Stevens, Phys. Rev. D11 (1975) 2449.
[263] M.J. Emms et al., Phys. Letters 58B (1975) 117.
[264] M.J. Emms et al., Nucl. Phys. B98 (1975) 1.
[265] Fermilab Single Arm Spectrometer Group, Phys. Rev. Letters 35 (1975) 1195.
[266] H. Genzel et al., Nucl. Phys. B92 (1975) 196.
[267] M.S. Groom and B.R. Martin, Nucl. Phys. B97 (1975) 36.
[268] A. Guła and M.R. Pennington, Nucl. Phys. B97 (1975) 461.
[269] R.E. Hendrick et al., Phys. Rev. D11 (1975) 536.
[270] E.W. Hoffman et al., Phys. Rev. Letters 35 (1975) 138.
[271] A.C. Irving, Nucl. Phys. B86 (1975) 125.
[272] A.C. Irving, Phys. Letters 59B (1975) 451.
[273] A.C. Irving, Nucl. Phys. B101 (1975) 263.
[274] A.C. Irving and L.G.F. Vanryckeghem, Nucl. Phys. B93 (1975) 324.
[275] L.M. Jones and P.V. Landshoff, Nucl. Phys. B94 (1975) 145.
[276] D.W.G.S. Leith, Proc. of the 1974 SLAC Summer Institute on Particle Physics, SLAC-PUB-1526 (1975).
[277] A.J. Lennox et al., Phys. Rev. D11 (1975) 1777.
[278] A.D. Martin and C. Michael, Nucl. Phys. B84 (1975) 83.
[279] R.G. Moorhouse, Proc. Palermo Conf., 1975.
[280] J.F. Owens, R.L. Eisner, S.U. Chung and S.D. Protopopescu, Nucl. Phys. B94 (1975) 77.
[281] J.F. Owens, R.L. Eisner, S.U. Chung and S.D. Protopopescu, Phys. Letters 58B (1975) 376.
[282] K. Paler et al., Nucl. Phys. B96 (1975) 1.
[283] A.J. Pawlicki et al., Argonne preprint ANL-HEP-CP-75-50 (1975).
[284] D.J. Quinn et al., Phys. Rev. Letters 34 (1975) 543.
[285] A.W. Reid, Nuovo Cimento 28A (1975) 519.
[286] C. Rosenzweig and G.F. Chew, Phys. Letters 48B (1975) 93.
[287] F. Schrempp and B. Schrempp, CERN preprint 1975, TH-2054; Proc. Palermo Conf. on High Energy Physics, 1975.
[288] J.K. Storrow and G. Winbow, J. Phys. G: Nucl. Phys. Vol. 1, No. 3 (1975) 263.
[289] L.G.F. Vanryckeghem, Nucl. Phys. B90 (1975) 161.
[290] D.R. Yennie, Rev. Mod. Phys. 47 (1975) 311.
[291] H.D.I. Abarbanel, Rev. Mod. Phys. 48 (1976) 417.
[292] M. Aguilar-Benitez et al., CERN preprint, submitted to Nucl. Phys. (1976).
[293] P. Auer et al., Nucl. Phys. B113 (1976) 279.
[294] C. Avilez-Valdez and G. Cocho, Nucl. Phys. B108 (1976) 335.
[295] A. Babaev et al., Nucl. Phys. B110 (1976) 189.
[296] M. Baker and K.A. Ter-Martirosyan, Phys. Reports 28C (1976) 1.
[297] I.S. Barker and J.K. Storrow, submitted to Nucl. Phys. (1976).
[298] A.V. Barnes et al., Phys. Rev. Letters 37 (1976) 76.
[299] H. Becker et al., preprint submitted to the Tbilisi Conference on High Energy Physics, 1976.
[300] E.L. Berger and C. Sorensen, Phys. Letters 62B (1976) 303.
[301] P.J. Busey et al., Phys. Letters 61B (1976) 479.
[302] G.W. Brandenburg et al., Nucl. Phys. B104 (1976) 413.
[303] A.S. Carroll et al., Phys. Letters 61B (1976) 303.
[304] D. Cohen et al., Phys. Rev. Letters 38 (1977) 269.
[305] P.D.B. Collins, An Introduction to Regge theory and high energy physics (Cambridge U.P., 1976).
[306] O.I. Dahl et al., Phys. Rev. Letters 37 (1976) 80.
[307] J.D. Dowell et al., Nucl. Phys. B108 (1976) 30.
[308] D.W. Duke, Phys. Letters 61B (1976) 103.
[309] K.W. Edwards et al., Contribution to the 18th Int. Conf. on High Energy Physics, Tbilisi, 1976.
[310] P. Estabrooks and A.D. Martin, Nucl. Phys. B102 (1976) 537.
[311] P. Estabrooks et al., Nucl. Phys. B106 (1976) 61.
[312] C.D. Frogatt and N.H. Parsons, Glasgow University preprint (1976).
[313] J. Gallivan et al., Nucl. Phys. B117 (1976) 269.
[314] G. Giacomelli, Phys. Reports 23 (1976) 123.
[315] G. Goldhaber et al., Phys. Rev. Letters 37 (1976) 255.
[316] S.-O. Holmgren et al., submitted to Nucl. Phys. B (1976).
[317] T. Inami, K. Kawarabayashi and S. Kitakado, Tokyo preprint UT-Komado 76-5 (1976).
[318] A.C. Irving, Nucl. Phys. B105 (1976) 491.
[319] G.L. Kane and A. Seidl, Rev. Mod. Phys. 48(2) (1976) 309.

[320] F. Marzano et al., CERN preprint submitted to Nucl. Phys. (1976).
[321] G.G.G. Massaro et al., Phys. Letters 66B (1977) 385.
[322] M.M. Nagels et al., Nucl. Phys. B109 (1976) 1.
[323] H. Navelet and P.R. Stevens, Nucl. Phys. B104 (1976) 171.
[324] J.F. Owens et al., Nucl. Phys. B112 (1976) 514.
[325] A.J. Pawlicki et al., Phys. Rev. Letters 37 (1976) 971.
[326] J.J. Phelan et al., Phys. Letters 61B (1976) 483.
[327] C. Quigg and J.L. Rosner, Phys. Rev. D14 (1976) 160.
[328] M. Shaevitz et al., Phys. Rev. Letters 36 (1976) 5.
[329] M. Shaevitz et al., Phys. Rev. Letters 36 (1976) 8.
[330] D. Sivers, S.J. Brodsky and R. Blankenbeckler, Phys. Reports 23C (1976) 1.
[331] A.B. Wicklund et al., private communication; to be published (1976).
[332] R.P. Worden, unpublished work (1976).